Approche multi-échelle pour la modélisation de fluides de travail des procédés de revalorisation de la chaleur fatale

Thomas Di Pietro

Thèse

Présentée et soutenue publiquement pour l'obtention du titre de

DOCTEUR DE l'UNIVERSITE DE LORRAINE

Spécialité : Génie des Procédés, des Produits et des Molécules

Par

Thomas DI PIETRO

Approche multi-échelle pour la modélisation de fluides de travail des procédés de revalorisation de la chaleur fatale

Le 25 Novembre 2022

Devant la commission d'examen composée de :

Présidente :	Mme Christelle GOUTAUDIER	Professeure, Université Claude Bernard Lyon 1, Villeurbanne
Rapporteurs :	Mme Margarida COSTA GOMES	Directrice de recherche, ENS de Lyon, Lyon
	M. Patrice PARICAUD	Professeur, ENSTA ParisTech, Palaiseau
Examinateurs :	M. Baptiste BOUILLOT	Maître de conférences, Ecole des Mines de Saint-Etienne, Saint-Etienne
	M. Fabrice MUTELET	Maître de conférences, Université de Lorraine, Nancy *Directeur de thèse*
	Mme Laëtitia CESARI	Maîtresse de conférences, Université de Lorraine, Nancy *Directrice de thèse*

Remerciements

Avant toute chose, je tiens à adresser mes sincères remerciements à Laurent FALK, directeur du Laboratoire Réactions et Génie des Procédés pour son accueil.

Envers Fabrice MUTELET mon directeur de thèse, pour le soutien, l'humour et les connaissances scientifiques : j'ai une profonde gratitude. L'expérience accumulée pendant ces trois années ainsi que les opportunités d'encadrement offertes grâce à lui me seront incontestablement précieuses.

Ma co-directrice de thèse Laëtitia CESARI a toujours su apporter une excellente complémentarité scientifique et humaine et a toujours répondu présente dans les moments difficiles comme les moments de célébrations. Je la remercie donc de tout cœur.

J'ai une profonde reconnaissance envers Christelle GOUTAUDIER pour avoir accepté d'endosser le rôle de présidente du jury et l'avoir fait avec énergie et bonté. Un remerciement particulier à Margarida COSTA GOMES et Patrice PARICAUD, rapporteurs de ce travail, pour leur examen attentif, constructif et pertinent, et les discussions enrichissantes sur la réalité expérimentale et la modélisation des pompes à chaleur qui en ont découlé. Un grand merci également à Baptiste BOUILLOT pour ses remarques très judicieuses.

Aux membres du comité de suivi Nicolas BROSSE et Christophe NICOLAS, qui par deux fois m'ont écouté et conseillé avec bienveillance au regard de ce projet de recherche, j'adresse mes plus sincères remerciements.

Je tiens à chaleureusement remercier les personnes qui m'ont donné accès sans hésitation à leur matériel informatique. Jean-Noël JAUBERT, Mohammed BOUROUKBA et Cindy TRINH, je vous dois une fière chandelle.

J'ai une pensée affectueuse envers mes collègues de l'IUT de Nancy-Brabois pour leur soutien depuis trois ans. Un remerciement particulier à Dominique ALONSO pour sa présence jusqu'au bout.

Je remercie de tout cœur toutes les personnes qui m'ont soutenu par leur présence ou en pensées en ce jour si particulier. Un mot pour les membres du couloir de l'équipe ThermE passés et présents, Jean-Noël, Romain, Silvia, Dominique, Mohammed, Roland, Andrès, Nicolas, Aghilas, Aya, Francisco, Konstantin, Fatima, Amine et Camille. Je suis ravi d'avoir partagé tous ces moments avec vous. J'ai eu la chance de rencontrer de nombreuses personnes sur le site du laboratoire et d'avoir notamment bénéficié du soutien et de l'amitié des personnes suivantes : Manon, P.A., Eya, Momo, Saad, Nabil, Rémi, Matteo, Stéphanie, Cristian, Iliàs, Flora, Laurène, Paul, Hao et Pan. Petite dédicace à Pierre-Alann. Liloo, Bubulle & Co et toi êtes toujours les bienvenus à la maison.

Un mot pour mes amis et camarades de promo que j'ai eu la joie d'appeler collègues doctorants et membres de la pandemic party. Dr. Alexis, pour tous les repas passés en ta compagnie et les discussions sur tout sujet. Je te souhaite d'apprécier un jour la supériorité de la pétanque sur le Mölkky. Madame Fátima, avec qui j'ai partagé les derniers moments de difficulté avant la délivrance. Je ne me lasse pas de partager musiques et films avec toi et je te suis très reconnaissant. Cindy-sensei, ta gentillesse et ta douceur font de toi une amie précieuse et une alliée de choix quand il s'agit de jeux de société. Je te souhaite toute la motivation et l'envie nécessaire pour mener à bien ton projet avec fierté, force et courage.

Enfin, c'est avec l'émotion la plus vive que je remercie ma famille. Les plus grands encouragements proviennent sans aucun doute de mes parents, prêts à tout pour ma réussite. C'est une chose de le savoir, c'en est une autre de le vivre. Je puise de la force dans l'assistance que vous me portez sans faille. Je ne le dis jamais assez : merci.

Table des matières

Liste des figures

Liste des Tableaux

Liste des tableaux

Introduction générale

Introduction générale

La gestion des énergies est un levier économique et écologique au cœur des discussions et débats depuis maintenant de nombreuses années. Les Conferences of the Parties (COP) successives sur les actions pour le climat ou les nombreuses conférences nationales ou internationales sur la gestion des ressources et des consommations énergétiques fixent des objectifs de plus en plus exigeants : abandon des énergies fossiles, financement de solutions de remplacement et transition vers des énergies et des économies moins carbonées. Le but est de limiter la production des gaz à effets de serre et ainsi de lutter contre le réchauffement climatique. Dans la conjoncture actuelle, également impactée par les conflits internationaux, le coût des énergies sans cesse croissant est une difficulté majeure et quotidienne pour les industries comme pour les particuliers. Une maîtrise de l'énergie passant par une utilisation et une réutilisation plus efficace devient dès lors une clef de succès et de longévité.

Dans ce contexte d'économie et de revalorisation des énergies, des pertes conséquentes de chaleur sont observées sur les sites industriels. Ainsi, fours, rejets de fumées et autres sources d'effluents thermiques émettent une chaleur résiduaire évaluée à environ 109.5 TWh par an en France en 2017 d'après l'Agence de l'Environnement et de la Maîtrise de l'Energie (ADEME) et le Centre d'Etudes et de Recherches Economiques sur l'éNergie (CEREN). Cette chaleur produite mais non utilisée dans sa totalité, appelée chaleur fatale, est souvent libérée à proximité d'un site ou d'une ligne de procédés consommateurs de chaleur. Le pas qui reste à faire pour revaloriser la chaleur fatale peut être franchi à l'aide de pompes à chaleur à absorption (PACA) de type II, appelées aussi thermo-transformateurs à absorption. Cette technologie permet d'obtenir à partir de chaleur fatale (température moyenne, 60 - 80 °C, chaleur de moyen à bas niveau) de la chaleur plus utile énergétiquement (température > 100 °C). Néanmoins, les fluides de travail traditionnels que sont les mélanges bromure de lithium/eau et eau/ammoniac comportent des inconvénients qui limitent une mise en place plus répandue de ces installations

dans l'industrie. Parmi ces inconvénients figurent les risques de corrosion et de cristallisation pour le premier mélange et une certaine toxicité ainsi que le besoin d'ajouter une étape de distillation pour le second. En remplacement, les liquides ioniques (LIs ou Ionic Liquids, ILs) ont été envisagés au début des années 2000. Plus récemment, ce sont les solvants eutectiques profonds (SEPs ou Deep Eutectic Solvents, DESs) mélangés à de l'eau qui ont attiré l'attention de la communauté scientifique. Il existe toutefois un nombre infini de mélanges de travail qui comportent des LIs et/ou des SEPs. Mesurer les propriétés de tous les LIs/SEPs purs et de leurs mélanges avec d'autres composés afin de choisir les plus adaptés à la technologie PACA n'étant pas concevable, une approche par modélisation est envisagée.

Ce travail de recherche a pour objectif de proposer un outil de modélisation prédictif qui permette de présélectionner des fluides aux performances intéressantes avec les thermo-transformateurs avant une éventuelle application expérimentale. Une approche multi-échelle sera employée. Le premier axe de réflexion explorera les interactions moléculaires au sein de solvants eutectiques profonds au moyen de la chimie quantique. Ces informations seront fournies à un modèle thermodynamique suffisamment robuste pour représenter les propriétés physico-chimiques et thermodynamiques de ces solvants. Enfin, l'intégration de ce modèle thermodynamique dans un logiciel de simulation de procédés permettra d'évaluer à l'échelle industrielle les performances de ces fluides dans les pompes à chaleur à absorption et de proposer des mélanges adaptés en fonction des performances et des caractéristiques de la pompe.

Dans une première partie, une description du fonctionnement des pompes à chaleur à absorption ainsi que des informations générales sur les solvants eutectiques profonds et leur modélisation seront données.

Le deuxième chapitre de ce rapport sera consacré à l'influence de molécules d'eau sur les conformations et les interactions au sein de deux solvants eutectiques profonds composés

de chlorure de choline et de phénol et de chlorure de choline et d'acide glycolique. Pour cela, une méthode de calcul quantique utilisant la théorie de la fonctionnelle de la densité (DFT pour density functional theory) sera utilisée.

Ensuite, un modèle thermodynamique basé sur l'approche COSMO (COnductor-like Screening Model) exploitera des informations issues de la DFT ainsi que de la thermodynamique statistique afin de prédire les équilibres de phases se produisant dans les mélanges comportant des solvants eutectiques profonds. Une modification du modèle pour prendre en compte les liaisons hydrogène entre d'une part les molécules d'eau ou les groupes hydroxyles et d'autre part les atomes de chlore et de brome sera également présentée.

Une quatrième partie permettra au moyen de bases de données de propriétés physico-chimiques (masse volumique, capacité thermique) de développer des modèles de contributions de groupes pour les solvants eutectiques profonds afin de compléter les informations nécessaires à la modélisation du procédé de pompe à chaleur.

Enfin, les différents modèles présentés précédemment seront intégrés à un code de thermotransformateur à absorption afin de simuler les propriétés de multiples fluides constitués de solvants eutectiques profonds et d'eau. Il sera alors possible de se servir de cet outil prédictif afin d'estimer les performances de fluides de travail constitués de solvants eutectiques profonds et d'eau dans des PACA de type II.

Chapitre 1

Généralités - Introduction aux thermotransformateurs à absorption et aux solvants eutectiques profonds

Life is so uncertain - Eat dessert first.

-- Gaussian software quote

Chapitre 1 : Généralités - Introduction aux thermotransformateurs à absorption et aux solvants eutectiques profonds

1.1 Cadre de l'étude - Revalorisation de la chaleur fatale

La chaleur fatale correspond à une énergie thermique produite par des procédés industriels mais qui ne peut être utilisée dans sa totalité et dont la partie restante est fatalement perdue et rejetée. D'après une étude de l'Agence de l'Environnement et de la Maîtrise de l'Energie (ADEME) [1], on distingue trois types de rejets :

- Les rejets liquides, tels que les eaux usées, les eaux de refroidissement, les eaux de lavage, les purges et les condensats de vapeur,

- Les rejets gazeux comme l'air de conditionnement, l'air de séchage, l'air sortant de compresseurs, l'air de refroidissement, les buées et les vapeurs de procédés (gaz de combustion, etc…),

- Les rejets diffus, du fait d'un défaut d'isolation, du refroidissement naturel des produits et de la chaleur rayonnée (four, réaction exothermique, etc…).

Ainsi, 109.5 TWh de chaleur seraient « parties en fumée » en France métropolitaine en 2017 [1]. Par comparaison, un rapport de l'Institut National de la Statistique et des Etudes Economiques (INSEE) estime que la consommation brute d'énergie des grands secteurs de l'industrie en 2017 en France s'élève à environ 435 TWh (valeur convertie depuis des milliers de tonnes d'équivalent pétrole, hors industrie de l'énergie et de l'artisanat) [2]. D'après l'ADEME [1], l'industrie est en troisième position des secteurs les plus consommateurs d'énergie après le secteur résidentiel et celui des transports. La **Figure 1.1** détaille au sein de l'industrie les secteurs d'activités qui consomment le plus, avec en tête le domaine de la chimie et des plastiques, suivie de l'agro-alimentaire et de la sidérurgie. En comparaison, la **Figure 1.2**

donne l'origine des rejets de chaleur fatale par secteur, avec plus de 50 % des rejets qui sont issus de l'industrie agro-alimentaire et du secteur de la chimie et des plastiques.

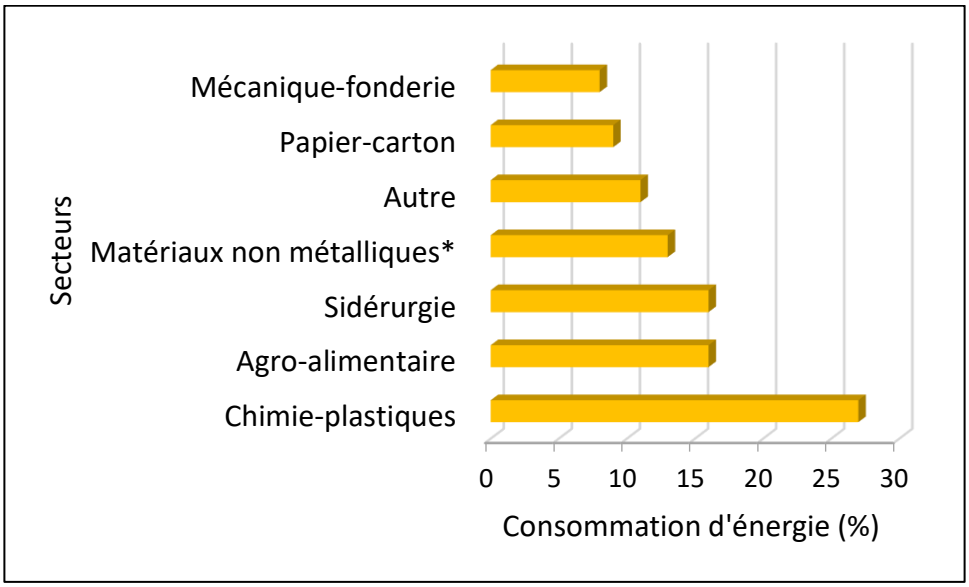

Figure 1.1. Pourcentage de la consommation d'énergie par secteur d'activité de l'industrie [1]
* Ciment, verre, tuile et brique

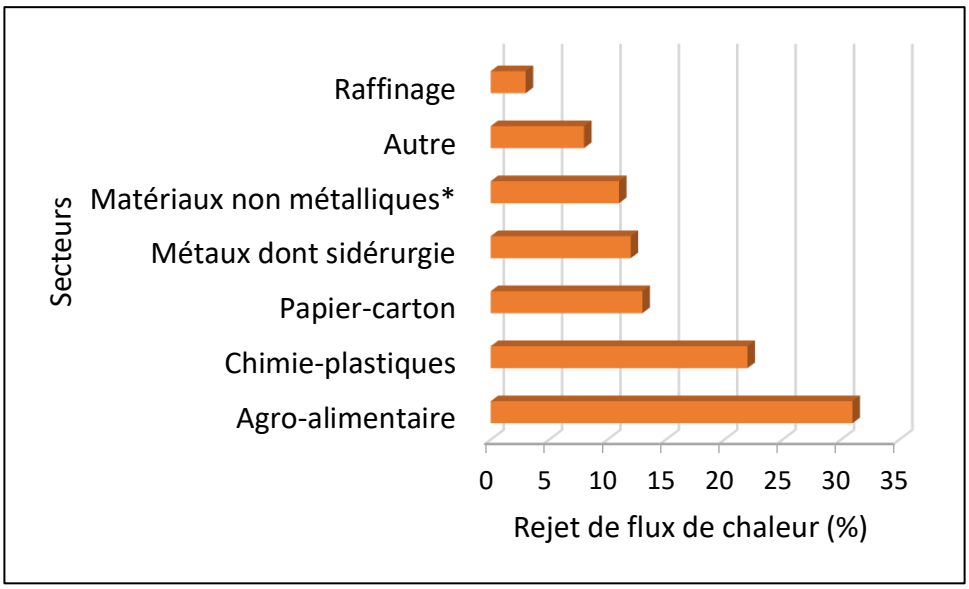

Figure 1.2. Pourcentage des rejets totaux de chaleur fatale par secteur d'activité industriel en France métropolitaine [1]

Pour les industries, les enjeux sont une réduction des émissions de gaz à effet de serre ainsi qu'un gain économique et donc une meilleure compétitivité. Notamment, ces rejets peuvent induire un double coût, par leur production d'une part, et par la nécessité de les refroidir

pour des raisons techniques ou dans le cadre de la réglementation des rejets à l'environnement d'autre part. Il y a donc d'autant plus intérêt à les revaloriser. Deux voies de récupération de la chaleur fatale sont envisageables. Une première approche consiste à permettre à des entreprises ou des territoires de récupérer la chaleur fatale afin de l'utiliser pour le chauffage des collectivités. Cette option nécessite la construction d'un réseau énergétique. Autre alternative, l'industrie source des rejets les réutilise en interne comme source de chaleur dans la même ligne de production ou au sein d'une autre ligne de production. Trois critères permettent d'identifier les rejets les plus facilement valorisables :

- Les rejets issus des procédés les plus énergivores, par exemple les fours, les séchoirs ou les chaudières,
- Les rejets les plus accessibles, par exemple les fumées ou les buées,
- Les rejets aux niveaux de température les plus hauts.

Une émission respectant ces trois critères est d'autant plus facile à utiliser directement. Toutefois, les rejets aux niveaux de température les plus faibles restent les plus abondants. Plus en détail, la **Figure 1.3** montre la répartition des sources de chaleur fatale selon l'échelle de température en France métropolitaine.

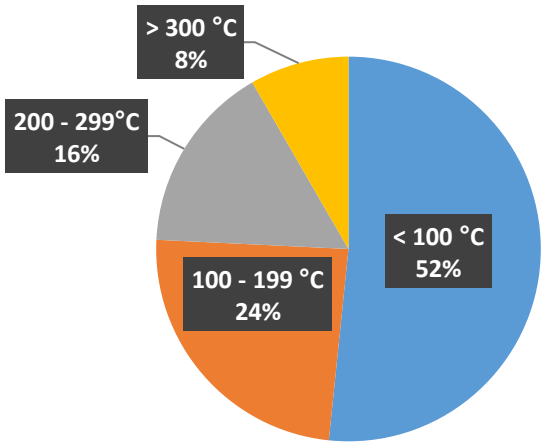

Figure 1.3. Gammes de température des sources de chaleur fatale à l'échelle de la France métropolitaine [1]

Les rejets aux températures inférieures à 100 °C représentent ainsi 52 % du gisement potentiel de chaleur fatale, soit 56.54 TWh. Ils correspondent principalement aux industries de la chimie, de l'agro-alimentaire et du papier-carton. Les rejets dont les températures dépassent les 100 °C correspondent quant à eux plutôt aux industries des métaux et des matériaux non métalliques et notamment aux gaz de combustion. Pour valoriser les rejets aux températures les plus faibles, il est nécessaire de recourir au préalable à une élévation du niveau thermique, en d'autres termes, d'élever la température du flux de chaleur au-dessus de 100 °C.

Les pompes à chaleur à absorption (PACA) de type II sont capables d'élever la température de sources de chaleur très variées, dont les énergies renouvelables comme la géothermie. Elles sont donc une solution intéressante pour les entreprises. Ainsi, Cudok et al. ont recensé un total de 48 installations de PACA de type II sur 43 sites industriels dans le monde entre 1981 et 2019 [3]. La **Figure 1.4** indique dans quels secteurs se répartissent ces installations.

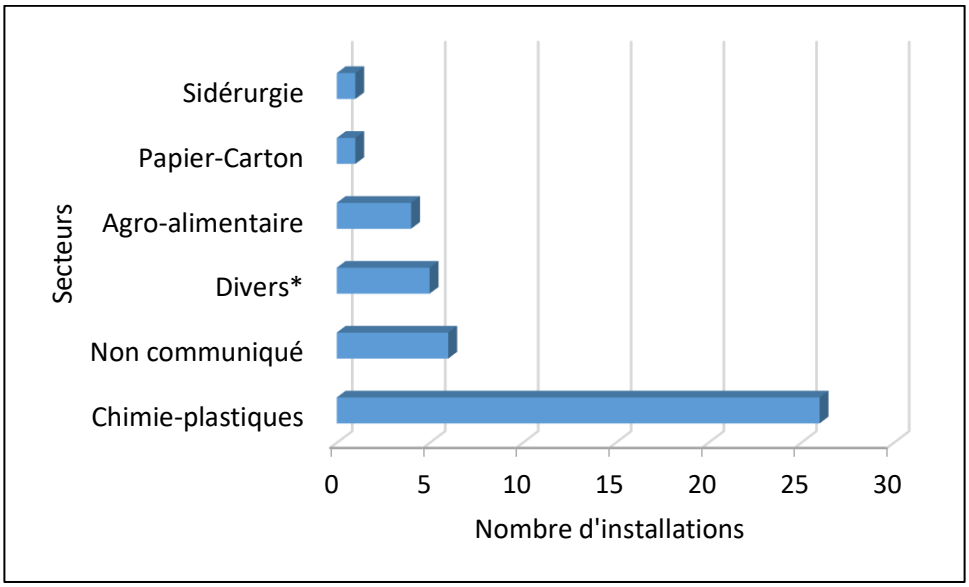

Figure 1.4. Secteur d'activité qui ont bénéficié de l'installation d'une pompe à chaleur à absorption de type II entre 1981 et 2019 [3]
*Eau chaude, incinération de déchets

Environ 60 % des installations ont eu lieu dans des entreprises du secteur de la chimie et des plastiques. Du point de vue de la production d'énergie, Cudok et al. font état de capacités entre 450 kW et 42.17 MW pour des machines installées entre 2013 et 2019 [3].

C'est donc à cette technologie que nous allons nous intéresser.

1.2 Les pompes à chaleur à absorption (PACA)

Une pompe à chaleur est une machine thermique qui permet le transfert de chaleur d'une source à basse température vers un puits à une température plus élevée. Le sens de ce transfert thermique n'est pas naturel et nécessite un apport d'énergie sous la forme de chaleur dans le cas des pompes à chaleur à absorption. On distingue deux types de PACA.

1.2.1 Principe de fonctionnement de la PACA de type I

Une pompe à chaleur à absorption fonctionne à l'aide d'un fluide de travail constitué du mélange d'un composé volatil, le réfrigérant, et d'un composé lourd, l'absorbant. Le réfrigérant représente le composé clef, de sorte que les notions de richesse et de pauvreté se rapportent à la concentration en réfrigérant dans les différents flux de matière. La première étape d'un procédé de PACA de type I (voir **Figure 1.5**) consiste à séparer les constituants du fluide de travail dans le générateur (aussi appelé désorbeur) à l'aide de chaleur reçue d'une source à haute température, et ce à haute pression. Par évaporation du réfrigérant, une vapeur riche et un liquide pauvre sont ainsi obtenus. La vapeur riche est envoyée au condenseur où de la chaleur est libérée vers un puits à moyenne température lors de la condensation de la vapeur à haute pression. Le liquide riche obtenu est détendu avant de rejoindre à basse pression un évaporateur. Le liquide reçoit alors de l'énergie d'une source à basse température afin d'être évaporé et d'atteindre, toujours à basse pression, l'absorbeur sous forme de vapeur. Dans l'absorbeur, le liquide pauvre issu du générateur absorbe la vapeur riche obtenue à l'évaporateur, ce qui libère de la chaleur vers un puits à moyenne température et produit un mélange liquide riche. Celui-ci est pompé vers le générateur en vue de subir un nouveau cycle. L'ensemble générateur +

condenseur représente ainsi un séparateur à haute pression tandis que l'association évaporateur + absorbeur forme un mélangeur basse pression. Dans cette étude, trois températures différentes seront considérées, la température du condenseur et de l'absorbeur étant égales, dans un cycle dit tritherme.

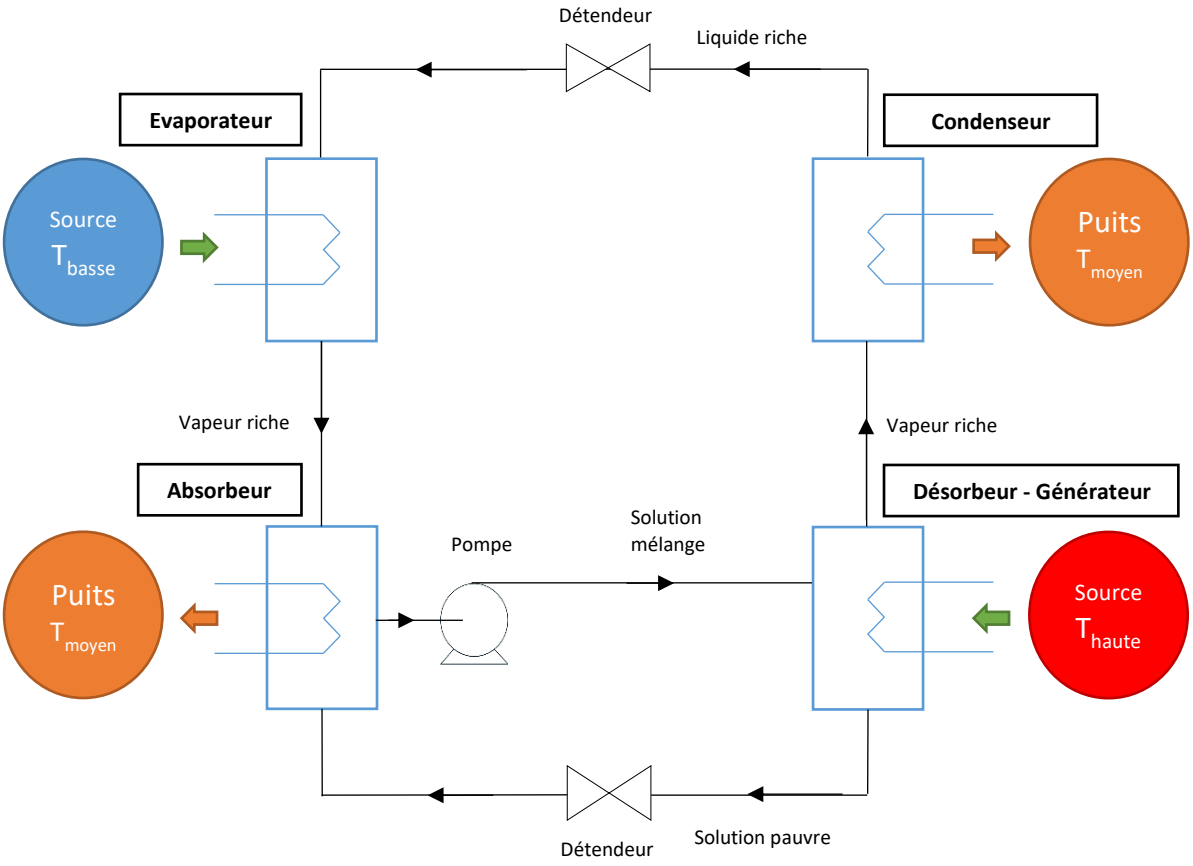

Figure 1.5. Schéma de présentation du procédé de pompe à chaleur à absorption de type I

On dénombre trois types d'applications des PACA de type I :

- Frigopompe est le nom donné aux pompes utilisées dans la production de froid,
- Thermopompe est celui donné aux pompes dont l'objectif est de produire un flux de chaleur chaud,
- Thermofrigopompe concerne les pompes dédiées à la production simultanée de chaud et de froid.

Ces trois modes de fonctionnement sont présentés dans la **Figure 1.6**.

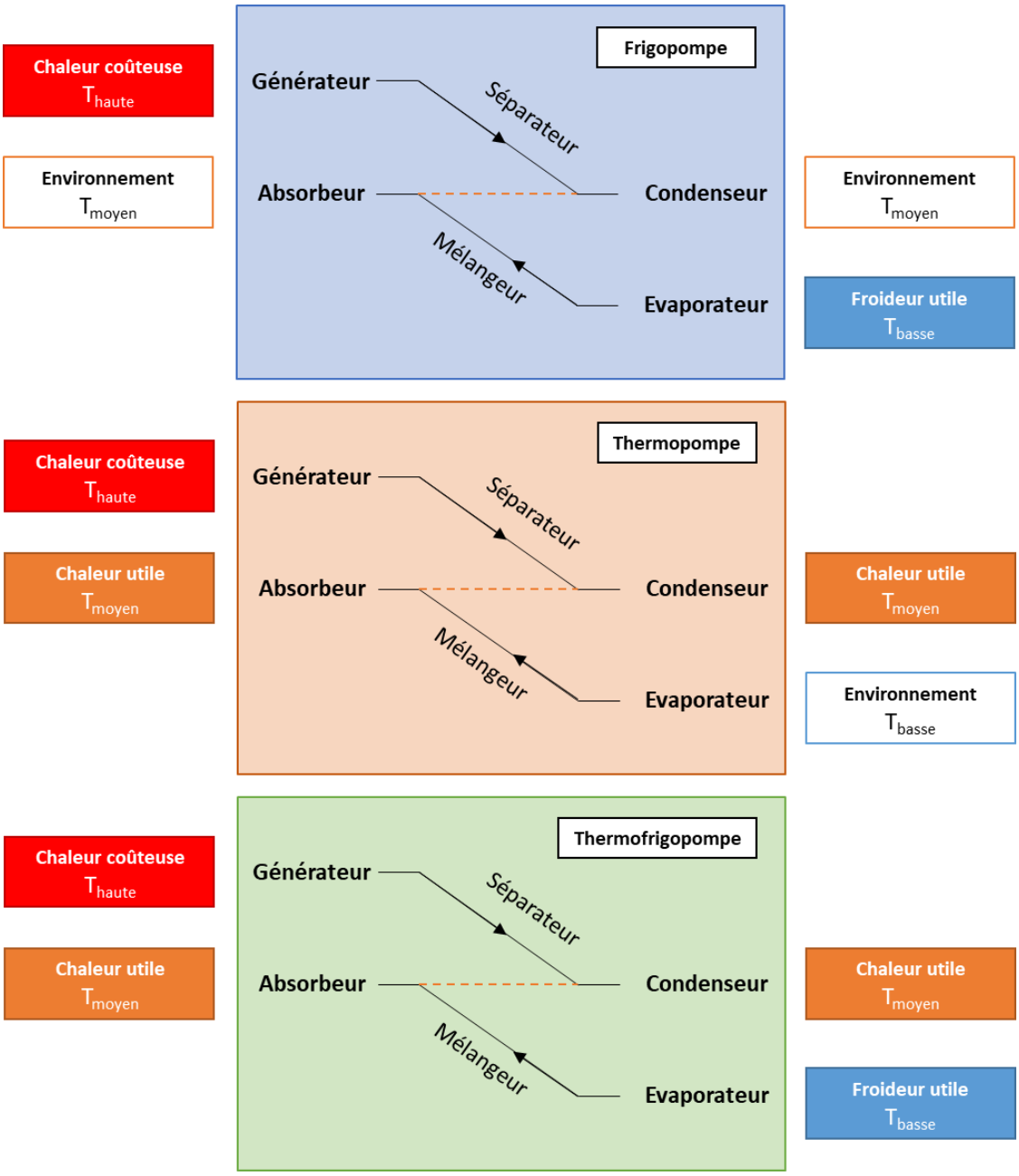

Figure 1.6. Différents modes de fonctionnement des PACA de type I [4]

1.2.2 Inversion du cycle - PACA de type II

Une PACA de type II possède un fonctionnement similaire à celui d'une PACA de type I, notamment au regard des sources et des puits de chaleur qui vont respectivement fournir de l'énergie à l'évaporateur et au générateur et recevoir de l'énergie du condenseur et de l'absorbeur qu'il s'agisse d'une pompe de type I ou II. Cependant, les niveaux de température

et de pression diffèrent, de sorte que le cycle est dit inversé. Un schéma permettant de présenter le fonctionnement d'une PACA de type II est donné en **Figure 1.7**.

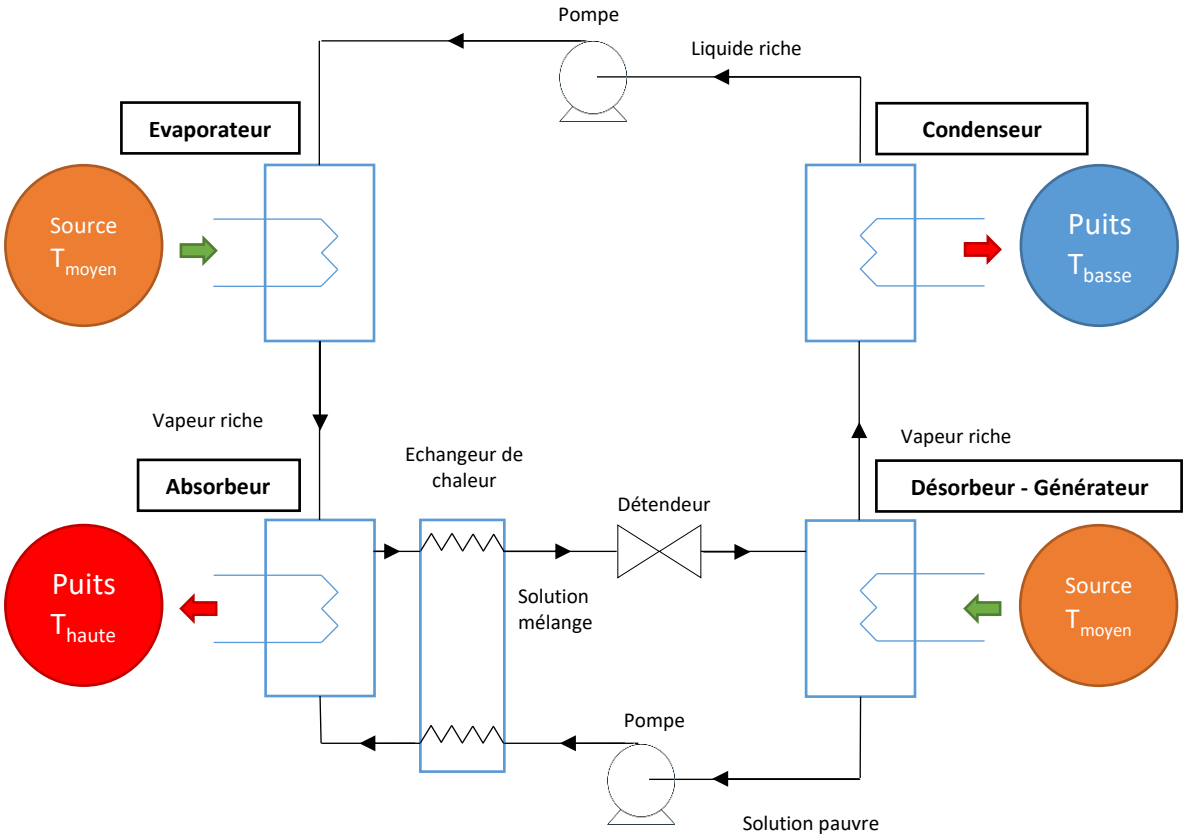

Figure 1.7. Schéma de présentation d'une pompe à chaleur à absorption de type II

Dans le générateur, le mélange de travail est chauffé à basse pression par une source de chaleur à moyen niveau. Une vapeur riche est séparée d'une solution pauvre et envoyée dans un condenseur où elle se retrouvera sous forme de liquide riche après avoir libérée de la chaleur transmise à un puits à basse température. Une fois pompé et amené à haute pression, le liquide riche rejoint l'évaporateur où il recevra de la chaleur provenant d'une source à moyenne température et sera évaporé. Sous forme de vapeur riche, le fluide atteint l'absorbeur où la vapeur est absorbée par le liquide pauvre provenant du générateur. Le phénomène d'absorption libère de la chaleur vers un puits à haute température. Le mélange liquide résultant est ensuite détendu et amené vers le générateur. Un échangeur de chaleur peut également être ajouté entre le générateur et l'absorbeur afin que le mélange issu de l'absorbeur réchauffe en partie le liquide

pauvre juste avant qu'il n'atteigne l'absorbeur. Ceci améliore le rendement du phénomène d'absorption.

Contrairement à une PACA de type I, le mélangeur (évaporateur + absorbeur) d'un thermotransformateur fonctionne à haute pression et le séparateur (générateur + condenseur) fonctionne quant à lui à basse pression. Les différents niveaux de température et de pression sont rappelés dans la **Figure 1.8**. Ce mode de fonctionnement permet ainsi de valoriser des flux de chaleur à moyenne température comme la chaleur fatale et d'obtenir des flux à un niveau thermique plus élevé. Les PACA de type II sont également appelées thermotransformateurs à absorption.

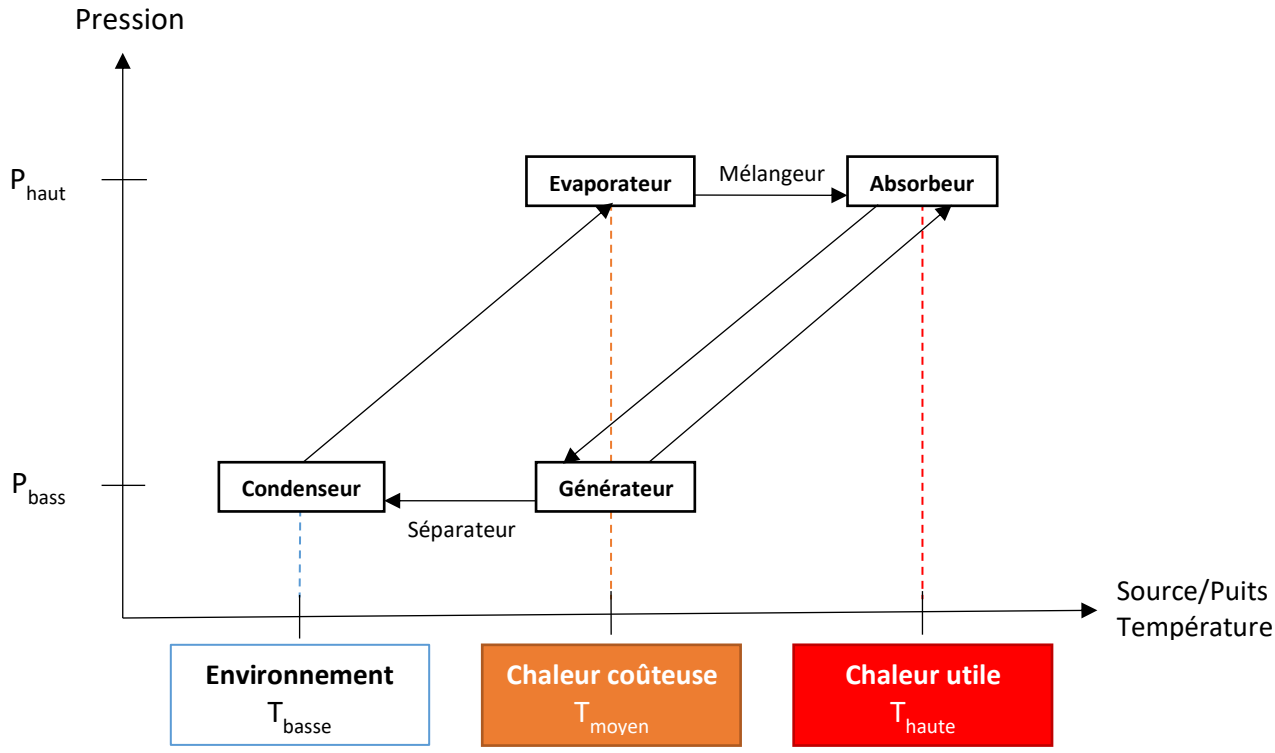

Figure 1.8. Niveaux de température et de pression des différents constituants d'une PACA de type II

1.2.3 Fluides de travail traditionnels

Le bon fonctionnement ainsi que les performances d'une pompe à chaleur sont directement liés au fluide de travail utilisé. Les propriétés idéales pour le réfrigérant et l'absorbant qui composent le fluide de travail sont désormais bien connues [5], [6]. Celles-ci sont présentées dans le **Tableau 1.1**.

Tableau 1.1. Propriétés du réfrigérant et de l'absorbant idéalement recherchées

Composé	Propriété visée	Objectif
Réfrigérant	Haute enthalpie d'évaporation	Débit de réfrigérant plus faible
	Pression de vapeur réduite en présence de l'absorbant	Pression de travail modérée et coûts d'investissement réduits
	Température critique élevée	Plage étendue de températures de travail
	Faible capacité thermique	Plus grande fraction de chaleur utile à l'évaporation
Absorbant	Grande capacité d'absorption du réfrigérant	Absorption possible et efficace à l'absorbeur
Absorbant et réfrigérant	Miscibilité parfaite	Absence de phases dans le procédé
	Points d'ébullition très différents	Séparation aisée à l'évaporateur
	Conductivité thermique élevée	Transferts de chaleur améliorés
	Stabilité thermique et chimique	Durée de vie étendue du fluide de travail
	Ininflammables, faibles corrosivité et toxicité	Sécurité et durée de vie étendue du procédé
	Faible coût et grande accessibilité	Coûts d'investissement réduits
	Faible viscosité	Pertes de charge réduites

Les PACA fonctionnent traditionnellement avec les couples réfrigérant/absorbant suivants : eau/bromure de lithium (LiBr) et ammoniac (NH_3)/eau [7]. Dans le cas du couple eau/LiBr, l'eau possède une haute enthalpie d'évaporation et constitue l'un des solvants les moins chers et les moins dangereux à utiliser. Les températures de travail mènent cependant à des pressions de vapeurs inférieures à la pression atmosphérique et il faut donc faire attention

aux infiltrations d'air. Le bromure de lithium est soluble dans l'eau (1667 $g.L^{-1}$ à 20 °C) sans pour autant être volatil, de sorte qu'une large plage de température peut être utilisée, et ce sans risque de retrouver LiBr en phase vapeur. De plus, le mélange est très stable. Toutefois, l'utilisation du couple eau/LiBr s'accompagne de risques de cristallisation [3], [8] qui peuvent mener à l'obstruction des tuyaux dès que la concentration en LiBr est élevée. Ceci est d'autant plus vrai dans le cas des frigopompes qui fonctionnent à basses températures. Les solutions aqueuses de bromure de lithium sont également très corrosives pour de nombreux matériaux, et en particulier à haute température [3]. Ceci est souvent responsable de la durée de vie limitée du procédé. Ces inconvénients ont conduit au développement de nombreux inhibiteurs de corrosion et de cristallisation [3], [8]. On retrouve ainsi le chromate de lithium (Li_2CrO_4) et le molybdate de lithium (Li_2MoO_4) [3]. Le premier est un inhibiteur efficace de corrosion bien que toxique et coûteux à gérer vis-à-vis des normes de sécurité. De plus, il n'empêche pas les problèmes de corrosion par piqûres. Comparé au chromate de lithium, le molybdate de lithium est efficace contre la corrosion par piqûres et n'est pas toxique. Il requiert néanmoins un prétraitement afin que la solution soit bien mélangée du fait de sa faible solubilité. Du point de vue de la cristallisation, Ring et al. ont étudié l'effet de 27 inhibiteurs sur des solutions aqueuses de LiBr (concentrée à 60 % en masse) [9], réduisant au maximum la température de cristallisation de 13 °C. Certains de ces inhibiteurs comme l'acide méthylène diphosphonique (MDPA) ou l'acide 1-hydroxyéthylidène-1,1-diphosphonique (HEDP) ont ensuite été testés avec des solutions utilisées dans l'industrie afin de vérifier leur efficacité et valider leur stabilité thermique [10]. Bien évidemment, ces additifs représentent un coût supplémentaire.

Le second couple de travail évoqué précédemment utilise cette fois l'eau en tant qu'absorbant. Celle-ci a une très bonne capacité d'absorption de l'ammoniac en phase gaz (bonne affinité), et la chaleur latente de l'ammoniac est élevée [7]. Les deux composés sont très stables et ils sont également compatibles avec la plupart des matériaux, à l'exception du cuivre

et de ses alliages. L'utilisation de l'ammoniac n'est cependant pas exempte de défauts. La volatilité de l'eau fait que les vapeurs d'ammoniac entrainent également une certaine quantité d'eau en sortie du générateur. La séparation de l'eau et de l'ammoniac nécessite une étape de distillation supplémentaire, ce qui augmente les coûts et la complexité de l'installation. Enfin, les pressions de travail sont plus élevées, ce qui augmente les coûts de pompage. De plus, la gestion de l'ammoniac à haute pression est plus exigeante du point de vue sécurité car il est toxique et inflammable.

Tous ces inconvénients limitent le développement de la technologie des PACA dans l'industrie et il y a donc beaucoup d'avantages à trouver des remplacements pour ces mélanges de travail. Ce rapport s'inscrit dans un cadre de recherche ayant pour objectif d'utiliser de nouveaux fluides de travail, notamment les solvants eutectiques profonds comme absorbants dans des mélanges de travail avec de l'eau.

1.3 Solvants eutectiques profonds dans les fluides de travail

1.3.1 Avant les solvants eutectiques profonds, les liquides ioniques

De nombreuses pistes ont été suivies pour tenter de remplacer les fluides de travail traditionnels dans les cycles à absorption [5], [11], [12]. Parmi elles, les liquides ioniques (LIs, ou ILs pour ionic liquids) sont apparus très prometteurs grâce à leurs propriétés. Ceux-ci sont constitués d'un anion et d'un cation dont les combinaisons quasi infinies offrent une grande liberté quant à l'ajustement des propriétés du mélange [13], [14]. Très stables thermiquement et chimiquement, ils ont également une pression de vapeur saturante considérée comme négligeable. De nombreuses études ont porté sur l'utilisation des LIs en tant qu'absorbants dans des procédés de PACA. Dans le cas particulier des thermotransformateurs, les performances des couples suivants ont été simulées et comparées à celles de mélanges de travail plus classiques :

- Eau/1-ethyl-3-méthylimidazolium diméthylphosphate ([EMIM][DMP]) [15]
- 2,2,2-Trifluoroéthanol (TFE) couplé soit au 1-éthyl-3-méthylimidazolium tétrafluoroborate ([EMIM][BF_4]) soit au 1-butyl-3-méthylimidazolium tétrafluoroborate ([BMIM][BF_4]) [16],
- Eau/1,3-diméthylimidazolium méthylsulfate ([MMIM][$MeSO_4$]) et eau/[EMIM][$MeSO_4$]) [17],
- Eau/1,3-diméthylimidazolium diméthylphosphate [MMIM][DMP] et méthanol/[MMIM][DMP] [18],
- Eau/1-éthyl-3-méthylimidazolium méthanesulfonate ([EMIM][OMs]) [19].

Parmi ces LI, quelques exemples sont illustrés **Tableau 1.2**.

Tableau 1.2. Exemples de liquides ioniques utilisés dans des simulations de PACA de type II [16], [18]

Nom	1-Ethyl-3-méthylimidazolium tétrafluoroborate	1,3-Diméthylimidazolium diméthylphosphate
Abréviation	[EMIM][BF_4]	[MMIM][DMP]
Représentation 2D	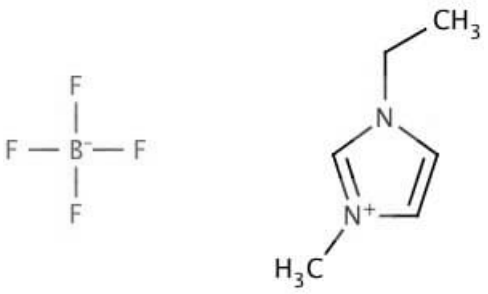	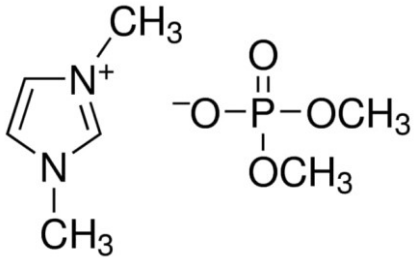

Ces études concluent que les performances de ces mélanges sont proches de celles des couples traditionnels et en font des pistes prometteuses. Toutefois, le coût et la toxicité potentielle de ces solvants mirent un frein à leur utilisation [20], [21].

1.3.2 Présentation des solvants eutectiques profonds

Les solvants eutectiques profonds (SEPs, ou DESs pour deep eutectic solvents) sont apparus comme les héritiers potentiels des liquides ioniques. Les SEPs furent décrits pour la première fois par Abbot et al. en 2003 avec un solvant constitué de chlorure de choline et d'urée [22], avant que le nom de SEP n'apparaisse ensuite en 2004 dans une étude sur des solvants constitués de chlorure de choline et d'acides carboxyliques [23]. Les SEPs sont formés par l'association d'au moins deux molécules avec un donneur et un accepteur de liaisons hydrogène [24]. Ils sont souvent formés avec des ions ammonium quaternaires, des alcools, des acides carboxyliques ou des amides. Si le SEP contient un ammonium, le contre ion associé œuvrera en tant qu'accepteur de liaison hydrogène, tandis que les alcools et les acides carboxyliques sont donneurs d'hydrogène via leur groupe hydroxyle. Néanmoins, de multiples liaisons peuvent être créées, de sorte qu'un composé peut à la fois prendre le rôle de donneur et d'accepteur de liaisons hydrogène. Ainsi, le chlorure de choline (voir **Tableau 1.3**) peut à la fois accepter des liaisons hydrogène via l'ion chlorure et donner un hydrogène via son groupement hydroxyle. Une catégorie de SEPs composés de constituants naturels est appelée NADES (Natural Deep Eutectic Solvent) [24]. Elle comporte des SEPs dont les constituants sont principalement issus des plantes, comme par exemple des molécules de sucre (glucose, fructose, etc…) ou des acides organiques (acide citrique, acide L-(+)-ascorbique ou vitamine C, etc…). Les SEPs ont donc l'avantage de pouvoir être formés avec des composés dits « verts » et peu coûteux [25], [26].

1.3.2.1 Appellation des solvants eutectiques profonds

Les SEP sont parfois aussi appelés « Low Transition Temperature Mixtures » (LTTM). LTTM et SEP font référence au fait que ces solvants se comportent comme un corps pur et possède une température de fusion propre, inférieure à celle des composés du SEP purs pris séparément. La diminution du point de fusion peut être telle qu'ils deviennent liquides à

température ambiante. La définition de SEP peut parfois porter à confusion et se rapprocher de celle d'un simple mélange eutectique. Martin et al. ont donc insisté sur le terme « profond » en proposant de rajouter comme critère que la nouvelle température de fusion doit également être nettement inférieure à celle du mélange liquide idéal des composés du SEP [27].

Outre la nature des constituants, le ratio entre accepteur et donneur d'hydrogène est capital pour décrire un SEP. Un mélange de composés A et B et de ratio [m:n] contient donc m molécules de A pour n molécules de B. La masse molaire du DES obtenu M_{DES} est une moyenne des masses molaires de A, M_A, et de B, M_B, pondérée par m et n :

$$M_{DES} = \frac{m}{m+n} * M_A + \frac{n}{m+n} M_B \quad (1)$$

Les ratios peuvent être obtenus expérimentalement à l'aide d'un diagramme de phases des constituants du SEP afin de déterminer les concentrations adaptées pour que le solvant soit liquide aux températures de travail. Certains SEP couramment étudiés ont même reçu un nom qui correspond à un rapport de donneur et d'accepteur de liaison H fixé. Des exemples sont donnés dans le **Tableau 1.3**.

Tableau 1.3. Exemple de DES couramment rencontrés dans la littérature

Nom courant	Ethaline	Glyceline	Reline
Constituants et ratios	{Chlorure de choline:Ethylène glycol} [1:2]	{Chlorure de choline:Glycérol} [1:2]	{Chlorure de choline:Urée} [1:2]
Représentation 2D	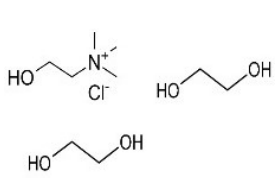	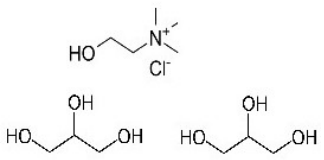	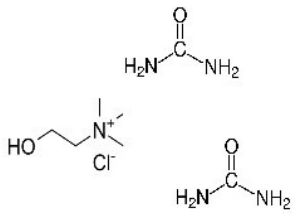

1.3.2.2 Solvants eutectiques profonds dans les pompes à chaleur

A ce jour, il n'existe que peu d'études faisant intervenir les SEP dans des cycles d'absorption. Haghbakhsh et al. ont étudié les performances de fluides de travail composés des SEP présentés dans le **Tableau 1.3** comme absorbant et d'eau comme réfrigérant [28], soulignant les bonnes performances de ces fluides dans les simulations et la nécessité d'étendre la recherche à de nouveaux SEP. Il n'y a aujourd'hui qu'une seule étude sur l'utilisation de SEP au sein de thermotransformateurs à absorption [29]. Les auteurs ont étudié les SEP {Betaine:Ethylene glycol} et {[Choline][Chloride]:Glycerol} en tant qu'absorbants couplés à de l'eau et ont simulé leurs performances. Les auteurs ont ainsi montré que ces deux SEP offraient des résultats concluants qui s'apparentaient à ceux du couple eau/LiBr.

Cependant, les propriétés des SEPs ne sont pas encore toujours bien connues, et des outils de modélisations puissants sont nécessaires afin de pallier le manque de données.

1.4 Approche multi-échelle : modélisation des solvants eutectiques profonds

Du fait de leur multitude, sélectionner des composés parmi tous ceux qui peuvent constituer un SEP n'est pas une tâche triviale. Des outils et modèles thermodynamiques sont cependant disponibles afin de prédire les propriétés des SEP et faciliter le choix du ratio et des constituants qui seront les plus adaptés à l'application visée avant de lancer le travail expérimental. Ces modèles permettent ainsi d'obtenir des informations de l'échelle microscopique (interactions entre les molécules) à l'échelle intermédiaire (propriétés physicochimiques, équilibres de phases) utilisables ensuite dans le cadre d'applications industrielles (échelle macroscopique). Quelques modèles traditionnels appliqués aux SEPs sont présentés dans la suite de ce rapport.

1.4.1 Calculs quantiques

La modélisation moléculaire basée sur la chimie quantique constitue la première étape de l'approche multi-échelle. Elle permet de mieux comprendre les interactions entre les molécules étudiées et de disposer d'informations sur la géométrie et la structure électronique de différentes conformations de molécules, avec entre autres, l'énergie des conformations, les distances et les angles des liaisons ou les spectres infrarouge.

Parmi les méthodes de calculs quantiques, la théorie de la fonctionnelle de la densité (DFT pour density functional theory) est basée sur des fonctions de densité électronique, c'est-à-dire des fonctions qui décrivent la probabilité de trouver un électron dans un élément de volume (aussi appelé orbitale). Le résultat des calculs dépendra à la fois du niveau de théorie (comment sont approximées les fonctions de densité) et de la base choisie (description mathématique des orbitales d'un système : taille, forme et combinaison linéaire des orbitales).

Dans le cas des SEPs, les calculs ont soit pour but de s'intéresser à la structure de SEPs isolés, soit d'analyser leurs interactions en présence d'autres molécules. Zhu et al. ont étudié les conformations stables de SEP formés de chlorure de choline, de glycérol, d'acide acétique et d'urée [30]. Les interactions entre le chlorure de choline et 9 polyols ont été analysées par Wang et al. [31]. Ils ont confirmé que l'interaction principale avait lieu entre l'atome de chlore et l'hydrogène du groupe hydroxyle des polyols et que la force de celle-ci était dépendante du nombre de carbone et de groupe alcool dans les polyols. Zhang et al ont déterminé les structures stables et réalisé des calculs de fréquences pour des complexes comprenant des molécules de choline et des ions de chlorure et de magnésium hydratés [32].

1.4.2 Contributions de groupes

Dans les modèles de contributions de groupes, les molécules sont décomposées en groupes fonctionnels simples. A chacun de ces groupes est attribuée une contribution. La somme des contributions pondérées par le nombre de fois qu'un groupe apparaît dans le

système étudié doit donner la propriété visée.

Des modèles appliqués aux SEPs ont été développés pour les propriétés suivantes : propriétés critiques [33]–[35], masse volumique [33], [34], [36], [37], capacité thermique [36], [38], indice de réfraction [36], vitesse de propagation du son [36] et tension de surface [36].

Les modèles de contributions de groupes sont simples à mettre en place et rapides d'utilisation mais sont fortement dépendants de la base de données utilisée pour ajuster leurs paramètres. Il est souvent avantageux d'effectuer un nouveau paramétrage quand de nouvelles bases plus étendues sont disponibles.

1.4.3 Equations d'état

Les équations d'état (EoS pour equation of state) permettent d'obtenir des informations sur l'état des phases d'un système à partir d'une relation entre les variables de pression (P), de volume (v pour le volume molaire), de température et de quantité de matière.

1.4.3.1 L'équation d'état cubique de Peng-Robinson

L'équation d'état cubique de Peng-Robinson (PR-EoS) a ainsi été utilisée pour prédire la solubilité de gaz dans des SEPs. L'équation est de la forme [39] :

$$P = \frac{RT}{v-b} - \frac{a}{v(v+b)+b(v-b)} \quad (2)$$

Avec R la constante des gaz parfaits, a un paramètre d'attraction et b un paramètre de covolume. Ces deux paramètres dépendent des propriétés critiques des constituants. Dans le cas d'étude de mélange, le paramètre a dépend également de paramètres d'interaction binaires k_{ij} entre le composé i et le composé j qui sont ajustés à l'aide de données expérimentales. Cette équation a ainsi permis d'obtenir les solubilités du CO_2 dans l'éthaline et la réline [39], [40], dans un SEP constitué d'éthylene glycol, d'acide malique et de chlorure de choline [40], dans des SEPs à base d'acide lactique [41], dans 17 SEPs basés sur des ions ammonium et phosphonium [42], et enfin dans des SEPs formés à partir de glycols ou d'amines [43]. Elle a

également été utilisée pour déterminer la solubilité du CH_4 dans l'éthaline et la réline [39].

1.4.3.2 Equations de type SAFT

Les équations de type SAFT (pour Statistical Associating Fluid Theory) forment une famille d'équations qui expriment l'enthalpie libre d'Helmoltz résiduelle A^{res} (différence entre l'énergie totale du système et celle d'un état de référence) à partir de différentes contributions. L'équation originelle SAFT représente les molécules comme des chaînes de sphères dures, une sphère pouvant se rapporter à un atome ou un groupe fonctionnel. L'équation fait intervenir des termes de formation, d'interaction et d'association entre chaînes. A partir de cette équation, d'autres modèles ont été développés.

Dans la version Perturbed-Chain SAFT (PC-SAFT), l'état de référence est un fluide de chaînes de sphères dures de tailles identiques. Interviennent des termes de répulsion des chaînes dures A^{hc}, de dispersion A^{disp} et d'association A^{assoc} :

$$A^{res} = A^{hc} + A^{disp} + A^{assoc} \quad (3)$$

L'utilisation de paramètres d'interaction binaire k_{ij} est également possible dans le cadre de mélanges. Du point de vue du calcul de propriétés de SEP, l'équation PC-SAFT a eu de nombreuses applications. Samarov et al ont prédit des équilibres liquide-liquide faisant intervenir un SEP composé de chlorure de choline et d'acide glutarique [44]. Pontes et al. ont retrouvé les valeurs de masses volimiques et les diagrammes de phases solide-liquide déterminés au préalable expérimentalement [45]. Les coefficients d'activité à dilution infinie de mélanges contenant des SEP à base de chlorure de choline et de glycérol ont été calculés par Verevkin et al. [46]. Dietz et al. ont prédit la solubilité du CO_2 dans 5 SEPs hydrophobes [47].

Néanmoins, la nécessité de paramètres d'interaction dépendants de la température et ajustés à l'aide de données expérimentales limite l'emploi des équations d'état pour les systèmes {eau + SEP} du fait de la faible quantité de données disponibles.

1.4.4 Modèles de coefficient d'activité

Les modèles de coefficient d'activité permettent de déterminer le coefficient d'activité γ_i d'un composé i dans un mélange. Pour cela, ils font intervenir dans leurs équations une contribution résiduelle (ou contribution enthalpique, interactions entre molécules) et une combinaison combinatoire (ou contribution entropique, place que prennent les molécules et désordre généré). Le logarithme népérien du coefficient d'activité s'exprime sous la forme :

$$\ln(\gamma_i) = \ln(\gamma_i^{res}) + \ln\left(\gamma_i^{comb}\right) \quad (4)$$

1.4.4.1 Non-Random Two Liquids NRTL

Le modèle NRTL [48] exprime l'énergie libre de Gibbs g^E d'un mélange binaire sous la forme :

$$\frac{g^E}{RT} = x_1 x_2 \left(\frac{\tau_{21} G_{21}}{x_1 + x_2 G_{21}} + \frac{\tau_{12} G_{12}}{x_2 + x_1 G_{12}}\right) \quad (5)$$

Avec x_i la composition molaire du composé i. Les paramètres G_{ij} et τ_{ij} dépendent des paramètres d'interaction g_{ij} qui sont ajustés à l'aide de données expérimentales :

$$\tau_{ij} = \frac{g_{ij} - g_{jj}}{RT} \quad (6)$$

$$G_{ij} = e^{-\alpha_{ij}\tau_{ij}} \quad (7)$$

Avec α_{ij} un paramètre de dispersion non aléatoire de la solution. Le modèle NRTL a été appliqué pour le calcul d'équilibre liquide-liquide de systèmes impliquant des SEPs {chlorure de choline:acide glutarique} [44], la solubilité de différents gaz dans des SEPs composés de chlorure de choline et d'urée à différents ratios [49], ou encore la représentation de données expérimentales d'enthalpies molaires de mélanges contenant des SEPs constitués du chlorure de choline et de l'urée [50]. L'utilisation du modèle NRTL requiert la connaissance des paramètres d'interaction binaire. A ce jour, il n'existe pas de méthode générale pour calculer ce paramètre et il est très souvent ajustés sur des données expérimentales Ceci limite donc l'utilisation du modèle NRTL dans le cadre des mélanges qui comportent des SEPs.

1.4.4.2 Modèles COSMO (COnductor-like Screening MOdel)

Apparu au début des années 90, le modèle COSMO fut rapidement suivi par le modèle COSMO for Real Solvents dit aussi COSMO-RS [51], [52]. Le principe consiste à plonger une molécule dans un solvant conducteur parfait puis d'effectuer une comparaison avec un solvant réel (écart à l'idéalité). Ces modèles nécessitent en entrée une description des molécules du mélange sous la forme de densités de charge surfaciques σ. Ces densités de charge correspondent à des éléments de surface chargés qui entourent les atomes d'une molécule plongée dans un solvant conducteur. Par exemple, un atome électronégatif aura tendance à s'entourer de charges positives. Ces densités de charge sont obtenues par le biais de calculs de DFT. Les modèles du type COSMO font ainsi le lien entre les calculs quantiques et la thermodynamique statistique pour prédire les contributions combinatoire et résiduelle des coefficients d'activité des molécules dans un mélange et obtenir ensuite les équilibres de phases.

Les seules informations nécessaires sont la structure des molécules étudiées. Ceci en fait un modèle prédictif et théoriquement applicable à tout type de mélange une fois les descripteurs issus de la DFT obtenus. Les modèles COSMO ont donc rapidement gagné en popularité et de nouvelles versions ont vu le jour comme les modèles COSMO Segment Activity Coefficient (COSMO-SAC) en 2002 [53] ou COSMO-RS(Ol) en 2005 [54]. Le modèle COSMO-SAC de 2010 comprend notamment des paramètres dédiés aux liaisons hydrogène formées par des atomes d'oxygène, d'azote et de fluor [55].

Ces modèles ont été appliqués à des mélanges contenant des SEPs. Le modèle COSMO-RS a ainsi été utilisé dans la prédiction de solubilités de gaz dans des SEPs {chlorure de choline:urée} [49] et la prédiction de coefficient de distribution et de sélectivité dans le cadre de l'extraction de terpénoïdes à l'aide de SEPs à base de diols [56]. Le modèle COSMO-SAC a, par exemple, permis de prédire des équilibres liquide-liquide faisant intervenir des alcools et

des SEPs formés d'acide laurique et de menthol [57].

1.4.5 Récapitulatif

Le **Tableau 1.4** reprend les propriétés calculées à l'aide des différents modèles présentés précédemment.

Tableau 1.4. Exemples de propriétés modélisées à l'aide de différents modèles thermodynamiques

Modèle	Exemples de propriétés modélisées	Remarques
Contributions de groupes	Propriétés critiques, masse volumique, capacité thermique, indice de réfraction, vitesse du son, tension de surface	Très faciles à mettre en place, efficacité dépendante de la taille de la banque de données
Equation d'état de Peng-Robinson	Equilibres de phases	Paramètres d'interaction binaires à ajuster sur les données expérimentales
Equations d'état type SAFT	Equilibres de phases	
Coefficient d'activité NRTL	Equilibres de phases, enthalpie de mélange	
Modèles COSMO	Equilibres de phases	Prédictif

Il est bien sûr tout à fait possible de combiner plusieurs méthodes pour obtenir un jeu de propriétés physico-chimiques et représenter un équilibre entre phases. Ainsi, les méthodes de contributions de groupes permettant d'obtenir les propriétés critiques de SEPs ont été utilisées conjointement à l'équation de Rackett, modifiée par Spencer et Danner pour prédire la masse volumique des SEP [34], [35] et l'équation d'état cubique de Peng-Robinson pour la solubilité de gaz dans les SEPs [42], [43]. De même, Ojeda et Llovell se sont servis de COSMO-RS et Soft-SAFT afin de déterminer la solubilité de SO_2 et CO_2 dans des SEP à base d'acide lévulinique et d'éthylène glycol [58].

1.5 Conclusion

De par leur capacité à élever la température de sources de chaleur à bas niveau, les thermotransformateurs à absorption représentent une solution élégante pour la revalorisation de la chaleur fatale. Un des paramètres qui impacte le plus les performances de cette technologie est le fluide de travail. Les mélanges traditionnellement utilisés, eau/LiBr ou ammoniac/eau, comportent des inconvénients qui motivent le développement de nouveaux fluides. Le sujet de ce rapport se concentre ainsi sur l'utilisation de SEP en tant qu'absorbants couplés à de l'eau. Leur multitude et grande diversité font qu'une étude expérimentale exhaustive des propriétés d'un nombre conséquent de SEP serait bien trop coûteuse. De ce fait, une approche théorique multi-échelle est proposée afin de permettre la prédiction des propriétés d'un grand nombre de SEPs sans ajustement de paramètres. Dans un premier temps, le chapitre suivant permettra de présenter des résultats issus du calcul quantique et d'aborder l'échelle moléculaire de cette étude. Il traitera de l'optimisation et de l'analyse de la structure de deux DES seuls et en présence d'eau afin d'étudier la structure de ces systèmes. Un intérêt particulier sera porté aux liaisons hydrogènes. Ensuite, le modèle COSMO-SAC a été choisi afin de prédire les équilibres de phases de systèmes contenant des SEPs à partir de descripteurs moléculaires (échelle microscopique). Une modification de ce modèle sera présentée afin de permettre une meilleure prédiction des équilibres liquide-vapeur de systèmes eau/SEP. De plus, des modèles de contributions de groupes seront mis en place afin de calculer les masses volumiques et les capacités thermiques de SEPs (échelle intermédiaire). L'utilisation du modèle COSMO-SAC modifié couplé aux méthodes de contributions de groupes permettra de modéliser le fonctionnement d'un thermotransformateur à absorption avec des mélanges de travail de type {eau + SEP} (échelle macroscopique).

Références bibliographiques

[1] *La chaleur fatale*, ADEME Editions. 2017.

[2] « Les entreprises en France. Section 4.1 Consommation d'énergie dans l'industrie », Institut national de la statistique et des études économiques (INSEE), Edition 2019.

[3] F. Cudok *et al.*, « Absorption heat transformer - state-of-the-art of industrial applications », *Renew. Sustain. Energy Rev.*, vol. 141, p. 110757, mai 2021, doi: 10.1016/j.rser.2021.110757.

[4] H. Noubli, « Développement d'un nouveau thermo-transformateur à absorption-démixtion: optimisation conjointe du cycle et du mélange de travail », Institut National Polytechnique de Lorraine, 2010. [En ligne]. Disponible sur: https://hal.univ-lorraine.fr/tel-01748808

[5] J. Sun, L. Fu, et S. Zhang, « A review of working fluids of absorption cycles », *Renew. Sustain. Energy Rev.*, vol. 16, p. 1899-1906, 2012.

[6] D. Alonso, « Thermotransformateur à absorption-demixtion: simulation et expérimentation », Institut National Polytechnique de Lorraine, 2000.

[7] E. Kurem et I. Horuz, « A comparison between ammonia-water and water-lithium bromide solutions in absorption heat transformers », *Int. Commun. Heat Mass Transf.*, vol. 28, nº 3, p. 427-438, avr. 2001, doi: 10.1016/S0735-1933(01)00247-0.

[8] K. Wang, O. Abdelaziz, P. Kisari, et E. A. Vineyard, « State-of-the-art review on crystallization control technologies for water/LiBr absorption heat pumps », *Int. J. Refrig.*, vol. 34, nº 6, p. 1325-1337, sept. 2011, doi: 10.1016/j.ijrefrig.2011.04.006.

[9] T. A. Ring, J. A. Dirksen, K. N. Duvall, et N. Jongen, « LiBr · 2H2O Crystallization Inhibition in the Presence of Additives », *J. Colloid Interface Sci.*, vol. 239, nº 2, p. 399-408, juill. 2001, doi: 10.1006/jcis.2001.7620.

[10] J. A. Dirksen, T. A. Ring, K. N. Duvall, et N. Jongen, « Testing of crystallization inhibitors in industrial LiBr solutions », *Int. J. Refrig.*, vol. 24, nº 8, p. 856-859, déc. 2001, doi: 10.1016/S0140-7007(01)00006-8.

[11] M. Khamooshi, K. Parham, et U. Atikol, « Overview of Ionic Liquids Used as Working Fluids in Absorption Cycles », *Adv. Mech. Eng.*, vol. 5, p. 620592, janv. 2013, doi: 10.1155/2013/620592.

[12] W. Rivera, R. Best, M. J. Cardoso, et R. J. Romero, « A review of absorption heat transformers », *Appl. Therm. Eng.*, vol. 91, p. 654-670, déc. 2015, doi: 10.1016/j.applthermaleng.2015.08.021.

[13] I. Bandrés, F. M. Royo, I. Gascón, M. Castro, et C. Lafuente, « Anion Influence on Thermophysical Properties of Ionic Liquids: 1-Butylpyridinium Tetrafluoroborate and 1-Butylpyridinium Triflate », *J. Phys. Chem. B*, vol. 114, nº 10, p. 3601-3607, mars 2010, doi: 10.1021/jp9120707.

[14] T. Vogl, P. Goodrich, J. Jacquemin, S. Passerini, et A. Balducci, « The Influence of Cation Structure on the Chemical–Physical Properties of Protic Ionic Liquids », *J. Phys. Chem. C*, vol. 120, nº 16, p. 8525-8533, avr. 2016, doi: 10.1021/acs.jpcc.6b01945.

[15] X. Zhang et D. Hu, « Performance analysis of the single-stage absorption heat transformer using a new working pair composed of ionic liquid and water », *Appl. Therm. Eng.*, vol. 37, p. 129-135, mai 2012, doi: 10.1016/j.applthermaleng.2011.11.006.

[16] D. S. Ayou, M. R. Currás, D. Salavera, J. García, J. C. Bruno, et A. Coronas, « Performance analysis of absorption heat transformer cycles using ionic liquids based on imidazolium cation as absorbents with 2,2,2-trifluoroethanol as refrigerant », *Energy Convers. Manag.*, vol. 84, p. 512-523, août 2014, doi: 10.1016/j.enconman.2014.04.077.

[17] E.-S. Abumandour, F. Mutelet, et D. Alonso, « Performance of an absorption heat transformer using new working binary systems composed of {ionic liquid and water} », *Appl. Therm. Eng.*, vol. 94, p. 579-589, févr. 2016, doi: 10.1016/j.applthermaleng.2015.10.107.

[18] W. Chen et S. Liang, « Thermodynamic analysis of absorption heat transformers using [mmim]DMP/H 2 O and [mmim]DMP/CH 3 OH as working fluids », *Appl. Therm. Eng.*, vol. 99, p. 846-856, avr. 2016, doi: 10.1016/j.applthermaleng.2016.01.135.

[19] N. Merkel, M. Bücherl, M. Zimmermann, V. Wagner, et K. Schaber, « Operation of an absorption heat transformer using water/ionic liquid as working fluid », *Appl. Therm. Eng.*, vol. 131, p. 370-380, févr. 2018, doi: 10.1016/j.applthermaleng.2017.11.147.

[20] T. P. T. Pham, C.-W. Cho, et Y.-S. Yun, « Environmental fate and toxicity of ionic liquids: A review », *Water Res.*, vol. 44, nº 2, p. 352-372, janv. 2010, doi: 10.1016/j.watres.2009.09.030.

[21] W. Kunz et K. Häckl, « The hype with ionic liquids as solvents », *Chem. Phys. Lett.*, vol. 661, p. 6-12, sept. 2016, doi: 10.1016/j.cplett.2016.07.044.

[22] A. P. Abbott, G. Capper, D. L. Davies, R. K. Rasheed, et V. Tambyrajah, « Novel solvent properties of choline chloride/urea mixtures », *Chem. Commun.*, nº 1, p. 70-71, janv. 2003, doi: 10.1039/B210714G.

[23] A. P. Abbott, D. Boothby, G. Capper, D. L. Davies, et R. K. Rasheed, « Deep Eutectic Solvents Formed between Choline Chloride and Carboxylic Acids: Versatile Alternatives to Ionic Liquids », *J. Am. Chem. Soc.*, vol. 126, nº 29, p. 9142-9147, juill. 2004, doi:

10.1021/ja048266j.

[24] T. MOUFAWAD, M. COSTA GOMES, et S. FOURMENTIN, « Solvants eutectiques profonds Vers des procédés plus durables », *Techniques de l'ingénieur Chimie verte*, vol. base documentaire : TIP142WEB., nº ref. article : chv4002. Editions T.I., 2021. doi: 10.51257/a-v1-chv4002.

[25] S. Khandelwal, Y. K. Tailor, et M. Kumar, « Deep eutectic solvents (DESs) as eco-friendly and sustainable solvent/catalyst systems in organic transformations », *J. Mol. Liq.*, vol. 215, p. 345-386, mars 2016, doi: 10.1016/j.molliq.2015.12.015.

[26] Y. Marcus, *Deep Eutectic Solvents*. Cham: Springer International Publishing, 2019. doi: 10.1007/978-3-030-00608-2.

[27] M. A. R. Martins, S. P. Pinho, et J. A. P. Coutinho, « Insights into the Nature of Eutectic and Deep Eutectic Mixtures », *J. Solut. Chem.*, 2018, doi: https://doi.org/10.1007/s10953-018-0793-1.

[28] R. Haghbakhsh, H. Peyrovedin, S. Raeissi, A. R. C. Duarte, et A. Shariati, « Energy Conservation in Absorption Refrigeration Cycles Using DES as a New Generation of Green Absorbents », *Entropy*, vol. 22, nº 4, p. 409, avr. 2020, doi: 10.3390/e22040409.

[29] F. Z. Nessakh, F. Mutelet, et A. Negadi, « Efficiency of two working fluids constituted of a deep eutectic solvent and water in absorption heat transformer », *Int. J. Energy Res.*, p. er.8658, sept. 2022, doi: 10.1002/er.8658.

[30] S. Zhu *et al.*, « Vibrational analysis and formation mechanism of typical deep eutectic solvents: An experimental and theoretical study », *J. Mol. Graph. Model.*, vol. 68, p. 158-175, juill. 2016, doi: 10.1016/j.jmgm.2016.05.003.

[31] H. Wang, S. Liu, Y. Zhao, J. Wang, et Z. Yu, « Insights into the Hydrogen Bond Interactions in Deep Eutectic Solvents Composed of Choline Chloride and Polyols », *ACS Sustain. Chem. Eng.*, vol. 7, nº 8, p. 7760-7767, avr. 2019, doi: 10.1021/acssuschemeng.8b06676.

[32] C. Zhang, Y. Jia, Y. Jing, H. Wang, et K. Hong, « Main chemical species and molecular structure of deep eutectic solvent studied by experiments with DFT calculation: a case of choline chloride and magnesium chloride hexahydrate », *J. Mol. Model.*, vol. 20, nº 8, p. 2374, août 2014, doi: 10.1007/s00894-014-2374-6.

[33] K. Shahbaz, F. S. Mjalli, M. A. Hashim, et I. M. AlNashef, « Prediction of deep eutectic solvents densities at different temperatures », *Thermochim. Acta*, vol. 515, nº 1-2, p. 67-72, mars 2011, doi: 10.1016/j.tca.2010.12.022.

[34] K. Shahbaz, S. Baroutian, F. S. Mjalli, M. A. Hashim, et I. M. AlNashef, « Densities of

ammonium and phosphonium based deep eutectic solvents: Prediction using artificial intelligence and group contribution techniques », *Thermochim. Acta*, vol. 527, p. 59-66, janv. 2012, doi: 10.1016/j.tca.2011.10.010.

[35] N. R. Mirza, N. J. Nicholas, Y. Wu, S. Kentish, et G. W. Stevens, « Estimation of Normal Boiling Temperatures, Critical Properties, and Acentric Factors of Deep Eutectic Solvents », *J. Chem. Eng. Data*, vol. 60, nº 6, p. 1844-1854, juin 2015, doi: 10.1021/acs.jced.5b00046.

[36] R. Haghbakhsh, S. Raeissi, et A. R. C. Duarte, « Group contribution and atomic contribution models for the prediction of various physical properties of deep eutectic solvents », *Sci. Rep.*, vol. 11, nº 1, p. 6684, déc. 2021, doi: 10.1038/s41598-021-85824-z.

[37] X.-J. Hou, L.-Y. Yu, Y.-X. Wang, K.-J. Wu, et C.-H. He, « Comprehensive Prediction of Densities for Deep Eutectic Solvents: A New Bonding-Group Interaction Contribution Scheme », *Ind. Eng. Chem. Res.*, vol. 60, nº 35, p. 13127-13139, sept. 2021, doi: 10.1021/acs.iecr.1c02260.

[38] M. Taherzadeh, R. Haghbakhsh, A. R. C. Duarte, et S. Raeissi, « Estimation of the heat capacities of deep eutectic solvents », *J. Mol. Liq.*, vol. 307, p. 112940, juin 2020, doi: 10.1016/j.molliq.2020.112940.

[39] D.-Y. Peng et D. B. Robinson, « A New Two-Constant Equation of State », *Ind. Eng. Chem. Fundam.*, vol. 15, nº 1, p. 59-64, févr. 1976, doi: 10.1021/i160057a011.

[40] M. B. Haider, D. Jha, B. Marriyappan Sivagnanam, et R. Kumar, « Modelling and simulation of CO2 removal from shale gas using deep eutectic solvents », *J. Environ. Chem. Eng.*, vol. 7, nº 1, p. 102747, févr. 2019, doi: 10.1016/j.jece.2018.10.061.

[41] N. R. Mirza, N. J. Nicholas, Y. Wu, K. A. Mumford, S. E. Kentish, et G. W. Stevens, « Experiments and Thermodynamic Modeling of the Solubility of Carbon Dioxide in Three Different Deep Eutectic Solvents (DESs) », *J. Chem. Eng. Data*, vol. 60, nº 11, p. 3246-3252, nov. 2015, doi: 10.1021/acs.jced.5b00492.

[42] L. F. Zubeir, M. H. M. Lacroix, et M. C. Kroon, « Low Transition Temperature Mixtures as Innovative and Sustainable CO_2 Capture Solvents », *J. Phys. Chem. B*, vol. 118, nº 49, p. 14429-14441, déc. 2014, doi: 10.1021/jp5089004.

[43] E. Ali *et al.*, « Solubility of CO2 in deep eutectic solvents: Experiments and modelling using the Peng–Robinson equation of state », *Chem. Eng. Res. Des.*, vol. 92, nº 10, p. 1898-1906, oct. 2014, doi: 10.1016/j.cherd.2014.02.004.

[44] M. B. Haider, D. Jha, B. Marriyappan Sivagnanam, et R. Kumar, « Thermodynamic and Kinetic Studies of CO_2 Capture by Glycol and Amine-Based Deep Eutectic Solvents », *J.*

Chem. Eng. Data, vol. 63, nº 8, p. 2671-2680, août 2018, doi: 10.1021/acs.jced.8b00015.

[45] A. Samarov, I. Prikhodko, N. Shner, G. Sadowski, C. Held, et A. Toikka, « Liquid–Liquid Equilibria for Separation of Alcohols from Esters Using Deep Eutectic Solvents Based on Choline Chloride: Experimental Study and Thermodynamic Modeling », *J. Chem. Eng. Data*, vol. 64, nº 12, p. 6049-6059, déc. 2019, doi: 10.1021/acs.jced.9b00884.

[46] P. V. A. Pontes *et al.*, « Measurement and PC-SAFT modeling of solid-liquid equilibrium of deep eutectic solvents of quaternary ammonium chlorides and carboxylic acids », *Fluid Phase Equilibria*, vol. 448, p. 69-80, sept. 2017, doi: 10.1016/j.fluid.2017.04.007.

[47] S. P. Verevkin, A. Yu. Sazonova, A. K. Frolkova, D. H. Zaitsau, I. V. Prikhodko, et C. Held, « Separation Performance of BioRenewable Deep Eutectic Solvents », *Ind. Eng. Chem. Res.*, vol. 54, nº 13, p. 3498-3504, avr. 2015, doi: 10.1021/acs.iecr.5b00357.

[48] C. H. J. T. Dietz *et al.*, « PC-SAFT modeling of CO2 solubilities in hydrophobic deep eutectic solvents », *Fluid Phase Equilibria*, vol. 448, p. 94-98, sept. 2017, doi: 10.1016/j.fluid.2017.03.028.

[49] H. Renon et J. M. Prausnitz, « Local compositions in thermodynamic excess functions for liquid mixtures », *AIChE J.*, vol. 14, nº 1, p. 135-144, janv. 1968, doi: 10.1002/aic.690140124.

[50] A. Kamgar, S. Mohsenpour, et F. Esmaeilzadeh, « Solubility prediction of CO 2 , CH 4 , H 2 , CO and N 2 in Choline Chloride/Urea as a eutectic solvent using NRTL and COSMO-RS models », *J. Mol. Liq.*, vol. 247, p. 70-74, déc. 2017, doi: 10.1016/j.molliq.2017.09.101.

[51] C. Ma, Y. Guo, D. Li, J. Zong, X. Ji, et C. Liu, « Molar enthalpy of mixing and refractive indices of choline chloride-based deep eutectic solvents with water », *J. Chem. Thermodyn.*, vol. 105, p. 30-36, févr. 2017, doi: 10.1016/j.jct.2016.10.002.

[52] A. Klamt, « Conductor-like Screening Model for Real Solvents: A New Approach to the Quantitative Calculation of Solvation Phenomena », *J. Phys. Chem.*, vol. 99, nº 7, p. 2224-2235, févr. 1995, doi: 10.1021/j100007a062.

[53] A. Klamt, V. Jonas, T. Bürger, et J. C. W. Lohrenz, « Refinement and Parametrization of COSMO-RS », *J. Phys. Chem. A*, vol. 102, nº 26, p. 5074-5085, juin 1998, doi: 10.1021/jp980017s.

[54] S.-T. Lin et S. I. Sandler, « A Priori Phase Equilibrium Prediction from a Segment Contribution Solvation Model », *Ind. Eng. Chem. Res.*, vol. 41, nº 5, p. 899-913, mars 2002, doi: 10.1021/ie001047w.

[55] H. Grensemann et J. Gmehling, « Performance of a Conductor-Like Screening Model

for Real Solvents Model in Comparison to Classical Group Contribution Methods », *Ind. Eng. Chem. Res.*, vol. 44, nº 5, p. 1610-1624, mars 2005, doi: 10.1021/ie049139z.

[56] C.-M. Hsieh, S. I. Sandler, et S.-T. Lin, « Improvements of COSMO-SAC for vapor–liquid and liquid–liquid equilibrium predictions », *Fluid Phase Equilibria*, vol. 297, nº 1, p. 90-97, oct. 2010, doi: 10.1016/j.fluid.2010.06.011.

[57] B. Ozturk et M. Gonzalez-Miquel, « Alkanediol-based deep eutectic solvents for isolation of terpenoids from citrus essential oil: Experimental evaluation and COSMO-RS studies », *Sep. Purif. Technol.*, vol. 227, p. 115707, nov. 2019, doi: 10.1016/j.seppur.2019.115707.

[58] R. Verma et T. Banerjee, « Liquid–Liquid Extraction of Lower Alcohols Using Menthol-Based Hydrophobic Deep Eutectic Solvent: Experiments and COSMO-SAC Predictions », *Ind. Eng. Chem. Res.*, vol. 57, nº 9, p. 3371-3381, mars 2018, doi: 10.1021/acs.iecr.7b05270.

[59] R. M. Ojeda et F. Llovell, « Soft-SAFT Transferable Molecular Models for the Description of Gas Solubility in Eutectic Ammonium Salt-Based Solvents », *J. Chem. Eng. Data*, vol. 63, nº 7, p. 2599-2612, juill. 2018, doi: 10.1021/acs.jced.7b01103.

Chapitre 2

Influence of water on the conformations and interactions within two chloride-based deep eutectic solvents: a density functional theory investigation

We are reaching the stage where the problems we must solve are going to become insoluble without computer.
I do not fear computers. I fear the lack of them.

-- Isaac Asimov

Chapitre 2 : Influence of water on the conformations and interactions within two chloride-based deep eutectic solvents: a density functional theory investigation

Thomas Di Pietro[a], Laetitia Cesari[a], Fabrice Mutelet[a]

a - Université de Lorraine, Ecole Nationale Supérieure des Industries Chimiques, Laboratoire Réactions et Génie des Procédés (UMR CNRS 7274), 1 rue Grandville, 54000 Nancy, France

Article à soumettre

Résumé

Ce travail présente l'étude des conformations des solvants eutectiques profonds {Chlorure de choline:Phénol} ratio [1:2] et {Chlorure de choline:Acide glycolique} ratio [1:1] dans leur état isolé et en présence d'eau. Les optimisations de géométries ont été effectuées en utilisant la théorie de la fonctionnelle de la densité avec la fonctionnelle B3LYP et la base 6-311(++)G(d,p). Les conformations les plus stables de la choline, du chlorure de choline, des deux solvants eutectiques profonds précédemment évoqués et des systèmes formés en présence d'eau sont détaillées à travers l'étude de l'optimisation de géométrie et de la distribution de charge. Les liaisons hydrogène principales sont identifiées à l'aide des valeurs des énergies de stabilisation issues des interactions entre orbitales. Les résultats mettent en avant que la liaison hydrogène de type OH--Cl est une des interactions clef. Ils permettent également d'observer que l'ion chlorure se comporte comme un accepteur de liaisons hydrogène tandis que la choline fonctionne agit principalement en tant que donneur de liaisons hydrogène, et que l'acide glycolique et le phénol peuvent jouer les deux rôles. L'ajout d'eau montre que la molécule

d’eau est capable de former des liaisons hydrogène variées. Cependant, les liaisons hydrogène formées entre l’ion chlorure et les groupes hydroxyles demeurent les plus fortes. Enfin, un nombre croissant de liaisons hydrogène dans un système diminue la force globale des interactions.

Abstract

This work presents the study of the conformations of {[Choline][Chloride]:Phenol} ratio [1:2] and {[Choline][Chloride]:Glycolic acid} ratio [1:1] deep eutectic solvents in their isolated state and with the presence of water. The optimization of the geometries were carried out using density functional theory with the B3LYP functional and the 6-311(++)G(d,p) basis set. Through the study of the geometry optimization and the charge distribution, the most stable conformations of choline, choline chloride, the two aforementioned deep eutectic solvents and their cluster with water are detailed. The main hydrogen bonds are identified using the values of stabilizing energies between interacting orbitals. The results highlight the OH--Cl type of hydrogen bonds as one of the key interactions. They also allow to observe that the chloride ion acts as a hydrogen bond acceptor while the choline ion acts primarily as a hydrogen bond donor, and that glycolic acid and phenol can play both roles. The addition of water shows that the molecule of water is able to form various hydrogen bonds. However, hydrogen bonds formed between the chloride ion and a hydroxyl group remain the strongest ones. Finally, an increasing total number of hydrogen bonds in a system decreases the strength of the overall interactions.

2.1 Introduction

Since the beginning of the 2000s, deep eutectic solvents (DESs) have appeared as promising new solvents [1,2]. They are comprised of hydrogen bond donors (HBD) and acceptors (HBA). Through the multiple interactions within the mixture, in particular the hydrogen bonds, the resulting solvent acts as a pure compound with a lowered temperature of fusion compared to the one of the hydrogen bond donors and acceptors taken separately. Incidentally, some components of DESs can take the role of both donor and acceptor of hydrogen. A suitable choice of the component of the DES leads to a liquid solvent with a low vapour pressure at room temperature.

In many DESs, choline chloride has been chosen as a primary hydrogen bond acceptor because of its availability and its pharmaceutically acceptable toxicity [3]. Choline chloride has often been paired with alcohol [4–8] or carboxylic acid [2,9–12] molecules. Regarding the first group, many were formed using phenolic compounds, and more specifically phenol with the ratios of choline chloride and phenol varying from [1:1] to [1:4]. The DES {[Choline][Chloride]:Phenol} ratio [1:2] has notably been investigated for the microextraction of polycyclic compounds [13], cobalt [14], malachite green [15], sulphonamides [16], arsenic [17], selenium [18], aluminium [19] and vanadium [20] from water. However, Shishov et al. [21] warned against the fact that a DES made of choline chloride and phenol can disassociate itself in an aqueous phase. In the organic phase resulting from an extraction, no choline chloride was found in their experiments. Thus, the DES in itself may not be reckoned as the extracting solvent. This kind of result prompts the need to investigate the interactions between the compounds of the DESs and water in order to get a better understanding of the behaviour of the DESs in mixtures. Over the past few years, many experimental and theoretical studies have been conducted on the interactions within phenol and water clusters [22–31]. The methods ranged from spectroscopy measurements to *ab initio* calculations. Within the *ab initio* methods,

the density functional theory (DFT) allows to access energy and bonding predictions from electron distribution via a functional and a basis set [32]. Using DFT, a few articles tackled the interactions within DESs containing phenol molecules [33,34], highlighting the main hydrogen bonds that can be found in the systems. In particular, the DESs involving phenol and choline chloride exhibited a strong hydrogen bond between the chloride ion and the hydroxyl group of phenol [33,34]. The next step is the study of the interactions between the DESs and water.

In the same vein, DESs composed of choline chloride and carboxylic acid are of interest. The DES {[Choline][Chloride]:Glycolic acid} [1:1] was chosen for comprising the shortest α-hydroxy acid and therefore a simple molecule with multiple hydrogen bonding atoms. They are in particular able to form intramolecular hydrogen bonds between the hydroxyl and carboxylic groups. Glycolic acid with choline chloride has previously been used for the extraction of dye from aqueous solution [35] and the separation of azeotropic mixtures comprised of hexane or heptane and ethanol [36] and of water and ethanol [37]. Similarly to phenol, glycolic acid and water clusters have been investigated [38–40]. A few DFT studies also includes DESs containing glycolic acid. Yu et al. [41] used DFT to understand the mechanism behind the extraction of flavonoids with several DESs. The authors have obtained the best extracting results with the DES containing choline chloride and glycolic acid (ratio [1:2]). The hydrogen bonds of the DES {proline:glycolic acid} and the DES {proline:malic acid} were compared to understand their impact on viscosity [42]. Regarding clusters containing glycolic acid-based DESs, Wang et al. [43] investigated the DES {glycolic acid:xylitol} in water. The authors observed that an increasing number of molecules of water increases the number of hydrogen bonds but decreases their strength.

Consequently, this work aims at investigating the interactions found in two DESs: {[Choline][Chloride]:Phenol} [1:2] and {[Choline][Chloride]:Glycolic acid} [1:1], using DFT to identify the hydrogen bonds and the most stabilizing interactions. A comparison of the

isolated conformations and their possible associations and pairwise interactions of the components constituting the two DESs and a molecule of water will be presented in the following order: (i) choline cation, (ii) choline chloride, (iii) choline chloride and two phenols (DES 1), (iv) choline chloride and two phenols and water (cluster 1), (v) choline chloride and glycolic acid (DES 2), (vi) choline chloride and glycolic acid and water (cluster 2).

2.2 Method and computational details

The geometries of the molecules, the DESs and their complexes with water were built with GaussView 5.0.9 [44]. Geometry optimizations, frequency and energy calculations were performed using Gaussian 09 Revision D.01 [45]. To do so, the B3LYP functional was employed [46,47] with the symmetry ignored. Empirical dispersion was accounted for using the D3 version of Grimme's dispersion, which adds Becke-Johnson damping and is called D3BJ [48]. The 6-311++G(d,p) basis set has been chosen in this work. This triple zeta basis set adds diffuse functions for both hydrogen and heavy atoms as well as polarization functions [49]. With it, a good compromise between computation time and accurate calculations can be reached as shown in previous works [50,51]. More details about this basis set are provided in the supporting information. Counterpoise corrections were computed to calculate the basis set superposition error (BSSE) [52,53]. Moreover, each geometry optimization was supported with a frequency calculation. It allowed to ensure that minima are valid (no vibrational frequencies with a virtual value) and provided the zero-point energy (ZPE) correction as well. Population analyses were performed with the Gaussian natural bond orbital (NBO) method (version 3.1) [54–60]. It provides a second order perturbation theory analysis of Fock matrix in NBO basis. This corresponds to an examination of the possible interactions between donor Lewis-type NBOs and acceptor non-Lewis NBOs. Among the donor NBOs can be found 1-center lone pair NBOs (LP, nonbonding) and 2-center bond NBOs (BD, linear combination of two bonding natural hybrid orbitals). BD NBOs are complemented by 2-center antibond NBOs (BD*, main

non-Lewis NBOs). BD* NBOs can take part in the stabilization of structures through resonance or hydrogen bonding. The NBOs are characterized by their occupancy and energy. Interactions between donor and acceptor NBOs causes a shift of occupancy from Lewis-type NBOs to unoccupied non-Lewis NBOs, called delocalization. This is typical of a stabilization of the system and is supported with a second order perturbation (stabilization) energy $E_{(2)}$. The higher this energy is, the stronger the interaction stabilizes the molecule. A threshold of 0.5 kcal.mol^{-1} has to be reached for the energies to be taken into account. The NBO method was also used to compute the charge distribution of the isolated molecules with both natural population analysis and CHarges from electrostatic potentials using a Grid-based method (CHelpG) scheme of Breneman [61]. Input keywords for all of the calculations are provided in the supplementary material.

Finally, the binding energy (or association energy) is defined as the energy of the system minus the sum of the energies of the individual components of the system. In this work, several binding energies can be calculated:

Choline chloride (ChCl):

$$\Delta E_b^{ChCl} = E_{ChCl} - (E_{choline} + E_{chloride}) \quad (1)$$

{[Choline][Chloride]:Phenol} [1:2]:

$$\Delta E_b^{DES1} = E_{DES1} - \left(E_{choline\ chloride} + 2 * E_{phenol}\right) \quad (2)$$

{[Choline][Chloride]:Glycolic acid} [1:1]:

$$\Delta E_b^{DES2} = E_{DES2} - \left(E_{choline\ chloride} + E_{glycolic\ acid}\right) \quad (3)$$

{DES + water} cluster [1:1]:

$$\Delta E_b^{cluster} = E_{cluster} - (E_{DES} + E_{water}) \quad (4)$$

All of them were both BSSE and ZPE corrected. The lower they are, the stronger the association is.

2.3 Results and discussion

2.3.1 Choline cation

The choline cation is a quaternary ammonium derivative with a hydroxyl group. Different conformations can be obtained through the variation of the C-C-O and C-O-H angles and the rotation of the corresponding groups (related to the N-C-C-O and C-C-O-H dihedra).

The optimization calculations using input files with different angles resulted in three conformations of choline that are presented **Figure 2.1**. **Table S.A1** in the supporting material provides the energies related to the conformers. The most stable one corresponds to the gauche conformation (gauche effect) with respect to the C-C bond. The anti conformer was found less stable with a relative energy (compared to the gauche conformer, energies counterpoised and ZPE corrected) around 18 $kJ.mol^{-1}$. As shown by Ashworth et al. [51], the optimization of a second anti conformation is possible using redundant coordinates to maintain the dihedron C-C-O-H at an angle of -90°. No negative frequencies were observed after the frequency calculation, ensuring a valid minimum. This last conformer has a relative energy slightly over 23 $kJ.mol^{-1}$. Values for the energies are consistent with the ones provided by Ashworth et al. [51].

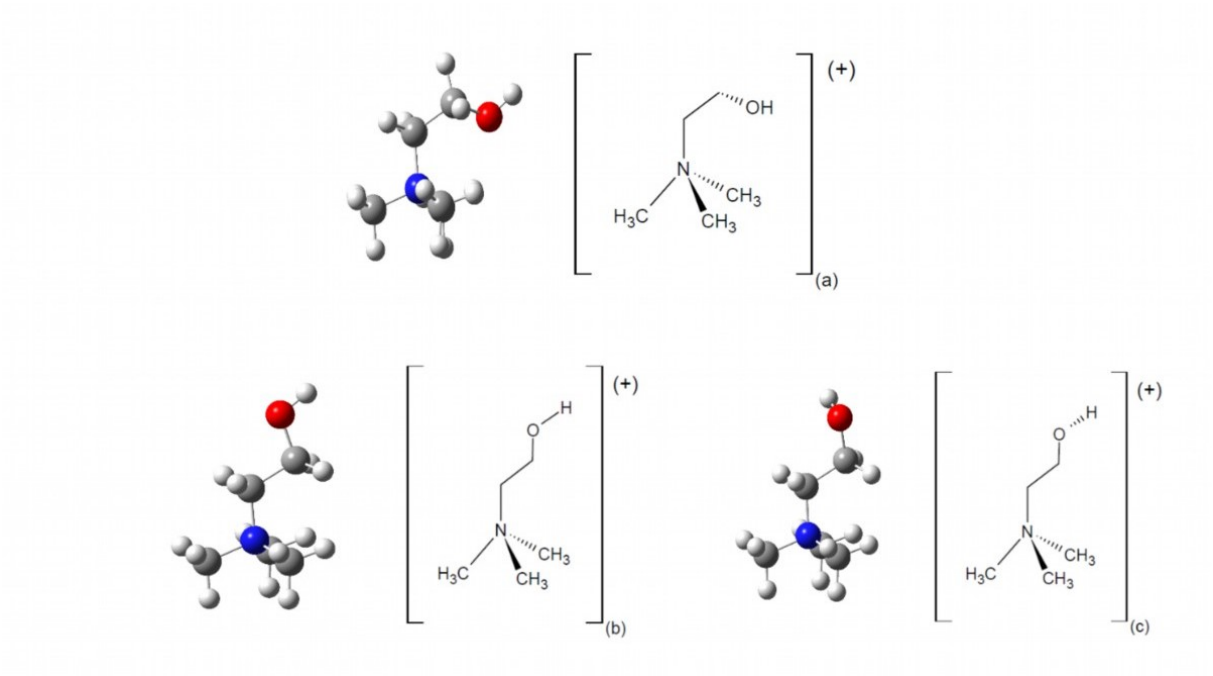

Figure 2.1. 3D representation of three conformations of choline: (a) gauche, (b) anti, (c) anti with a C-C-O-H dihedral angle of -90°

The charge distribution for the gauche conformer has been obtained with a natural population analysis from the NBO population analysis and with the CHelpG scheme of Breneman. They are provided in the supporting material, **Table S.A2**, along with a numbering of the atoms in **Figure S.A1**. NBO gives a minimum charge around -0.75 e on the oxygen atom and a maximum charge of 0.49 e on the hydrogen H^2 from the hydroxyl group. The corresponding values with CHelpG are -0.65 and 0.45 e. Overall, ChelpG tends to give less variable charges with absolute values closer to 0 compared to the NBO method. Negative charges are primarily placed on the atom of oxygen, then distributed on the atoms of carbon with no covalent bond with the atom of oxygen. The NBO analysis also places negative charges on the remaining atom of carbon (C^3) and on the nitrogen. The positive charges are divided between the hydrogen atoms and the aforementioned carbon and nitrogen atoms for the CHelpG method. It is to be noted that the hydrogen atoms H^4 and H^5 on the carbon bonded to the oxygen are less positively charged compared to the other hydrogen atoms due to the influence of the hydroxyl group. They are also not equivalent since H^4 is even less charged than H^5. This

distribution supports a favourable interaction between the atom of oxygen and the atoms of hydrogen on the methyl groups [51,62].

2.3.2 Choline chloride

The starting point of each geometry optimization was determined by positioning a chloride ion on a different side of the choline conformations. Eight different choline chloride conformations were obtained in accordance with Ashworth et al. [51] and are presented in **Table S.A3**. The different conformations were sorted by their relative energy and named accordingly with a diminutive of choline chloride and a letter of the alphabet. The results related to their energies are reported in **Table S.A4**. The conformations with the lowest energies also have the lowest free energies, in the same order.

The three most stable conformations are gathered in **Figure 2.2**, where the lengths of their main hydrogen bonds are indicated as well. Atoms have been numbered so that bonds can be clearly identified. All three conformations are derived from the gauche conformation of the choline ion. In the first conformation ChCl_A, the chloride ion is in the centre of a clamp made of three atoms of hydrogen, including the one linked to the atom of oxygen.

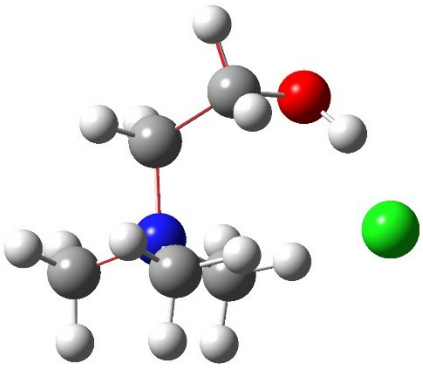

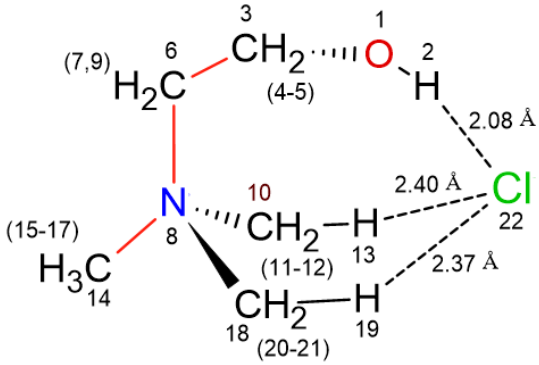

ChCl_A, $\Delta E = 0.000$ kJ.mol^{-1}

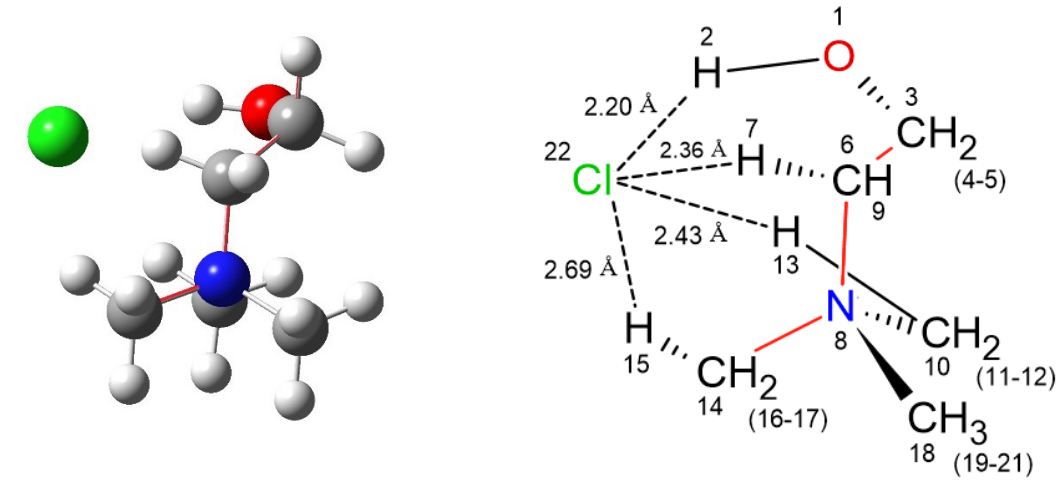

ChCl_B, $\Delta E = 1.633$ kJ.mol^{-1}

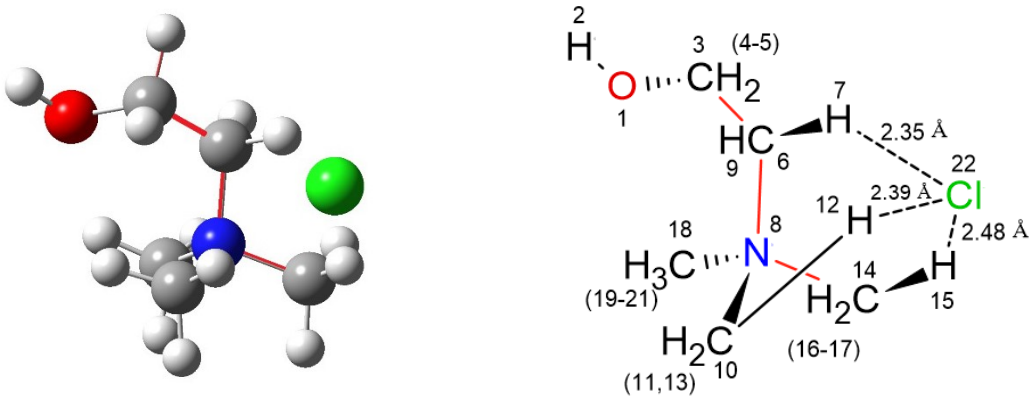

ChCl_C, $\Delta E = 12.461$ kJ.mol^{-1}

Figure 2.2. 3D and schematic representations of the three most stable conformations of choline chloride with the length of the main hydrogen bonds.
Red bonds are here as a key visual for the central plane

This is the conformation that has the lowest energy. The Cl--OH bond is the shortest of all the hydrogen bonds that have been indicated in **Figure 2.2**. The binding energy ΔE_b^{ChCl} of ChCl_A has been calculated with the ZPE and counterpoise corrected energy and is around -408 kJ.mol^{-1}. This is almost identical to the value of -409 kJ.mol^{-1} calculated by Ashworth et al. [51]. The second most stable configuration ChCl_B has a relative energy of 1.63 kJ.mol^{-1}. The chloride ion is on the other side of the central plane (plane formed by the red bonds in **Figure 2.2**) compared to ChCl_A. The chloride ion is surrounded by four atoms of

hydrogen and is a little further away from the hydrogen of the hydroxyl group (2.20 Å against 2.08 Å in ChCl_A). In the ChCl_C conformation, the chloride ion is not on a side close to the hydroxyl group and is instead encased in a “three-prong clamp” formed by hydrogen atoms from the ammonium group. The relative energy of ChCl_C is around 12.46 $kJ.mol^{-1}$. This relative energy is almost ten times higher compared to the one of ChCl_B. This indicates that the Cl--CH bonds are much less stabilizing compared to the Cl--OH bond. This is also consistent with the charge distribution of the choline ion with the hydrogen atom from the hydroxyl group having the highest positive charge.

Natural bond orbital interactions of interest are presented in **Table 2.1**. The most stabilizing NBO interaction for ChCl_A was found to occur between the lone pair orbital of the chloride ion and the antibonding orbital from the hydroxyl group. This confirms that the hydrogen bond between the chlorine ion and the hydrogen from the O-H bond is the strongest of the hydrogen bonds in the choline chloride. It is completed by hydrogen bonds of lower strength between lone pairs from the oxygen and chlorine atoms and hydrogen atoms from alkyl groups. In ChCl_B, the same interactions can be found. However, the atom of chlorine provides less stabilization and the hydrogen bonds formed with the chloride ion are less strong compared to ChCl_A. For the third conformation ChCl_C, the stabilization energies of the interactions involving the chloride ion do not stand out as much anymore compared to the energies of the interactions with the lone pairs of the oxygen atoms.

Table 2.1. Main interactions between NBOs within the three most stable conformations of choline chloride

Conformation	NBOs interactions	Stabilization energy $E^{(2)}$ ($kJ.mol^{-1}$)
ChCl_A	LP O^1 → BD* C^3-H^5	23.0
	LP Cl^{22} → BD* O^1-H^2	**81.5**
	LP Cl^{22} → BD* C^{18}-H^{19}	29.5
	LP Cl^{22} → BD* C^{10}-H^{13}	15.06
ChCl_B	LP O^1 → BD* C^3-H^5	39.4
	LP Cl^{22} → BD* O^1-H^2	**52.2**
	LP Cl^{22} → BD* C^6-H^7	12.3
	LP Cl^{22} → BD* C^{10}-H^{12}	10.1
ChCl_C	**LP O^1 → BD* C^3-H^4**	**26.8**
	LP O^1 → BD* C^3-H^5	22.5
	LP Cl^{22} → BD* C^6-H^7	19.7
	LP Cl^{22} → BD* C^{10}-H^{12}	17.2

Thus, the first two conformations display a hydrogen bond between the chloride ion and the hydrogen from the hydroxyl group. In both cases, it corresponds to the shortest hydrogen bond of the conformation. This hydrogen bond is actually found in three out of the four most stable conformations, and not at all in the four less stable ones. This suggests that it is one the most stabilizing interaction that is possible within choline chloride. The chloride ion also tends to surround itself with three or four hydrogen atoms that form a clamp. Overall, only three choline chloride conformations out of the eight show a choline ion with an anti conformation (namely ChCl_D and the two less stable ones ChCl_G and ChCl_H), which indicates that the gauche conformation remains more stable.

2.3.3 {[Choline][Chloride]:Phenol} [1:2]

A short presentation of the optimization of the molecule of phenol with matching results compared to the ones from Feller et al. [22] and Cesari et al. [63] can be found in section 4 in the supporting information. Two phenols have been introduced alongside the choline chloride ion pair. They bring one hydroxyl group each to contribute to the hydrogen bond interactions, as well as benzene rings, more than doubling the number of atoms in the system compared to choline chloride. Molecules have been moved around in order to get diverse starting points before the optimization of the geometry of the systems. The eight conformations with the lowest energies have been gathered in **Table S.A6** and the three most stable can be found in **Figure 2.3**. Out of the eight, most of them are derived from the conformation ChCl_A of the ion pair. Only conformations DES1_C, DES1_E and DES1_F display a choline chloride ion pair with a conformation ChCl_D. In particular, the difference between the most stable conformation DES1_A and DES1_E is the conformation of the choline chloride since the phenol molecules have a similar positioning. In DES1_A, the molecules of phenol complete the clamp formation of choline, with the hydroxyl groups "spiralling" around the chloride ion. The two phenols belong to planes that are almost perpendicular to each other so that the benzene rings can get as close as possible from the choline cation. Conformation DES1_B has a relative energy of 3.628 kJ.mol^{-1} compared to DES1_A. This time, the phenol molecules are placed on each side of the choline cation, leading the hydroxyl groups to form a pyramid shape with the chloride ion at its pinnacle. DES1_C trades the classical Cl--OH^{choline} hydrogen bond for a bond between the choline as HBD and the second molecule of phenol as HBA. Therefore, the chloride ion is placed in a clamp formed by three hydrogen atoms belonging to methyl groups from the choline and the hydrogen from the OH group of the phenol molecules. The bonding energy ΔE_b^{DES1} calculated with the conformation DES1_A is around -126 kJ.mol^{-1} and is less negative compared to the one of choline chloride. This may be because the addition of molecules makes

it more energy-demanding to bind together the molecules of the system.

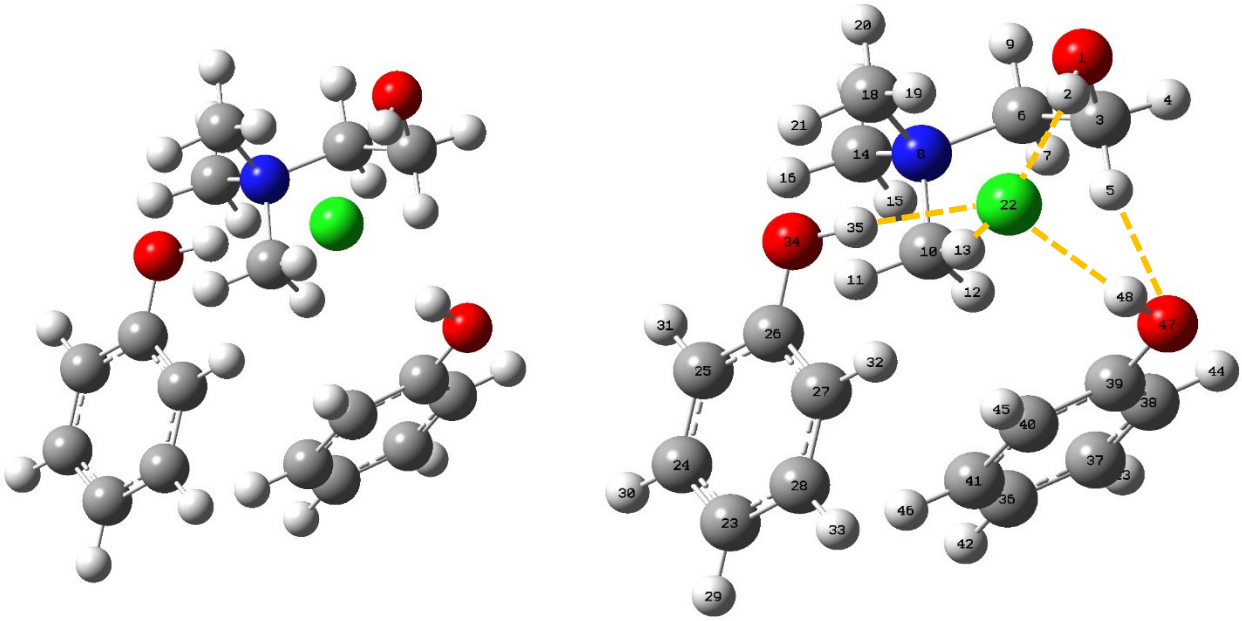

DES1_A, $\Delta E = 0.000$ kJ.mol^{-1}

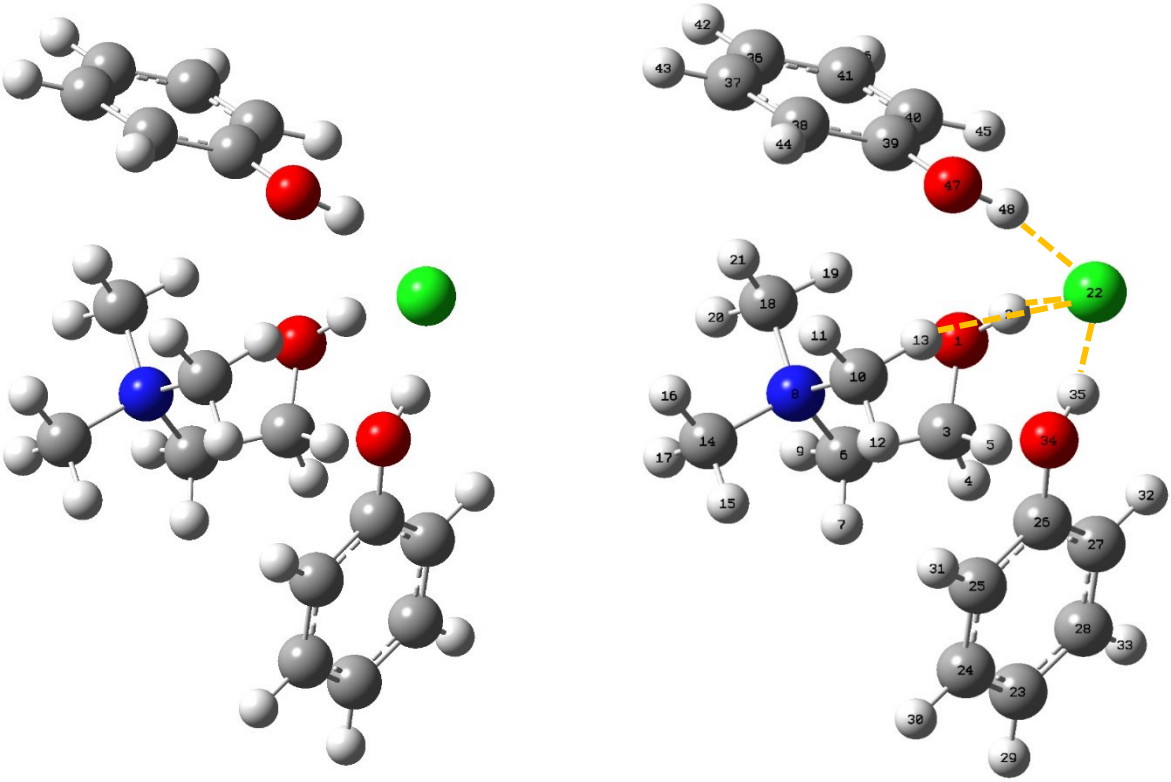

DES1_B, $\Delta E = 3.628$ kJ.mol^{-1}

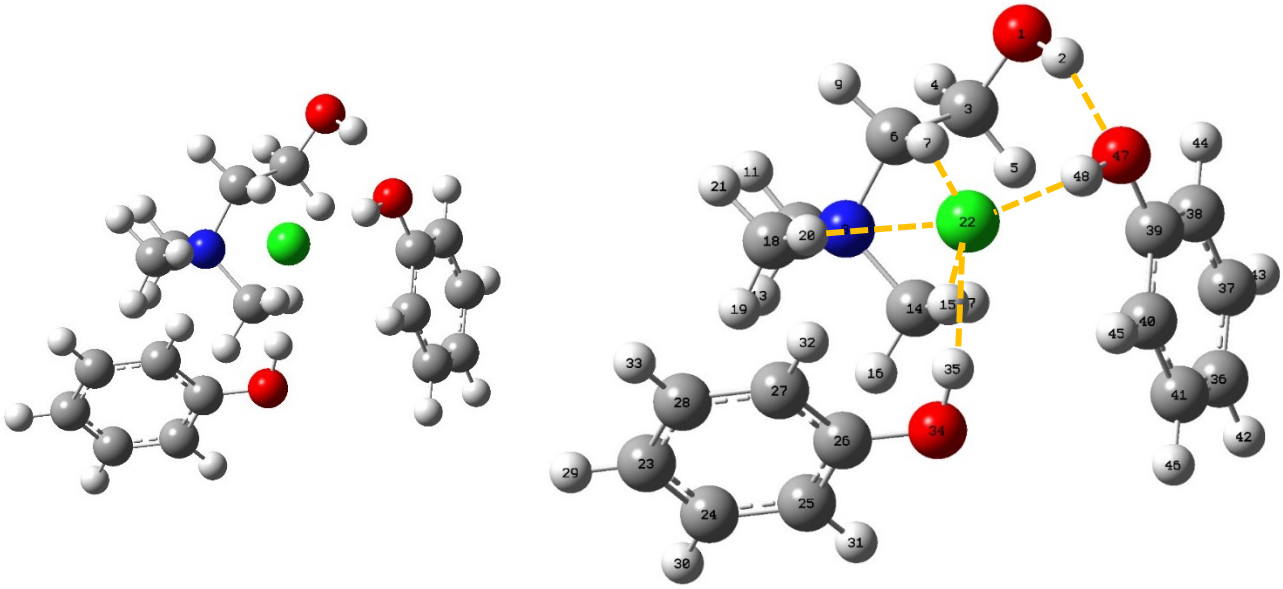

DES1_C, $\Delta E = 4.684$ kJ.mol^{-1}

Figure 2.3. 3D representations of the three most stable conformations of DES 1 {Choline chloride:Phenols} with the main hydrogen bonds as yellow dash lines

Hydrogen bonds with lengths and stabilizing energies from the NBO analysis are presented in **Table 2.2**. The values of the stabilizing energies are much lower compared to the ones from the choline chloride conformations. The number of molecules and of hydrogen bonds has increased, weakening the strength of each individual hydrogen bonds as the stabilization phenomenon is spread and shared between more bonds. This is also consistent with the decrease in the binding energy. For DES1_A, the main hydrogen bonds are formed between the chloride as HBA and the two molecules of phenol and the choline as HBD. The strongest interaction occurs between the chloride ion and a hydroxyl group from the phenols with a stabilization energy of 13.76 kJ.mol^{-1}. The other molecule of phenol also acts as a HBA with a hydrogen from choline, creating a weak interaction of 1.02 kJ.mol^{-1}. The same main hydrogen bonds are found in DES1_B, although the Cl--OH^{choline} interaction (Cl^{22}--O^{1}-H^{2}) is roughly twice weaker compared to DES1_A. Compared to the ChCl_A conformation, the distance between the chloride ion and the atoms of the choline has increased in both DES1_A and DES1_B: the Cl--OH^{choline} bond going from 2.08 to around 2.2 Å and the Cl--CH^{choline} bonds from around 2.4

to 2.5 Å. The conformation DES1_C exhibits the highest stabilization energy for the Cl^{22}--O^{47}-H^{48} interaction between the chloride and a phenol with a value of 14.77 kJ.mol^{-1}, although the differences in terms of energy values between the conformations of the DES are much smaller compared to the ones between the choline chloride conformations. In replacement of the Cl--$OH^{choline}$ bond, DES1_C displays a hydrogen bond between a phenol and the choline (O^{47}--O^{1}-H^{2}) weaker than the Cl--$OH^{choline}$ from the other two conformations. The interactions between the chloride and the hydrogen atoms from the methyl groups of the choline are also weaker compared to the one observed in DES1_A. Rain et al. also performed the optimization of the same DES [34] with a different method, namely the 6-31++G(d,p) basis set with the ωB97XD functional. In their conformations, the chloride ion is placed on a side away from the hydroxyl group of the choline and only one hydroxyl group from a phenol molecule interacts with the anion. Nonetheless, they find Cl--OH^{phenol} to be the main hydrogen bond in their system, with 2.07 Å between the hydroxyl group of one of the phenol molecules and the chloride ion, which is on par with the lengths provided in **Table 2.2** for similar interactions.

Overall, a preference for hydrogen bonds between the chloride ion and a hydrogen from a OH group is observed. In the conformations DES1_A, B, E and F all the hydroxyl groups form a direct hydrogen bond with the chloride ion. The remaining conformations still have two hydroxyl groups interacting with the chloride ion, the third OH group bonding with the oxygen of another hydroxyl group with the following interactions: choline (HBD) with a phenol (DES1_C), phenol with phenol (DES1_D and DES1_G) and phenol (HBD) with choline (DES1_H). Compared to the conformations of choline chloride, the addition of the molecules of phenol weakened all the hydrogen bonds between the choline and the chloride. Due to the steric hindrance induced by the phenols, the methyl groups from the ammonium part of choline got further away from the chloride ion, leading to the weakening (Cl^{22}--C^{10}-H^{13}) or disappearance (Cl^{22}--C^{18}-H^{19}) of some of the hydrogen bonds compared to the ChCl_A

conformation.

Table 2.2. Main interactions between NBOs LP → BD* of hydrogen bonds within the three most stable conformations of DES 1

Conformation	Units involved	Hydrogen bond	Length (Å)	Stabilization energy $E^{(2)}$ ($kJ.mol^{-1}$)
DES1_A	Chloride and choline	**Cl^{22}--O^{1}-H^{2}**	**2.19**	**9.78**
		Cl^{22}--C^{10}-H^{13}	2.53	3.64
	Chloride and phenol 1	**Cl^{22}--O^{34}-H^{35}**	**2.14**	**13.76**
	Chloride and phenol 2	**Cl^{22}--O^{47}-H^{48}**	**2.22**	**4.49**
	Phenol 2 and choline	O^{47}--C^{3}-H^{5}	2.44	1.02
DES1_B	Chloride and choline	**Cl^{22}--O^{1}-H^{2}**	**2.18**	**5.55**
		Cl^{22}--C^{10}-H^{13}	2.57	2.43
	Chloride and phenol 1	**Cl^{22}--O^{34}-H^{35}**	**2.17**	**8.73**
	Chloride and phenol 2	**Cl^{22}--O^{47}-H^{48}**	**2.15**	**9.00**
DES1_C	Chloride and choline	Cl^{22}--C^{6}-H^{7}	2.54	2.83
		Cl^{22}--C^{18}-H^{20}	2.66	2.32
		Cl^{22}--C^{14}-H^{15}	2.63	2.04
	Chloride and phenol 1	**Cl^{22}--O^{34}-H^{35}**	**2.13**	**10.21**
	Chloride and phenol 2	**Cl^{22}--O^{47}-H^{48}**	**2.10**	**14.77**
	Phenol 2 and choline	**O^{47}--O^{1}-H^{2}**	**1.96**	**4.74**

2.3.4 Cluster 1: DES 1 {[Choline][Chloride]:Phenol} [1:2] and water

The molecules composing cluster 1 have been placed in various positions before optimization to test as many interactions as possible and derive the most stable conformations. The eight conformations with the lowest energies are gathered in **Table S.A8** and the first three are presented in **Figure 2.4**. The molecule of water is the smallest fragment of the system after the chloride and was able to adopt diverse positioning, forming a hydrogen bond with the chloride ion in only two of the conformations, namely Cluster1_C and Cluster1_G.

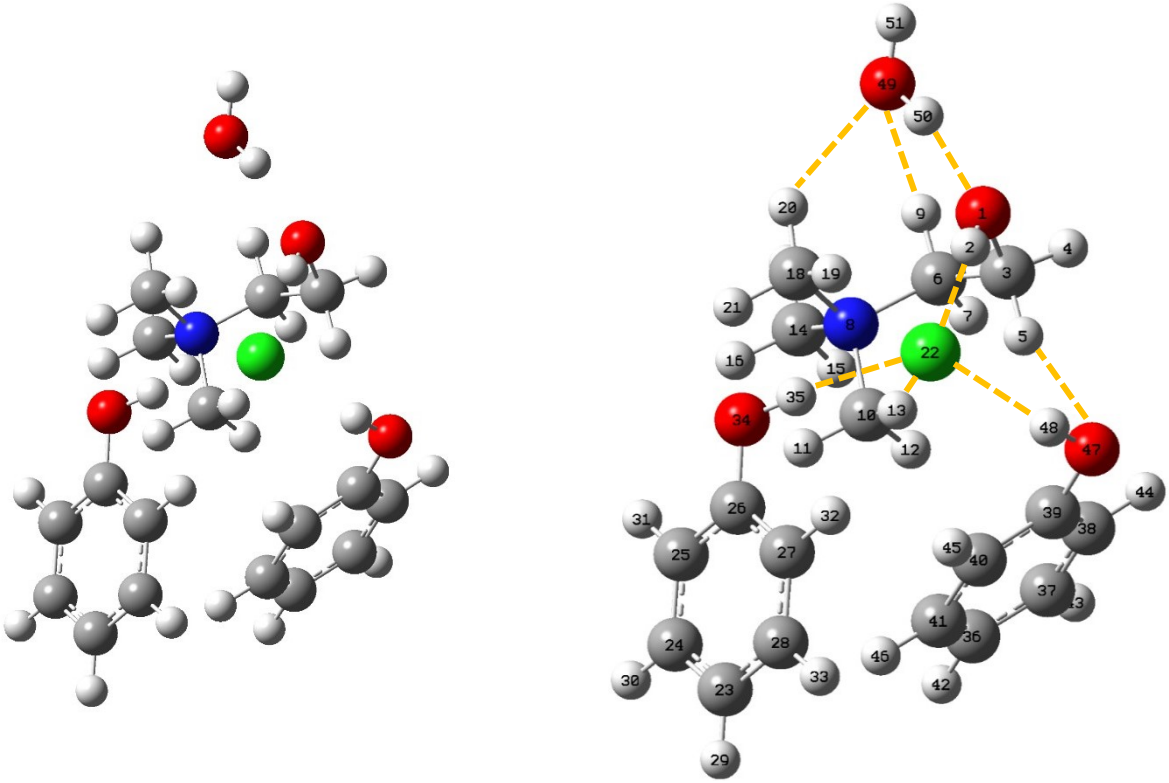

Cluster1_A, $\Delta \boldsymbol{E} = \mathbf{0.000}$ kJ.mol^{-1}

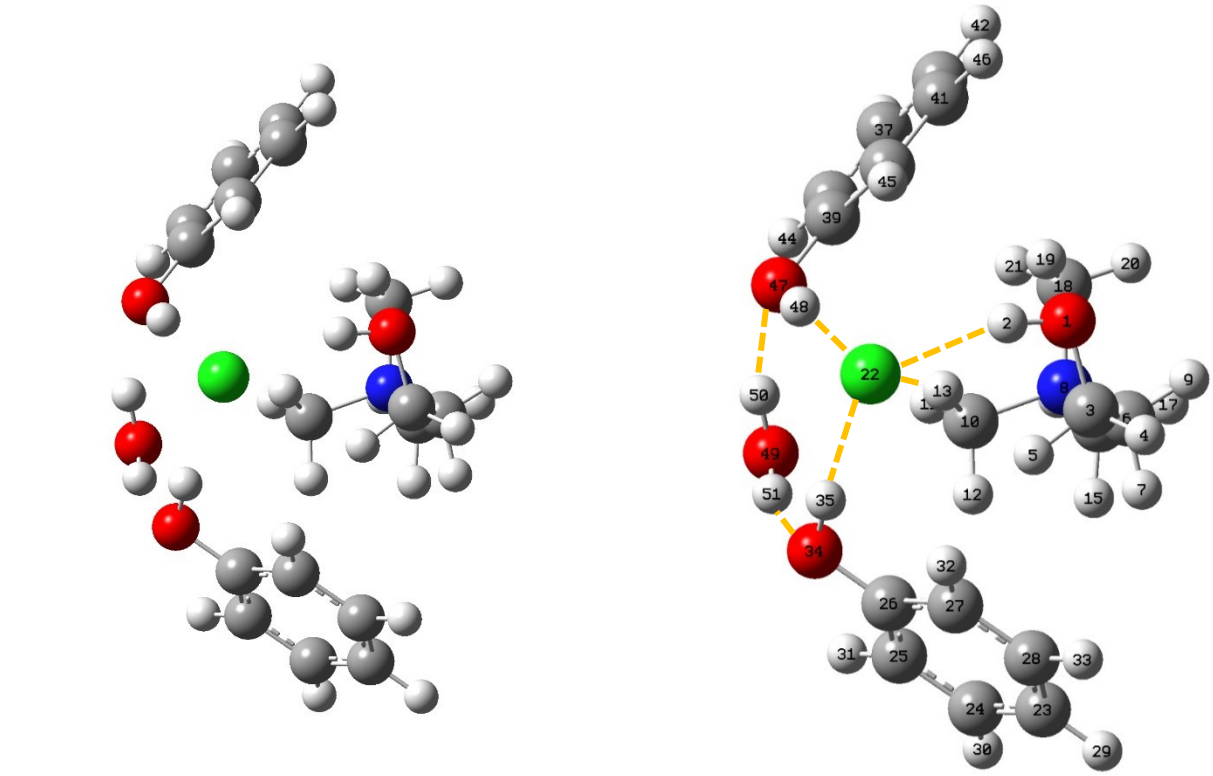

Cluster1_B, $\Delta \boldsymbol{E} = \mathbf{1.003}$ kJ.mol^{-1}

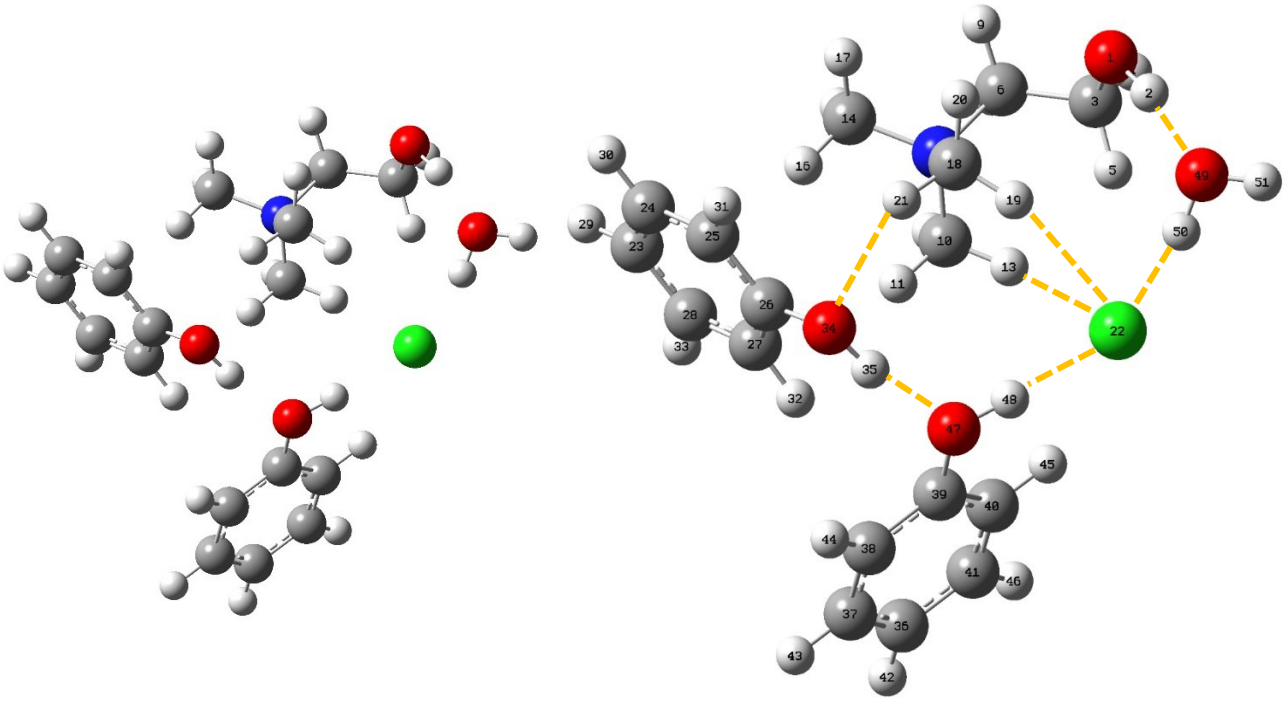

Cluster1_C, $\Delta \boldsymbol{E} = \mathbf{1.927}$ kJ.mol^{-1}

Figure 2.4. 3D representations of the three most stable conformations of cluster 1 {Choline chloride:Phenols} + Water with the main hydrogen bonds as yellow dash lines

Cluster1_A is derived from DES1_A with the molecule of water positioned over the choline ion so that the oxygen atom O^1 from the hydroxyl group of choline can accept a hydrogen bond from water. This way, the molecule of water assumes both roles of HBD and HBA, interacting also with hydrogen atoms from CH_2 and CH_3 groups from the choline. The Cluster1_B conformation corresponds to DES1_B with the molecule of water placed so that it acts solely as a HBD and interacts with both molecules of phenol. A structure combining the positioning of the molecule of water in Cluster1_A and the conformation DES1_B has also been obtained, called Cluster1_F. Remarkably, it has the lowest value of free energy G despite having a higher relative energy compared to Cluster 1_A and Cluster1_B. Compared to Cluster1_F, the conformation of the DES in Cluster1_A is more stable as seen in the previous section while in Cluster1_B, the molecule of water was able to adopt a more stabilizing position. This underlines the balance between the importance of the initial stability of the components of the cluster and the new possibilities of stabilisation introduced with the formation of the cluster. In particular, the water molecule has adopted the positioning above the hydroxyl group of choline in three conformations (Cluster1_A, Cluster1_E and Cluster1_F) and was placed so that it could interact with the hydroxyl group of the molecules of phenol in also three conformations (Cluster1_B, Cluster1_D and Cluster1_H). In contrast, the chloride ion has adopted less variable positioning, remaining mainly at the centre of cluster 1. Specifically, in the Cluster1_C conformation the clamp around the chloride ion is formed by water, the second molecule of phenol and hydrogen atoms from methyl groups belonging to the choline ion. This is the conformation in which the molecule of water had the most impact on the configuration of the DES. The water was inserted between the choline and the chloride, causing the $Cl\text{--}OH^{choline}$ interaction to disappear. The first molecule of phenol acts as a HBD for the second phenol. This interaction is found in three conformations out of the eight in **Table S.A8** (Cluster1_C, Cluster1_D and Cluster1_E). Every time, the molecules of phenol are in

perpendicular planes because of steric hindrance. This is also consistent with the work of Słupek et al. [33] who studied a DES formed with choline chloride, two molecules of phenol and one molecule of dimethyl disulphide. Using diagrams of electron density, they noted the repulsive effect between the benzene rings of the molecules of phenol. Cluster1_A and Cluster1_B have close energy values while Cluster1_C has a relative energy around 1.9 kJ.mol^{-1}. Therefore, these conformers have a comparable stability. In all three most stable conformations of cluster 1, choline has adopted the gauche conformations, and the ion pair formation ChCl_A is maintained in both Cluster1_A and B. In fact, only the least stable conformation Cluster1_H out of the eight does not comprise a gauche choline. The binding energy $\Delta E_b^{cluster1}$ using Cluster1_A is equal to -34.47 kJ.mol^{-1}. It has been reduced compared to ΔE_b^{DES1} with the addition of water.

Table 2.3 presents the main hydrogen bonds for the three most stable conformations. Cluster1_A retains the same interactions from the conformation DES1_A, mostly related to the chloride ion. They have similar lengths and stabilization energies, apart from the energy of the interaction between the chloride ion and the first molecule of phenol that dropped from 13.76 to 9.17 kJ.mol^{-1}. It is possible that a redistribution of the effect of stabilization has occurred with the addition of water. The interaction between the oxygen of the choline O^1 and the hydrogen of water H^{51} is the weakest of the main hydrogen bonds of Cluster1_A with an energy of 5.49 kJ.mol^{-1} while also being the shortest (1.86 Å). This is consistent with the fact that the chloride ion is more negatively charged and results in stronger hydrogen bonds compared to the oxygen of choline. Besides, the chloride ion is submitted to more interactions than O^1, resulting in steric hindrance between the HBDs and longer hydrogen bonds. In the conformation Cluster1_B, the same interactions as DES1_B can be found. However, the interactions between the chloride and the molecules of phenol have a higher energy in Cluster1_B, going from 8.73 and 9.00 kJ.mol^{-1} to 10.24 and 12.76 kJ.mol^{-1}. A possible explanation is that the addition of

water caused the oxygen atoms from the phenol molecules to be less electronegative towards the hydrogen atoms, which in turn get more attracted to the chloride ion. Along with the increase in stabilizing energy, the length of the bonds Cl^{22}--O^{34}-H^{35} and Cl^{22}--O^{47}-H^{48} decreased, going from 2.17 and 2.15 Å to 2.14 and 2.10 Å, respectively. In contrast, the hydrogen bonds between water and the oxygen atoms of the phenol molecules are shorter (around 2.00 Å) and weaker (between 2.68 and 3.50 $kJ.mol^{-1}$). They are also weaker compared to the main hydrogen bond O^{1}-- O^{49}-H^{51} with water as HBD and choline as HBA in Cluster1_A. The highest stabilization energy of Cluster1_C occurs between the chloride and the second molecule of phenol with 22.31 $kJ.mol^{-1}$. The other main hydrogen bonds correspond to the Cl--OH^{water} interaction, the bond between the two molecules of phenol and the interaction between water and choline. The strongest interactions with water occur in Cluster1_C. Due to its position, the first molecule of phenol displays weak interactions with the methyl groups of choline. Cluster1_C also has a phenol--phenol interaction (O^{47}--O^{34}-H^{35}) with a stabilization energy of 11.47 $kJ.mol^{-1}$. This way, the second molecule of phenol acts both as a HBA and a HBD. This bond O^{47}-- O^{34}-H^{35} and the bond O^{49}-- O^{1}-H^{2} between the water and the choline correspond to the shortest hydrogen bonds to be formed in cluster 1 with a length of 1.77 Å. The difference in stability between Cluster1_A and Cluster1_C does not seem to be explainable with hydrogen bonds only, and could originate from ionic contributions or steric effects instead.

Overall, the addition of the molecule of water led to the formation of short bonds (between 1.77 and 2.03 Å) in all three conformations of cluster 1. In the first two clusters, the water positioned itself in a way it could maximize the stabilization effect via hydrogen bonds without modifying the conformation of the DES. In the third conformation, the water caused the formation of a new organisation of the molecules. It resulted in the disappearance of the traditional Cl--$OH^{choline}$ bond and the formation of the strongest hydrogen bond involving phenol in this work. Nonetheless, the Cl--OH type of hydrogen bond remained the overall most

frequent interaction. In particular, all of the conformations exhibit a Cl--$OH^{phenol\ 2}$ bond. In each conformation, at least one molecule of phenol acts both as a HBA and a HBD, interacting with hydrogen atoms from the choline in Cluster1_A, water in Cluster1_B and another phenol in Cluster1_C.

Table 2.3. Main interactions between the NBOs (LP → BD*) of hydrogen bonds within the three most stable conformations of cluster 1

Conformation	Units involved	Hydrogen bond	Length (Å)	Stabilization energy $E^{(2)}$ ($kJ.mol^{-1}$)
Cluster1_A	Choline and water	**O^{1}-- O^{49}-H^{51}**	**1.86**	**5.49**
	Chloride and choline	**Cl^{22}--O^{1}-H^{2}**	**2.13**	**9.81**
		Cl^{22}--C^{10}-H^{13}	2.61	2.93
	Chloride and phenol 1	**Cl^{22}--O^{34}-H^{35}**	**2.16**	**9.17**
	Chloride and phenol 2	**Cl^{22}--O^{47}-H^{48}**	**2.23**	**5.86**
	Phenol 2 and choline	O^{47}-- C^{3}-H^{5}	2.42	1.09
	Water and choline	O^{49}-- C^{6}-H^{9}	2.37	0.87
		O^{49}-- C^{18}-H^{20}	2.41	0.70
Cluster1_B	Chloride and choline	**Cl^{22}--O^{1}-H^{2}**	**2.19**	**5.25**
		Cl^{22}--C^{10}-H^{13}	2.65	2.09
	Chloride and phenol 1	**Cl^{22}--O^{34}-H^{35}**	**2.14**	**10.24**
	Chloride and phenol 2	**Cl^{22}--O^{47}-H^{48}**	**2.10**	**12.76**
	Phenol 1 and water	O^{34}-- O^{49}-H^{51}	2.03	2.68
	Phenol 2 and water	O^{47}-- O^{49}-H^{50}	1.99	3.50

Cluster1_C	Chloride and choline	Cl^{22}--C^{10}-H^{13}	2.48	4.53
		Cl^{22}--C^{18}-H^{19}	2.65	1.93
	Chloride and phenol 2	**Cl^{22}--O^{47}-H^{48}**	**2.05**	**22.31**
	Chloride and water	**Cl^{22}--O^{49}-H^{50}**	**2.12**	**7.86**
	Phenol 1 and choline	O^{34}-- C^{18}-H^{21}	2.44	0.80
	Phenol 2 and Phenol 1	**O^{47}-- O^{34}-H^{35}**	**1.77**	**11.47**
	Water and choline	**O^{49}-- O^{1}-H^{2}**	**1.77**	**16.80**

2.3.5 {[Choline][Chloride]:Glycolic acid} [1:1]

An optimization of the isolated molecule of glycolic acid is presented in the supporting information (section 7) along with charge distributions matching the calculations from van den Bruinhorst et al. [42]. Glycolic acid comprises both a carboxyl group and a hydroxyl group. They introduce three oxygen and at least two hydrogen atoms that can form hydrogen bonds and interact with choline chloride. Several inputs were tried out in order to maximize the number of interactions within the DES and the results of the eight most stable conformations are gathered in **Table S.A12**.

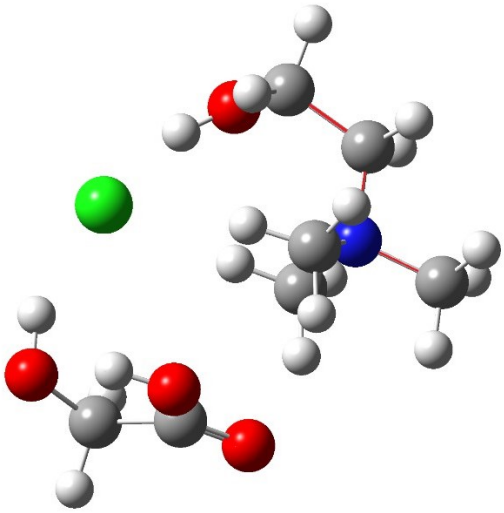

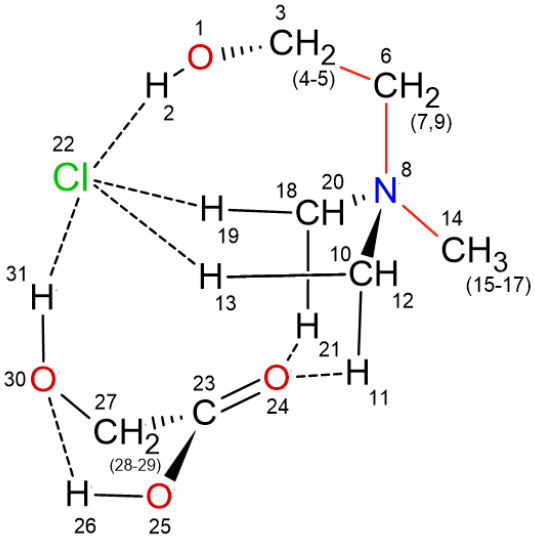

DES2_A, $\Delta E = 0.000$ kJ.mol^{-1}

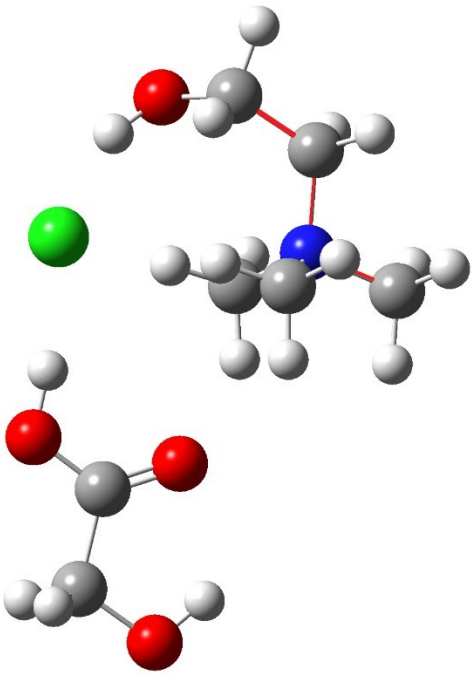

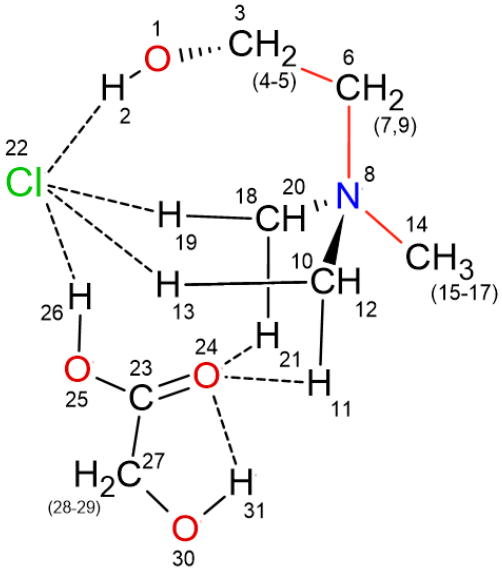

DES2_B, $\Delta E = 0.585$ kJ.mol^{-1}

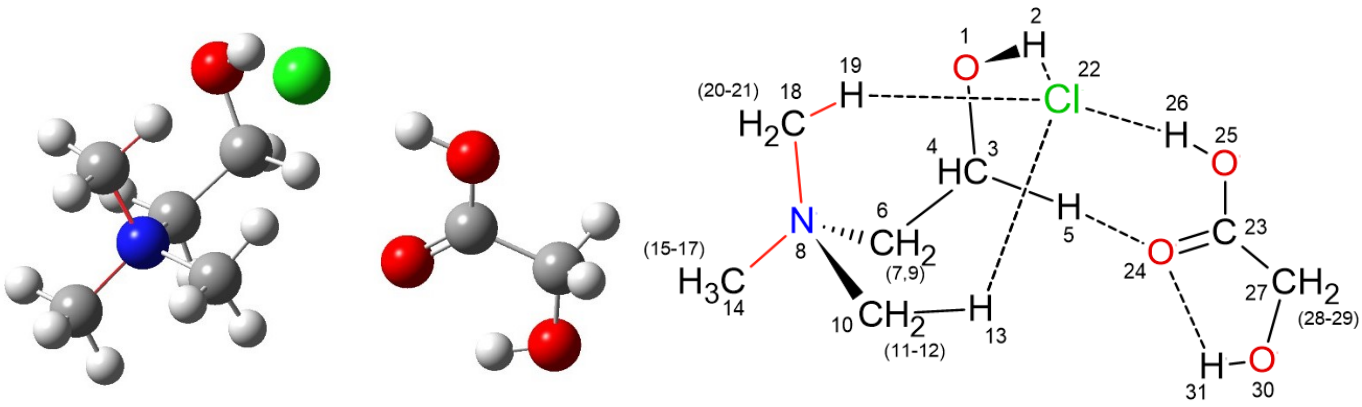

DES2_C, $\Delta E = 3.736$ kJ.mol^{-1}

Figure 2.5. 3D and schematic representations of the three most stable conformations of DES 2 {[Choline][Chloride]:Glycolic acid} [1:1] with the main hydrogen bonds as dashed lines - Red bonds are here as a key visual for the central plane of the choline cation

The three most stable conformations of DES 2, shown in **Figure 2.5**, are all derived from the gauche conformation of choline with the glycolic acid completing the clamp formation around the chloride ion. When comparing the conformations, the glycolic acid is orbiting around the chloride ion while maximizing the interactions that can be formed with choline. Hence, it acts both as a hydrogen bond donor and a hydrogen bond acceptor. With the chloride ion, the glycolic acid creates each time a single main hydrogen bond using a hydrogen from a OH group, from the alcohol group for DES2_A and from the carboxyl group for DES2_B and DES2_C. Between DES2_B and DES2_C, the molecule of glycolic acid has rotated 90°. Despite having the lowest energy, the conformation DES2_A has the highest free energy G. Overall, conformations DES2_A and DES2_B have very close energy values with the relative energy of DES2_B being less than 1 kJ.mol^{-1}, indicating that they are of equivalent stability. They also both display hydrogen bonds between the oxygen from the C^{23}=O^{24} part of the carboxyl group and hydrogen atoms from the methyl groups of the choline ion. On the other hand, the oxygen O^{24} of DES2_C interacts with the hydrogen H^5 from the CH_2 group of choline. Since H^5 is less positively charged compared to the hydrogen atoms from the methyl groups as seen in the charge distribution of choline, the resulting interaction is less favourable which is consistent

with the higher value of relative energy of DES2_C, namely 3.74 kJ.mol^{-1}. The binding energy ΔE_b^{DES2} calculated using conformation DES2_A has a value of -78.68 kJ.mol^{-1}. Compared to the systems previously investigated, the value of the binding energy continues to get closer to zero as the number of hydrogen bonds increases.

The main orbital interactions for the hydrogen bonds in DES 2 can be found in **Table 2.4** along with the corresponding distances and stabilization energies. The most stabilizing hydrogen bonds of DES2_A involve the chloride anion and the hydroxyl groups from both the choline and the glycolic acid with stabilization energies of 11.63 and 12.55 kJ.mol^{-1}, respectively. In comparison, the resonance stabilization occurring via the delocalization of the electrons within the carboxyl group (LP O^{25} → BD* C^{23}=O^{24}) is higher, reaching 43.99 kJ.mol^{-1}. The third main hydrogen bond in DES2_A is the intramolecular bond within the glycolic acid with a stabilization energy of 7.82 kJ.mol^{-1}. Unlike the balanced repartition of energy for DES2_A, the conformation DES2_B displays one main stabilizing energy value of 30.94 kJ.mol^{-1} for the hydrogen bond between the chloride and the OH group of the carboxyl group. The other interactions are less impactful, though the usual choline chloride Cl--O^1H^2 interaction has a value of 6.81 kJ.mol^{-1}. For DES2_C, the main hydrogen bond is found to be between the chloride anion and the OH of the group carboxyl with the value of 33.12 kJ.mol^{-1}. DES2_C also has a noteworthy Cl--O^1H^2 interaction of 12.79 kJ.mol^{-1}. Hence, the two most stable conformations do not have the strongest interactions in terms of stabilization energy. However, a reason explaining the stability of DES2_A could be that it presents the strongest stabilization through the intramolecular hydrogen bond within the glycolic acid, with a stabilization energy three times higher compared to the other two conformations. This hydrogen bond is also the shortest of the bonds (1.91 Å) presented in **Table 2.4**.

Although no DFT study of the same DES has been found in the literature, some authors investigated DESs made with carboxylic acids and choline chloride. Gautam et al. [11] studied

acetic and formic acids and observed that they formed strong hydrogen bonds with the chloride ion. They also noted that choline can act as a HBD with the acids, the double-bonded atom of oxygen from the carboxyl group forming a hydrogen bond with the hydrogen from the methyl groups of choline. This is similar to what is observed in the conformations of DES 2 in this work.

Finally, in spite of the addition of the glycolic acid, the choline chloride main interaction $Cl\text{--}OH^{choline}$ is retained. It is only in the eighth most stable conformation that this interaction disappears. Instead, the DES2_H conformation displays the choline directing the hydrogen of its hydroxyl group toward an oxygen of the glycolic acid.

Table 2.4. Main interactions between NBOs LP → BD* of hydrogen bonds within the three most stable conformations of DES 2

Conformation	Units involved	Hydrogen bond	Length (Å)	Stabilization energy $E^{(2)}$ ($kJ.mol^{-1}$)
DES2_A	Chloride and choline	**$Cl^{22}\text{--}O^{1}\text{-}H^{2}$**	**2.17**	**11.63**
		$Cl^{22}\text{--}C^{18}\text{-}H^{19}$	2.53	2.97
		$Cl^{22}\text{--}C^{10}\text{-}H^{13}$	2.50	2.86
	Chloride and glycolic acid	**$Cl^{22}\text{--}O^{30}\text{-}H^{31}$**	**2.14**	**12.55**
	Glycolic acid and choline	$O^{24}\text{--}C^{18}\text{-}H^{21}$	2.31	0.64
		$O^{24}\text{--}C^{10}\text{-}H^{11}$	2.43	0.52
	Glycolic acid (intra)	**$O^{30}\text{--}O^{25}\text{-}H^{26}$**	**1.91**	**7.82**
DES2_B	Chloride and choline	**$Cl^{22}\text{--}O^{1}\text{-}H^{2}$**	**2.17**	**6.81**
		$Cl^{22}\text{--}C^{18}\text{-}H^{19}$	2.52	3.72
		$Cl^{22}\text{--}C^{10}\text{-}H^{13}$	2.45	3.62
	Chloride and glycolic acid	**$Cl^{22}\text{--}O^{25}\text{-}H^{26}$**	**1.98**	**30.94**

	Glycolic acid and choline	O^{24}--C^{18}-H^{21}	2.38	0.44
		O^{24}--C^{10}-H^{11}	2.35	0.65
	Glycolic acid (intra)	O^{24}--O^{30}-H^{31}	2.07	2.83
DES2_C	Chloride and choline	**Cl^{22}--O^{1}-H^{2}**	**2.16**	**12.79**
		Cl^{22}--C^{18}-H^{19}	2.51	1.54
		Cl^{22}--C^{10}-H^{13}	2.50	3.52
	Chloride and glycolic acid	**Cl^{22}--O^{25}-H^{26}**	**1.98**	**33.12**
	Glycolic acid and choline	O^{24}--C^{3}-H^{5}	2.35	1.07
	Glycolic acid (intra)	O^{24}--O^{30}-H^{31}	2.07	2.87

2.3.6 Cluster 2: DES 2 {[Choline][Chloride]:Glycolic acid} [1:1] and water

The initial inputs consisted of placing water around the different conformations of DES 2 to see how the interactions were impacted and which stable conformations could be derived. The eight most stable results are presented in **Table S.A14**. The three of the conformations with the lowest relative energy can be found in **Figure 2.6**.

Cluster2_A corresponds to the conformation DES2_A for which a molecule of water has been added under the tetrahedron structure of the choline. As a result, the molecule of glycolic acid has been slightly shifted to permit the water to create hydrogen bonds with the hydrogen of the alkyl groups of the choline ion. This is in line with the fact that these hydrogen atoms are the most positively charged hydrogen bar the one from the hydroxyl group as seen in the charge distribution of choline. Cluster2_B also corresponds to the conformation DES2_A, although this time the molecule of water has been inserted between the choline and the chloride

ions. Consequently, the dihedral C-O-O-H of the choline has rotated to favour the hydrogen bond with the oxygen of water while the traditional Cl--OH^{choline} bond disappeared in the process. Cluster2_C consists of a modification of DES2_B with the added molecule of water joining the clamp formation around the chloride ion on a side of the choline cation. Despite the addition of water, the two most stable conformations of DES 2 remain predominant. As a matter of fact, among the eight more stable conformations of cluster 2, four are derived from the DES2_A structure (clusters A, B, D and F) and three from DES2_B (clusters C, E and H). Only cluster2_G corresponds to another organisation of the molecules, with a gauche choline and water surrounding the chloride ion while the glycolic acid has moved around to form a hydrogen bond with the atom of oxygen from the choline. Using the conformation of Cluster2_A, the binding energy $\Delta E_b^{cluster2}$ is around -20.55 kJ.mol^{-1}.

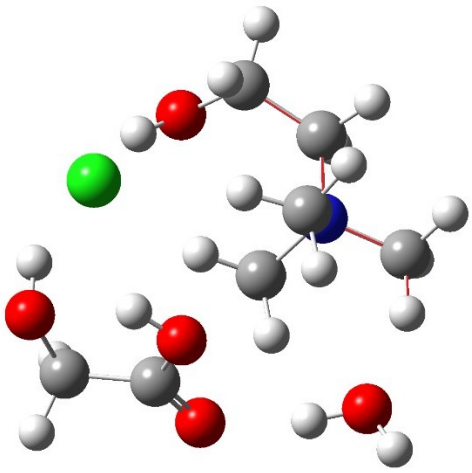

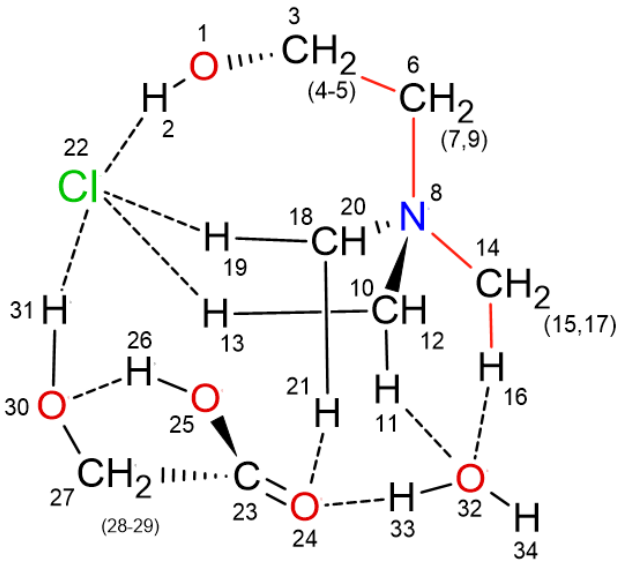

Cluster2_A, $\Delta E = 0.000$ kJ.mol^{-1}

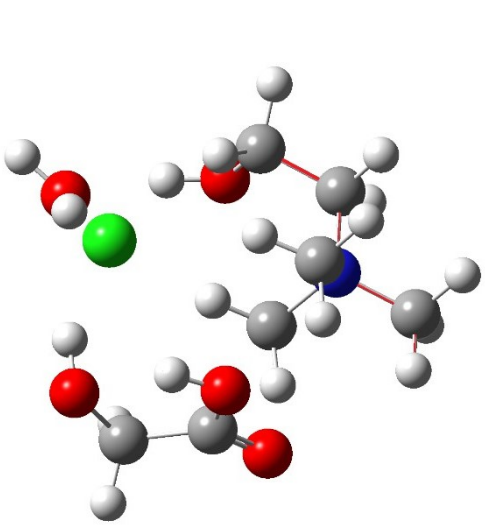

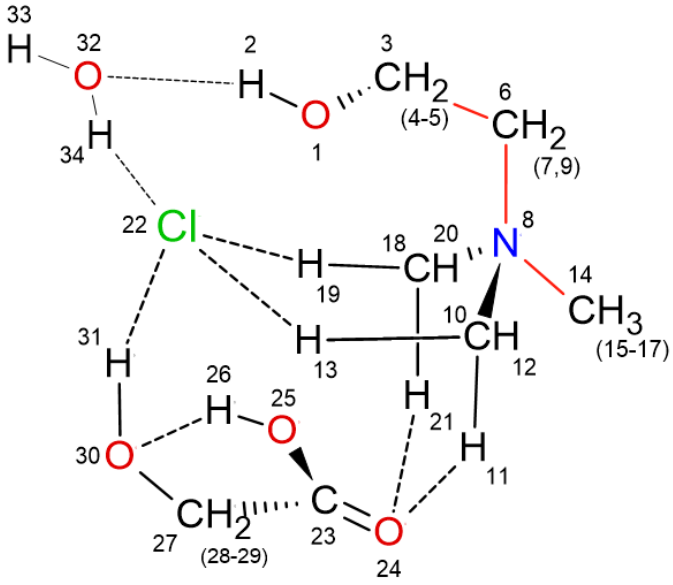

Cluster2_B, $\Delta E = 1.738$ kJ.mol^{-1}

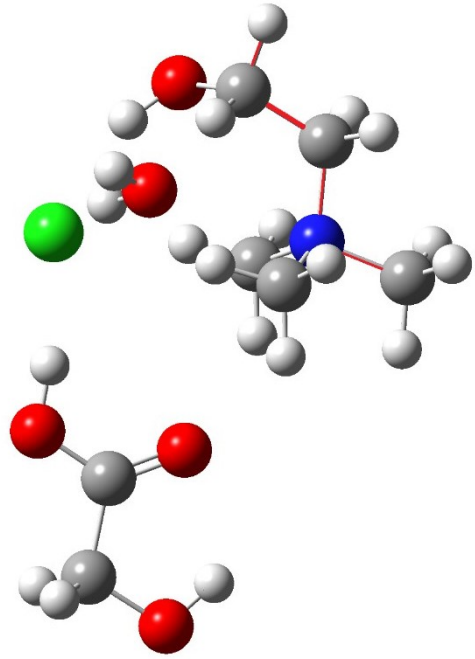

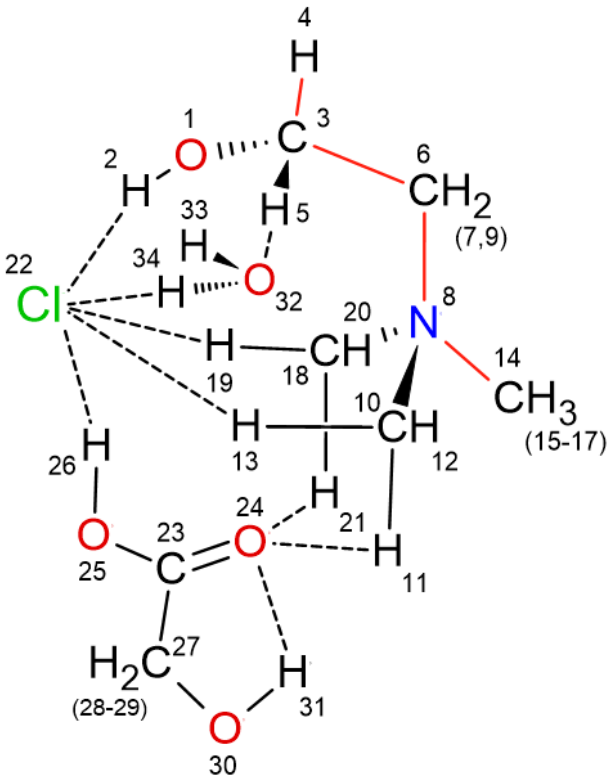

Cluster2_C, $\Delta E = 4.421$ kJ.mol^{-1}

Figure 2.6. 3D and schematic representations of the three most stable conformations of Cluster 2 {Choline chloride:Glycolic acid} [1:1] + Water with the main hydrogen bonds as dashed lines - Red bonds are here as a key visual for the central plane of the choline cation

The main orbital interactions for the hydrogen bonds in the conformations A, B and C of cluster 2 are presented in **Table 2.5**. Cluster2_A shows two main stabilizing interactions between the chloride ion and the hydroxyl groups from the choline and the glycolic acid with energies of 10.58 and 14.28 kJ.mol^{-1}, respectively. The other main hydrogen bonds are the intramolecular bond within the glycolic acid (the strongest of the kind compared to the other two conformations) and the interaction between a lone pair of an oxygen atom from the carboxyl group and a hydrogen of water O^{24}--O^{32}-H^{33}. This interaction with water results in the shortest bond of Cluster1_A with a length of 1.80 Å. Cluster2_B lacks the usual Cl--$OH^{choline}$ interaction which has been replaced by a strong bond of 17.08 kJ.mol^{-1} between water and choline. This corresponds to the shortest hydrogen bond (1.77 Å) of all conformations of cluster 2 and the strongest that involves water, being the only one in which water receives a hydrogen bond from a hydroxyl group. Cluster2_C has the weakest intramolecular hydrogen bond in the glycolic acid with a value of 2.73 kJ.mol^{-1}, as well as a weaker Cl--$OH^{choline}$ interaction compared to Cluster2_A. This observation is consistent with the observations in the section dedicated to DES 2. Cluster2_C maintains the interaction between the chloride ion and a hydroxyl group of the glycolic acid. This is the bond with the highest energy of Cluster2_C with a value of 26.68 kJ.mol^{-1}, which is only a bit lower compared to the energy of the same bond in DES2_B (30.94 kJ.mol^{-1}). However, Cluster2_C is the conformation with the least stabilizing interactions with water. Comparing the stabilizing energy of the interaction for which water plays the role of HBD, the corresponding energy in reaches 6.79 kJ.mol^{-1} in Cluster2_C against 9.39 kJ.mol^{-1} and 10.36 kJ.mol^{-1} in Cluster2_A and Cluster2_B, respectively.

Table 2.5. Main interactions between NBOs LP → BD* of hydrogen bonds within the three most stable conformations of cluster 2

Conformation	Units involved	Hydrogen bond	Length (Å)	Stabilization energy $E^{(2)}$ ($kJ.mol^{-1}$)
Cluster2_A	Chloride and choline	**Cl^{22}--O^{1}-H^{2}**	**2.17**	**10.58**
		Cl^{22}--C^{18}-H^{19}	2.59	2.48
		Cl^{22}--C^{10}-H^{13}	2.54	2.23
	Chloride and glycolic acid	**Cl^{22}--O^{30}-H^{31}**	**2.11**	**14.28**
	Glycolic acid and choline	O^{24}--C^{18}-H^{21}	2.59	0.14
	Glycolic acid (intra)	**O^{30}--O^{25}-H^{26}**	**1.90**	**8.26**
	Glycolic acid and water	**O^{24}--O^{32}-H^{33}**	**1.80**	**9.39**
	Water and choline	O^{32}--C^{14}-H^{16}	2.20	3.28
		O^{32}--C^{10}-H^{11}	2.45	0.80
Cluster2_B	Chloride and choline	Cl^{22}--C^{18}-H^{19}	2.64	2.21
		Cl^{22}--C^{10}-H^{13}	2.50	1.95
	Chloride and glycolic acid	**Cl^{22}--O^{30}-H^{31}**	**2.13**	**11.01**
	Chloride and water	**Cl^{22}--O^{32}-H^{34}**	**2.11**	**10.36**
	Glycolic acid and choline	O^{24}--C^{18}-H^{21}	2.29	0.69
		O^{24}--C^{10}-H^{11}	2.41	0.47
	Glycolic acid (intra)	**O^{30}--O^{25}-H^{26}**	**1.91**	**7.67**
	Water and choline	**O^{32}--O^{1}-H^{2}**	**1.77**	**17.08**
Cluster2_C	Chloride and choline	**Cl^{22}--O^{1}-H^{2}**	**2.21**	**5.13**
		Cl^{22}--C^{18}-H^{19}	2.58	1.81
		Cl^{22}--C^{10}-H^{13}	2.57	3.11

	Chloride and glycolic acid	**Cl^{22}--O^{25}-H^{26}**	**2.02**	**26.68**
	Chloride and water	**Cl^{22}--O^{32}-H^{34}**	**2.21**	**6.79**
	Glycolic acid and choline	O^{24}--C^{18}-H^{21}	2.37	0.54
		O^{24}--C^{10}-H^{11}	2.39	0.48
	Glycolic acid (intra)	O^{24}--O^{30}-H^{31}	2.07	2.73
	Water and choline	O^{32}--C^{3}-H^{5}	2.41	2.23

.

Although the chloride ion remained the centre of the stabilization of the cluster, all three of the available hydroxyl groups of the cluster did not always elect to form a hydrogen bond with the anion. Half of the eight conformations of cluster 2 have a chloride ion forming three Cl--OH bonds, the other half (including Cluster2_A and B) having only two. However, a Cl--OH interaction is always the one with the highest stabilizing interaction for all three most stable conformations, and water interacts with the chloride ion in six out of the eight conformations. Thus, the addition of water induced deep modification of the organisation of DES 2 in only two conformations (Cluster2_C and Cluster2_G). Water is also involved in the shortest hydrogen bonds of the two most stable conformations. Finally, all the conformations maintain hydrogen bonds between the double bonded oxygen from the carboxyl group and hydrogen atoms from the methyl groups of choline. That way, the glycolic acid keeps both roles of HBA and HBD.

2.3.7 Comparison between the two DESs

Despite having different numbers of components and different numbers of hydrogen bonding groups, the DESs {[Choline][Chloride]:Phenol} ratio [1:2] and {[Choline][Chloride]:Glycolic acid} ratio [1:1] are both choline chloride-based and present

comparable structures. Both displayed hydrogen from hydroxyl groups organised like a clamp around the chloride ion with similar lengths (roughly between 2 and 2.5 Å) and a choline ion with a primarily gauche conformation. Regarding the stabilizing energies from the natural orbital analysis, the DES containing the glycolic acid was the one with the overall higher energies, with some values reaching over 30 $kJ.mol^{-1}$ against 20 $kJ.mol^{-1}$ for the conformations of the DES made of phenol molecules. This in turn can be related to the binding energy of the systems. All binding energies are gathered in the **Table S.A17**. The binding energies are observed to be decreasing with an increasing number of hydrogen bonds. For the DESs studied in this work, the glycolic acid is able to form various hydrogen bonds with three potential hydrogen bonding groups. On the other hand, the molecules of phenol are limited with the number of hydrogen bonds they can form due to steric effects and having only one hydroxyl group each. Thus, the DES with the two molecules of phenol is expected to form less hydrogen bonds compared to the DES with the glycolic acid. The binding energies of the systems involving the glycolic acid are lower compared to the binding energies of the systems with phenol molecules.

The formation of hydrogen bonds can be related to physicochemical properties such as density and viscosity [64] as well. An increase in density values can notably be observed with an increasing number of hydrogen bonds in a system. In terms of density, Zhu et al. [65] measured the density of DES 1 from 293.15 to 333.15 K and obtained values ranging from 1.10 to 1.07 $g.cm^{-3}$. At the same temperatures, the densities measured by Florindo et al. [9] for DES 2 ranges from 1.20 to 1.18 $g.cm^{-3}$. The higher values for the DES containing the glycolic acid are consistent with a greater number of hydrogen bonds compared to DES 1. Moreover, compared to the DES made of phenol, the stabilizing energies of DES 2 reach higher values, indicating overall stronger hydrogen bonds. This can be correlated to the values of viscosity of the two DESs that are found in the literature. According to Guo et al. [66], the viscosity of the DES

{[Choline][Chloride]:Phenol} ratio [1:2] ranges from 0.034 to 0.12 Pa.s for temperatures from 318.2 to 293.2 K. At the same temperatures, Florindo et al. [9] measured viscosities between 0.167 and 0.7794 Pa.s for the DES {[choline][chloride]:glycolic acid} ratio [1:1]. Thus, higher values of viscosities are consistent with stronger hydrogen bonds.

The formation of the clusters by addition of water logically resulted in an increase in the number of hydrogen bonds. In most cases, the molecule of water ended positioned around an existing conformation of DES, optimizing the number of hydrogen bonds that can be created, being equally able to interact with the chloride, the choline, the phenols and the glycolic acid. However, it was able to disrupt the most stabilizing interactions within the DESs, as seen when water gets inserted between the choline cation and the chloride ion in Cluster 1_C and in Cluster2_B. In both clusters 1 and 2, the water is the source of the shortest hydrogen bonds of the systems (around 1.8 Å), although the strongest interactions often stem from the chloride ion. In particular, the Cl--$OH^{choline}$ bond inherited from the choline chloride ion pair conformation was observed in almost all of the conformations of the clusters bar two. However, as more molecules are added, a progressive weakening of the Cl--$OH^{choline}$ bond in favour of other hydrogen bonds can be observed, notably of the Cl--OH type. In spite of this, not all of the available hydroxyl groups will necessarily interact with the chloride ion. Regarding the most stable conformations of both clusters, there is almost always one of the molecules with a hydroxyl group that will not form a strong hydrogen bond with the chloride ion. The only exception is Cluster2_C. For the other conformations, either the molecule of water will interact with another HBD (Cluster1_A, Cluster1_B, Cluster2_A) or it will be inserted between one HBD and the chloride ion, acting both as a HBD and a HBA (Cluster1_C and Cluster2_B).

2.4 Conclusion

In this work, DFT was used to shed light on the favoured interactions between the components of two choline chloride-based DESs: the {[Choline][Chloride]:Phenol}, ratio [1:2] and the {[Choline][Chloride]:Glycolic acid}, ratio [1:1]. Furthermore, the goal was to see how the addition of a molecule of water could disrupt and modify these interactions. The optimization of the geometries established the gauche conformation of choline as the most stable and favourable, with Cl--$OH^{choline}$ being the most stabilizing interaction. The study of the DESs confirmed that there is a higher probability to encounter Cl--OH interactions compared to OH--OH as more of the formers are found in the most stable conformations of the DESs. With the addition of water, the Cl--OH interactions remain predominant. Nevertheless, a molecule of water is able to get inserted between the chloride ion and another HBD thanks to its small size. This complements the capacity of glycolic acid and phenol to act both as HBD and HBA while chloride plays the role of HBD and choline primarily the one of HBD. However, the addition of water did not have any impact on the conformation of choline in itself since the gauche conformations remained the most frequent to be observed. Finally, the greater the number of hydrogen bonds, the weaker the individual interactions and the lower the binding energy become.

This work represents a first step and a more comprehensive study could allow to get a better depiction of the interactions between the molecules of DESs and water. In particular, the addition of more molecules of water by means of molecular dynamics would allow to investigate systems containing many more molecules and more complex and varied interactions.

References

[1] A.P. Abbott, G. Capper, D.L. Davies, R.K. Rasheed, V. Tambyrajah, Novel solvent properties of choline chloride/urea mixturesElectronic supplementary information (ESI) available: spectroscopic data. See http://www.rsc.org/suppdata/cc/b2/b210714g/, Chem. Commun. (2003) 70–71. https://doi.org/10.1039/b210714g.

[2] A.P. Abbott, D. Boothby, G. Capper, D.L. Davies, R.K. Rasheed, Deep Eutectic Solvents Formed between Choline Chloride and Carboxylic Acids: Versatile Alternatives to Ionic Liquids, J. Am. Chem. Soc. 126 (2004) 9142–9147. https://doi.org/10.1021/ja048266j.

[3] H.G. Morrison, C.C. Sun, S. Neervannan, Characterization of thermal behavior of deep eutectic solvents and their potential as drug solubilization vehicles, International Journal of Pharmaceutics. 378 (2009) 136–139. https://doi.org/10.1016/j.ijpharm.2009.05.039.

[4] A. Korotkevich, D.S. Firaha, A.A.H. Padua, B. Kirchner, Ab initio molecular dynamics simulations of SO 2 solvation in choline chloride/glycerol deep eutectic solvent, Fluid Phase Equilibria. 448 (2017) 59–68. https://doi.org/10.1016/j.fluid.2017.03.024.

[5] V. Alizadeh, F. Malberg, A.A.H. Pádua, B. Kirchner, Are There Magic Compositions in Deep Eutectic Solvents? Effects of Composition and Water Content in Choline Chloride/Ethylene Glycol from Ab Initio Molecular Dynamics, J. Phys. Chem. B. 124 (2020) 7433–7443. https://doi.org/10.1021/acs.jpcb.0c04844.

[6] E.S.C. Ferreira, I.V. Voroshylova, N.M. Figueiredo, C.M. Pereira, M.N.D.S. Cordeiro, Computational and experimental study of propeline: A choline chloride based deep eutectic solvent, Journal of Molecular Liquids. 298 (2020) 111978. https://doi.org/10.1016/j.molliq.2019.111978.

[7] K. Biernacki, H.K.S. Souza, C.M.R. Almeida, A.L. Magalhães, M.P. Gonçalves, Physicochemical Properties of Choline Chloride-Based Deep Eutectic Solvents with Polyols: An Experimental and Theoretical Investigation, ACS Sustainable Chem. Eng. 8 (2020) 18712–18728. https://doi.org/10.1021/acssuschemeng.0c08288.

[8] H. Moradi, N. Farzi, Experimental and computational assessment of the physicochemical properties of choline chloride/ ethylene glycol deep eutectic solvent in 1:2 and 1:3 mole fractions and 298.15–398.15 K, Journal of Molecular Liquids. 339 (2021) 116669. https://doi.org/10.1016/j.molliq.2021.116669.

[9] C. Florindo, F.S. Oliveira, L.P.N. Rebelo, A.M. Fernandes, I.M. Marrucho, Insights into the Synthesis and Properties of Deep Eutectic Solvents Based on Cholinium Chloride and Carboxylic Acids, ACS Sustainable Chem. Eng. 2 (2014) 2416–2425.

https://doi.org/10.1021/sc500439w.

[10] A. kumar Jangir, D. Patel, R. More, A. Parmar, K. Kuperkar, New insight into experimental and computational studies of Choline chloride-based 'green' ternary deep eutectic solvent (TDES), Journal of Molecular Structure. 1181 (2019) 295–299. https://doi.org/10.1016/j.molstruc.2018.12.106.

[11] R. Gautam, N. Kumar, J.G. Lynam, Theoretical and experimental study of choline chloride-carboxylic acid deep eutectic solvents and their hydrogen bonds, Journal of Molecular Structure. 1222 (2020) 128849. https://doi.org/10.1016/j.molstruc.2020.128849.

[12] O. Sethi, M. Singh, T. Singh Kang, A. Kumar Sood, Volumetric and compressibility studies on aqueous mixtures of deep eutectic solvents based on choline chloride and carboxylic acids at different temperatures: Experimental, theoretical and computational approach, Journal of Molecular Liquids. 340 (2021) 117212. https://doi.org/10.1016/j.molliq.2021.117212.

[13] T. Khezeli, A. Daneshfar, R. Sahraei, Emulsification liquid–liquid microextraction based on deep eutectic solvent: An extraction method for the determination of benzene, toluene, ethylbenzene and seven polycyclic aromatic hydrocarbons from water samples, Journal of Chromatography A. 1425 (2015) 25–33. https://doi.org/10.1016/j.chroma.2015.11.007.

[14] M.B. Arain, E. Yilmaz, M. Soylak, Deep eutectic solvent based ultrasonic assisted liquid phase microextraction for the FAAS determination of cobalt, Journal of Molecular Liquids. 224 (2016) 538–543. https://doi.org/10.1016/j.molliq.2016.10.005.

[15] F. Aydin, E. Yilmaz, M. Soylak, A simple and novel deep eutectic solvent based ultrasound-assisted emulsification liquid phase microextraction method for malachite green in farmed and ornamental aquarium fish water samples, Microchemical Journal. 132 (2017) 280–285. https://doi.org/10.1016/j.microc.2017.02.014.

[16] L. Liu, T. Zhu, Emulsification liquid–liquid microextraction based on deep eutectic solvents: an extraction method for the determination of sulfonamides in water samples, Anal. Methods. 9 (2017) 4747–4753. https://doi.org/10.1039/C7AY01332A.

[17] R.A. Zounr, M. Tuzen, M.Y. Khuhawar, Ultrasound assisted deep eutectic solvent based on dispersive liquid liquid microextraction of arsenic speciation in water and environmental samples by electrothermal atomic absorption spectrometry, Journal of Molecular Liquids. 242 (2017) 441–446. https://doi.org/10.1016/j.molliq.2017.07.053.

[18] A.H. Panhwar, M. Tuzen, T.G. Kazi, Ultrasonic assisted dispersive liquid-liquid microextraction method based on deep eutectic solvent for speciation, preconcentration and determination of selenium species (IV) and (VI) in water and food samples, Talanta. 175 (2017) 352–358. https://doi.org/10.1016/j.talanta.2017.07.063.

[19] A.H. Panhwar, M. Tuzen, T.G. Kazi, Deep eutectic solvent based advance microextraction method for determination of aluminum in water and food samples: Multivariate study, Talanta. 178 (2018) 588–593. https://doi.org/10.1016/j.talanta.2017.09.079.

[20] R.A. Zounr, M. Tuzen, M.Y. Khuhawar, Novel ultrasonic-assisted deep eutectic solvent-based dispersive liquid–liquid microextraction for determination of vanadium in food samples by electrothermal atomic absorption spectrometry: A multivariate study, Appl Organometal Chem. 32 (2018) e4144. https://doi.org/10.1002/aoc.4144.

[21] A. Shishov, A. Gorbunov, L. Moskvin, A. Bulatov, Decomposition of deep eutectic solvents based on choline chloride and phenol in aqueous phase, Journal of Molecular Liquids. 301 (2020) 112380. https://doi.org/10.1016/j.molliq.2019.112380.

[22] D. Feller, M.W. Feyereisen, Ab initio study of hydrogen bonding in the phenol-water system, J. Comput. Chem. 14 (1993) 1027–1035. https://doi.org/10.1002/jcc.540140904.

[23] F. Ramondo, L. Bencivenni, G. Portalone, A. Domenicano, Effect of intermolecular O-H ⋯ O hydrogen bonding on the molecular structure of phenol: An ab initio molecular orbital study, Struct Chem. 6 (1995) 37–45. https://doi.org/10.1007/BF02263526.

[24] M. Gerhards, M. Schmitt, K. Kleinermanns, W. Stahl, The structure of phenol(H 2 O) obtained by microwave spectroscopy, The Journal of Chemical Physics. 104 (1996) 967–971. https://doi.org/10.1063/1.470820.

[25] W.-H. Fang, Theoretical characterization of the excited-state structures and properties of phenol and its one-water complex, The Journal of Chemical Physics. 112 (2000) 1204–1211. https://doi.org/10.1063/1.480673.

[26] D.M. Benoit, D.C. Clary, Quantum Simulation of Phenol−Water Clusters, J. Phys. Chem. A. 104 (2000) 5590–5599. https://doi.org/10.1021/jp994420q.

[27] A. Lüchow, D. Spangenberg, C. Janzen, A. Jansen, M. Gerhards, K. Kleinermanns, Structure and energetics of phenol(H2O)n, n 7: Quantum Monte Carlo calculations and double resonance experiments, Phys. Chem. Chem. Phys. 3 (2001) 2771–2780. https://doi.org/10.1039/b101779i.

[28] Y. Dimitrova, Ab initio and DFT studies of the vibrational spectra of hydrogen-bonded PhOH…(H2O)4 complexes, Spectrochimica Acta Part A: Molecular and Biomolecular Spectroscopy. 60 (2004) 3049–3057. https://doi.org/10.1016/j.saa.2004.01.026.

[29] I. Bandyopadhyay, H.M. Lee, K.S. Kim, Phenol vs Water Molecule Interacting with Various Molecules: σ-type, π-type, and χ-type Hydrogen Bonds, Interaction Energies, and Their Energy Components, J. Phys. Chem. A. 109 (2005) 1720–1728. https://doi.org/10.1021/jp0449657.

[30] R. Parthasarathi, V. Subramanian, N. Sathyamurthy, Hydrogen Bonding in Phenol, Water, and Phenol−Water Clusters, J. Phys. Chem. A. 109 (2005) 843–850. https://doi.org/10.1021/jp046499r.

[31] L. Cesari, L. Canabady-Rochelle, F. Mutelet, Computational study of phenolic compounds-water clusters, Struct Chem. 29 (2018) 625–643. https://doi.org/10.1007/s11224-018-1081-9.

[32] E. Lewars, Computational chemistry: introduction to the theory and applications of molecular and quantum mechanics, 2nd ed, Springer, Dordrecht [Netherlands] ; London ; New York, 2011.

[33] E. Słupek, P. Makoś, Absorptive Desulfurization of Model Biogas Stream Using Choline Chloride-Based Deep Eutectic Solvents, Sustainability. 12 (2020) 1619. https://doi.org/10.3390/su12041619.

[34] M.I. Rain, H. Iqbal, M. Saha, M.A. Ali, H.K. Chohan, M.S. Rahman, M.A. Halim, A comprehensive computational and principal component analysis on various choline chloride-based deep eutectic solvents to reveal their structural and spectroscopic properties, J. Chem. Phys. 155 (2021) 044308. https://doi.org/10.1063/5.0052569.

[35] P. Kaur, N. Rajani, P. Kumawat, N. Singh, J.P. Kushwaha, Performance and mechanism of dye extraction from aqueous solution using synthesized deep eutectic solvents, Colloids and Surfaces A: Physicochemical and Engineering Aspects. 539 (2018) 85–91. https://doi.org/10.1016/j.colsurfa.2017.12.013.

[36] N.R. Rodriguez, B.S. Molina, M.C. Kroon, Aliphatic+ethanol separation via liquid–liquid extraction using low transition temperature mixtures as extracting agents, Fluid Phase Equilibria. 394 (2015) 71–82. https://doi.org/10.1016/j.fluid.2015.03.017.

[37] S. Ma, Y. Hou, Y. Sun, J. Li, Y. Li, L. Sun, Simulation and experiment for ethanol dehydration using low transition temperature mixtures (LTTMs) as entrainers, Chemical Engineering and Processing: Process Intensification. 121 (2017) 71–80. https://doi.org/10.1016/j.cep.2017.08.009.

[38] A.J. Thakkar, N.E.-B. Kassimi, S. Hu, Hydrogen-bonded complexes of glycolic acid with one and two water molecules, Chemical Physics Letters. 387 (2004) 142–148. https://doi.org/10.1016/j.cplett.2004.02.012.

[39] A.K. Roy, J.R. Hart, A.J. Thakkar, Clusters of glycolic acid and 16 water molecules, Chemical Physics Letters. 434 (2007) 176–181. https://doi.org/10.1016/j.cplett.2006.12.010.

[40] Q. Gu, D. Shen, Z. Tang, W. Wu, P. Su, Y. Xia, Z. Yang, C.O. Trindle, Dissection of H-bonding interactions in a glycolic acid–water dimer, Phys. Chem. Chem. Phys. 19 (2017)

14238–14247. https://doi.org/10.1039/C7CP02234D.

[41] Q. Yu, F. Wang, Y. Jian, V.M. Chernyshev, Y. Zhang, Z. Wang, Z. Yuan, X. Chen, Extraction of flavonoids from Glycyrrhiza residues using deep eutectic solvents and its molecular mechanism, Journal of Molecular Liquids. 363 (2022) 119848. https://doi.org/10.1016/j.molliq.2022.119848.

[42] A. van den Bruinhorst, T. Spyriouni, J.-R. Hill, M.C. Kroon, Experimental and Molecular Modeling Evaluation of the Physicochemical Properties of Proline-Based Deep Eutectic Solvents, J. Phys. Chem. B. 122 (2018) 369–379. https://doi.org/10.1021/acs.jpcb.7b09540.

[43] X. Wang, B. Liu, H. Yang, J. Tian, Properties of binary mixtures of a novel natural deep eutectic solvent (glycolic acid + xylitol) and water at several temperatures, Fluid Phase Equilibria. 556 (2022) 113390. https://doi.org/10.1016/j.fluid.2022.113390.

[44] R. Dennington, T.A. Keith, J.M. Millam, GaussView, (2008).

[45] M.J. Frisch, G.W. Trucks, H.B. Schlegel, G.E. Scuseria, M.A. Robb, J.R. Cheeseman, G. Scalmani, V. Barone, G.A. Petersson, H. Nakatsuji, X. Li, M. Caricato, A. Marenich, J. Bloino, B.G. Janesko, R. Gomperts, B. Mennucci, H.P. Hratchian, J.V. Ortiz, A.F. Izmaylov, J.L. Sonnenberg, D. Williams-Young, F. Ding, F. Lipparini, F. Egidi, J. Goings, B. Peng, A. Petrone, T. Henderson, D. Ranasinghe, V.G. Zakrzewski, J. Gao, N. Rega, G. Zheng, W. Liang, M. Hada, M. Ehara, K. Toyota, R. Fukuda, J. Hasegawa, M. Ishida, T. Nakajima, Y. Honda, O. Kitao, H. Nakai, T. Vreven, K. Throssell, J.A. Montgomery, Jr., J.E. Peralta, F. Ogliaro, M. Bearpark, J.J. Heyd, E. Brothers, K.N. Kudin, V.N. Staroverov, T. Keith, R. Kobayashi, J. Normand, K. Raghavachari, A. Rendell, J.C. Burant, S.S. Iyengar, J. Tomasi, M. Cossi, J.M. Millam, M. Klene, C. Adamo, R. Cammi, J.W. Ochterski, R.L. Martin, K. Morokuma, O. Farkas, J.B. Foresman, D.J. Fox, Gaussian 09, Revision D.01, (2016).

[46] A.D. Becke, Density-functional thermochemistry. III. The role of exact exchange, The Journal of Chemical Physics. 98 (1993) 5648–5652. https://doi.org/10.1063/1.464913.

[47] C. Lee, W. Yang, R.G. Parr, Development of the Colle-Salvetti correlation-energy formula into a functional of the electron density, Phys. Rev. B. 37 (1988) 785–789. https://doi.org/10.1103/PhysRevB.37.785.

[48] S. Grimme, S. Ehrlich, L. Goerigk, Effect of the damping function in dispersion corrected density functional theory, J. Comput. Chem. 32 (2011) 1456–1465. https://doi.org/10.1002/jcc.21759.

[49] J.B. Foresman, A. Frisch, Exploring chemistry with electronic structure methods, 2nd ed., Gaussian, Inc., Pittsburgh, PA, 1996.

[50] L.F. Pacios, O. Gálvez, P.C. Gómez, Variation of geometries and electron properties along proton transfer in strong hydrogen-bond complexes, The Journal of Chemical Physics. 122 (2005) 214307. https://doi.org/10.1063/1.1899103.

[51] C.R. Ashworth, R.P. Matthews, T. Welton, P.A. Hunt, Doubly ionic hydrogen bond interactions within the choline chloride–urea deep eutectic solvent, Phys. Chem. Chem. Phys. 18 (2016) 18145–18160. https://doi.org/10.1039/C6CP02815B.

[52] S.F. Boys, F. Bernardi, The calculation of small molecular interactions by the differences of separate total energies. Some procedures with reduced errors, Molecular Physics. 100 (2002) 65–73. https://doi.org/10.1080/00268970110088901.

[53] S. Simon, M. Duran, J.J. Dannenberg, How does basis set superposition error change the potential surfaces for hydrogen-bonded dimers?, The Journal of Chemical Physics. 105 (1996) 11024–11031. https://doi.org/10.1063/1.472902.

[54] J.P. Foster, F. Weinhold, Natural hybrid orbitals, J. Am. Chem. Soc. 102 (1980) 7211–7218. https://doi.org/10.1021/ja00544a007.

[55] A.E. Reed, F. Weinhold, Natural bond orbital analysis of near-Hartree–Fock water dimer, The Journal of Chemical Physics. 78 (1983) 4066–4073. https://doi.org/10.1063/1.445134.

[56] A.E. Reed, R.B. Weinstock, F. Weinhold, Natural population analysis, The Journal of Chemical Physics. 83 (1985) 735–746. https://doi.org/10.1063/1.449486.

[57] A.E. Reed, F. Weinhold, Natural localized molecular orbitals, The Journal of Chemical Physics. 83 (1985) 1736–1740. https://doi.org/10.1063/1.449360.

[58] J.E. Carpenter, Extension of Lewis structure concepts to open-shell and excited-state molecular species, University of Wisconsin, 1987.

[59] J.E. Carpenter, F. Weinhold, Analysis of the geometry of the hydroxymethyl radical by the “different hybrids for different spins” natural bond orbital procedure, Journal of Molecular Structure: THEOCHEM. 169 (1988) 41–62. https://doi.org/10.1016/0166-1280(88)80248-3.

[60] A.E. Reed, L.A. Curtiss, F. Weinhold, Intermolecular interactions from a natural bond orbital, donor-acceptor viewpoint, Chem. Rev. 88 (1988) 899–926. https://doi.org/10.1021/cr00088a005.

[61] C.M. Breneman, K.B. Wiberg, Determining atom-centered monopoles from molecular electrostatic potentials. The need for high sampling density in formamide conformational analysis, J. Comput. Chem. 11 (1990) 361–373. https://doi.org/10.1002/jcc.540110311.

[62] M. Moosavi, N. Banazadeh, M. Torkzadeh, Structure and Dynamics in Amino Acid Choline-Based Ionic Liquids: A Combined QTAIM, NCI, DFT, and Molecular Dynamics

Study, J. Phys. Chem. B. 123 (2019) 4070–4084. https://doi.org/10.1021/acs.jpcb.9b01799.

[63] L. Cesari, L. Canabady-Rochelle, F. Mutelet, Computational study on the molecular conformations of phenolic compounds, Struct Chem. 29 (2017) 179–194. https://doi.org/10.1007/s11224-017-1017-9.

[64] B.B. Hansen, S. Spittle, B. Chen, D. Poe, Y. Zhang, J.M. Klein, A. Horton, L. Adhikari, T. Zelovich, B.W. Doherty, B. Gurkan, E.J. Maginn, A. Ragauskas, M. Dadmun, T.A. Zawodzinski, G.A. Baker, M.E. Tuckerman, R.F. Savinell, J.R. Sangoro, Deep Eutectic Solvents: A Review of Fundamentals and Applications, Chem. Rev. 121 (2021) 1232–1285. https://doi.org/10.1021/acs.chemrev.0c00385.

[65] J. Zhu, K. Yu, Y. Zhu, R. Zhu, F. Ye, N. Song, Y. Xu, Physicochemical properties of deep eutectic solvents formed by choline chloride and phenolic compounds at T = (293.15 to 333.15) K: The influence of electronic effect of substitution group, Journal of Molecular Liquids. 232 (2017) 182–187. https://doi.org/10.1016/j.molliq.2017.02.071.

[66] W. Guo, Y. Hou, S. Ren, S. Tian, W. Wu, Formation of Deep Eutectic Solvents by Phenols and Choline Chloride and Their Physical Properties, J. Chem. Eng. Data. 58 (2013) 866–872. https://doi.org/10.1021/je300997v.

Chapitre 3

Modified version of the COSMO-SAC model for the prediction of vapour-liquid equilibria of mixtures containing halogen compounds

We make a living by what we get,
we make a life by what we give.

-- Sir Winston Churchill

Chapitre 3 : Modified version of the COSMO-SAC model for the prediction of vapour-liquid equilibria of mixtures containing halogen compounds

Thomas Di Pietro[a], Laetitia Cesari[a], Fabrice Mutelet[a]

a - Université de Lorraine, Ecole Nationale Supérieure des Industries Chimiques, Laboratoire Réactions et Génie des Procédés (UMR CNRS 7274), 1 rue Grandville, 54000 Nancy, France.

Article accepté dans Fluid Phase Equilibria

Résumé

Ce chapitre traite de l'étude des équilibres de phase de mélanges qui contiennent des atomes de chlore ou de brome susceptibles de former des liaisons hydrogène. Les modèles utilisés sont basés sur le modèle COSMO-SAC (2010) pour qui la contribution liée à la formation de liaisons H a été modifiée. Deux paramètres ont ainsi été ajoutés au sein d'une équation empirique introduisant une dépendance en température. Ces paramètres ont été optimisés à l'aide de données d'équilibre liquide-vapeur de mélanges contenant des liquides ioniques et/ou des solvants à eutectique profond, de même que des composés plus habituels. Les mélanges étudiés font toujours intervenir des ions halogénures ou des halocarbures avec des molécules d'eau, d'alcool ou d'acide carboxylique. Les modèles étendus sont nommés COSMO-SAC (+OH-Cl), COSMO-SAC (+OH-Br) et COSMO-SAC (+OH-ClBr) suivant que les nouveaux paramètres ont été optimisés avec des données concernant des mélanges contenant des atomes de chlore uniquement, des atomes de brome uniquement, ou à la fois des atomes de chlore et de brome,

respectivement. Il est montré que ces modèles améliorent pour ces systèmes la prédiction des équilibres liquide-vapeur tout en maintenant des résultats satisfaisants à la fois pour des équilibres liquide-liquide et des équilibres solide-liquide.

Abstract

In this work, the prediction of the phase behaviour of mixtures containing chlorine or bromine atoms involved in hydrogen bonding is investigated. Based on the COSMO-SAC (2010) model, extended models named COSMO-SAC (+OH-Cl), COSMO-SAC (+OH-Br) and COSMO-SAC (+OH-ClBr) are presented. The extension of the base model focuses on the hydrogen bond contribution. For this contribution, the addition of two parameters in an empirical equation introduces a dependence in temperature. The parameters were optimized using a databased composed of vapour-liquid equilibria data of mixtures comprised of both ionic liquids or deep eutectic solvents and regular compounds. The mixtures always involve halides or halocarbons as well as molecules of water, alcohol or carboxylic acids. The extended models are shown to improve the predictions of such systems for vapour-liquid equilibria as well as being able to keep providing satisfying results for both liquid-liquid and solid-liquid equilibria.

3.1 Introduction

New working fluids have continuously been investigated as a way to enhance and optimize the performances of energy recovery processes such as absorption heat exchangers [1–3]. Over the past few years, ionic liquids (ILs) have proven to be efficient albeit costly promising alternatives to traditional fluids such as H_2O/LiBr or NH_3/H_2O. For example, they have been coupled with ammonia [4,5], alcohols and water [6] or other non-aqueous refrigerants [7]. However, to avoid the potential pitfalls of cost and toxicity [8] other solutions such as deep eutectic solvents (DESs) have been studied. A DES is composed of at least two components that can form hydrogen bonds together in a way that a eutectic mixture is obtained [9,10]. Martins et al. [11] have proposed to additionally precise that the temperature of phase transition of the mixture must be both below the ones of the pure components and the one of an ideal liquid mixture of these compounds. DESs are similar to ILs in that they also have low vapour pressures [12], which can be a key property for solvents if liquid at room temperature. Moreover, they offer the possibility of adjusting the mixture properties such as viscosity or density or their ecological impact by modifying the constituting components. Many different combinations and properties have been presented in various reviews [9,10] or books [13]. Properties can also be altered via the composition of the DES, as showcased by Francisco et al. with choline chloride and lactic acid [14].-

Working fluids are traditionally modelled using two methods, the equations of state (EOS) and the excess Gibbs free energy models [15]. The use of cubic EOS requires the knowledge of critical properties. However, these are most of the time non-measurable for DESs since they are not stable at high temperature. They can nonetheless be calculated through group contribution methods [16,17]. Besides, when predicting the behaviour of these solvents mixed with other molecules, interaction parameters are required for both methods. In most cases, they are obtained by fitting experimental data such as vapour-liquid equilibria [18] or molar

enthalpies of mixing [19]. In that regard, EOS or excess Gibbs free energy models are not predictive. The huge number of possible pairings of compounds forming DESs makes it practically impossible to perform experiments for all of them. This underlines the usefulness of models that would be able to bypass the need of experimental data.

In the 1990s, the COnductor-like Screening MOdel (COSMO) was released, before being followed by the COSMO-RS model (COSMO for real solvents). Based on quantum chemistry and statistical thermodynamics, it consists on placing molecules in a perfect conductor solvent and then calculates the deviation from ideality in terms of screening of the charge densities compared to real solvents [20]. The model is able to provide the activity coefficient of compounds in a mixture, from which are derived properties such as phase equilibria or excess properties like excess molar enthalpies. Soon after its release, modifications began to be made to improve the results, then other versions of the model started to be developed and proposed. Among others, COSMO-SAC [21] (COSMO segment activity coefficient) or COSMO-RS(Ol) [22], which have also been improved on a regular basis. The version of COSMO-SAC 2010 comprises 10 parameters including 5 parameters for the electrostatic interaction and the hydrogen bonds [23].

For chemicals not taken into account, discrepancies can arise between prediction and experimental data, rendering the predictive power of these models unsuitable for industrial processes. Reparameterizations have thus been conducted in the literature for liquid-liquid equilibria (LLE) of ether-water mixtures [24] or for chemical functions such as carboxylic acid [25].

Ionic liquids have also needed a special attention in the way they were dealt with within the COSMO models. Notably, three different approaches have been reported for their representation: the “ion pair” or “molecule” approach, the “meta-file” approach and the “electroneutral” or “ions” approach [26,27]. Literature agrees that the first approach leads to

less accurate predictions [26,27]. Regarding ILs mixtures and electrolytes, models combining COSMO models, Pitzer Debye-Hückel model and empirical interaction equations have also been implemented in order to increase the accuracy of the predictions of phase equilibria and thermodynamics properties [28–30].

For DESs, the same considerations could be applied. However, a difficulty of using the electroneutral approach when deriving the liquid phase composition of DESs containing ionic components (ionic DESs) is that it would require the calculations of mean activity coefficients from ionic compounds and non-ionic compounds. Thus, detailed phase equilibria predictions of mixtures containing DESs with the COSMO-SAC model have primarily been computed using the meta-file approach [31].

Many liquid-liquid or vapour-liquid equilibrium (VLE) data involve mixtures of DESs comprising bromide or chloride anions [32–34]. These kinds of components undergo hydrogen bonds that are not taken into account with COSMO-SAC (2010) since no parameters have been implemented for halogen atoms beside fluorine.

The aim of this work is to propose additional parameters to improve the prediction of properties of mixtures containing DESs and in particular mixtures with halogens (halogenated or halide compounds with chlorine or bromine atoms) and water or compounds with hydroxyl groups as well. This functional group is able to form a hydrogen bond with halogens and is likely to appear within working fluids of absorption heat exchanger. The new versions of this model are called COSMO-SAC (+OH-Cl), COSMO-SAC (+OH-Br) and COSMO-SAC (+OH-ClBr) for whether chlorine atoms, bromine atoms or both have been taken into account respectively. The parameters have been optimized using VLE data. These models have then been tested with VLE, LLE and SLE to make sure that the added parameters provide good performances.

3.2 Theory

3.2.1 COSMO-SAC model - Activity coefficient calculations

As previously mentioned, the COSMO-SAC model is used for the calculation of activity coefficients of molecules in a mixture. Activity coefficients of ILs and DESs in mixtures can also be derived from excess Gibbs free energy models such as the UNIFAC, UNIQUAC or NRTL models [15,35]. In the case of UNIQUAC or NRTL models, the interaction parameters required for the representation of mixtures are mainly determined using experimental data [36]. There is no universal method to determine these parameters. To overcome this problem, UNIFAC approach based on group contribution method can be used [37]. This model allows to predict with good accuracy phase diagrams of organic compounds. However, it was demonstrated that UNIFAC model underestimates the strength of the interaction between the components of the DES. According to Xin et al [38], an addition and reparameterization of group-interaction parameters should lead to better estimates. The use of COSMO models and their universal parameters was chosen in this work. The proposed approach of adding new hydrogen bond parameters can be applied to COSMO models to increase their predictive power in regard to the phase diagrams of mixtures containing DESs. COSMO-SAC (2010) corresponds to the version in which hydrogen bond parameters have been introduced. This is before the authors of the COSMO-SAC model directed their work toward dispersion [39]. By using the 2010 version, the optimization of additional hydrogen bond parameters could be performed in similar conditions compared to the development of the first parameters, which are still used to this day [40,41].

The model described in the following section is derived from the equations presented by Hsieh et al. [23]. Another more recent description is also provided by Bell et al. [41]. The first step consists on retrieving the ideal surface charge densities σ_j derived from quantum chemical calculations (method further displayed in the computational details section). An averaging of

the charges is then performed over an area of radius r_{eff} to take into account the fact that the charge density is not constant over a surface segment [20]:

$$\sigma_{k,av} = \frac{\sum_j^{N_{segments}} \sigma_j \frac{r_j^2 r_{eff}^2}{r_j^2 + r_{eff}^2} exp\left(-f_{decay} \frac{d_{j,k}^2}{r_j^2 + r_{eff}^2}\right)}{\sum_j^{N_{segments}} \frac{r_j^2 r_{eff}^2}{r_j^2 + r_{eff}^2} exp\left(-f_{decay} \frac{d_{j,k}^2}{r_j^2 + r_{eff}^2}\right)} \quad (1)$$

With $r_j = \sqrt{a_j/\pi}$ the radius of a surface segment j, calculated from its area a_j, and $r_{eff} = \sqrt{a_{eff}/\pi}$ the effective radius calculated from the parameter a_{eff}. All the parameters of the model are given in **Table 3.1**. f_{decay} is an empirical parameter. Also, $d_{j,k}$ represents the distance between two segments j and k and is given by

$d_{j,k} = \sqrt{(x_j - x_k)^2 + (y_j - y_k)^2 + (z_j - z_k)^2}$ with *x*, *y* and *z* the coordinates of the segments in 3D (see also the COSMO files generation section). The averaged density values $\sigma_{k,av}$ are then allocated to one of the 51 discretized values σ_d ranging from -0.025 to 0.025 e.Å^{-2} with a step $\Delta\sigma$ of 0.001 e.Å^{-2}. The sigma profile of a molecule $p(\sigma_d)$ is designed to represent the number of density values within each interval, weighted by the surface associated to the segments from which originate the averaged charges. Sigma profiles give an insight on the affinity between the molecules considered. The repartition follows the lever rule.

Thus, for a given molecule, for all k so that $\sigma_d \leq \sigma_{k,av} < \sigma_{d+1} = \sigma_d + \Delta\sigma$:

$$p(\sigma_d) = \sum_k \frac{A_k}{A_{tot}} * \frac{\sigma_{d+1} - \sigma_{k,av}}{\Delta\sigma} \quad (2)$$

$$p(\sigma_{d+1}) = \sum_k \frac{A_k}{A_{tot}} * \frac{\sigma_{k,av} - \sigma_d}{\Delta\sigma} \quad (3)$$

Where A_k is the surface of the segment k and A_{tot} is the sum of the surface of all the segments of the molecule. In the case of a mixture S, the mole fractions x_i of each compound i in the liquid phase are taken into account:

$$p_S(\sigma_d) = \frac{\sum_i x_i * A_{tot,i} * p_i(\sigma_d)}{\sum_i x_i * A_{tot,i}} \quad (4)$$

In COSMO-SAC (2010) and onward, sigma profiles are also divided in different categories depending on the kind of hydrogen bonds that the molecules are able to form. In the version of 2010, 3 contributions are differentiated: NHB, OH and OT. The segments are sorted depending on the kind of atom they come from, and corresponding sigma profiles are created, with the original $p(\sigma_d)$ corresponding to the sum of the categorized sigma profiles:

$$p(\sigma_d) = p^{NHB}(\sigma_d) + p^{OH}(\sigma_d) + p^{OT}(\sigma_d) \quad (5)$$

NHB applies to atoms not able to do any hydrogen bonds. OH is the class that contains atoms of hydrogen and oxygen that are part of a hydroxyl group.

Table 3.1. Parameters used in the COSMO-SAC (2010) [23] model and in the extended versions (+OH-Cl, +OH-Br and +OH-ClBr)

Model	Parameters	Value
From 2010 onwards	a_{eff} (Å²)	7.25
From 2010 onwards	f_{decay} (/)	3.57
From 2010 onwards	σ_0 (e.Å^{-2})	0.007
From 2010 onwards	A_{ES} (kcal.Å^4.mol^{-1}.e^{-2})	6525.69
From 2010 onwards	B_{ES} (K².kcal.Å^4.mol^{-1}.e^{-2})	1.4859*10^8
From 2010 onwards	$C_{OH\text{-}OH}$ (kcal.Å^4.mol^{-1}.e^{-2})	4013.78
From 2010 onwards	$C_{OT\text{-}OT}$ (kcal.Å^4.mol^{-1}.e^{-2})	932.31
From 2010 onwards	$C_{OH\text{-}OT}$ (kcal.Å^4.mol^{-1}.e^{-2})	3016.43
+OH-Cl	$a_{C_{OH-Cl}}$ (K².kcal.Å^4.mol^{-1}.e^{-2})	5.8703*10^3
+OH-Cl	$b_{C_{OH-Cl}}$ (kcal.Å^4.mol^{-1}.e^{-2})	- 4.2517*10^8
+OH-Br	$a_{C_{OH-Br}}$ (K².kcal.Å^4.mol^{-1}.e^{-2})	4.4157*10^3
+OH-Br	$b_{C_{OH-Br}}$ (kcal.Å^4.mol^{-1}.e^{-2})	- 2.3054*10^8
+OH-ClBr	$a_{C_{OH-ClBr}}$ (K².kcal.Å^4.mol^{-1}.e^{-2})	5.7823*10^3
+OH-ClBr	$b_{C_{OH-ClBr}}$ (kcal.Å^4.mol^{-1}.e^{-2})	- 4.1518*10^8

Finally, OT is for hydrogen, oxygen, nitrogen and fluorine atoms prone to hydrogen bonds but not part of a hydroxyl group. Moreover, to be qualified as hydrogen-bonding (whether it is of

the OH or OT type), the sign of the charge density of the segments is checked. For hydrogen atoms, the charges need to be negative while for oxygen, nitrogen and fluorine the charges have to be positive. Indeed, during the quantum chemical calculations, negative screening charge densities around a hydrogen atom account for a positive polarity of the hydrogen, which is suitable for hydrogen bonding. The opposite is true for the other aforementioned atoms. Once this is done, a Gaussian-type correction is applied to adjust the probability of a hydrogen bond formation [42]:

$$p^{NHB,corr}(\sigma_d) = p^{NHB}(\sigma_d) + \left(p^{OH}(\sigma_d) + p^{OT}(\sigma_d)\right) * \left(1 - P^{HB}(\sigma_d)\right) \quad (6)$$

$$p^{OH\ or\ OT,corr}(\sigma_d) = p^{OH\ or\ OT}(\sigma_d) * P^{HB}(\sigma_d) \quad (7)$$

With the probability function $P^{HB}(\sigma_d) = 1 - exp\left(\frac{\sigma^2}{2\sigma_0^2}\right)$ and σ_0, a parameter related to the shape of the function. In the case of a DES composed of the molecules M_1 and M_2 with the ratio [m_1:m_2], the meta-file approach is applied and the following sigma profile p_{DES}^t is also calculated, with t standing for NHB, OH or OT:

$$p_{DES}^t(\sigma_d) = \frac{\sum_m ratio(m) * A_{tot,m} * p_m^t(\sigma_d)}{\sum_m ratio(m) * A_{tot,m}} \quad (8)$$

In this work, a new class is introduced for atoms of chlorine or bromine that can form hydrogen bonds with hydrogen from hydroxyl groups. 3 approaches were considered, called Cl, Br or ClBr. In the Cl approach, chlorine atoms are the only halogen atoms to be found in the dataset used to optimize the new parameters. The added parameters are labelled +OH-Cl. Likewise regarding the Br approach and bromine atoms. For the ClBr approach, Cl and Br atoms are treated as similar. The main idea was to determine if a distinction between chlorine and bromine was necessary or if their interaction with hydrogens could be comparable within the model. Thus, in the case of the ClBr category both chlorine and bromine atoms share the same parameters. The new class is treated in a comparable way to the OH and OT ones regarding the atoms of oxygen, nitrogen and fluorine. Thus, for a given molecule, equation (5) becomes:

$$p(\sigma_d) = p^{NHB}(\sigma_d) + p^{OH}(\sigma_d) + p^{OT}(\sigma_d) + p^{Cl}(\sigma_d) \quad (9)$$

This modification also affects equations (6) to (8). In the equations (9), (12) and (13) the superscript Cl is used as an example, but could well be replaced by Br or ClBr.

As part of the calculation of the residual contribution of the activity coefficient γ_i^r, the exchange energy ΔW is computed for two charge densities σ_j and σ_k.

$$\Delta W(\sigma_j, \sigma_k) = C_{ES}(T) * (\sigma_j + \sigma_k)^2 - C_{HB}(\sigma_j, \sigma_k) * (\sigma_j - \sigma_k)^2 \quad (10)$$

$$C_{ES}(T) = A_{ES} + \frac{B_{ES}}{T^2} \quad (11)$$

With C_{ES} the electrostatic interaction parameter and T being the temperature of the system. A_{ES} and B_{ES} are universal – not-dependent-on-the-molecule type of – parameters. In contrast, the hydrogen bonding parameter C_{HB} is equal to $C_{OH\text{-}OH}$, $C_{OT\text{-}OT}$, $C_{OH\text{-}OT}$ or $C_{OH\text{-}Cl}$ depending on the type of hydrogen bond that is involved between the two atoms from which are derived σ_j and σ_k. More specifically:

$$C_{HB}(\sigma_j, \sigma_k) = \begin{cases} C_{OH-OH} & \sigma_j \text{ and } \sigma_k \text{ are both OH type and } \sigma_j * \sigma_k < 0 \\ C_{OT-OT} & \sigma_j \text{ and } \sigma_k \text{ are both OT type and } \sigma_j * \sigma_k < 0 \\ C_{OH-OT} & \text{one of } \sigma_j \text{ and } \sigma_k \text{ is OH type, the other OT type and } \sigma_j * \sigma_k < 0 \\ C_{OH-Cl} & \text{one of } \sigma_j \text{ and } \sigma_k \text{ is OH type, the other Cl type and } \sigma_j * \sigma_k < 0 \\ 0 & \text{otherwise} \end{cases} \quad (12)$$

Moreover, the modification of the hydrogen bonding parameter C_{HB} for systems with chlorine atoms consists of the replacement of a fixed value with an empirical equation similar to the one for the electrostatic interaction parameter C_{ES}, introducing a temperature dependence:

$$C_{OH-Cl}(T) = a_{C_{OH-Cl}} + \frac{b_{C_{OH-Cl}}}{T^2} \quad (13)$$

The units of the parameters are found in **Table 3.1** and allow for the homogeneity of the equations. The fact that the other parameters are unaltered allows for this modification to be transferable to other versions of the model. A slight adjustment of the new parameters may nonetheless be beneficial if the creation of the COSMO files and descriptors of the molecules

has been conducted with a different ab initio software or a different basis set.

The exchange energy is then used for the calculations of the segment activity coefficient Γ, which requires to solve a self-consistency equation that converges by damping method, with a damping factor of 0.5. This value allows for fast calculations and has been found in previous implementations of COSMO-SAC codes [43]. This equation is applied to both pure compounds i and their mixture S. Both cases are gathered under the subscript X for the sake of simplicity:

$$\Gamma_X^t(\sigma_d) = \exp\left(-ln\left(\sum_j p_X^t(\sigma_j) * \Gamma_X^t(\sigma_j) * exp\left[-\frac{\Delta W(\sigma_j^t, \sigma_d)}{RT}\right]\right)\right) \quad (14)$$

The segment activity coefficients Γ are needed in the calculation of the restoring free energy, which accounts for the residual part of the activity coefficient:

$$ln(\gamma_i^r) = \frac{A_{tot,i}}{a_{eff}} \sum_t \sum_j p_i^t(\sigma_j) * \left[ln\left(\Gamma_S^t(\sigma_j)\right) - ln\left(\Gamma_i^t(\sigma_j)\right)\right] \quad (15)$$

Subsequently, the calculation of the cavity formation free energy provides the combinatorial part of the activity coefficient.

$$ln(\gamma_i^c) = ln\left(\frac{\Phi_i}{x_i}\right) + \frac{z}{2} q_i ln\left(\frac{\theta_i}{\Phi_i}\right) + l_i - \frac{\Phi_i}{x_i} \sum_n x_n l_n \quad (16)$$

$$With: \theta_i = \frac{x_i q_i}{\sum_n x_n q_n}, \qquad \Phi_i = \frac{x_i r_i}{\sum_n x_n r_n}, \quad l_i = \frac{z}{2}(r_i - q_i) - (r_i - 1)$$

This operates using the Staverman-Guggenheim combinatorial parameters [44], including the coordination parameter $z = 10$, $r_i = \frac{V^{COSMO}}{V^{standard}}$, $q_i = \frac{A^{COSMO}}{A^{standard}}$, with $V^{standard} = 66.69$ Å^3, $A^{standard} = 79.53$ Å^2. V^{COSMO} and A^{COSMO} are the cavity volume and area of the molecule i, derived from the COSMO calculations. Within the meta-file approach:

$$A_{DES}^{COSMO} = \sum_i \frac{ratio(i)}{\sum_n ratio(n)} * A_{tot,i} \quad (17)$$

$$V_{DES}^{COSMO} = \sum_i \frac{ratio(i)}{\sum_n ratio(n)} * V_i^{COSMO} \quad (18)$$

Finally, both residual and combinatorial contributions are summed:

$$\gamma_i = exp\left(ln(\gamma_i^r) + ln(\gamma_i^c)\right) \quad (19)$$

The aim of this study is mainly to develop a model able to predict the behaviour of working fluids containing halogen compounds in energy recovery processes. In such processes, the mixtures are in vapour-liquid equilibria. Therefore, the new parameters were fitted using VLE data from various sources [45–54]. The parameters of the models are summarised in **Table 3.1**. Since LLE and SLE can be more sensitive, the modified model was also used to predict such phase diagrams to make sure that the addition of new parameters did not have any adverse effect.

3.2.2 Phase Equilibria

3.2.2.1 Vapour-liquid equilibrium (VLE)

The equilibrium between the gas phase and the liquid phase is rendered by equation (20).

$$P = \sum_i P_i^{sat}\, x_i \gamma_i \quad (20)$$

Saturation vapour pressures of component i, P_i^{sat}, were calculated using the Antoine equation provided by the NIST database [55]. Judging by the almost null molar fraction of ILs or DESs in the vapour phase, their saturation vapour pressures were considered to be negligible and were not considered in the calculation of the total pressure.

3.2.2.2 Liquid-liquid equilibrium (LLE)

The gamma-gamma method for the LLE can be defined by equation (21):

$$x_i^A \gamma_i^A = x_i^B \gamma_i^B \quad (21)$$

For any component i in liquid phases A and B. LLE are solved iteratively following the Rachford-Rice algorithm [56]. The fraction of total material in one phase R was initialized to 0.5.

3.2.2.3 Solid-liquid equilibrium (SLE)

SLE and solubility are determined using equations (22-23) [57]:

$$\ln x_i\gamma_i = \frac{\Delta H_{fus,i}}{RT_{fus,i}}\left(1 - \frac{T_{fus,i}}{T}\right) \quad (22)$$

$$\ln x_i = \frac{\Delta H_{fus,i}}{RT_{fus,i}}\left(1 - \frac{T_{fus,i}}{T}\right) - \ln \gamma_i \quad (23)$$

With $\Delta H_{fus,i}$ and $T_{fus,i}$ the enthalpy and temperature of fusion of the solute i, respectively. At first, the liquid phase compositions of the solute are calculated considering the ideal case with the activity coefficient equal to 1. Then, the activity coefficients are computed using these ideal compositions within COSMO-SAC. The actual compositions are finally derived from equation (23).

3.3 Computational details

3.3.1 COSMO files generation

Gaussian 09 Revision D.01 [58] was used to generate the COSMO files. These files contain the ideal surface charge densities σ_j, the coordinates *x*, *y* and *z* of the segments as well as their area and the cavity volume V^{COSMO} of the molecule. The files can also provide the cavity area A^{COSMO}. However, this quantity was rather recalculated by summing the areas of the charge densities in order to get a more accurate value. With Gaussian 09, density functional theory (DFT) was performed with the following settings: BVP86 [59–61] for the functional, Triple Zeta Valence plus Polarization (TZVP) [62,63] for the basis set, DGA1 [64,65] for the fitting set and tight Self-Consistent Field (SCF) for the convergence method. These are recommended when generating COSMO files with Gaussian 09 and have previously been applied for similar calculations [31,66,67]. In addition, the keywords SCRF=COSMO (replaced by SCRF=COSMORS in the writing step), NoSymm and NoVaracc were also used. An example of syntax for the key words is provided in the supplementary material. Additionally, COSMO-SAC (2010) paper authors also warn that an adjustment of the parameters of the COSMO

models may be necessary depending on the package of quantum modelling used to obtain the COSMO files.

3.3.2 Optimization and databank description

The optimization of the following objective function was performed using a gradient-based method:

$$obj = \frac{1}{N_{data}} * \left(\sum_{i=1}^{n} \frac{\left| P_i^{calc} - P_i^{exp} \right|}{P_i^{exp}} * 100 \right) \quad (24)$$

With N_{data} the number of data points involved in the calculations and P_i the vapour pressure of the system for a given composition. The subscripts calc and exp stand for the calculated and experimental values respectively. This corresponds to the mean absolute percentage error (MAPE). 702 experimental VLE data points were used to optimize the parameters $a_{C_{OH-Cl}}$ and $b_{C_{OH-Cl}}$. They consist of 166 points of binary mixtures containing choline chloride based DESs and 536 points from mixture containing chloride based ILs. The second component is either water or an alcohol (primary or secondary) so there can be a hydrogen bond between the chlorine and an atom of hydrogen covalently linked to an atom of oxygen. Temperatures range from 298.15 to 444.55 K. Details are provided in **Table 3.2**. These points form the dataset A.

Table 3.2. Description of the dataset used in the optimization of COSMO-SAC (+OH-Cl) and COSMO-SAC (+OH-ClBr) (dataset A)

System	Temperature range (K)	Number of data points	Reference
{Glycerol:[Choline] [Chloride]} [2:1] + Water	298.15 - 338.15	86	[45]
{Phenol:[Choline] [Chloride]} [2:1] + Water	298.15 - 333.15	80	[45]
[EMIM] [Chloride] + Water	355.58 - 435.03	92	[46]
[BMIM] [Chloride] + Methanol	320.8 - 361.74	69	[47]
[BMIM] [Chloride] + 1-Propanol	352.75 - 410.89	66	[47]
[BMIM] [Chloride] + 2-Propanol	338.67 - 388.75	100	[47]
[BMIM] [Chloride] + 1-Butanol	372.25 - 431	58	[47]
[BMIM] [Chloride] + 2-Butanol	354.75 - 398.75	87	[47]
[BMIM] [Chloride] + 1-Pentanol	389.91 - 444.55	64	[47]
	Total	**702**	

A different set of 1464 points - dataset B (found in the supplementary material) - was used to test the new parameters. The OH-Br type parameters were optimized via a dataset of 700 points called dataset C. **Table 3.3** displays the details of the systems used for this. In this dataset, the systems are constituted of bromide-based IL or 1-bromopropane in binary mixtures with either an alcohol (63 points), a carboxylic acid (69 points) or water (568 points). Temperatures range from 304.8 to 457.4 K. A dataset D (see the supplementray materials) different from dataset C

was used to test the new parameters.

Finally, the optimization of the OH-ClBr parameters made use of the two previously mentioned datasets A and C, thus regrouping data with both chlorine and bromine atoms. The optimized parameters were then tested using datasets B and D.

The performances of the models were evaluated using the average deviation between predicted and experimental pressures for the VLE and the root-mean-square deviation (RMSD) for the LLE/SLE given in equation (25).

$$RMSD = \sqrt{\frac{\sum_{i=1}^{N}\left(x_{i,exp} - x_{i,calc}\right)^2}{N_{data}}} \quad (25)$$

With x_i the molar fraction of the considered component in the liquid phase.

3.4 Results and discussion

The optimized parameters can be found in **Table 3.1**.

Table 3.3. Description of the dataset used in the optimization of COSMO-SAC (+OH-Br) and COSMO-SAC (+OH-ClBr) (dataset C)

System	Temperature range (K)	Number of data points	Reference
1-Bromopropane + Acetic acid	344.75 – 383.05	29	[48]
1-Bromopropane + Propionic acid	345.7 – 411.32	40	[48]
[1-Ethyl-1-methylpiperidinium] [Bromide] + Water	338.15 – 368.15	89	[49]
[1-Ethylpyridinium] [Bromide] + Water	338.15 – 368.15	76	[49]
[N-Hydroxyethylpyridinium] [Bromide] + Water	338.15 – 368.15	46	[49]
[1-Ethyl-1-methylmorpholinium]	338.15 – 368.15	87	[49]

[Bromide] + Water			
[1-Hydroxyethyl-1-methylmorpholinium] [Bromide] + Water	338.15 – 368.15	70	[49]
[Choline] [Bromide] + Water	338.15 – 368.15	49	[49]
[1-Butyl-3-methylimidazolium] [Bromide] + Water	304.8 – 457.4 355.24 – 399.88	64 65	[50] [51]
[1-Methyl-1-pentylmorpholinium] [Bromide] + Water	368.15	22	[52]
1-Bromopropane + Methanol	339.45 – 354.85	14	[53]
1-Bromopropane + Propan-2-ol	327.62 – 339.78	26	[53]
1-Bromopropane + 2-Methylpropan-2-ol	341.58 – 353.65	23	[54]
	Total	**700**	

3.4.1 VLE

The database for the VLE is divided in 4 parts A, B, C and D, depending on whether the studied mixture contains chlorine or bromine atoms and whether it has been used for optimization or not:

A - Dataset comprised of mixtures containing chlorine atoms and used to optimize parameters
B - Dataset comprised of mixtures containing chlorine atoms not used for optimization
C - Dataset comprised of mixtures containing bromine atoms and used to optimize parameters
D - Dataset comprised of mixtures containing bromine atoms not used for optimization.

As presented before, datasets A and C are found in **Table 3.2** and **Table 3.3**, respectively. Datasets B and D can be found in **Table S.B19** and **Table S.B20**, respectively. There is a total of 2639 data points. The results are presented in **Table 3.4**.

Table 3.4 Comparison of the average deviations obtained from the 2010 and modified COSMO-SAC models for the different databases

Database	Number of data points	Average Deviation COSMO-SAC (2010) (%)	Average Deviation COSMO-SAC +OH-Cl (%)	Average Deviation COSMO-SAC +OH-Br (%)	Average Deviation COSMO-SAC +OH-ClBr (%)
Dataset A[a]	702	36.32	6.25	/	6.47
Dataset B	1464	23.03	10.30	/	10.33
Dataset C[b]	700	65.59	/	16.45	17.16
Dataset D	773	11.16	/	4.19	4.01
Dataset (A+C)[c]	1402	47.10	/	/	10.41
Dataset B+D	2237	19.26	/	/	8.32

[a] used to optimize OH-Cl parameters
[b] used to optimize OH-Br parameters
[c] used to optimize OH-ClBr parameters

The performances of the (+OH-Cl) model have been evaluated over 1464 points from systems not included in the dataset used for the optimization (dataset B). These systems also contain chlorine atoms which are able to form a hydrogen bond with a hydrogen linked to an oxygen. Compared to the 2010 model, the average deviation of these systems was roughly reduced by half, from 23.03% with COSMO-SAC (2010) in average to 10.30% with COSMO-SAC (+OH-Cl). Concerning the (+OH-Br) model, a smaller validating dataset of 773 points (dataset D) has been used with systems containing bromine atoms susceptible to form hydrogen bonds with hydrogen in a hydroxyl group. For this dataset, the average deviation was reduced from 11.16% with COSMO-SAC (2010) to 4.19%. Finally, a dataset gathering both the 1464 points and the 773 points (dataset B+D) was run with the COSMO-SAC (2010) and COSMO-SAC (+OH-ClBr) models. In each case, the modified models demonstrated better predictions. As an illustration, the comparison between experimental and predicted vapour pressure for the system containing the DES (phenol:choline chloride) [2:1] and water is shown in **Figure 3.1**. The addition of the parameters in the modified COSMO-SAC enables to correct

the trend and the values for the prediction of the vapour pressures. Likewise, **Figure 3.2** represents the comparison between experimental and predicted vapour pressure for the system {1-methyl-1-pentylpyrrolidinium bromide + water}, for which analogous comments can be made with respect to **Figure 3.1**. One can also notice that the (+OH-Cl)/(+OH-Br) and the (+OH-ClBr) predictions are too close in values to be discernible. Furthermore, generally speaking the COSMO-SAC (+OH-ClBr) model displays very close results to the other two. In the case of the (+OH-Cl) model, this is expected because of the values of the parameters $a_{C_{OH-Cl}}$ and $a_{C_{OH-ClBr}}$ and of $b_{C_{OH-Cl}}$ and $b_{C_{OH-ClBr}}$ are extremely similar. Nevertheless, the results obtained with COSMO-SAC (+OH-ClBr) indicate that differentiating between chlorine and bromine atoms within the model is not necessary since the predictions are better for both kinds of datasets when the same set of parameters is applied for both bromine and chlorine.

In the supplementary material, the average deviation between predicted and experimental vapour pressures are presented for the entirety of the database. Notably, the results have been compiled for the base model as well as for all three modified models for the sake of comparison and completeness. Overall, the results show that the addition and implementation of a new set of parameters to better describe the hydrogen bond with chlorine and bromine atoms is beneficial to the accuracy of the predictions.

Figure 3.3 shows the values of the pressures calculated with both COSMO-SAC (2010) and COSMO-SAC (+OH-ClBr) as a function of the experimental data points for the entire dataset. The 2010 version has a clear tendency to overestimate the values. Almost all of the points are on or above the y=x line. The +OH-ClBr model corrects this tendency. This is particularly significant for pressures under 50 kPa, for which most of the database is properly represented. Even beyond, aside from a handful of points, the majority of the points are along the y=x line. In particular, the behaviour of the VLE of most of the systems of the database are properly predicted up to 85 kPa. The most problematic mixtures are some composed of ILs and ethanol

and some binaries of alcohol + 1-Bromopropane, which are badly represented with all of the models used in this work. The experimental points have been obtained at constant pressure, varying only in the composition of the binaries. These points correspond to the vertical lines that can be observed in **Figure 3.3** at 50, 70 and 100 kPa (300 points from 6 sets of data). Nevertheless, for mixtures composed of ethanol and either 1-ethyl-3-methylimidazolium (EMIM) chloride, 1-butyl-3-methylimidazolium (BMIM) chloride (2 sets of data) or 1-hexyl-3-methylimidazolium (HMIM) chloride, the average deviation between calculated and experimental vapour pressure has dropped from respectively 91.7, 122.4 (or 105.5) and 133.3% to 31.5, 44.2 (32.15) and 47.3% after using the modified model COSMO-SAC (+OH-ClBr) compared to the 2010 version. The deviation has been divided roughly by 3. To reduce the remaining deviation from the experimental data an idea not implemented in this work could be to introduce a special bonding parameter when modelling mixtures with ethanol.

Figure 3.4 displays for both COSMO-SAC (2010) and COSMO-SAC (+OH-ClBr) the abundance of values in percentage of rounded relative deviations (RD) between calculated and experimental pressures for the entire dataset. The peak of the 2010 model is centred on a value slightly above 0%. Besides, the area under the curve is more important after 0, confirming the fact that the values tend to be overestimated with this model. On the other hand, the peak corresponding to the +OH-ClBr model is better centred around 0 and the area under the curve decreases fast after +10 and -10 RD% indicating that the model does not show any particular bias toward over or underestimated values. Finally, the peak for the modified model reaches a value around 11%, compared to a value slightly above 6% for the 2010 model. This is characteristic of an increase in the abundance of well-represented data, which is consistent with an overall improvement of the results.

The impact of the origin of the OH groups on the performances of the COSMO-SAC (+OH-ClBr) model has been compared. In the database, OH groups can come from water,

alcohol and carboxylic acid. The corresponding average deviations are summarized in **Table 3.5**. There are 1790 data points for mixtures with water, 2247 data points with alcohol molecules and 351 with carboxylic acid molecules. The average deviations are 5.96, 12.95 and 23.86%, respectively. The model has better performances when water is involved, and overall when more than one source of hydrogen is available in the mixture compared to when there is only water (6.22%), alcohol (15.77%) or carboxylic acid (43.34%). The highest deviations are observed when carboxylic acids are involved. This can be linked to the fact that carboxylic acids are much less represented in the dataset compared to water and alcohols. One way to improve the COSMO-SAC (+OH-ClBr) model would be to determine specific $a_{C_{OH-ClBr}}$ et $b_{C_{OH-ClBr}}$ parameters for water, alcohols and carboxylic acids. This would be possible when larger database of VLE are available.

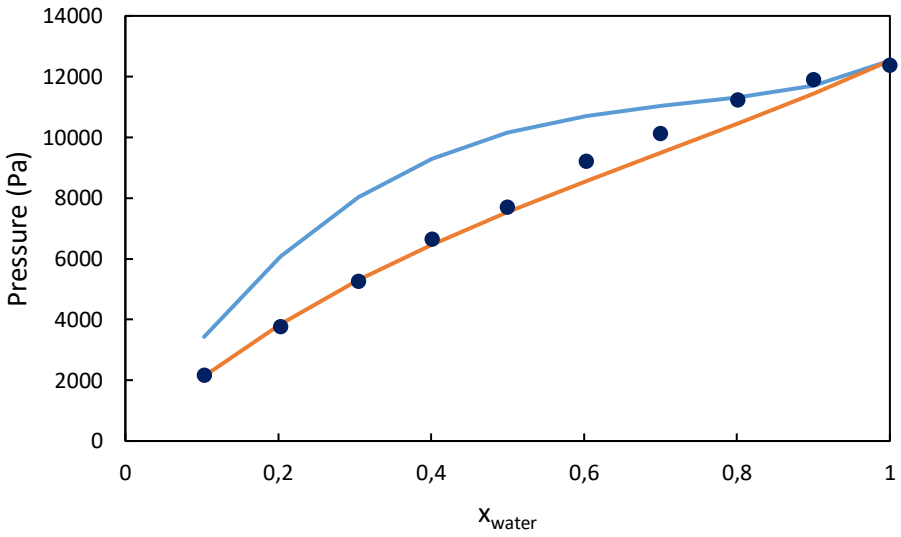

Figure 3.1. Isothermal vapour pressure versus mole fraction of water for the system {(Phenol:Choline chloride) [2:1] + Water} at 323.15K, ● experimental data [45], — COSMO-SAC (2010) model, — COSMO-SAC (+OH-Cl) model, — COSMO-SAC (+OH-ClBr) model (the two +OH-X models coincide)

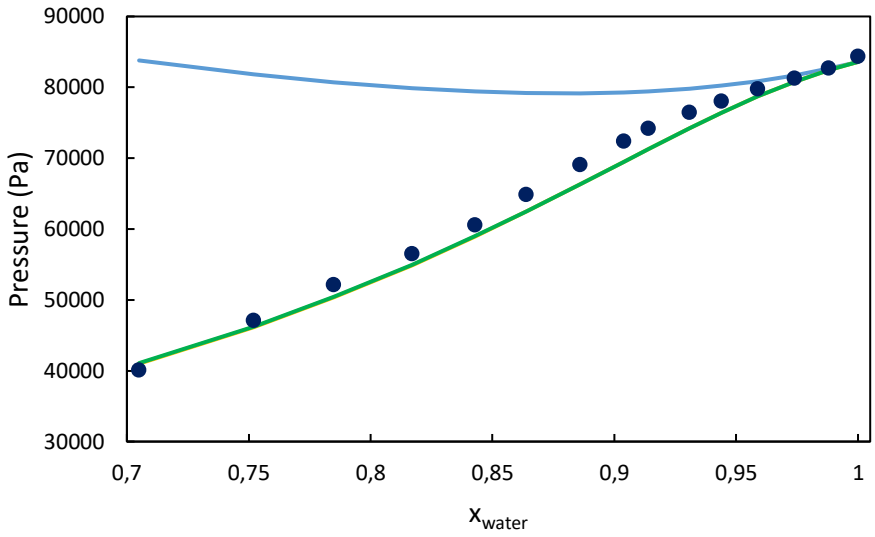

Figure 3.2. Isothermal vapour pressure versus mole fraction of water for the system {1-Methyl-1-pentylpyrrolidinium bromide + Water} at 368.15K, ● experimental data [68], — COSMO-SAC (2010) model, — COSMO-SAC (+OH-Br) model, — COSMO-SAC (+OH-ClBr) model (the two +OH-X models coincide)

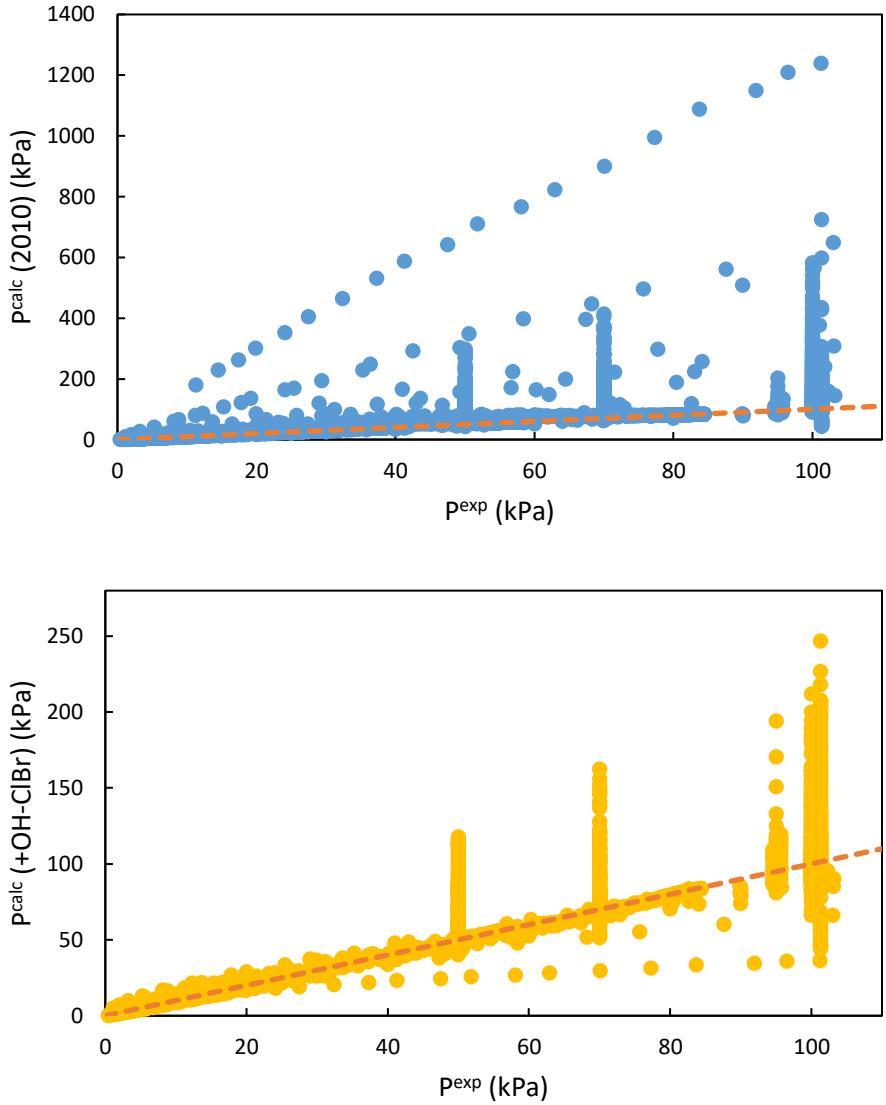

Figure 3.3. Discrepancy between calculated and experimental values of pressure for the VLE database - Comparison between ● COSMO-SAC (2010) and ● COSMO-SAC (+OH-ClBr) models, -- y = x line

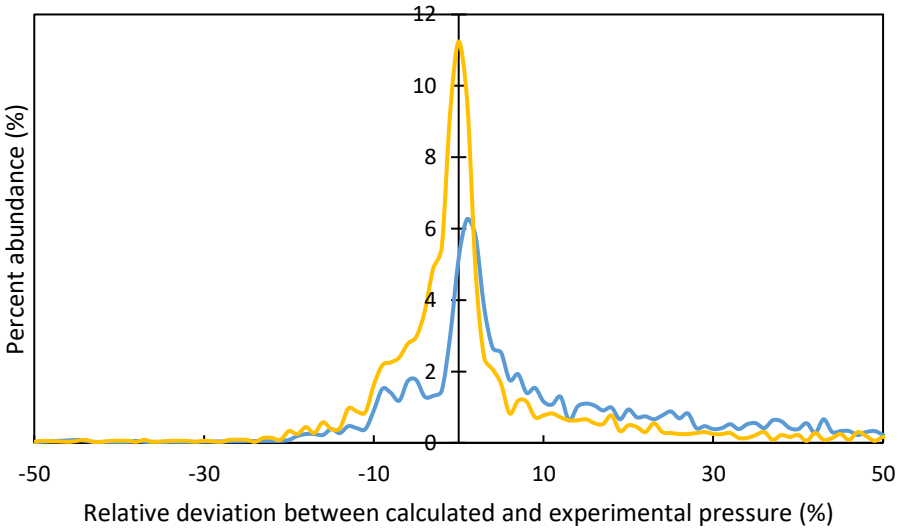

Figure 3.4. Percent abundance of the relative deviation in percentage for the entire VLE dataset, comparison between — COSMO-SAC (2010) and — COSMO-SAC (+OH-ClBr) models

Table 3.5. Average deviations obtained with COSMO-SAC (+OH-ClBr) depending on the sources of the hydrogens involved in the hydrogen bond

OH source contained in the systems	Number of data points	Average deviation (%)
Water	1790	5.96
Water only	1215	6.22
Alcohol	2247	12.95
Alcohol only	1613	15.77
Water and alcohol	460	5.18
Carboxylic acid	351	23.86
Carboxylic acid only	162	43.34

3.4.2 LLE and SLE

Results for LLE and SLE are compiled in the supplementary material. Due to the fact that the values of the parameters for the extended models are very resembling, only the results derived from the COSMO-SAC (+OH-ClBr) model have been generated.

For the LLE, 787 data points for a total of 106 systems have been investigated. As a reference, the average RMSD on this database is 0.08 for both COSMO-SAC (2010) and COSMO-SAC (+OH-ClBr). Results from both the 2010 and the extended version are extremely close. Therefore, the modification of the model did not have any adverse impact on the predictions of LLE.

Regarding the SLE, the comparison between prediction and experimental data has been carried out for 34 systems and 503 data points. Very good results for systems comprised of a binary mixture of 2 ILs have been obtained. An example is illustrated in **Figure 3.5**. These systems behave closely to an ideal mixture, with activity coefficients close to the unity, and most of them share a cation or an anion. For other systems, in particular the ones involving carboxylic acids, a part of the phase diagram is characterized by a small variation of the temperature over a large range of compositions. In these cases, the models are capable of predicting the right trend, although the actual values of compositions are a bit off compared to the experimental data. This leads to rather large values of RMSD. Taking the entire dataset into account, the extended model was able to provide better results. Notably, phase diagrams could be obtained for systems in which carboxylates were part of the mixture with COSMO-SAC (+OH-ClBr) and not with the original model. **Figure 3.6** is set as an example of such a system. In fact, the ideal case in which the activity coefficient is equal to 1 provides a very good estimation of the phase diagram for these systems. However, the COSMO-SAC (2010) model tends to underestimate the values of the activity coefficients at low temperature. COSMO-SAC (+OH-ClBr) improves this, although it is not able to reach the entire range of compositions. The same issue has been observed with COSMO-RS for the system {choline chloride + choline acetate} [69]. **Figure 3.7** displays the percent abundance of values for the difference between modelled and experimental mole fractions of the first compound of the mixture. The trend is similar for both COSMO-SAC (2010) and (+OH-ClBr) models, with a peak centred on 0. The main difference is that COSMO-SAC (+OH-ClBr) results in less negative differences.

Finally, in the case of the LLE and SLE the calculations between the 2010 and the +OH-ClBr versions are very comparable, or even improved for some SLE. The fact that the added parameters convey a temperature dependence and that the temperature ranges for SLE and LLE are lower than for VLE is a possible explanation of the limited impact of the extension of the

model. At the very least, the addition of the new parameters does not seem to compromise the predictions for LLE and SLE.

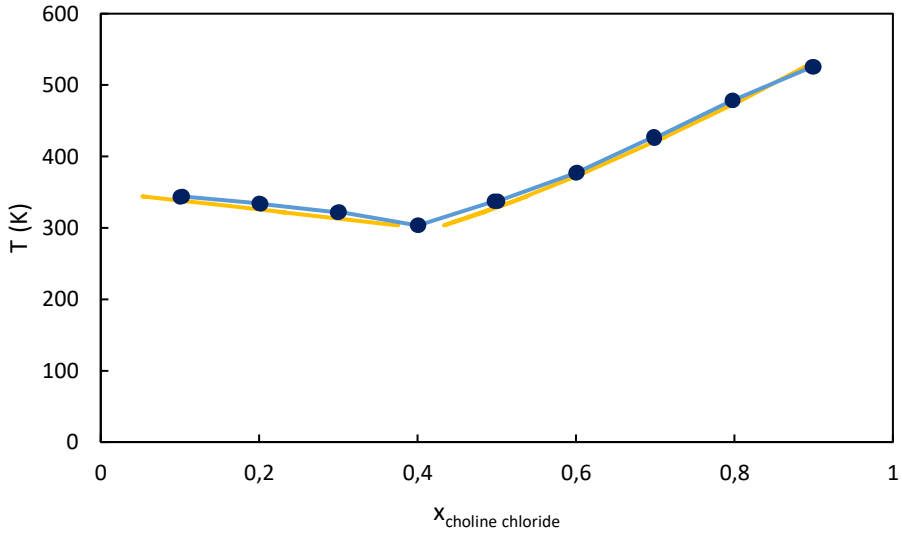

Figure 3.5. SLE - Temperature versus mole fraction of choline chloride for the system {Choline chloride + EMIM chloride}, ● experimental data [69], — COSMO-SAC (2010) model, — COSMO-SAC (+OH-ClBr) model

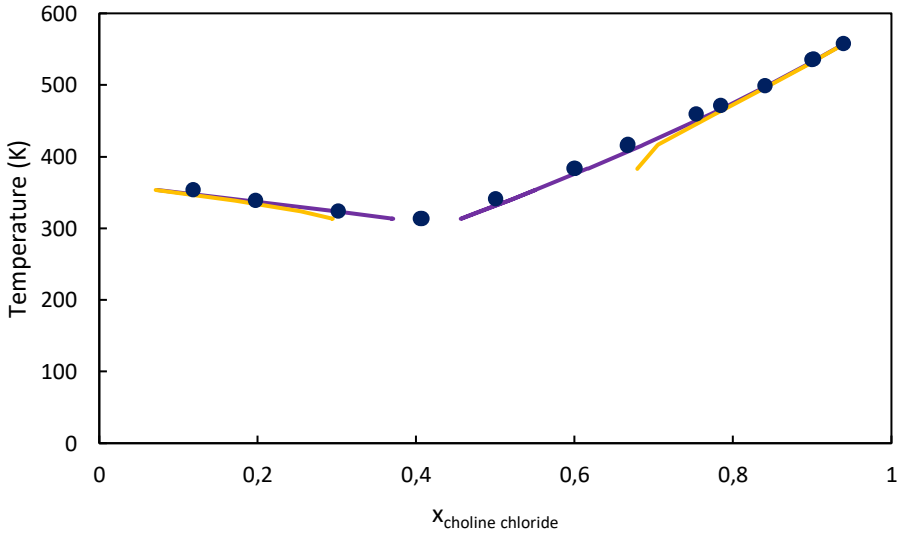

Figure 3.6. SLE - Temperature versus mole fraction of choline chloride for the system {Choline chloride + Choline acetate}, ● experimental data [69], — ideal case ($\gamma_i = 1$), — COSMO-SAC (+OH-ClBr) model

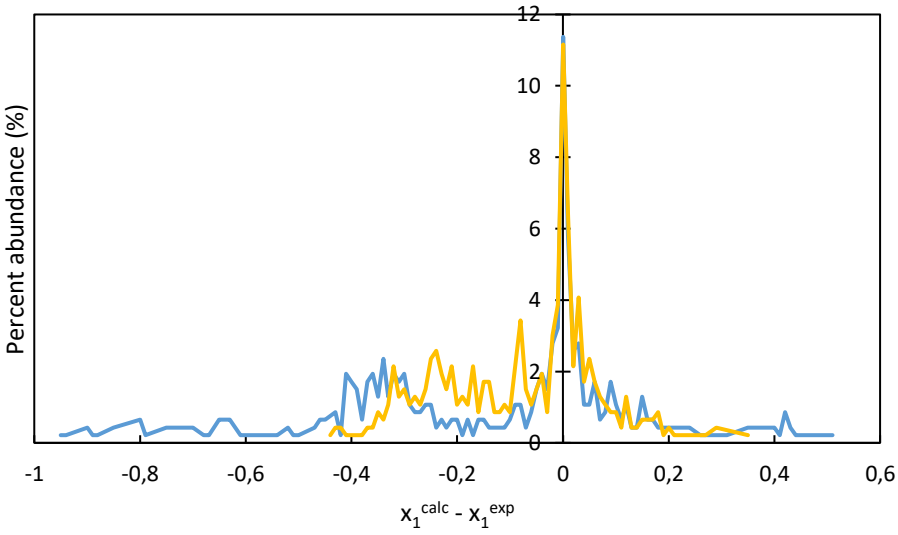

Figure 3.7. Percent abundance of the difference between predicted and experimental mole fraction for the first compound of the mixtures investigated in the SLE study (mixtures for which COSMO-SAC (2010) was able to converge) – Comparison between — COSMO-SAC (2010) and — COSMO-SAC (+OH-ClBr) models

3.5 Conclusion

An extension of the COSMO-SAC model was presented in this work. The aim was to improve the predictions of the phase behaviour of mixtures containing chlorine or bromine atoms, and in particular when the systems included DESs. To do so, a set of two parameters corresponding to the hydrogen bonding interactions were added, introducing a temperature dependence. They were optimized using a database constituted of VLE data of systems containing hydroxyl groups and chlorine or bromine atoms. The resulting COSMO-SAC (+OH-ClBr) model displays performances that are improved in terms of VLE predictions compared to those of COSMO-SAC (2010). COSMO-SAC (+OH-ClBr) is shown to successfully predict the behaviour of mixtures containing many ionic and non-ionic compounds with halogen atoms. LLE and SLE predictions are shown to be on par with those of COSMO-SAC (2010). Besides, judging on the results of this work, the distinction between bromine et chlorine atoms appears not to be impactful. Thus, its implementation is seemingly not required. A further investigation to see if applying the new sets of parameters to fluorine atoms (although already described with parameters shared with oxygen and nitrogen atoms) could be interesting regarding the accuracy

of the model. The investigation of the hydrogen bonding between chlorine/bromine atoms and hydrogen atoms not involved in a hydroxyl group could also be conducted, requiring the optimization of additional parameters with a corresponding database.

3.6 Supplementary material description

The supplementary material contains keywords for the generation of COSMO files with Gaussian, tables of the detailed databank with average deviations for each system (VLE, LLE and SLE) and tables with the description of the dataset used to assess the performances of the new parameters, namely datasets B and D.

3.7 Abbreviations

BMIM, 1-butyl-3-methylimidazolium cation; DES, deep eutectic solvent; DFT, density functional theory; EMIM, 1-ethyl-3-methylimidazolium cation; EOS, equation of state; HMIM, 1-hexyl-3-methylimidazolium cation; IL, ionic liquid; LLE, liquid-liquid equilibrium; MAPE, mean absolute percentage error; RD, relative deviation; RMSD, root-mean-square deviation; SCF, Self-Consistent Field; SLE, solid-liquid equilibrium; TZVP, Triple Zeta Valence plus Polarization; VLE, vapour-liquid equilibrium.

References

[1] H. Perez-Blanco, Absorption heat pump performance for different types of solutions, Int. J. Refrig. 7 (1984) 115–122.

[2] U. Nowaczyk, F. Steimle, Thermophysical properties of new working fluid systems for absorption processes, Int. J. Refrig. 15 (1992).

[3] J. Sun, L. Fu, S. Zhang, A review of working fluids of absorption cycles, Renew. Sustain. Energy Rev. 16 (2012) 1899–1906.

[4] M. Wang, C.A.I. Ferreira, Absorption heat pump cycles with NH3 – ionic liquid working pairs, Appl. Energy. 204 (2017) 819–830.

[5] W. Wu, T. You, X. Li, Performance comparisons of NH3/ionic liquid absorption-compression heat pump for increasing the utilization of geothermal energy, Int. J. Refrig. 104 (2019) 19–33.

[6] Z. He, Thermodynamic properties of new heat pump working pairs: 1,3-Dimethylimidazolium dimethylphosphate and water, ethanol and methanol, Fluid Phase Equilibria. 298 (2010) 83–91.

[7] M. Seiler, A. Kühn, F. Ziegler, X. Wang, Sustainable Cooling Strategies Using New Chemical System Solutions, Ind. Eng. Chem. Res. 52 (2013) 16519–16546. https://doi.org/10.1021/ie401297u.

[8] T.P.T. Pham, C.-W. Cho, Y.-S. Yun, Environmental fate and toxicity of ionic liquids: A review, Water Res. 44 (2010) 352–372. https://doi.org/10.1016/j.watres.2009.09.030.

[9] E.L. Smith, A.P. Abbott, K.S. Ryder, Deep Eutectic Solvents (DESs) and Their Applications, Chem Rev. 114 (2014) 11060–11082.

[10] M. Francisco, A. van den Bruinhorst, M.C. Kroon, Low-Transition-Temperature Mixtures (LTTMs): A New Generation of Designer Solvents, Angew Chem Int Ed. 52 (2013) 3074–3085.

[11] M.A.R. Martins, S.P. Pinho, J.A.P. Coutinho, Insights into the Nature of Eutectic and Deep Eutectic Mixtures, J. Solut. Chem. 48 (2019) 962–982. https://doi.org/10.1007/s10953-018-0793-1.

[12] K. Shahbaz, F.S. Mjalli, G. Vakili-Nezhaad, I.M. AlNashef, A. Asadov, M.M. Farid, Thermogravimetric measurement of deep eutectic solvents vapor pressure, J. Mol. Liq. 222 (2016) 61–66.

[13] Y. Marcus, Deep Eutectic Solvents, 1st ed. 2019, Springer International Publishing : Imprint: Springer, Cham, 2019. https://doi.org/10.1007/978-3-030-00608-2.

[14] M. Francisco, A. van den Bruinhorst, L.F. Zubeir, C.J. Peters, M.C. Kroon, A new low transition temperature mixture (LTTM) formed by choline chloride+lactic acid: Characterization as solvent for CO2 capture, Fluid Phase Equilibria. 340 (2013) 77–84. https://doi.org/10.1016/j.fluid.2012.12.001.

[15] A. González de Castilla, J.P. Bittner, S. Müller, S. Jakobtorweihen, I. Smirnova, Thermodynamic and Transport Properties Modeling of Deep Eutectic Solvents: A Review on g^E -Models, Equations of State, and Molecular Dynamics, J. Chem. Eng. Data. 65 (2020) 943–967. https://doi.org/10.1021/acs.jced.9b00548.

[16] K. Shahbaz, F.S. Mjalli, M.A. Hashim, I.M. AlNashef, Prediction of deep eutectic solvents densities at different temperatures, Thermochim. Acta. 515 (2011) 67–72. https://doi.org/10.1016/j.tca.2010.12.022.

[17] N.R. Mirza, N.J. Nicholas, Y. Wu, S. Kentish, G.W. Stevens, Estimation of Normal Boiling Temperatures, Critical Properties, and Acentric Factors of Deep Eutectic Solvents, J. Chem. Eng. Data. 60 (2015) 1844–1854. https://doi.org/10.1021/acs.jced.5b00046.

[18] L.F. Zubeir, M.H.M. Lacroix, M.C. Kroon, Low Transition Temperature Mixtures as Innovative and Sustainable CO_2 Capture Solvents, J. Phys. Chem. B. 118 (2014) 14429–14441. https://doi.org/10.1021/jp5089004.

[19] C. Ma, Y. Guo, D. Li, J. Zong, X. Ji, C. Liu, Molar enthalpy of mixing and refractive indices of choline chloride-based deep eutectic solvents with water, J. Chem. Thermodyn. 105 (2017) 30–36. https://doi.org/10.1016/j.jct.2016.10.002.

[20] A. Klamt, V. Jonas, T. Bürger, J.C.W. Lohrenz, Refinement and Parametrization of COSMO-RS, J. Phys. Chem. A. 102 (1998) 5074–5085. https://doi.org/10.1021/jp980017s.

[21] S.-T. Lin, S.I. Sandler, A Priori Phase Equilibrium Prediction from a Segment Contribution Solvation Model, Ind. Eng. Chem. Res. 41 (2002) 899–913. https://doi.org/10.1021/ie001047w.

[22] H. Grensemann, J. Gmehling, Performance of a Conductor-Like Screening Model for Real Solvents Model in Comparison to Classical Group Contribution Methods, Ind. Eng. Chem. Res. 44 (2005) 1610–1624. https://doi.org/10.1021/ie049139z.

[23] C.-M. Hsieh, S.I. Sandler, S.-T. Lin, Improvements of COSMO-SAC for vapor–liquid and liquid–liquid equilibrium predictions, Fluid Phase Equilibria. 297 (2010) 90–97. https://doi.org/10.1016/j.fluid.2010.06.011.

[24] S.-T. Lin, L.-H. Wang, W.-L. Chen, P.-K. Lai, C.-M. Hsieh, Prediction of miscibility gaps in water/ether mixtures using COSMO-SAC model, Fluid Phase Equilibria. 310 (2011) 19–24. https://doi.org/10.1016/j.fluid.2011.06.015.

[25] S.S. Kang, J. Lee, J.W. Kang, An extended COSMO-SAC method for the prediction of carboxylic acid solubility, Fluid Phase Equilibria. 521 (2020) 112673. https://doi.org/10.1016/j.fluid.2020.112673.

[26] M. Diedenhofen, A. Klamt, COSMO-RS as a tool for property prediction of IL mixtures—A review, Fluid Phase Equilibria. 294 (2010) 31–38. https://doi.org/10.1016/j.fluid.2010.02.002.

[27] L. Yang, S.I. Sandler, C. Peng, H. Liu, Y. Hu, Prediction of the Phase Behavior of Ionic Liquid Solutions, Ind. Eng. Chem. Res. 49 (2010) 12596–12604.

[28] M.-T. Hsieh, S.-T. Lin, A predictive model for the excess gibbs free energy of fully dissociated electrolyte solutions, AIChE J. 57 (2011) 1061–1074. https://doi.org/10.1002/aic.12325.

[29] B.-S. Lee, S.-T. Lin, Prediction of phase behaviors of ionic liquids over a wide range of conditions, Fluid Phase Equilibria. 356 (2013) 309–320. https://doi.org/10.1016/j.fluid.2013.07.046.

[30] T. Gerlach, S. Müller, I. Smirnova, Development of a COSMO-RS based model for the calculation of phase equilibria in electrolyte systems, AIChE J. 64 (2018) 272–285. https://doi.org/10.1002/aic.15875.

[31] R. Verma, T. Banerjee, Liquid–Liquid Extraction of Lower Alcohols Using Menthol-Based Hydrophobic Deep Eutectic Solvent: Experiments and COSMO-SAC Predictions, Ind. Eng. Chem. Res. 57 (2018) 3371–3381. https://doi.org/10.1021/acs.iecr.7b05270.

[32] S.-H. Wu, A.R. Caparanga, R.B. Leron, M.-H. Li, Vapor pressure of aqueous choline chloride-based deep eutectic solvents (ethaline, glyceline, maline and reline) at 30–70°C, Thermochim. Acta. 544 (2012) 1–5. https://doi.org/10.1016/j.tca.2012.05.031.

[33] B. Sharma, N. Singh, T. Jain, J.P. Kushwaha, P. Singh, Acetonitrile Dehydration via Extractive Distillation Using Low Transition Temperature Mixtures as Entrainers, J. Chem. Eng. Data. 63 (2018) 2921–2930. https://doi.org/10.1021/acs.jced.8b00228.

[34] M.K. Hadj-Kali, H.F. Hizaddin, I. Wazeer, L. El blidi, S. Mulyono, M.A. Hashim, Liquid-liquid separation of azeotropic mixtures of ethanol/alkanes using deep eutectic solvents: COSMO-RS prediction and experimental validation, Fluid Phase Equilibria. 448 (2017) 105–115. https://doi.org/10.1016/j.fluid.2017.05.021.

[35] G. Yu, Z. Wei, K. Chen, R. Guo, Z. Lei, Predictive molecular thermodynamic models for ionic liquids, AIChE J. 68 (2022). https://doi.org/10.1002/aic.17575.

[36] R. Haghbakhsh, S. Raeissi, Modeling vapor-liquid equilibria of mixtures of SO2 and deep eutectic solvents using the CPA-NRTL and CPA-UNIQUAC models, J. Mol. Liq. 250

(2018) 259–268. https://doi.org/10.1016/j.molliq.2017.11.161.

[37] G. Yu, C. Dai, Z. Lei, Modified UNIFAC-Lei Model for Ionic Liquid–CH $_4$ Systems, Ind. Eng. Chem. Res. 57 (2018) 7064–7076. https://doi.org/10.1021/acs.iecr.8b00986.

[38] K. Xin, I. Roghair, F. Gallucci, M. van Sint Annaland, Total vapor pressure of hydrophobic deep eutectic solvents: Experiments and modelling, J. Mol. Liq. 325 (2021) 115227. https://doi.org/10.1016/j.molliq.2020.115227.

[39] C.-M. Hsieh, S.-T. Lin, J. Vrabec, Considering the dispersive interactions in the COSMO-SAC model for more accurate predictions of fluid phase behavior, Fluid Phase Equilibria. 367 (2014) 109–116. https://doi.org/10.1016/j.fluid.2014.01.032.

[40] R. Fingerhut, W.-L. Chen, A. Schedemann, W. Cordes, J. Rarey, C.-M. Hsieh, J. Vrabec, S.-T. Lin, Comprehensive Assessment of COSMO-SAC Models for Predictions of Fluid-Phase Equilibria, Ind. Eng. Chem. Res. 56 (2017) 9868–9884. https://doi.org/10.1021/acs.iecr.7b01360.

[41] I.H. Bell, E. Mickoleit, C.-M. Hsieh, S.-T. Lin, J. Vrabec, C. Breitkopf, A. Jäger, A Benchmark Open-Source Implementation of COSMO-SAC, J. Chem. Theory Comput. 16 (2020) 2635–2646. https://doi.org/10.1021/acs.jctc.9b01016.

[42] S. Wang, S.I. Sandler, C.-C. Chen, Refinement of COSMO−SAC and the Applications, Ind. Eng. Chem. Res. 46 (2007) 7275–7288. https://doi.org/10.1021/ie070465z.

[43] B. Bouillot, Approches Thermodynamiques pour la Prédiction de la Solubilité de Molécules d'Intérêt Pharmaceutique, Doctoral dissertation, Université de Toulouse, Institut National Polytechnique de Toulouse, 2011.

[44] A.J. Staverman, The entropy of high polymer solutions. Generalization of formulae, Recl. Trav. Chim. Pays-Bas. 69 (1950) 163–174. https://doi.org/10.1002/recl.19500690203.

[45] F.Z. Nessakh, Etude de nouveaux fluides de travail constitués de solvants eutectiques profonds pour les pompes à chaleur, Ph.D. Thesis, Université de Tlemcen, Algeria, Université de Lorraine, France, 2022.

[46] P.J. Carvalho, I. Khan, A. Morais, J.F.O. Granjo, N.M.C. Oliveira, L.M.N.B.F. Santos, J.A.P. Coutinho, A new microebulliometer for the measurement of the vapor–liquid equilibrium of ionic liquid systems, Fluid Phase Equilibria. 354 (2013) 156–165. https://doi.org/10.1016/j.fluid.2013.06.015.

[47] N. Chouireb, I. Khan, E.A. Crespo, M.B. Oliveira, F. Llovell, L.F. Vega, O. Tafat-Igoudjilene, A.A. Kaci, L.M.N.B.F. Santos, P.J. Carvalho, J.A.P. Coutinho, Evaluation of the solvent structural effect upon the vapor –liquid equilibrium of [C4C1im][Cl] + alcohols, Fluid Phase Equilibria. 440 (2017) 36–44. https://doi.org/10.1016/j.fluid.2017.02.016.

[48] J. Wisniak, A. Tamir, Vapor-liquid equilibrium in the systems propyl bromide-acetic acid, propyl bromide-propionic acid and propyl bromide-acetic acid-propionic acid, J. Chem. Eng. Data. 27 (1982) 430–435. https://doi.org/10.1021/je00030a019.

[49] M. Królikowska, K. Paduszyński, M. Zawadzki, (Vapor + liquid) phase equilibria of an aqueous solution of bromide-based ionic liquids – measurements, correlations and application to absorption cycles, Fluid Phase Equilibria. 494 (2019) 201–211. https://doi.org/10.1016/j.fluid.2019.05.003.

[50] K.-S. Kim, S.-Y. Park, S. Choi, H. Lee, Vapor Pressures of the 1-Butyl-3-methylimidazolium Bromide + Water, 1-Butyl-3-methylimidazolium Tetrafluoroborate + Water, and 1-(2-Hydroxyethyl)-3-methylimidazolium Tetrafluoroborate + Water Systems, J. Chem. Eng. Data. 49 (2004) 1550–1553. https://doi.org/10.1021/je034210d.

[51] H. Passos, I. Khan, F. Mutelet, M.B. Oliveira, P.J. Carvalho, L.M.N.B.F. Santos, C. Held, G. Sadowski, M.G. Freire, J.A.P. Coutinho, Vapor–Liquid Equilibria of Water + Alkylimidazolium-Based Ionic Liquids: Measurements and Perturbed-Chain Statistical Associating Fluid Theory Modeling, Ind. Eng. Chem. Res. 53 (2014) 3737–3748. https://doi.org/10.1021/ie4041093.

[52] M. Zawadzki, M. Królikowska, J. Antonowicz, P. Lipiński, M. Karpińska, Physicochemical and thermodynamic properties of the {1-alkyl-1-methylmorpholinium bromide, [C1Cn=3,4,5MOR]Br, or 1-methyl-1-pentylpiperidinium bromide, [C1C5PIP]Br+water} binary systems, J. Chem. Thermodyn. 98 (2016) 324–337. https://doi.org/10.1016/j.jct.2016.03.030.

[53] J. Wisniak, A. Tamir, Vapor-liquid equilibria at 760 mmHg in the system methanol-2-propanol-propyl bromide and its binaries, J. Chem. Eng. Data. 30 (1985) 339–344. https://doi.org/10.1021/je00041a032.

[54] J. Wisniak, A. Tamir, Vapor-liquid equilibria at 760 mm Hg in the systems propyl bromide-tert-butyl alcohol and propyl bromide-p-xylene, J. Chem. Eng. Data. 33 (1988) 106–108. https://doi.org/10.1021/je00052a012.

[55] V.K. Shen, D.W. Siderius, W.P. Krekelberg, H.W. Hatch, NIST Standard Reference Simulation Website, NIST Standard Reference Database Number 173, National Institute of Standards and Technology, Gaithersburg MD, 20899, http://doi.org/10.18434/T4M88Q, NIST. (2021). https://www.nist.gov/ (accessed October 18, 2021).

[56] J.P. O'Connell, J.M. Haile, Thermodynamics: Fundamentals for Applications, Cambridge University Press, 2005.

[57] J.M. Prausnitz, R.N. Lichtenthaler, E.G. de Azevedo, Molecular Thermodynamics of

Fluid-Phase Equilibria, Pearson Education, 1998.

[58] M.J. Frisch, G.W. Trucks, H.B. Schlegel, G.E. Scuseria, M.A. Robb, J.R. Cheeseman, G. Scalmani, V. Barone, G.A. Petersson, H. Nakatsuji, X. Li, M. Caricato, A. Marenich, J. Bloino, B.G. Janesko, R. Gomperts, B. Mennucci, H.P. Hratchian, J.V. Ortiz, A.F. Izmaylov, J.L. Sonnenberg, D. Williams-Young, F. Ding, F. Lipparini, F. Egidi, J. Goings, B. Peng, A. Petrone, T. Henderson, D. Ranasinghe, V.G. Zakrzewski, J. Gao, N. Rega, G. Zheng, W. Liang, M. Hada, M. Ehara, K. Toyota, R. Fukuda, J. Hasegawa, M. Ishida, T. Nakajima, Y. Honda, O. Kitao, H. Nakai, T. Vreven, K. Throssell, J.A. Montgomery, Jr., J.E. Peralta, F. Ogliaro, M. Bearpark, J.J. Heyd, E. Brothers, K.N. Kudin, V.N. Staroverov, T. Keith, R. Kobayashi, J. Normand, K. Raghavachari, A. Rendell, J.C. Burant, S.S. Iyengar, J. Tomasi, M. Cossi, J.M. Millam, M. Klene, C. Adamo, R. Cammi, J.W. Ochterski, R.L. Martin, K. Morokuma, O. Farkas, J.B. Foresman, D.J. Fox, Gaussian 09, Revision D.01, Gaussian Inc., Wallingford CT, 2016.

[59] A.D. Becke, Density-functional exchange-energy approximation with correct asymptotic behavior, Phys. Rev. A. 38 (1988) 3098–3100. https://doi.org/10.1103/PhysRevA.38.3098.

[60] J.P. Perdew, Density-functional approximation for the correlation energy of the inhomogeneous electron gas, Physical review B. 33 (1986) 8822–8824.

[61] S.H. Vosko, L. Wilk, M. Nusair, Accurate spin-dependent electron liquid correlation energies for local spin density calculations: a critical analysis, Can. J. Phys. 58 (1980) 1200–1211. https://doi.org/10.1139/p80-159.

[62] A. Schäfer, H. Horn, R. Ahlrichs, Fully optimized contracted Gaussian basis sets for atoms Li to Kr, J. Chem. Phys. 97 (1992) 2571–2577. https://doi.org/10.1063/1.463096.

[63] A. Schäfer, C. Huber, R. Ahlrichs, Fully optimized contracted Gaussian basis sets of triple zeta valence quality for atoms Li to Kr, J. Chem. Phys. 100 (1994) 5829–5835. https://doi.org/10.1063/1.467146.

[64] N. Godbout, D.R. Salahub, J. Andzelm, E. Wimmer, Optimization of Gaussian-type basis sets for local spin density functional calculations. Part I. Boron through neon, optimization technique and validation, Can. J. Chem. 70 (1992) 560–571. https://doi.org/10.1139/v92-079.

[65] C. Sosa, J. Andzelm, B.C. Elkin, E. Wimmer, K.D. Dobbs, D.A. Dixon, A local density functional study of the structure and vibrational frequencies of molecular transition-metal compounds, J. Phys. Chem. 96 (1992) 6630–6636. https://doi.org/10.1021/j100195a022.

[66] T. Banerjee, M.K. Singh, A. Khanna, Prediction of Binary VLE for Imidazolium Based Ionic Liquid Systems Using COSMO-RS, Ind. Eng. Chem. Res. 45 (2006) 3207–3219.

https://doi.org/10.1021/ie051116c.

[67] R. Verma, P.K. Naik, I. Diaz, T. Banerjee, Separation of low molecular weight alcohols from water with deep eutectic solvents: Liquid-liquid equilibria and process simulations, Fluid Phase Equilibria. 533 (2021) 112949. https://doi.org/10.1016/j.fluid.2021.112949.

[68] M. Zawadzki, M. Królikowska, P. Lipiński, Physicochemical and thermodynamic characterization of N -alkyl- N -methylpyrrolidinium bromides and its aqueous solutions, Thermochim. Acta. 589 (2014) 148–157. https://doi.org/10.1016/j.tca.2014.05.028.

[69] L. Fernandez, L.P. Silva, M.A.R. Martins, O. Ferreira, J. Ortega, S.P. Pinho, J.A.P. Coutinho, Indirect assessment of the fusion properties of choline chloride from solid-liquid equilibria data, Fluid Phase Equilibria. 448 (2017) 9–14. https://doi.org/10.1016/j.fluid.2017.03.015.

Chapitre 4

Group contribution models for densities and heat capacities of deep eutectic solvents

'Would you tell me please which way I ought to walk from here?'
'That depends a great deal on where you want to go,' said the cat.
'I don't much care where --', said Alice.
'Then it doesn't matter which way you walk,' said the cat.

-- Lewis Carroll

Chapitre 4 : Group contribution models for densities and heat capacities of deep eutectic solvents

Thomas Di Pietro[a], Laetitia Cesari[a], Fabrice Mutelet[a,*]

a - Université de Lorraine, Ecole Nationale Supérieure des Industries Chimiques, Laboratoire Réactions et Génie des Procédés (UMR CNRS 7274), 1 rue Grandville, 54000 Nancy, France

Article à soumettre

Résumé

Ce chapitre présente la plus récente base de données regroupant deux propriétés clef pour l'usage des solvants eutectiques profonds dans les procédés, à savoir la masse volumique et la capacité thermique. Cette banque de données a été utilisée dans le développement de modèles de contribution de groupes simples d'utilisation ayant pour but de prédire les propriétés de n'importe quel solvant à eutectique profond qui puisse être décrit à l'aide des groupes sélectionnés. La banque de données contient un total de 3266 points de masse volumique et 573 points de capacité thermique. Ces modèles nécessitent seulement une température et le nombre de groupes au sein de chaque molécule, sans limitation vis-à-vis du nombre de molécules pouvant composer le solvant à eutectique profond. Les écarts moyens obtenus sont de 1.95 % pour les masses volumiques et 3.09 % pour les capacités thermiques et sont comparés à des modèles de contribution de groupes plus complexes issus de la littérature. Ces modèles sont très faciles à mettre en place et à modifier, notamment lorsque de nouvelles données deviennent disponibles, et sont un pas en avant dans le domaine de la prédiction générale des propriétés des solvants à eutectique profond.

Abstract

The most recent database regrouping two key properties for the use of deep eutectic solvents in chemical processes, namely the density and the heat capacity, was used to develop simple group contribution models for predicting these properties. The databank contains a total of 3266 and 573 data points for density and heat capacity, respectively. These models only require the temperature and the number of each group in the molecules with no limitation on the number of molecules composing the studied deep eutectic solvent. The resulting average deviations are of 1.95% for density and 3.09% for heat capacity and are compared to more complex group contribution models from the literature. These models are easy to implement and to modify for when new data will be available are a step in the direction of general prediction of properties of deep eutectic solvents.

4.1 Introduction

Considerable efforts are made towards the development and use of sustainable and greener solvents in the industry [1,2]. Deep eutectic solvents (DESs) are among the promising and new categories of solvents. Appeared at the beginning of the 2000s [3,4], their fields of application have since largely been investigated, extending from synthesis [5–7] to analytical chemistry [8] or energy recovery [9]. Sometimes comprised of ionic liquids (ILs), DESs consist of the association of at least one donor and one acceptor of hydrogen to form a hydrogen bond. The resulting interactions within the mixture lead to a solvent behaving like a pure compound with a temperature of fusion below the one of the pure hydrogen bond donor and acceptor if they are taken individually. Moreover, the temperature of fusion of the DES should also be lower compared to the one of the ideal mixture [10]. If chosen appropriately the liquid solvent at the desired temperature should have negligible vapour pressure, which are very favourable properties for solvents. Depending on the constituents of the DESs, other wanted properties such as low cost and low ecotoxicity can be attained. Components and ratios of the DESs also greatly affect thermophysical properties such as density and heat capacity [11]. Of paramount importance in terms of processes design in which heat and/or mass transfers take place, the properties must be optimized and accurately determined. Due to the great number of possible associations for DESs, simulations are essential in order to lessen the need of experimental data. Moreover, the predictions ought to be reliable, hence the diverse modelling methods and approaches that have consistently increased in number over the past few years. They include empirical equations, activity coefficient models, equations of state, machine learning and methods based on critical properties or group contribution methods [12,13]. First developed for organic compounds and then extended to ILs, these models have in particular been applied to predict the densities [14–17], heat capacities [18,19] and viscosities [20–25] of DESs. They can be either specific of a sole DES with an optimization based on the ratio or the temperature or

with a more comprehensive applicability. Some thermodynamic models or correlations require the knowledge of critical properties. This limits the methods, especially since the critical properties of DESs are not easily available and cannot be measured. On the other hand, group contribution methods are being developed with the aim of providing a tool generally and readily usable with parameters working for any DES.

Group contribution methods (GCMs) are based on the description of compounds using molecular groups. To predict the property of a studied system, each group contributes to the calculations according to optimized parameters. The contributions are weighted by how many times the corresponding group appears in the system. Then, the contributions are summed to obtain the physicochemical property. This allows to have a general model with parameters fitting any DES as opposed to a model that would require specific parameters for each DES. In the case of DESs, it also offers the specific advantage of easily taking into account the ratios of the hydrogen bond donors and acceptors when counting the groups while being temperature-dependant.

For the densities, an early group contribution method depending on the volumes of the ions and cations has been developed using a databank of 9 ILs and 788 data points [26]. Another method described by Shahbaz et al. [27] made use of a modified Lydersen-Joback-Reid method to estimate the critical properties of DESs along with Lee-Kesler equations for their mixing critical properties. From these, densities were calculated via a Rackett equation modified by Spencer and Danner with the use of experimental data points for more accuracy. Thereafter, this method was applied to other datasets constituted of DESs [14,28]. Hou et al. based their work on the hydrogen bond interactions within the DESs to propose a bonding-group interaction contribution model to describe both the constituents and their interactions in the DESs [29]. They used 3647 data points of densities of binary DESs and an additional 174 points from ternary DESs. The model leads to an average deviation of 1.49% for their training set and

of 1.56% for their test set. Their studied systems include a few groups and atoms such as potassium, praseodymium, fluorine, zinc or cerium. Between the structural parameters, the parameters for the substitution patterns (the ortho, meta and para position for substituents in aromatic hydrocarbons) interaction parameters based on five types of DES and constant parameters, the model requires the implementation of up to 80 parameters to work for binary DESs plus one more for DESs made of three components. Besides, because of the consideration of the interactions, increasing the number of constituents in the system would require more parameters and the implementation of a Redlich-Kister type of equation. Haghbakhsh et al. developed several group contribution models as well as atomic contribution models for five properties of DESs including the density and heat capacity (along with refractive index, speed of sound and surface tension) [30]. The density and heat capacity dataset gathered 1239 and 461 data points, respectively, with a deviation of 1.44% for density and 3.26% for heat capacity. In their models, the correlations are functions of the temperature and of the molar mass of the DESs. In particular, the temperature dependences are not linear. Instead, a power of -0.6785 is applied to the temperature for the group contribution model for density while the model for heat capacity has the temperature to a power -0.4528. The density model requires 70 parameters for groups along with 3 constant ones (including the powers) for a total of 35 groups considered. For the heat capacity model, 44 parameters and 3 constant parameters were implemented for 22 groups differentiated.

Other group contribution methods for heat capacities include one by Gardas et Coutinho [31] for ILs. The parameters for their second-order, temperature-dependent correlation were optimized using 2400 data points. Ahmadi et al. also proposed an atomic contribution method using a dataset gathering 4822 heat capacities of ILs [32]. Another correlation involving the critical pressure and the acentric factor of a given DES, obtained via the Lydersen and Joback-Reid group contribution approach, was developed to estimate the heat capacities of DESs with

an overall deviation of 4.7% [33].

New correlations can be investigated as more data are produced. This work aims at presenting group contribution methods for the prediction of two different properties, namely the density and the heat capacity of DESs with the most recent database available and a straightforward and very easy-to-apply approach. The database comprises 3266 data points of densities and 573 data points of heat capacities. The databank is composed of binary and ternary DESs (DESs composed of two or three compounds, ILs counting as one). The method ambitions to present models that can be used with ease as well as modified with any new addition of groups as needed and according to the availability of the data.

4.2 Group contribution models

4.2.1 DESs description

The DESs are described with several groups in order to calculate their density and heat capacity with two different models. To describe the DESs and count the groups, ratios are always normalized. For instance, a ratio [1:2] in the literature will be changed to [0.333:0.667] in our calculations. For a DES {[Choline][Chloride]:Ethylene glycol}, [0.333:0.667], the counted groups are: 2*0.333 [-CH_2-], 3*0.333 [-CH_3], 1*0.333 [-OH], 1*0.333 [>$N^{(+)}$<] and 1*0.333 [Cl^-] for the choline chloride and 2*0.667 [-CH_2-] and 2*0.667 [-OH] for ethylene glycol.

4.2.2 Description of the models

For the densities of the DESs ρ_{liq}^{DES} (g.cm^{-3}), the properties are calculated using a linear dependence in temperature which is traditionally used for this kind of system [34,35] and is detailed in the following equations:

$$\rho_{liq}^{DES} = A^{\rho} + B^{\rho} * \frac{T}{100} \quad (1)$$

T is the temperature of the system in K. To obtain A^{ρ} and B^{ρ} for a given DES, the equations (2) and (3) are used:

$$A^{\rho} = a_0^{\rho} + \sum_{i=1}^{n_{group}^{tot}} n_i * a_i^{\rho} \quad (2)$$

$$B^{\rho} = b_0^{\rho} + \sum_{i=1}^{n_{group}^{tot}} n_i * b_i^{\rho} \quad (3)$$

n_i corresponds to the number of times the group i appears in the DES, with n_{group}^{tot} the total number of groups. a_i^{ρ} and b_i^{ρ} are the parameters obtained from the group contribution method related to density. a_0^{ρ} and b_0^{ρ} are constant and independent of the DES.

The molar heat capacities of the DESs Cp_m^{DES} (J.mol^{-1}.K^{-1}) are obtained using a method previously applied to ILs by Gardas et al. [36]:

$$Cp_m^{DES} = R * \left(A^{Cp} + B^{Cp} * \frac{T}{100} + C^{Cp} * \left(\frac{T}{100} \right)^2 \right) \quad (4)$$

R is the molar gas constant (R=8.314472 J.mol^{-1}K^{-1}). A^{Cp}, B^{Cp} and C^{Cp} are provided in a similar manner compared to density by the equations:

$$A^{Cp} = \sum_{i=1}^{n_{group}^{tot}} n_i * a_i^{Cp} \quad (5)$$

$$B^{Cp} = \sum_{i=1}^{n_{group}^{tot}} n_i * b_i^{Cp} \quad (6)$$

$$C^{Cp} = \sum_{i=1}^{n_{group}^{tot}} n_i * c_i^{Cp} \quad (7)$$

The parameters a_i^{Cp}, b_i^{Cp} and c_i^{Cp} are specific to the molar heat capacity model.

The objective function that has been minimized to obtain the parameters is equal to the mean absolute percentage error (MAPE) of the dataset considered for the optimization:

$$obj = \frac{1}{N_{data}} * \left(\sum_{i=1}^{N_{data}} \frac{\left| X_i^{calc} - X_i^{exp} \right|}{X_i^{exp}} * 100 \right) \quad (8)$$

With X_i^{calc} the calculated property, X standing for ρ_{liq}^{DES}or Cp_m^{DES} depending on the investigated property and X_i^{exp} the corresponding experimental value for the data point i. N_{data} is the total number of data points in the optimizing dataset. This formula also corresponds to the average deviation (%) that is used to assess the performances of the models, with N_{data} representing the total number of data points in the investigated set of data.

The standard deviation σ was also used to estimate the accuracy of the models:

$$\sigma = \sqrt{\frac{\sum_{i=1}^{N_{data}} (X_i^{calc} - X_i^{exp})^2}{N_{data}}} \quad (9)$$

Finally, the absolute average deviation (AAD) has also been considered:

$$AAD = \frac{1}{N_{data}} * \left(\sum_{i=1}^{N_{data}} \left| X_i^{calc} - X_i^{exp} \right| \right) \quad (10)$$

4.3 Databank description

The density and molar heat capacity values used to develop the models were measured at atmospheric pressure.

4.3.1 Density

The databank for the density is composed of 3266 data points for 231 DESs. This last number does not take into account the ratios of the systems but only the nature of the hydrogen donor and acceptor. The list of DESs is presented in **Table S.C23** in the supporting information. The databank has been divided in two datasets D1 and D2 for whether the data have been exploited for the optimization of the parameters (dataset D1, optimizing set, 79.8% of the data) or not (dataset D2, dataset used for testing only, 20.2% of the data). The latter allows to assess the robustness of the model by performing calculations with DESs not included during the optimization process.

The optimizing dataset D1 contains 188 DESs and a total of 2607 data points. Dataset D1 is detailed in

Table S.C24. The densities vary from 0.8051 (system made of menthol and dodecanoic acid) to 1.4712 g.cm^{-3} (choline chloride with trichloroacetic acid) while the range of temperature is 278.15 – 413.15 K.

Dataset D2 comprises 43 DESs (none of them included in D1) and 654 data points. The dataset is detailed in **Table S.C25**. The lowest density is 0.8102 g.cm^{-3} for a system containing dodecanoic and octanoic acids while the highest density is of 1.46 g.cm^{-3} for glucose with tartaric acid. Temperatures range from 278.15 to 413.15 K as well.

4.3.2 Heat capacity

The databank for heat capacity is composed of 573 data points and 27 systems. The list of systems is detailed in **Table S.C26**. Only sets of data containing at least 8 data points have been used in order to have a reliable variation of the heat capacity as a function of the temperature and the composition. Therefore, 3 single data points for the systems {Betaine:Glycerol}, {Betaine:Ethylene glycol} and {Betaine:Propylene glycol} [36] were excluded. The databank is divided in two datasets, the optimizing dataset H1 (73.1% of the data) and the data set used for testing only H2 (26.9% of the data).

There are 21 systems and 419 data points in dataset H1. These are detailed in **Table S.C27**. The minimum value of heat capacity is 109.6 J.mol^{-1}.K^{-1} for a DES containing malic acid, betaine and water and the maximum is 605.9 J.mol^{-1}.K^{-1} for a DES with tetrabutylammonium chloride and malonic acid. The temperature is ranging from 298.15 to 363.15 K.

Dataset H2 is composed of 6 systems and 154 data points. The details are given in **Table S.C28**. Extreme values for the heat capacities are 181.4 J.mol^{-1}.K^{-1} and 479.7 J.mol^{-1}.K^{-1} for the DESs containing choline chloride and urea and tetrabutylammonium chloride and triethylene

glycol, respectively. The range of temperature is 278.15 – 361.15 K.

4.4 Results and discussion

Groups have been chosen to best describe the data available in the literature. The total number of groups varies from one model to another since some molecules and functional groups are only available with enough data points in some datasets. Among the most notable choices, the several hybridisations of the atom of nitrogen have different groups depending on the number of hydrogen atoms and the charges that are on the atom of nitrogen. As in the model from Hou et al. [29], a group [H_2O] has been solely devoted to the molecule of water. Groups that are constituting a ring and groups that are not are differentiated. The only exception is the carbonyl group [>C=O] for which the distinction did not improve the results. The corresponding parameters are thus applied whether the group is part of a ring or not. On the other hand, no groups have been devoted to functional groups that are linked to a carbon that is forming a ring. Thus, a hydroxyl group [-OH] in a saturated ring (phenolic compound) is treated with the same parameters as a hydroxyl group from any other alcohol. This also helps reducing the number of parameters. In a similar vein, the group [-Cl] has been used for molecules containing a chlorine substituent or a chloride ion. The optimized parameters for each group and each model along with the average deviations obtained for each dataset are presented in the following sections.

4.4.1 Density

33 groups are used in this model for a total of 68 parameters, including parameters a_0^ρ and b_0^ρ used with any DES. The parameters for the density model are provided in **Table 4.1**.

Table 4.1. Parameters a_i^ρ and b_i^ρ and their values for each group within the group contribution model for density

Groups forming a ring or not	Groups	Parameters	
		a_i^ρ	b_i^ρ
	0 (for parameters a_0^ρ and b_0^ρ)	0.0102	1.1057
Not forming a ring	H_2O	-0.0851	0.3955
	>C<	0.0086	0.1974
	-CH<	0.0356	$6.5*10^{-5}$
	$-CH_2-$	-0.0067	0.0061
	$-CH_3$	-0.0019	-0.1371
	>C=	-0.0963	0.3746
	-CH=	0.0321	-0.0629
	$CH_2=$	-0.3792	1.0195
	-O-	0.0110	$3.9*10^{-4}$
	$-O^{(-)}$	-0.1149	0.3465
	-OH	-0.0348	0.0916
	-COOH	-0.0460	0.2069
	>C=O (*)	-0.0319	0.1692
	$>N^{(+)}<$	0.1026	0.1788
	$-NH^{(+)}<$	0.1100	-0.0016
	-NH-	$8.2*10^{-4}$	0.2012

	$-NH_2$	-0.0369	0.0122
	$-CONH_2$	-0.0392	0.2741
	>C=NH	$8.2*10^{-4}$	0.2000
	$>S(=O)_2$	0.2093	-0.5168
	$>P^{(+)}<$	0.1404	0.3911
	$-Cl^{(-)}$/HCl/-Cl	-0.0813	0.2920
	$-Br^{(-)}$	$-5.1*10^{-5}$	0.1698
Forming a ring	>C<	0.0240	$-4.6*10^{-4}$
	-CH<	0.0052	0.0363
	$-CH_2-$	-0.0308	0.0657
	>C=	-0.0287	0.1632
	-CH=	-0.0087	-0.0055
	-O-	0.0511	-0.1268
	>N-	-0.1745	0.5494
	>NH	0.0128	0.1516
	-N=	-0.0708	0.0909
	$>N^{+}=$	0.2290	-0.3583

(*) The group ">C=O (not forming a ring)" is applicable whether the carbonyl group is part of a ring or not

The deviations for the entire dataset between experimental and calculated densities are shown in **Figure 4.1**. Both optimizing and testing datasets have a similar repartition along the x=y line. Besides, average and standard deviations along with the characteristics of the databank are gathered in **Table 4.2**. Although there is a difference of almost 1% in terms of average deviation between dataset D1 and D2 (1.77 against 2.70%), both the figure and the results from the table show that the predictions for the testing and optimizing datasets are on par with each

other. The average deviation for the entire dataset of density is 1.95%. The distributions of the calculated values of deviation in percentage for each dataset have also been presented in **Table 4.3**. More than 50% of the deviations are below 2% for both datasets and almost 42.8% of the data points are below 1% of deviation for D1+D2. It is also interesting to note that the model is able to predict well the impact of the ratio of the DES. As presented in **Figure 4.2** for the DES {[Tetrabutylammonium][Chloride]:Triethylene glycol} with ratios from [1:1] to [4:1], a linear evolution of the density with increasing molar fraction of tetrabutylammonium chloride is predicted in accordance to the experimental data.

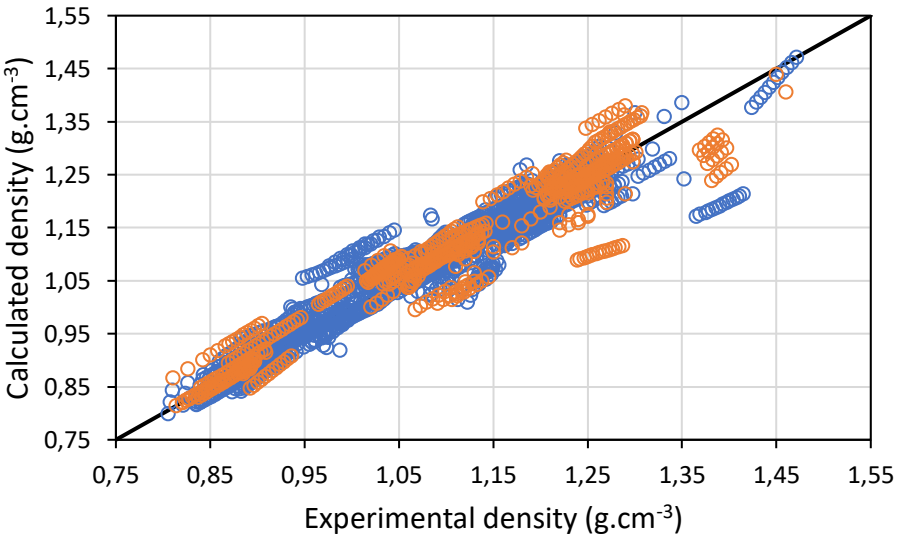

Figure 4.1. Deviation between experimental and modelled density for both the optimizing and testing sets, o optimizing set D1, o testing set D2.

Nevertheless, some discrepancies can be observed in the values of average deviations. Notably, the density values for some acids tend to not be well predicted. The high average deviation for small acids such as formic acid and pyruvic acid could be explained by the fact that these molecules are scarcely represented in the dataset with only two corresponding data points for the formic acid and 13 for the pyruvic acid. Some deviations higher than 5% are obtained when glycolic acid is one of the main components of the DES (for example, when forming a DES with xylitol). An overestimation of the densities for mixtures of two carboxylic

acids can also be observed, in particular for DESs composed of dodecanoic and octanoic acid. For these acids, there are interactions such as hydrogen bonds that could lead to lower the density values compared to what is expected by the model.

Table 4.2. Comparison of the statistical indicators for the different datasets used in the development of the group contribution models for density and heat capacity

Property	Dataset	Number of data points	Temperature range (K)	Property range	Absolute average deviation	Average deviation (%)	Maximum deviation	Maximum deviation (%)	Standard deviation σ
Density ($g.cm^{-3}$)	D1	2607	278.15 - 413.15	0.8051 - 1.4712	0.02 $g.cm^{-3}$	1.77	0.20 $g.cm^{-3}$	14.31	0.03 $g.cm^{-3}$
	D2	659	278.15 - 413.15	0.8102 - 1.46	0.03 $g.cm^{-3}$	2.70	0.17 $g.cm^{-3}$	13.28	0.05 $g.cm^{-3}$
	D1+D2	**3266**	**278.15 - 413.15**	**0.8051 - 1.4712**	**0.02 $g.cm^{-3}$**	**1.95**	**0.20 $g.cm^{-3}$**	**14.31**	**0.03 $g.cm^{-3}$**
Heat capacity ($J.mol^{-1}.K^{-1}$)	H1	419	298.15 - 363.15	109.6 - 605.9	10.11 $J.mol^{-1}.K^{-1}$	3.14	77.56 $J.mol^{-1}.K^{-1}$	28.25	22.53 $J.mol^{-1}.K^{-1}$
	H2	154	278.15 - 361.15	181.4 - 479.7	8.67 $J.mol^{-1}.K^{-1}$	2.95	36.46 $J.mol^{-1}.K^{-1}$	18.91	13.31 $J.mol^{-1}.K^{-1}$
	H1+H2	**573**	**278.15 - 363.15**	**109.6 - 605.9**	**9.72 $J.mol^{-1}.K^{-1}$**	**3.09**	**77.56 $J.mol^{-1}.K^{-1}$**	**28.25**	**20.46 $J.mol^{-1}.K^{-1}$**

Moreover, the stability of DESs composed of carboxylic acids has been reconsidered by Rodriguez et al [38]. The authors have shown that a reaction of esterification can occur between acids and choline chloride, leading to the degradation of the DESs and the presence of impurities. Finally, the densities of DESs containing guaiacol seem to systematically be underestimated although the highest AAD observed is around 0.09 $g.cm^{-3}$ for the system {[Acetylcholine][Chloride]:Guaiacol} [0.167:0.833] at 323.15 K. The average deviations of the ten most representative families of constituents of DESs are given in **Table 4.4**. The family with the highest number of points corresponds to the choline chloride based DESs with a total

of 1267 points. They account for more than a third of the entire database of density (38.8%). They are also one of the most well predicted family, alongside the betaine and the benzyltrialkylammonium type of DESs, with overall deviations around 1.5% or lower. Sugar-type DESs are also well modelled with deviations around 1.6% for both databanks. The other families with the highest numbers of points are the carboxylic acid and the diol families with 1118 and 817 points, respectively. For these two groups, an increase in terms of deviation can be observed between the optimising and the testing sets D1 and D2. In the case of the carboxylic acid family, the deviation goes from 2.06% to 3.15%, while it increases from 1.55 to 3.62% for the diol based DESs. Nonetheless, most families in **Table 4.4** present an overall deviation around 2% or lower.

Table 4.3. Repartition of the values of the deviation (%) between modelled and experimental properties for each dataset of density and heat capacity.

Property	Dataset	Range of deviation				
		< 1%	1-2%	2-5%	>5%	Total
Density	D1	1156 (44.3%)	610 (23.4%)	687 (26.4%)	154 (5.9%)	2607 (100%)
	D2	241 (36.6%)	97 (14.7%)	216 (32.8%)	105 (15.9%)	659 (100%)
	D1+D2	**1397 (42.8%)**	**707 (21.6%)**	**903 (27.6%)**	**259 (7.9%)**	**3266 (100%)**
Heat capacity	H1	269 (64.2%)	45 (10.7%)	37 (8.8%)	68 (16.2%)	419 (100%)
	H2	49 (31.8%)	22 (14.3%)	53 (34.4%)	30 (19.5%)	154 (100%)
	H1+H2	**318 (55.5%)**	**67 (11.7%)**	**90 (15.7%)**	**98 (17.1%)**	**573 (100%)**

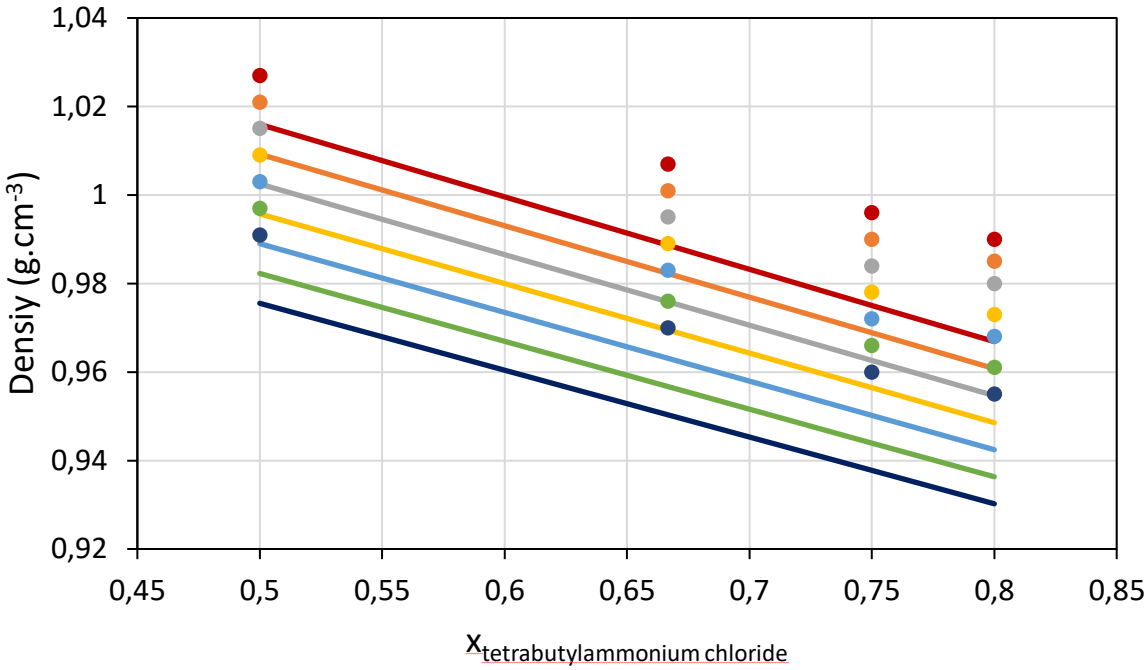

Figure 4.2. Evolution of the density of {[Tetrabutylammonium][Chloride]:Triethylene glycol} as a function of the ratio of salt in the DES at different temperatures - ● experimental data [39], ▬ calculated values:
▬ 298.15 K, ▬ 303.15 K, ▬ 313.15 K, ▬ 323.15 K, ▬ 333.15 K, ▬ 343.15 K, ▬ 353.15 K

Comparisons have been conducted between our model and the group contribution model from Haghbakhsh et al. [30]. A first comparison was drawn using their own databank, named here D3. In their work, the authors have proposed different groups compared to the group contribution method developed in this paper. In particular, they include no group for water, [-$O^{(-)}$] or [>N^{+}=]. Moreover, their model was developed using a smaller dataset: 1239 data points of binary DESs for them against 3266 in this work (including both binary and ternary DESs). The pool of data D3 is presented in the supplementary materials in **Table S.C29**. The comparison is presented in **Table 4.5**. With a more complex model, Haghbakhsh et al. achieve a lower average deviation of 1,44% against 1.90% for this work. It should be noted that this pool of data gathers between 70% and 80% of the data that has been used to optimize the parameters of their model while this dataset only involves 37% of the data used in our optimizing set. Standard deviations are nonetheless equal for both models and the correlation from Haghbakhsh et al. even gives a higher maximum deviation of 19.28% against 10.54%

when compared to our model.

Table 4.4. Average deviations between experimental and calculated densities depending on the family of molecules comprised in the DESs and the dataset of origin

Family of molecules	Dataset	Number of data points	Average deviation (%)
Choline Chloride	D1	1052	1.43
	D2	215	2.07
	D1+D2	**1267**	**1.54**
Betaine	D1	69	1.19
	D2	10	0.68
	D1+D2	**79**	**1.13**
Tetraalkylammonium	D1	470	1.86
	D2	52	3.91
	D1+D2	**522**	**2.06**
Benzyltrialkylammonium	D1	141	1.44
	D2	44	1.41
	D1+D2	**185**	**1.43**
Carboxylic acid	D1	870	2.06
	D2	248	3.15
	D1+D2	**1118**	**2.31**
Menthol	D1	238	2.45
	D2	86	0.51
	D1+D2	**324**	**1.96**
Thymol	D1	104	1.84
	D2	32	3.55
	D1+D2	**136**	**2.24**
Sugar	D1	161	1.60
	D2	105	1.63
	D1+D2	**266**	**1.61**
Diol	D1	688	1.55
	D2	129	3.62
	D1+D2	**817**	**1.88**
Glycerol	D1	240	2.35
	D2	77	2.54
	D1+D2	**317**	**2.40**

A second comparison was conducted using this time as many data points as possible with both models. Because of the different grouping, any data point involving water, hydrogen sulphate or 1-ethyl-3-methylimidazolium have been removed. Besides, the model from Haghbakhsh et al. was not able to provide suitable values in a few cases. Indeed, negative values had to be brought to the power -0.2045 which is not possible. Thus, systems involving trichloroacetic acid, glycolic acid with xylitol and alanine with malic acid had to be removed

from the testing pool as well. Eventually, a total of 3103 data points were used. Results are also shown in **Table 4.5**. With this pool of data, the average deviation of the model of Haghbakhsh et al. reaches 6.69% against 1.90% for this work. It can be expected that the performances of the model of Haghbakhsh et al. are lessened when using this pool of data containing systems not taken into account during the development of their model. However, another point can explain the multiplication of the deviation by more than 4.5. In their model, the normalization of the ratio of the DESs is made so that there is always one of the ratio equal to the unity. So, whenever the difference between the values of the ratios becomes large, for example [1:9] or [1:10], some of the parameters get much bigger multipliers than others. This is also true when a small ratio of compounds is added to a mixture to form a ternary DES with experimental ratios such as [1:2:0.05] for example. In our work, the normalization of the ratios is done in a way that the sum of the ratios is always equal to one, which prevents any "over the-top" multipliers in the calculations. Besides, it is consistent with how the molar masses of DESs are calculated. It can also be noted that the statistical indicators such as the average deviation for our model remained consistent compared to the other dataset that have been previously investigated.

Calculations with the GCM developed by Hou et al. [29] leads to a deviation of 2.29% for ternary DESs specifically. In comparison, the deviation for the ternary systems gathered in this work is of 1.05%. The lack of references for the data used by Hou et al. [29] made it difficult to compare with the rest of their results and their model was not further included in the comparison.

Overall, the performances of our model hold the comparison against other general GCMs for the prediction of density of DESs found in the literature with accurate and consistent results regardless of the dataset used for testing.

Table 4.5. Comparison between the group contribution models for density and heat capacity from this work and the literature

Property	Model	Number of data points	Average deviation (%)	Maximum deviation (%)	Standard deviation
Density	Haghbakhsh et al. [30]	1239	1.44	19.28	0.03 g.cm^{-3}
	This work		1.91	10.54	0.03 g.cm^{-3}
	Haghbakhsh et al. [30]	3103	6.69	128.79	0.15 g.cm^{-3}
	This work		1.90	13.28	0.04 g.cm^{-3}
Heat capacity	Haghbakhsh et al. [30]	452	2.99	32.97	21.31 J.mol^{-1}.K^{-1}
	This work		3.49	28.25	22.73 J.mol^{-1}.K^{-1}

4.4.2 Heat capacity

25 groups and 75 parameters are used in this GCM described by equations (4-7). The parameters $a_i^{C_p}$, $b_i^{C_p}$ and $c_i^{C_p}$ are provided in **Table 4.6**.

Table 4.6. Values of the parameters for the group contribution model for heat capacities

Group forming a ring or not	Groups	Parameters		
		$a_i^{C_p}$	$b_i^{C_p}$	$c_i^{C_p}$
Not forming a ring	H_2O	0.1467	2.5921	0.2605
	>C<	0.1095	11.2902	-2.0310
	-CH<	-0.0421	0.3631	-0.0074
	$-CH_2-$	0.1418	1.4328	0.0578
	$-CH_3$	2.1767	0.4656	-0.4257
	-O-	12.3367	-4.1952	$-7.2*10^{-4}$
	$-O^{(-)}$	7.4743	-0.1667	-0.0786
	-OH	3.5680	0.3931	0.0340
	-COOH	5.2284	1.6782	0.0021
	>C=O (*)	-0.3087	2.7267	0.0052
	$>N^{(+)}<$	0.1546	-0.0647	-0.1214
	$-NH^{(+)}<$	-0.0723	-1.1395	-0.4602
	-NH-	2.4030	2.3713	-0.9243
	$-NH_2$	5.4753	-0.6063	0.1386
	$-CONH_2$	5.1665	2.1204	0.1439
	>C=NH	2.4039	2.3695	-0.9232
	$>P^{(+)}<$	0.1424	0.1563	-1.9219
	$-Cl^{(-)}$	0.1535	5.3116	0.0019
	$-Br^{(-)}$	-0.1031	6.1957	$-9.8*10^{-4}$
Forming a ring	>C<	3.3459	0.1517	0.0136
	-CH<	0.0898	2.1618	-0.0497

	$-CH_2-$	3.3454	0.1516	0.0136
	>C=	-0.0230	0.3741	0.0413
	-CH=	-0.0054	1.8694	-0.1977
	-O-	-0.0995	0.1532	0.0081

(*) The group ">C=O (not forming a ring)" is applicable whether the carbonyl group is part of a ring or not

The deviations for both the optimizing and testing datasets H1 and H2 are shown in **Figure 4.3**. Due to the lack of data, the testing dataset has only six different systems mainly containing choline chloride. Nonetheless, the values are well predicted and close to the x=y line. Average deviations can be found in **Table 4.2**. The optimizing set has a higher average deviation compared to the testing dataset because of the presence of the system {[Choline][Chloride]:Oxalic acid}, [0.333:0.667] for which the average deviation is around 27.53%. This deviation can be explained by the fact that esterification can be observed with DESs based on choline chloride and carboxylic acid. In the case of the DES {[Choline][Chloride]:Oxalic acid}, the fraction of esterified choline chloride was found to be between 10% at 333.15 K and 29% at 353.15 K [38]. In comparison, the fraction of esterified choline chloride in the DES {[Choline][Chloride]:Malonic acid} is between 3 and 8% for temperatures ranging from 333.15 K to 353.15 K. In this case, this DES is well represented with our model with an average deviation of 0.58%. Overall, the databank H1+H2 has an average deviation of 3.09%, which is very promising in view of the amount of data available. The distributions of the calculated values of percentage deviation for each dataset can also be found in **Table 4.3**. Once again, the databank H1+H2 has more than 50% of its points that have an average deviation below 2%.

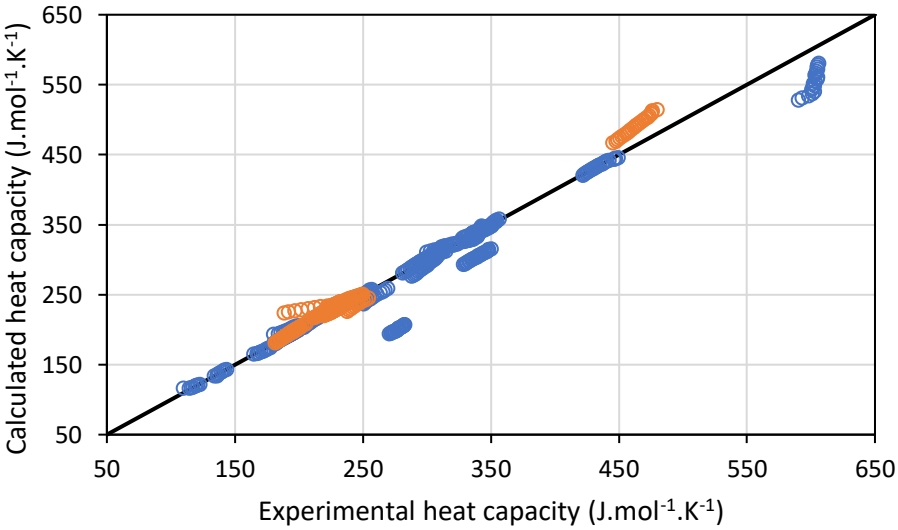

Figure 4.3. Deviation between experimental and modelled heat capacity for both the optimizing and testing sets, o optimizing set H1, o testing set H2.

The group contribution model proposed by Haghbakhsh et al. [30] for the prediction of heat capacities has been compared to the model presented in this work using a set of data H3 of 452 data points. This set of data presented in **Table S.C30** corresponds to the data that the authors employed to develop their model, minus 9 data points that could not be found or seemed to be used twice (exact same values from different references). Deviations for both models can be found in **Table 4.5**. The average deviation is lower with the model of Haghbakhsh et al. with a value of 2.99% compared to a deviation of 3.49% for our model. Nevertheless, standard deviations are very comparable and the model of Haghbakhsh et al. reaches the highest maximum deviation. Besides, both models struggle with the DES made of choline chloride and oxalic acid, for which the highest deviations are obtained in either case.

4.5 Conclusion

With the aim of being able to predict the properties of DESs without any more input than the temperature, the ratio and the structural groups composing a DES, a group contribution method based on simple correlations have been developed for the calculation of the density and the heat capacity of DESs using the most recent database. Among the two properties investigated in this work, density is the most well represented. Although the model developed in this work can be less accurate than more complex models, its simple approach allows for an easy implementation and quick modifications for the addition of any new group as well as a consistent accuracy. The linear dependence in temperature and the way the ratios are normalized ensure that virtually any DES could be investigated. For the heat capacity, results are very promising although the lack of data limits the model and its development.

Even though the goal is to be able to predict the properties of hypothetically any DES, the current number of data points is too small to derive robust modelling. Besides, more diverse data can only improve the accuracy of the models. The DESs used in this work were constituted of three or less compounds. In order to screen more data, this method could be tested with mixtures of DESs and other compounds. This has arguably been started since DESs formed of two compounds plus water are now more used for the development of predictive models.

References

[1] P. Pollet, E.A. Davey, E.E. Ureña-Benavides, C.A. Eckert, C.L. Liotta, Solvents for sustainable chemical processes, Green Chem. 16 (2014) 1034–1055. https://doi.org/10.1039/C3GC42302F.

[2] C.J. Clarke, W.-C. Tu, O. Levers, A. Bröhl, J.P. Hallett, Green and Sustainable Solvents in Chemical Processes, Chem. Rev. 118 (2018) 747–800. https://doi.org/10.1021/acs.chemrev.7b00571.

[3] A.P. Abbott, G. Capper, D.L. Davies, R.K. Rasheed, V. Tambyrajah, Novel solvent properties of choline chloride/urea mixturesElectronic supplementary information (ESI) available: spectroscopic data. See http://www.rsc.org/suppdata/cc/b2/b210714g/, Chem. Commun. (2003) 70–71. https://doi.org/10.1039/b210714g.

[4] A.P. Abbott, D. Boothby, G. Capper, D.L. Davies, R.K. Rasheed, Deep Eutectic Solvents Formed between Choline Chloride and Carboxylic Acids: Versatile Alternatives to Ionic Liquids, J. Am. Chem. Soc. 126 (2004) 9142–9147. https://doi.org/10.1021/ja048266j.

[5] D. Carriazo, M.C. Serrano, M.C. Gutiérrez, M.L. Ferrer, F. del Monte, Deep-eutectic solvents playing multiple roles in the synthesis of polymers and related materials, Chem. Soc. Rev. 41 (2012) 4996. https://doi.org/10.1039/c2cs15353j.

[6] H. Zhao, G.A. Baker, Ionic liquids and deep eutectic solvents for biodiesel synthesis: a review: Ionic liquids for biodiesel synthesis, J. Chem. Technol. Biotechnol. 88 (2013) 3–12. https://doi.org/10.1002/jctb.3935.

[7] E.L. Smith, A.P. Abbott, K.S. Ryder, Deep Eutectic Solvents (DESs) and Their Applications, Chem. Rev. 114 (2014) 11060–11082. https://doi.org/10.1021/cr300162p.

[8] A. Shishov, A. Bulatov, M. Locatelli, S. Carradori, V. Andruch, Application of deep eutectic solvents in analytical chemistry. A review, Microchem. J. 135 (2017) 33–38. https://doi.org/10.1016/j.microc.2017.07.015.

[9] R. Haghbakhsh, H. Peyrovedin, S. Raeissi, A.R.C. Duarte, A. Shariati, Energy Conservation in Absorption Refrigeration Cycles Using DES as a New Generation of Green Absorbents, Entropy. 22 (2020) 409. https://doi.org/10.3390/e22040409.

[10] M.A.R. Martins, S.P. Pinho, J.A.P. Coutinho, Insights into the Nature of Eutectic and Deep Eutectic Mixtures, J. Solut. Chem. 48 (2019) 962–982. https://doi.org/10.1007/s10953-018-0793-1.

[11] J. Cao, F. Zhu, Q. Dong, R. Wu, E. Su, Insight into the physicochemical properties of deep eutectic solvents by systematically investigating the components, J. Mol. Liq. 346 (2022) 118315. https://doi.org/10.1016/j.molliq.2021.118315.

[12] I.I.I. Alkhatib, D. Bahamon, F. Llovell, M.R.M. Abu-Zahra, L.F. Vega, Perspectives and guidelines on thermodynamic modelling of deep eutectic solvents, J. Mol. Liq. 298 (2020) 112183. https://doi.org/10.1016/j.molliq.2019.112183.

[13] A. Kovács, E.C. Neyts, I. Cornet, M. Wijnants, P. Billen, Modeling the Physicochemical Properties of Natural Deep Eutectic Solvents, ChemSusChem. 13 (2020) 3789–3804. https://doi.org/10.1002/cssc.202000286.

[14] K. Shahbaz, S. Baroutian, F.S. Mjalli, M.A. Hashim, I.M. AlNashef, Densities of ammonium and phosphonium based deep eutectic solvents: Prediction using artificial intelligence and group contribution techniques, Thermochim. Acta. 527 (2012) 59–66. https://doi.org/10.1016/j.tca.2011.10.010.

[15] R. Haghbakhsh, R. Bardool, A. Bakhtyari, A.R.C. Duarte, S. Raeissi, Simple and global correlation for the densities of deep eutectic solvents, J. Mol. Liq. 296 (2019) 111830. https://doi.org/10.1016/j.molliq.2019.111830.

[16] C. Wang, Q. Bi, Y. Huo, Z. Zhang, D. Tao, Y. Shen, Q. Zhu, Z. Chen, H. Li, W. Zhu, Investigation of Amine-Based Ternary Deep Eutectic Solvents for Efficient, Rapid, and Reversible SO_2 Absorption, Energy Fuels. 35 (2021) 20406–20410. https://doi.org/10.1021/acs.energyfuels.1c03807.

[17] A.K. Halder, R. Haghbakhsh, I.V. Voroshylova, A.R.C. Duarte, M.N.D.S. Cordeiro, Density of Deep Eutectic Solvents: The Path Forward Cheminformatics-Driven Reliable Predictions for Mixtures, Molecules. 26 (2021) 5779. https://doi.org/10.3390/molecules26195779.

[18] R.M.A. Bunquin, A.R. Caparanga, Predicting the heat capacities of ammonium- and phosphonium-based deep eutectic solvents using artificial neural network, J. Phys. Conf. Ser. 1893 (2021) 012001. https://doi.org/10.1088/1742-6596/1893/1/012001.

[19] A. Bagherzadeh, N. Shahini, D. Saber, P. Yousefi, S.M. Seyed Alizadeh, S. Ahmadi, F. Tat Shahdost, Developing a global approach for determining the molar heat capacity of deep eutectic solvents, Measurement. 188 (2022) 110630. https://doi.org/10.1016/j.measurement.2021.110630.

[20] F.S. Mjalli, J. Naser, Viscosity model for choline chloride-based deep eutectic solvents: VISCOSITY OF DES, Asia-Pac. J. Chem. Eng. 10 (2015) 273–281. https://doi.org/10.1002/apj.1873.

[21] J.M. Vuksanović, N.M. Todorović, M.L. Kijevčanin, S.P. Šerbanović, I.R. Radović, Experimental investigation and modeling of thermophysical and extraction properties of choline chloride + DL-malic acid based deep eutectic solvent, J. Serbian Chem. Soc. 82 (2017) 1287–1302.

[22] R. Haghbakhsh, K. Parvaneh, S. Raeissi, A. Shariati, A general viscosity model for deep eutectic solvents: The free volume theory coupled with association equations of state, Fluid Phase Equilibria. 470 (2018) 193–202. https://doi.org/10.1016/j.fluid.2017.08.024.

[23] J.N. Al-Dawsari, A. Bessadok-Jemai, I. Wazeer, S. Mokraoui, M.A. AlMansour, M.K. Hadj-Kali, Fitting of experimental viscosity to temperature data for deep eutectic solvents, J. Mol. Liq. 310 (2020) 113127. https://doi.org/10.1016/j.molliq.2020.113127.

[24] A. Bakhtyari, R. Haghbakhsh, A.R.C. Duarte, S. Raeissi, A simple model for the viscosities of deep eutectic solvents, Fluid Phase Equilibria. 521 (2020) 112662. https://doi.org/10.1016/j.fluid.2020.112662.

[25] G. Gygli, X. Xu, J. Pleiss, Meta-analysis of viscosity of aqueous deep eutectic solvents and their components, Sci. Rep. 10 (2020) 21395. https://doi.org/10.1038/s41598-020-78101-y.

[26] R.L. Gardas, J.A.P. Coutinho, Extension of the Ye and Shreeve group contribution method for density estimation of ionic liquids in a wide range of temperatures and pressures, Fluid Phase Equilibria. 263 (2008) 26–32. https://doi.org/10.1016/j.fluid.2007.09.016.

[27] K. Shahbaz, F.S. Mjalli, M.A. Hashim, I.M. AlNashef, Prediction of deep eutectic solvents densities at different temperatures, Thermochim. Acta. 515 (2011) 67–72. https://doi.org/10.1016/j.tca.2010.12.022.

[28] N.R. Mirza, N.J. Nicholas, Y. Wu, S. Kentish, G.W. Stevens, Estimation of Normal Boiling Temperatures, Critical Properties, and Acentric Factors of Deep Eutectic Solvents, J. Chem. Eng. Data. 60 (2015) 1844–1854. https://doi.org/10.1021/acs.jced.5b00046.

[29] X.-J. Hou, L.-Y. Yu, Y.-X. Wang, K.-J. Wu, C.-H. He, Comprehensive Prediction of Densities for Deep Eutectic Solvents: A New Bonding-Group Interaction Contribution Scheme, Ind. Eng. Chem. Res. 60 (2021) 13127–13139. https://doi.org/10.1021/acs.iecr.1c02260.

[30] R. Haghbakhsh, S. Raeissi, A.R.C. Duarte, Group contribution and atomic contribution models for the prediction of various physical properties of deep eutectic solvents, Sci. Rep. 11 (2021) 6684. https://doi.org/10.1038/s41598-021-85824-z.

[31] R.L. Gardas, J.A.P. Coutinho, A Group Contribution Method for Heat Capacity Estimation of Ionic Liquids, Ind. Eng. Chem. Res. 47 (2008) 5751–5757. https://doi.org/10.1021/ie800330v.

[32] A. Ahmadi, R. Haghbakhsh, S. Raeissi, V. Hemmati, A simple group contribution correlation for the prediction of ionic liquid heat capacities at different temperatures, Fluid Phase Equilibria. 403 (2015) 95–103. https://doi.org/10.1016/j.fluid.2015.06.009.

[33] M. Taherzadeh, R. Haghbakhsh, A.R.C. Duarte, S. Raeissi, Estimation of the heat capacities of deep eutectic solvents, J. Mol. Liq. 307 (2020) 112940. https://doi.org/10.1016/j.molliq.2020.112940.

[34] M.K. AlOmar, M. Hayyan, M.A. Alsaadi, S. Akib, A. Hayyan, M.A. Hashim, Glycerol-based deep eutectic solvents: Physical properties, J. Mol. Liq. 215 (2016) 98–103. https://doi.org/10.1016/j.molliq.2015.11.032.

[35] J. Zhu, K. Yu, Y. Zhu, R. Zhu, F. Ye, N. Song, Y. Xu, Physicochemical properties of deep eutectic solvents formed by choline chloride and phenolic compounds at T = (293.15 to 333.15) K: The influence of electronic effect of substitution group, J. Mol. Liq. 232 (2017) 182–187. https://doi.org/10.1016/j.molliq.2017.02.071.

[36] R.L. Gardas, J.A.P. Coutinho, A group contribution method for viscosity estimation of ionic liquids, Fluid Phase Equilibria. 266 (2008) 195–201. https://doi.org/10.1016/j.fluid.2008.01.021.

[37] K.Z. Kučan, M. Perković, K. Cmrk, D. Načinović, M. Rogošić, Betaine + (Glycerol or Ethylene Glycol or Propylene Glycol) Deep Eutectic Solvents for Extractive Purification of Gasoline, ChemistrySelect. 3 (2018) 12582–12590. https://doi.org/10.1002/slct.201803251.

[38] N. Rodriguez Rodriguez, A. van den Bruinhorst, L.J.B.M. Kollau, M.C. Kroon, K. Binnemans, Degradation of Deep-Eutectic Solvents Based on Choline Chloride and Carboxylic Acids, ACS Sustain. Chem. Eng. 7 (2019) 11521–11528. https://doi.org/10.1021/acssuschemeng.9b01378.

[39] F.S. Mjalli, J. Naser, B. Jibril, V. Alizadeh, Z. Gano, Tetrabutylammonium Chloride Based Ionic Liquid Analogues and Their Physical Properties, J. Chem. Eng. Data. 59 (2014) 2242–2251. https://doi.org/10.1021/je5002126.

Chapitre 5

Performances of an Absorption Heat Transformer cycle with water/deep eutectic solvents working fluids: modelling and screening of a database

Learn from yesterday,
Live for today,
Look for tomorrow,
Rest this afternoon.

-- SNOOPY

Chapitre 5 : Performances of an Absorption Heat Transformer cycle with water/deep eutectic solvents working fluids: modelling and screening of a database

Thomas Di Pietro[a], Laetitia Cesari[a], Fabrice Mutelet[a]

a - Université de Lorraine, Ecole Nationale Supérieure des Industries Chimiques, Laboratoire Réactions et Génie des Procédés (UMR CNRS 7274), 1 rue Grandville, 54000 Nancy, France

Article à soumettre

Résumé

Dans le cadre de la récupération et de la revalorisation de la chaleur fatale, ce chapitre présente un outil capable de modéliser les performances d'un thermotransformateur à absorption pouvant fonctionner avec des fluides qui contiennent des solvants eutectiques profonds (SEPs). En particulier, l'eau en tant que réfrigérant et les solvants eutectiques profonds en tant qu'absorbants constituent les composés d'intérêt. Les propriétés nécessaires à la simulation de la pompe à chaleur sont obtenues à l'aide des méthodes présentées dans les chapitres précédents au sein d'une approche multi-échelle. Les équilibres liquide-vapeur sont ainsi prédits grâce au modèle COSMO-SAC (+OH-ClBr) tandis que les masses volumiques et capacités thermiques des solvants à eutectique profond sont obtenues via des modèles de contribution de groupes. Les résultats obtenus ont été comparés à ceux d'une approche conventionnelle basée sur le modèle NRTL et des corrélations empiriques ajustées sur des données expérimentales afin de valider l'approche multi-échelle. Les performances du thermotransformateur à absorption ont

été évaluées à l'aide de différents critères dont le coefficient de performance, le coefficient de circulation et le débit de chaleur produite. Les résultats sont en accord avec ceux obtenus avec l'approche plus classique. Les performances de 32 solvants eutectiques profonds associés à l'eau ont été analysées, de même que l'influence des différentes températures du procédé sur les résultats. Ce chapitre met en valeur l'utilité du modèle en tant qu'outil de présélection de solvants eutectiques profonds utilisables comme absorbants dans un procédé de pompe à chaleur à absorption avant que ne soient menées des études expérimentales. Les résultats représentent également le premier screening de fluides de travail constitués de SEPs et d'eau. Les résultats montrent que les meilleures performances sont prédites pour des SEPs qui contiennent de l'éthylène glycol, du glycérol, du chlorure de tétraéthylammonium, du chlorure de choline et de la bétaïne. Un coefficient de performance de 0.441 a été obtenu avec le couple eau/{éthylène glycol:[tétraméthylammonium][chlorure]} ratio [2 :1]. Plus généralement, les SEPs qui ont un plus haut ratio d'accepteur de liaisons hydrogène et une masse molaire plus faible ont conduit à de meilleures performances en tant qu'absorbants au sein d'un thermotransformateur à absorption.

Abstract

With the goal of improving the recovery of industrial waste heat, a tool modelling the performances of working fluids composed of deep eutectic solvents (DESs) and water in a single-stage absorption heat transformer is presented in this work. In particular, the components of interest are water as refrigerant and deep eutectic solvents as absorbents. The thermophysical properties required for the simulation were obtained through a multiscale approach. Vapour-liquid equilibria were predicted using a modified version of the COSMO-SAC model called (+OH-ClBr) developed to improve the predictions for mixtures with chlorine atoms able to form hydrogen bonds. Group contribution models provided the densities and heat capacities of the DESs. The predictive power of the model has been assessed by comparing the results with the ones obtained with a conventional approach based on the NRTL model and empirical correlations derived from experimental data. The performances of the AHT were evaluated using several criteria including the coefficient of performance, the circulation ratio and the heat input. The results are in agreement with the ones obtained with the more classical approach. The performances of 32 DESs as well as the influence of the different temperatures of the process on the results are investigated. This allows to demonstrate the suitability of the model as a tool to select DESs that could potentially be used as absorbent in an AHT process before experimental testing. The results also consist of the first screening of potential working fluids constituted of DESs and water. Results show that the best performances are predicted with DESs made of ethylene glycol, glycerol, tetramethylammonium chloride, choline chloride and betaine. A coefficient of performance of 0.441 could be achieved with the pair water/{ethylene glycol:[tetramethylammonium][chloride]} ratio [2:1]. Overall, the DESs that have a higher ratio of hydrogen bond acceptor and lower molar masses showed better performances as absorbents in absorption heat transformers.

5.1 Introduction

Reducing energy consumption is at the heart of the efforts towards a better management of energy and resources. Among many leads, one way to do so is to retrieve and reuse waste heat to reduce operating costs and environmental footprint of industrial processes. Indeed, when rejected, this heat has no economical worth. Sometimes, costs are even added if cooling is required before the emission in the environment. Absorption heat transformers (AHTs), also called heat pump type II, can make use of medium-temperature heat such as waste heat to cause the absorption of a refrigerant by an absorbent and produce heat at an upgraded temperature. Cudok et al. have identified 48 AHTs put into use in industries (over the world but mainly in Asia) in the last 38 years, with 17 running in 2020[1]. They include in particular chemical and food industries. These installations were successful in turning waste heat from one component of a production line into upgraded heat to feed another component. The authors note the economic and environmental benefit of this technology. However, among limiting factors are the weight and the space taken by the equipment due to large exchange surface requirements and the high costs of installation before good return on investment. Another major challenge is the choice of the absorbent/refrigerant working pair which is one of the most crucial criterion for the performances of the AHT and absorption cycles in general[2].

Traditional and most common refrigerant/absorbent working fluids are water/LiBr and ammonia/water[2–4]. For the former, crystallisation and corrosion for most common metals as well as limited solubility and high viscosity are the main issues[4–6]. For the later, besides the toxicity of ammonia, water is a volatile absorbent. Thus, the separation of water from ammonia in the gas phase requires a distillation process (analyser) and a rectifier to remove the water vapour and improve the efficiency of the AHT, with the drawback of additional costs[5]. These have hindered the development and implementation of this technology.

As a replacement of common absorbents, ionic liquids (ILs) have been considered.

Composed of cations and anions, the virtually unlimited possibilities of combination of ions allow ILs to have very tuneable properties[7,8]. In addition to being thermally and chemically stable, they offer negligible vapour pressure. As absorbents, this prevents them from going in the vapour phase in the absorption cycle. Many studies have investigated the performances of AHTs with ILs with promising results, comparable to that of traditional working fluids[9–15]. However, these are mitigated by the fact that ILs have shortcomings of their own such as cost and ecotoxicity[16,17].

From the 2000s onward, deep eutectic solvents (DESs) have appeared as innovative mixtures for the replacement of problematic solvents[18,19]. They consist of the association of at least two compounds, one acting as a hydrogen bond donor (HBD) and one as a hydrogen bond acceptor (HBA). Even so, a component can fill several roles simultaneously and multiple hydrogen bonds can be formed as well. Due to the interactions within the DES, the resulting solvent is a eutectic mixture with a lower melting point compared to its individual components. One of the highlights of the DESs is that they retain the advantages of the ILs while being potentially cheap, easy to produce and "green" or natural, depending on their constituents[20–22].

In the literature, they are still few evaluations of the performances of absorption cycles working using working fluids containing DESs. To the best of our knowledge, Nessakh et al.[23] did the first study about AHT and DESs as absorbents. They measured the thermodynamic properties of the two DESs {Betaine:Ethylene glycol} and {[Choline][Chloride]:Glycerol}. With these data, they simulated the performances of an AHT with water as refrigerant and the DESs as absorbent using a classical approach: the vapour-liquid equilibria (VLE) were predicted with the NRTL model, densities and heat capacities were derived from empirical correlations while the excess properties were correlated using Redlich-Kister type equations. Both DESs had suitable properties for their use in an AHT and demonstrated slightly lower performances compared to the working fluid water/LiBr. The authors also underlined the need

for further investigation on the use of DESs as absorbent in AHT and in particular the impact of the components of the DESs on the results. Abedin et al. predicted the performances of an absorption refrigeration cycle with a working fluid mixing the hydrofluorocarbon R134a and a choline chloride-based DESs comprising urea, glycerol or ethylene glycol[24]. In their model, the energy input was derived from solar or waste heat sources. Using COSMO-RS, they demonstrated that the best results were obtained with the system R134a/{[Choline][Chloride]:Ethylene glycol}. Haghbakhsh et al. investigated the efficiency of three DESs made of choline chloride and either ethylene glycol, glycerol or urea as absorbents within a refrigeration cycle with water as refrigerant[25]. They demonstrated that these solvents have analogous performances compared to the more traditional water/LiBr mixture, thus proving their suitability. They also reached similar conclusions using the same three DESs with ammonia as refrigerant in their working fluids[26]. They also underlined the need for more data on new DESs. This way, it would become possible to choose from a larger pool of constituents and reach ever better results.

Thus, there is a need for a much greater number of DESs to be investigated. This would involve comprehensive and intensive experimental studies. To alleviate this work of data gathering, a simulation tool is presented in this work that enables to predict the performances of any working fluid made of water as refrigerant and DES as absorbents. Using a multiscale approach, the properties required for the simulations are no longer directly fitted to experimental measurements. Instead, the approach offers to derive the VLE from the COSMO-SAC (+OH-ClBr) model while the values of density and heat capacity are obtained via group contribution methods (GCMs). A first screening of the performances of 32 DESs has been performed.

5.2 Simulation of the AHT cycle

5.2.1 Description of the AHT cycle

A single-stage absorption heat transformer comprises four main parts: a generator, a condenser, an evaporator and an absorber. The process functions with a working fluid made of a mixture of the absorbent and the refrigerant. The refrigerant is considered the key component and the concepts of richness and poorness relate to the concentration of refrigerant in the material flows. A detailed scheme of the process can be found in **Figure 5.1**, with the state points from 1 to 10. Starting at the generator, the working fluid receives heat at medium temperature T_{medium} from the wast heat source. This enables to separate both compounds: the refrigerant is evaporated while the absorbent remains in a solution poor in refrigerant. The poor solution is pumped and sent at a higher pressure to the absorber (points 8-10). Meanwhile, the refrigerant is sent as vapour (rich in refrigerant) to the condenser (point 1). In the condenser, energy is released at low temperature T_{low} as the vapour condenses to become a rich liquid (point 2) that is pumped and brought to a higher pressure into the evaporator (point 3). Receiving once more energy from waste heat, it is evaporated again and goes as rich vapour in the absorber (point 4). There, the rich vapour is absorbed by the poor solution, which releases (upgraded) heat at a high temperature T_{high}. Then, the liquid mixture (rich in refrigerant) is expanded via a throttling valve and sent back to the generator for another cycle (points 5-7). A solution heat exchanger (SHE) is added between the rich solution exiting the absorber (point 5) and the poor solution that is entering (point 9). The poor solution is thus preheated for better efficiency and energy recovery. The evaporator and the absorber corresponds to a high pressure system while the generator and the condenser form a low pressure separator: $P_{Abs} = P_{Ev} = P_{high}$ and $P_{Con} = P_{Gen} = P_{low}$. The subscripts Abs, Ev, Con and Gen correspond to absorber, evaporator, condenser and generator, respectively.

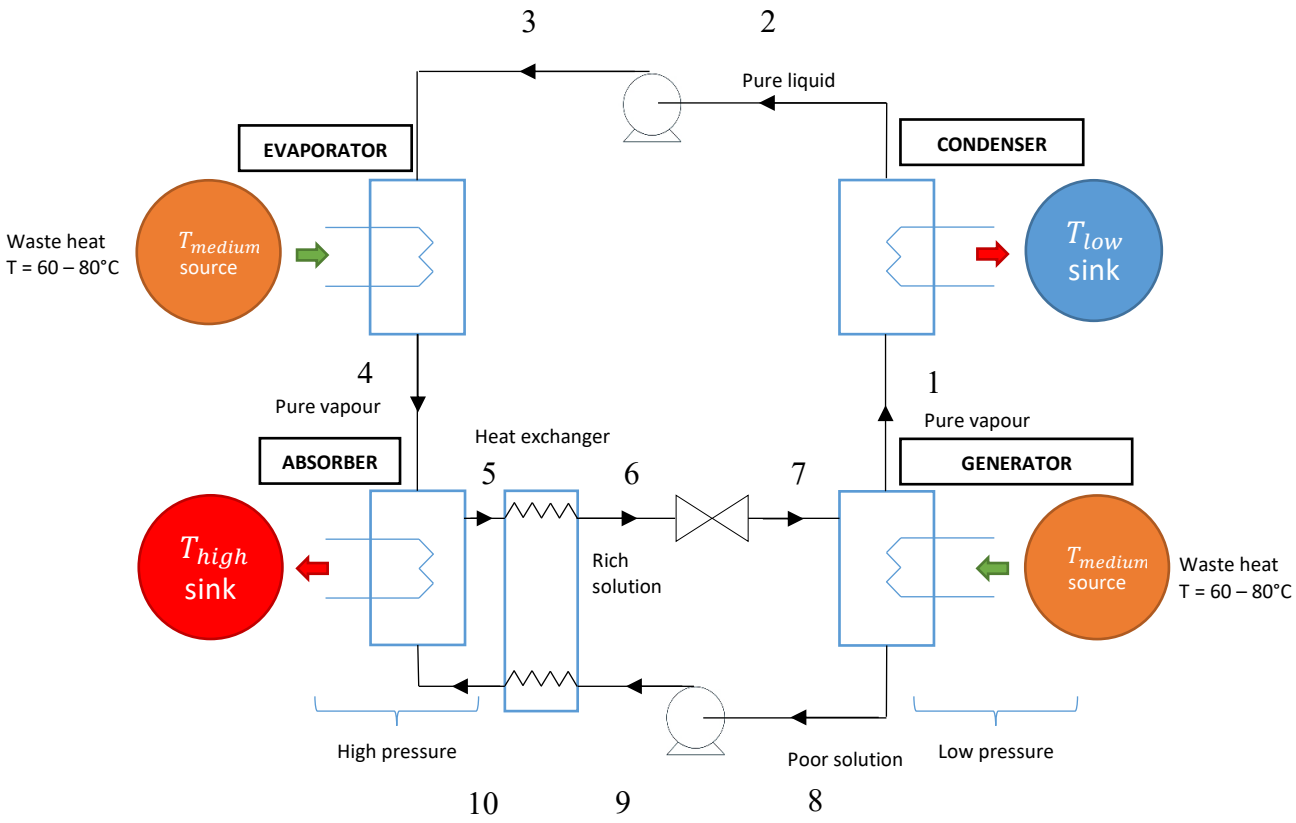

Figure 5.1. Schematic presentation of the AHT process with the state points

5.2.2 Description of the model

For the simulation of the AHT, several assumptions were made:

1) The process is under steady state conditions.

2) When leaving the generator and the absorber, the solutions are considered saturated liquids.

3) The liquid exiting the condenser is saturated, as well as the vapour exiting the evaporator.

4) Pressure and thermal losses are neglected within the whole cycle.

5) The throttling valve is isenthalpic.

6) In the solution heat exchanger, the minimum temperature difference between the hot and cold streams ΔT_{min} is 5 K. That way, the size of the SHE remains reasonable and excessive energy losses are prevented as well.

7) Compared to the heat output, the energy consumption of the pumps is neglected.

5.2.2.1 Pressure

The pressures of the state points can either be P_{low} (points 1,2 7 and 8) or P_{high} (points 3 to 6 and 9-10). Since DESs have negligible saturated pressures, only water goes in the vapour phase exiting the generator and from points 1 to 4 fluids are considered pure water. At the condenser and evaporator, because of the phase equilibria, the values of these pressures are determined using the saturated pressure for water P_{sat}^{w}, the superscript w standing for water. Thus, $P_{low} = P_{sat}^{w}(T_{Con})$ and $P_{high} = P_{sat}^{w}(T_{Ev})$. P_{sat}^{w} values were calculated with the Antoine equation using parameters from the NIST database[27]:

$$P_{sat}^{w} = 10^{\left(4.6543 - \frac{1435.264}{T - 64.848}\right)} * 10^{5} \ (Pa) \quad (1)$$

5.2.2.2 Composition

The compositions of the liquid mixture between the absorber and the generator (points 5 to 10) are derived from vapour-liquid equilibria (VLE). For the VLE calculations, activity coefficients γ are required. They are provided by the COSMO-SAC (+OH-ClBr) model, a modified version of COSMO-SAC (COSMO segment activity coefficient) with added parameters to take into account hydrogen bonds with chlorine and bromine atom. A full description can be found in our previous work[28]. According to the vapour-liquid equilibria, and since DESs have negligible saturated pressure, the mole fraction of refrigerant (i.e.: water) in the rich solution x_{rich}^{w} exiting the absorber shall ensure that:

$$P_5 = P_{sat}^{w}(T_{Abs}) * \gamma^{w} * x_{rich}^{w} = P_{high} \quad (2)$$

Similarly, the mole fraction of refrigerant in the poor solution x_{poor}^{w} is determined in such a way that for the liquid exiting the generator:

$$P_8 = P_{sat}^{w}(T_{Gen}) * \gamma^{w} * x_{poor}^{w} = P_{low} \quad (3)$$

From these, the corresponding mass fractions $x_{m,rich}^{w}$ and $x_{m,poor}^{w}$ are derived using the molar mass of water and of the DES.

5.2.2.3 Mass flowrates

The mass flow rate entering and exiting the condenser ($\dot{m}_1$ and $\dot{m}_2$) is set at 1 kg.s^{-1}. This also corresponds to the value of the flow rates $\dot{m}_3$ and $\dot{m}_4$ entering and exiting the evaporator. The other mass flowrates $\dot{m}_i$ are determined using mass balances. For the solution going from the absorber to the generator ($\dot{m}_5 = \dot{m}_6 = \dot{m}_7$), a global mass balance at the absorber gives:

$$\dot{m}_4 = \dot{m}_5 - \dot{m}_{10} \tag{4}$$

From the mass balance in the absorber in terms of absorbent:

$$\dot{m}_{10} = \frac{\dot{m}_5 . x_{m,5}^{DES}}{x_{m,10}^{DES}} \tag{5}$$

With $x_{m,i}^{DES}$ the mass fraction of DES in the mixture at point i. By replacing Eq. 5 in Eq. 4 and isolating $\dot{m}_5$:

$$\dot{m}_5 = \frac{\dot{m}_4}{1 - \frac{x_{m,5}^{DES}}{x_{m,10}^{DES}}} \tag{6}$$

With the superscript DES standing for the DES used as absorbent. For the solution going from the generator to the absorber ($\dot{m}_8 = \dot{m}_9 = \dot{m}_{10}$), the mass balance at the generator is derived:

$$\dot{m}_8 = \dot{m}_7 - \dot{m}_1 \tag{7}$$

With $\dot{m}_7 = \dot{m}_5$.

5.2.2.4 Enthalpies

The enthalpy of pure water for the point 1 to 4 depends on the state of the refrigerant. The enthalpy of the pure liquid exiting the condenser (points 2 and 3) is calculated according to:

$$h_{liq} = h_{ref} + \frac{1}{\rho_{liq}(T_{ref})} * \left(P - P_{ref}\right) + \int_{T_{ref}}^{T} c_p dT \tag{8}$$

With ρ_{liq} the density in kg.m^{-3} and c_p the heat capacity in kJ.kg^{-1}.K^{-1}. The reference is

arbitrarily chosen so that:

$$h_{ref} = 0\ kJ.kg^{-1}, T_{ref} = 273.15\ K\ and\ P_{ref} = 101325\ Pa$$

The physicochemical properties of water were determined using the data compilation of pure compound properties from the DIPPR[29]:

$$\rho_{liq}^{w}(T_{ref}) = 999.7884519\ kg.m^{-3} \quad (9)$$

$$c_p^w = A + B * T + C * T^2 + D * T^3 + E * T^4 \quad (10)$$

The enthalpy of water vapour h_{vap}^{w} (kJ.kg^{-1}) is determined at the points 1 and 4 using:

$$h_{vap}^{w} = h_{liq}^{w} + \Delta h_{vap} \quad (11)$$

With the enthalpy of vaporization Δh_{vap} calculated according to the following correlation, taken from the DIPPR:

$$\Delta h_{vap} = A * \left(1 - \frac{T}{T_C^w}\right)^{B+C*\frac{T}{T_C^w}+D*\left(\frac{T}{T_C^w}\right)^2} \quad (12)$$

With T_C^w= 647.096 K, the critical temperature of water. Parameters A, B, C, D and E for Eq. 10 and 12 are given in the supporting information.

Binary mixtures of DES and water are investigated for points 5 to 10 between the absorber and the generator. The enthalpy of a binary liquid mixture h_{mix} can be expressed as:

$$h_{mix} = x_m^w h_{liq}^w + x_m^{DES} h_{liq}^{DES} + \Delta h_{mix} \quad (13)$$

In this expression, the mixing enthalpy Δh_{mix} has been neglected. For the absorbent, the liquid enthalpy is calculated according to Eq. 8 and requires the density and the heat capacity that have been calculated using group contribution methods. These models were previously developed for DESs[30], with the base equations as follow:

$$\rho_{liq}^{DES} = A^{\rho} + B^{\rho} * \frac{T}{100} \quad (14)$$

$$Cp_m^{DES} = R * \left(A^{Cp} + B^{Cp} * \frac{T}{100} + C^{Cp} * \left(\frac{T}{100}\right)^2\right) \quad (15)$$

A^{ρ} and B^{ρ} are the parameters for the density of a given DES obtained via the group contribution method. Similarly, A^{C_p}, B^{C_p} and C^{C_p} enable to obtain the heat capacity of a given DES. R is the gas constant.

Finally, the possibility of a liquid + vapour mixture needs to be looked upon at the point 7 after the rich solution went through the valve and also at the point 10 after the poor solution has been heated by the SHE. If this is the case, the enthalpy of the mixture becomes:

$$h_{LV} = z * h_{vap}^{w} + (1 - z) * h_{mix} \quad (16)$$

With z the steam quality, namely the mass fraction of vapour in the liquid vapour mixture.

Table 5.1. Summary table and thermal properties of the reference points of the AHT schematic presentation

Reference point	**Temperature (K)**	**Pressure (Pa)**	**Mass fraction of refrigerant**	**Enthalpy (kJ.kg^{-1})**	**Mass flowrate (kg.s^{-1})**
1	$T_{Gen} = T_{medium}$	P_{low}	0	h_{vap}	1
2	$T_{Con} = T_{low}$	P_{low}	0	h_{liq}	1
3	T_{low}	P_{high}	0	h_{liq}	1
4	$T_{Ev} = T_{medium}$	P_{high}	0	h_{vap}	1
5	$T_{Abs} = T_{high}$	P_{high}	$x_{m,rich}^{w}$	h_{mix}	$\dot{m}_5 = \frac{\dot{m}_4}{1 - \frac{x_{m,5}^{DES}}{x_{m,10}^{DES}}}$
6	T_6*	P_{high}	$x_{m,rich}^{w}$	h_{mix}	$\dot{m}_5$
7**	T_7*	P_{low}	$x_{m,rich}^{w}$	h_{mix} or h_{LV}	$\dot{m}_5$
8	T_{medium}	P_{low}	$x_{m,poor}^{w}$	h_{mix}	$\dot{m}_7 - \dot{m}_1$
9	T_{medium}	P_{high}	$x_{m,poor}^{w}$	h_{mix}	$\dot{m}_8$
10**	T_{10}*	P_{high}	$x_{m,poor}^{w}$	h_{mix} or h_{LV}	$\dot{m}_8$

*To be determined by calculations

**Points 7 and 10 require to check whether the fluid is a liquid mixture or comprises both a gas phase and a liquid phase.

More details regarding the determination of the operating conditions at points 6, 7 and 10 are given in the supporting material. The characteristics of each state point are summarized in **Table 5.1**.

5.2.3 Performance criteria

The performances can be evaluated using a selection of criteria to compare the efficiency and the costs of different scenarios.

According to the energy balances for each main component of the AHT, heat flows (kW) can be expressed as follow:

$$\dot{Q}_{Ev} = -\dot{m}_3 h_3 + \dot{m}_4 h_4 = \dot{m}_1 (h_4 - h_3) \quad (17)$$

$$\dot{Q}_{Con} = \dot{m}_1 h_1 - \dot{m}_2 h_2 = \dot{m}_1 (h_1 - h_2) \quad (18)$$

$$\dot{Q}_{Gen} = \dot{m}_1 h_1 - \dot{m}_7 h_7 + \dot{m}_8 h_8 \quad (19)$$

$$\dot{Q}_{Abs} = \dot{m}_4 h_4 - \dot{m}_5 h_5 + \dot{m}_{10} h_{10} = \dot{Q}_{Gen} + \dot{Q}_{Ev} - \dot{Q}_{Con} \quad (20)$$

The coefficient of performance (COP) is defined as the ratio of heat obtained at the absorber (useful heat that has been upgraded to a higher temperature) to the energy provided to the system (heat input):

$$COP = \frac{\dot{Q}_{Abs}}{\dot{Q}_{Ev} + \dot{Q}_{Gen}} \quad (21)$$

When talking about input, the work of the pumps is neglected here. The COP is aimed to be as high as possible and helps quantify the performances of the AHT.

The circulation ratio f is the ratio of the mass flow of the solution rich in refrigerant that is entering the generator $\dot{m}_7$ to the mass flow of refrigerant exiting the generator as vapour $\dot{m}_1$. Using the following mass balances at the generator, f can also be expressed as a function of the mass fraction of refrigerant (Eq. 22-24):

$$1 * \dot{m}_1 + x^w_{m,poor} \dot{m}_8 = x^w_{m,rich} \dot{m}_7 \ \ (refrigerant\ mass\ balance) \quad (22)$$

$$\dot{m}_8 = \dot{m}_7 - \dot{m}_1 \ \ (total\ mass\ balance) \quad (23)$$

$$f = \frac{\dot{m}_7}{\dot{m}_1} = \frac{1 - x^w_{m,poor}}{x^w_{m,rich} - x^w_{m,poor}} \quad (24)$$

This ratio is related to the energy required to heat and pump within the process. It provides an insight on the dimension of the equipment per unit heat produced, and thus on the costs. It is sought to be as low as possible.

The gross temperature lift Δt indicates how much the temperature of the waste heat has been increased. It corresponds to the difference in K between the high temperature and the medium temperature and reflects the absorption potential and the thermal valorisation of the AHT:

$$\Delta t = T_{Abs} - T_{Ev} \quad (25)$$

Finally, the heat output at the absorber per unit mass of refrigerant q (kJ.kg^{-1}) has to be maximized:

$$q = \frac{\dot{Q}_{Abs}}{\dot{m}_1} \quad (26)$$

The influence of the different temperatures on the performance criteria was investigated in the results section.

5.2.4 Multiscale approach

The simulation of a AHT requires the following properties: the VLE, the densities and heat capacities. Excess properties can also be used when taking into account the mixing enthalpy. These properties were previously determined from experimental measurements in what is called the "classical approach"[12,23]. To develop a tool that does not depend on experimental data and to investigate as many DESs as possible, a multiscale approach was implemented in this work.

Through statistical thermodynamics and quantum chemical calculations, COSMO-SAC models allow to derived thermodynamics properties, including activity coefficients which can in turn be used to derive phase equilibria. In this work, the model COSMO-SAC (+OH-ClBr)[28]

is used for the predictions of the VLE. This model was developed to improve the predictions of phase diagrams of systems containing chlorine and bromine atoms susceptible to hydrogen bonding with hydroxyl groups, in particular in systems with DESs. Group contribution models[30] were previously developed to derive the density and heat capacity of DESs with any ratio.

The results derived from the multiscale approach are first compared to the results obtained with a more classical approach based on the NRTL model and empirical correlations.

5.3 Results and discussion

5.3.1 Comparison with a classical approach

At first, the results of our model (multiscale approach) were compared to the ones obtained by Nessakh et al.[23] (classical approach). They investigated two working fluids containing DESs as absorbent, namely water/{Glycerol:[Choline][Chloride]} ratio [2:1] and water/{Ethylene glycol:Betaine} ratio [3:1]. The authors used the NRTL model and empirical correlations (conventional approach) to derive the properties required in the simulations and predict the performances of an AHT. Their results regarding COP, circulation ratio and mass fractions are gathered in **Table 5.2** for the DES with glycerol and **Table 5.3** for the DES with ethylene glycol, along with the results obtained in this work in the same operating conditions.

Table 5.2. Simulations of the performances of an AHT with water as refrigerant and the DES {[Choline][Chloride]:Glycerol}, ratio [1:2] as absorbent - Comparison between this work and the work of Nessakh et al.[23]

T_{Con} (K)	$T_{Gen} = T_{Ev}$ (K)	T_{Abs} (K)	COP	f	$x^{w}_{m,rich} - x^{w}_{m,poor}$	Source
293.15	353.15	403.15	0.42	23.47	0.04	[23]
298.15			0.42	27.41	0.04	
308.15	363.15	403.15	0.44	16.61	0.06	
293.15	353.15	403.15	0.434	11.81	0.08	This work
298.15			0.435	12.83	0.08	
308.15	363.15	403.15	0.446	8.51	0.11	

Table 5.3. Simulations of the performances of an AHT with water as refrigerant and the DES {Betaine:Ethylene glycol}, ratio [1:3] as absorbent - Comparison between this work and the work of Nessakh et al.[23]

T_{Con} (K)	$T_{Gen} = T_{Ev}$ (K)	T_{Abs} (K)	COP	f	$x^{w}_{m,rich} - x^{w}_{m,poor}$	Source
298.15	343.15	373.15	0.44	10.73	0.09	[23]
293.15	353.15	403.15	0.42	17.91	0.05	
298.15			0.42	20.82	0.05	
308.15	363.15	403.15	0.44	12.57	0.08	
298.15	343.15	373.15	0.455	9.86	0.10	This work
293.15	353.15	403.15	0.424	18.30	0.05	
298.15			0.421	21.34	0.05	
308.15	363.15	403.15	0.44	12.21	0.08	

Comparisons between the classical and the multiscale approaches in terms of COP at different temperatures are also presented in **Figure 5.2** to **Figure 5.4**. For the DES {Glycerol:[Choline][Chloride]}, the results are of the same order of magnitude with corresponding trends and close values in terms of COP, although the model from this work predicts better performances compared to the classical approach. In particular, the differences in mass fractions $x^{w}_{m,rich} - x^{w}_{m,poor}$ from this work are twice higher compared to Nessakh et al., namely 0.09 compared to 0.05 in average. This leads to circulation ratios that are twice smaller, with values around 10 compared to values around 20. The differences could be explained by the uncertainties of the models. The average deviation for VLE of systems containing water and alcohol compounds is of 5.18%[28] with the COSMO-SAC (+OH-ClBr) model. The group contribution models also have an average deviation of 1.95% for density and of 3.09% for heat capacity[30]. In comparison, the classical approach has a deviation of 7.58% for the VLE, 0.2% for the densities and 1.47% for the heat capacities[23]. For the second DES comprised of {Ethylene glycol:Betaine}, the results are extremely close with all three of the criteria. Besides, the results obtained with both approaches **Figure 5.2** to **Figure 5.4** for this DES are almost overlapping.

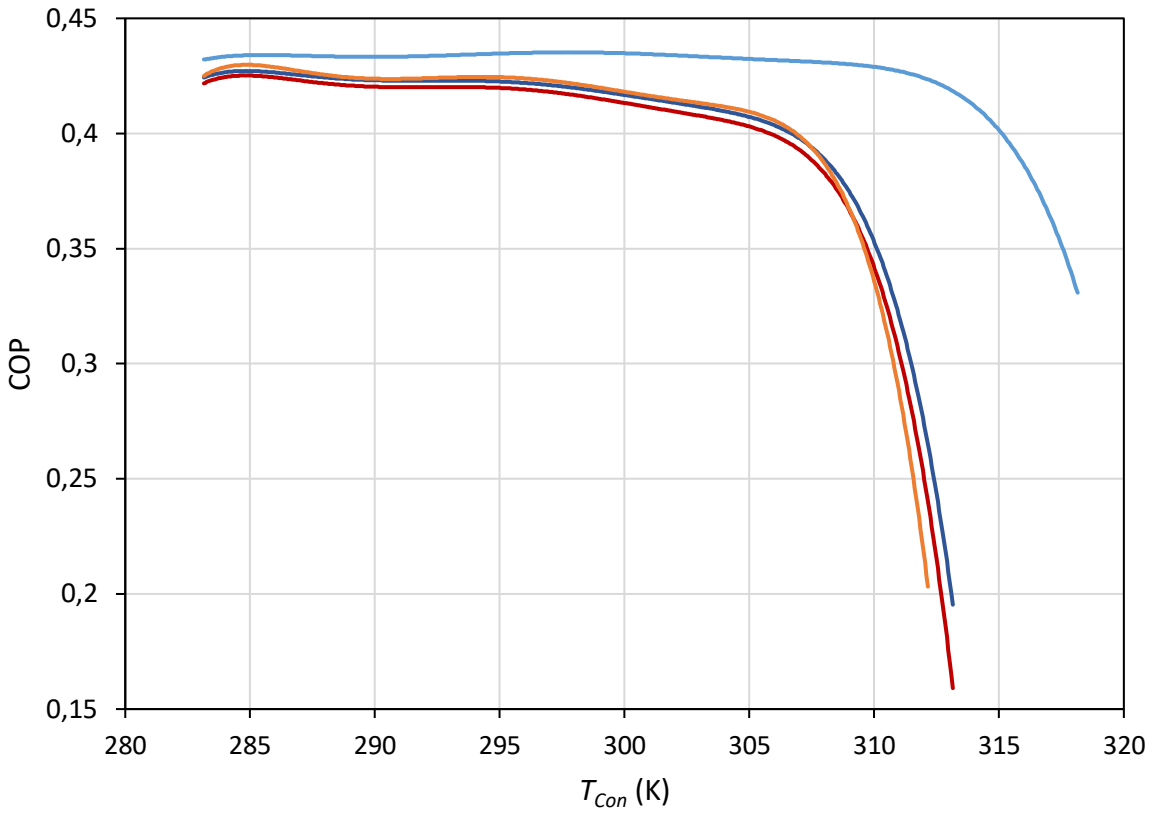

Figure 5.2. Prediction of the coefficient of performance of two working fluids as a function of the temperature of the condenser – $T_{Gen} = T_{Ev} = 353\ K$, $T_{Abs} = 403\ K$ – Comparison between two approaches. Water as refrigerant.
Absorbent:
– Glycerol : Choline chloride [2:1] - classical approach[23]
– Glycerol : Choline chloride [2:1] - multiscale approach (this work)
– Ethylene glycol : Betaine [3:1] - classical approach[23]
– Ethylene glycol : Betaine [3:1] - multiscale approach (this work)

Thus, compared to an approach based on experimentally measured properties, the multiscale approach provides very similar results, allowing to validate the models.

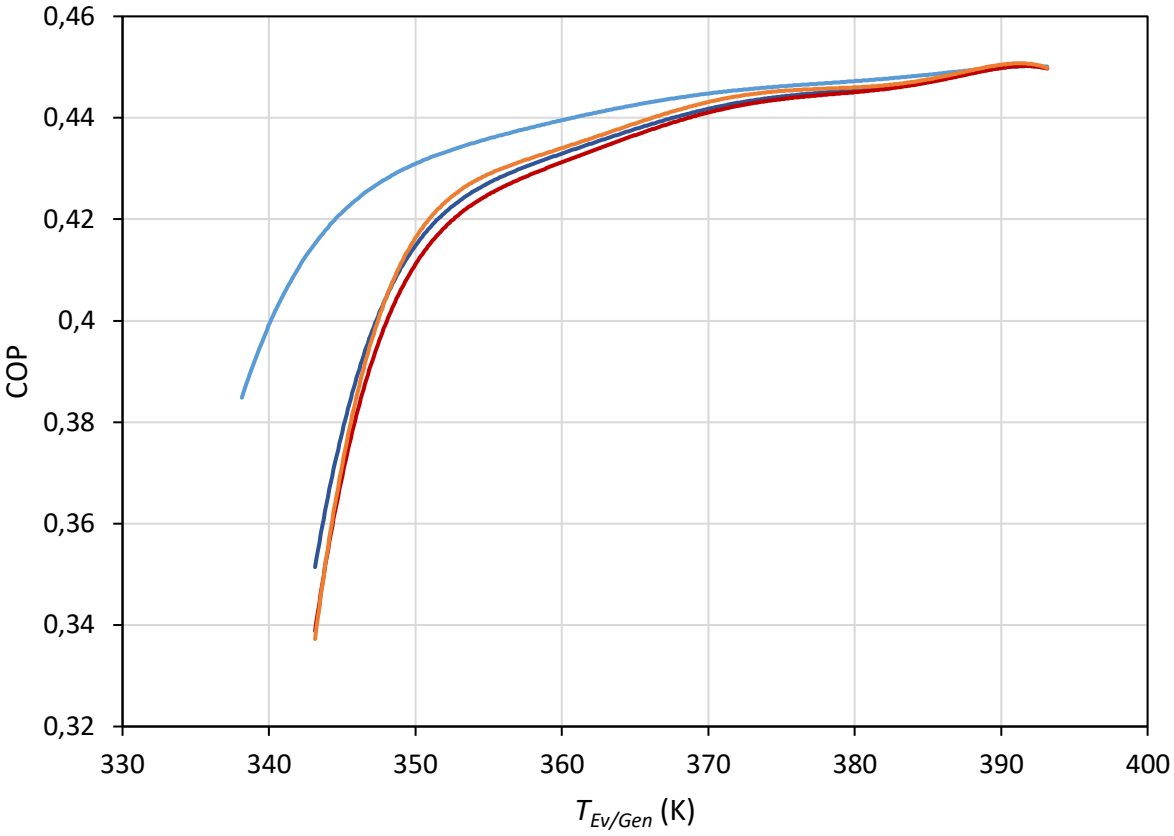

Figure 5.3. Prediction of the coefficient of performance of two working fluids as a function of the temperature of the evaporator and generator – $T_{Con} = 293\ K$, $T_{Abs} = 403\ K$ – Comparison between two approaches. Water as refrigerant.
Absorbent:
- Glycerol : Choline chloride [2:1] - classical approach[23]
- Glycerol : Choline chloride [2:1] - multiscale approach (this work)
- Ethylene glycol : Betaine [3:1] - classical approach[23]
- Ethylene glycol : Betaine [3:1] - multiscale approach (this work)

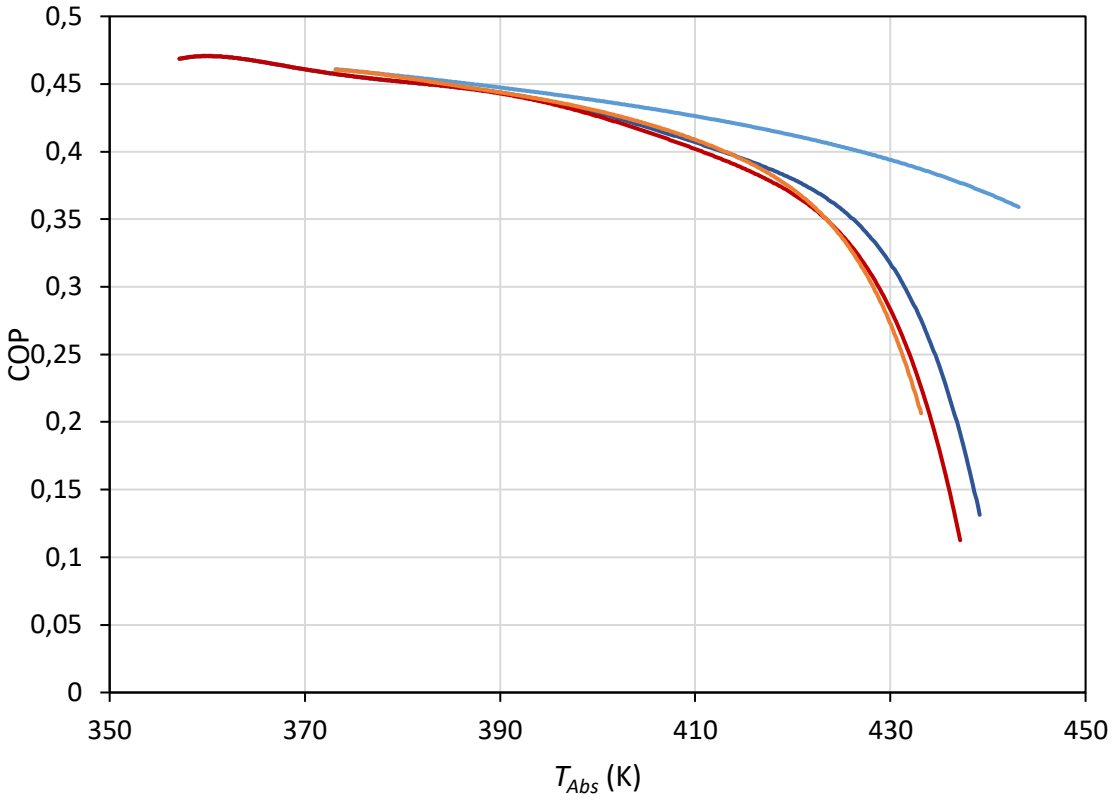

Figure 5.4. Prediction of the coefficient of performance of two working fluids as a function of the temperature of the absorber – $T_{Con} = 293\ K$, $T_{Gen} = T_{Ev} = 353\ K$ – Comparison between two approaches. Water as refrigerant.
Absorbent:
– Glycerol : Choline chloride [2:1] - classical approach[23]
– Glycerol : Choline chloride [2:1] - multiscale approach (this work)
– Ethylene glycol : Betaine [3:1] - classical approach[23]
– Ethylene glycol : Betaine [3:1] - multiscale approach (this work)

5.3.2 Screening of water/DES binary systems - Influence of the constituents of the DES

The simulations of the AHT were run with DESs reported in the literature[31]. The goal was to find the most efficient DES and to gain insight on the impact the constituents can have on the performances of the process. 21 pairs of HBA and HBD were investigated in this work. Considering the ratios of the DESs, 32 working mixtures have been studied. Their performances in terms of COP, circulation ratio and heat output per unit mass of refrigerant can be found in **Table 5.4**. The operating conditions have been arbitrarily chosen and are as follow: T_{Con} was set to 298.15 K, T_{Gen} and T_{Ev} to 353.15 K and T_{Abs} to 403.15 K. This way, the gross temperature

lift was constant and equal to 50 K. The best results are presented in **Figure 5.5**. Among them, the components appearing the most are ethylene glycol, glycerol, TMA chloride, choline chloride and betaine. The best performances were obtained with the DES {Ethylene glycol:TMA chloride}, ratio [2:1] with a COP of 0.441, a circulation ratio of 9.66 and a heat output of 2006.77 $kJ.kg^{-1}$, which is the only value over 2000 $kJ.kg^{-1}$. In comparison, the worst results correspond to a COP value of 0.385, a circulation ratio of 39.94 and a heat output of 1586.90 $kJ.kg^{-1}$ for the DES {Glycolic acid:Xylitol}, ratio [3:1].

The first criterion that has been investigated is the size of the components. Taking a look at the results of ammonium-based DESs, the best performances were obtained with the ammonium of smallest molar masses. For example, for the DESs {Glycerol:Ammonium chloride}, ratio [2:1], the COP values obtained with TMA, choline and TEA paired with chloride are 0.440, 0.435 and 0.432, respectively. When investigating DESs with glycol molecules, the same conclusion can be made, namely that smaller glycols are more likely to provide better results. When comparing {Glycol:Choline chloride} DESs, ratio [3:1], the COP values are as follow: 0.431 with ethylene glycol, 0.425 with diethylene glycol and 0.413 with triethylene glycol.

The second criterion is the impact of the ratios of the constituents. A good example would be the DES {Ethylene glycol:Betaine}. Depending on the ratio, the COP are 0.439 for a ratio [1:2], 0.435 with [1:1], 0.428 with [2:1] and 0.421 with [3:1], the best results being obtained when there is less ethylene glycol compared to betaine. This behaviour is also confirmed with the DESs {Glycerol:Betaine} and {Xylitol:Betaine}. Betaine acting as the HBA for these DESs, this would imply that better performances are favoured when the ratio of HBA is greater compared to the ratio of HBD within the DES.

Table 5.4. Comparison of the performances of several working fluids based on DESs as absorbent and water as refrigerant as part of the simulation of an AHT process. T_{Con} = 298 K, $T_{Ev} = T_{Gen}$ = 353.15 K and T_{Abs} = 403.15 K.

Absorbent		**Ratio**	**COP**	f	q (kJ.kg^{-1})
Compound #1	**Compound #2**				
Glycerol	Choline chloride	2:1	0.435	12.83	1953.29
	TMA chloride	2:1	0.440	10.98	1994.09
	TEA chloride	2:1	0.432	14.91	1932.00
	Betaine	1:2	0.438	14.75	1982.79
		1:1	0.434	16.46	1950.81
		2:1	0.428	19.29	1898.22
Ethylene glycol	Choline chloride	2:1	0.436	11.68	1961.71
		3:1	0.431	13.70	1926.20
	TMA chloride	2:1	0.441	9.66	2006.77
	TEA chloride	2:1	0.433	13.87	1939.11
	Betaine	1:2	0.439	14.42	1987.68
		1:1	0.435	15.98	1956.83
		2:1	0.428	18.98	1897.97
		3:1	0.421	21.34	1849.35
1,2-Propanediol	Choline chloride	2:1	0.438	13.57	1982.11
		3:1	0.435	16.62	1953.79
	Betaine	3:1	0.427	27.56	1890.63
1,3-Propanediol	Choline chloride	3:1	0.429	14.25	1908.81
Diethylene glycol	Choline chloride	2:1	0.431	15.73	1925.18
		3:1	0.425	19.44	1874.28
Triethylene glycol	Choline chloride	3:1	0.413	28.64	1784.46
		4:1	0.402	34.95	1708.15
Xylitol	Choline chloride	1:1	0.435	14.33	1952.12
	Betaine	1:2	0.434	18.58	1949.29
		1:1	0.425	24.05	1880.32
		2:1	0.409	33.78	1754.20
Glycolic acid	Choline chloride	1:1	0.439	11.18	1989.37

	Ethylene glycol	2:1	0.399	29.49	1686.74
	1,2-Propanediol	2:1	0.402	33.53	1705.55
	Betaine	2:1	0.422	26.42	1851.08
	Xylitol	3:1	0.385	39.94	1586.90
Urea	Choline chloride	2:1	0.424	33.64	1869.77

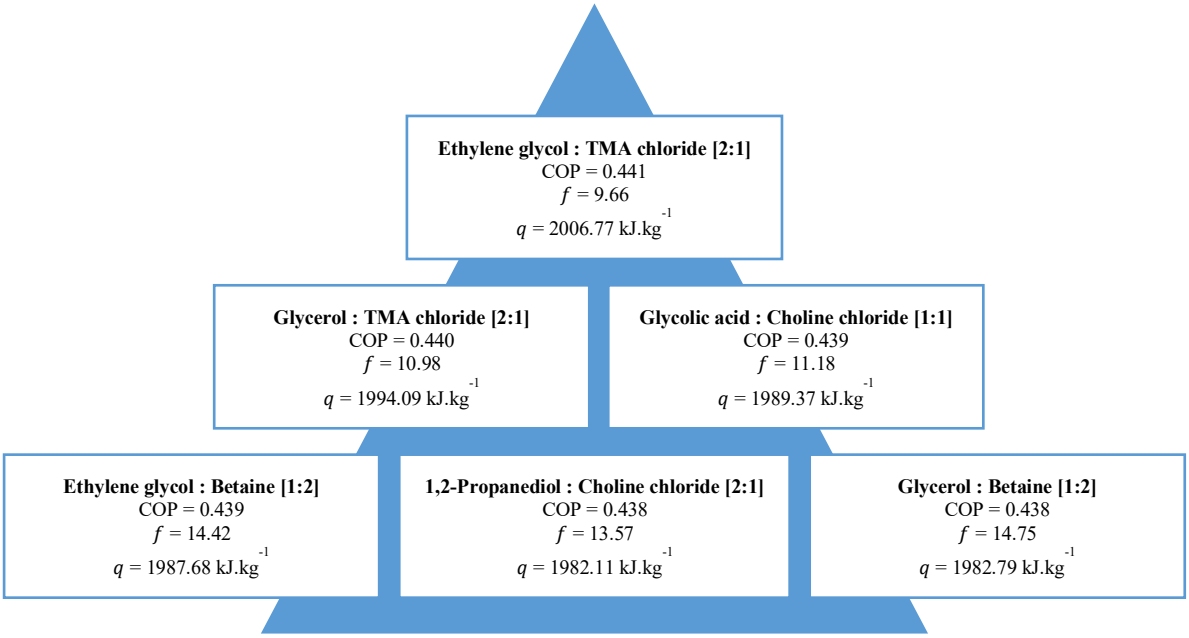

Figure 5.5. Pyramidal presentation of the DESs providing the best performances as absorbent in the working pairs water/DES within the multiscale approach.
T_{Con} = 298 K, $T_{Ev} = T_{Gen}$ = 353.15 K and T_{Abs} = 403.15 K.

It is important to note however that some of the results are very close to each other. In order to draw more general conclusions, a wider pool of DESs potentially suitable for absorption cycle applications would be required.

5.3.3 Influence of the temperatures

The influence of the temperatures of the four main parts of the process on the performances of the AHT was investigated. The working fluid was composed of water as refrigerant and DESs comprised of glycerol as absorbent, since they are among the most commonly studied DESs in the literature. Besides glycerol, the DESs are composed of either an ammonium (choline, tetramethylammonium [TMA] or tetraethylammonium [TEA]) with a

chloride or betaine at different ratios. Their performances were also compared to those obtained with ILs: the 1-Ethyl-3-methylimidazolium methylphosphonate [EMIM][MPH] the traditional working fluid made with LiBr (results taken from the literature[23]). All of the values used for the figures that follow are gathered in the supporting material.

5.3.3.1 Influence of T_{Con}

The temperature of the waste heat (T_{Gen} and T_{Ev}) was set to 353.15 K and the temperature of the upgraded heat (T_{Abs}) was set to 403.15 K. **Figure 5.6** shows the evolution of the COP values of the systems for T_{Con} varying from 283.15 to 318.15 K. For all of the working fluids, a low T_{Con} produces better results. Moreover, once a fluid-dependent threshold is reached, a dramatic drop in COP values can be observed. For the ILs and the betaine-based working fluids, this threshold is around 305 K while chloride-based fluids showed a threshold around 310 K. The water/LiBr working fluid results in the highest COP, namely around 0.5 before the threshold, while the values of COP for the other fluids are around 0.44. Horuz and Kurt computed the performances of an AHT using information from an industrial installation of a textile company and functioning with water/LiBr and obtained a very similar trend[32]. The COP of their AHT went from around 0.49 to below 0.46 for T_{Con} between 291.15 to 305.15 K with the same temperatures at the absorber and at the generator and evaporator. These results are also close to the ones of Rivera et al.[33] who investigated the performances of an AHT working with water/LiBr coupled with a distillation process. Although in their study, T_{Con} varied from 293.15 K up to 303.15 K with slightly different operating temperatures: T_{Gen} and T_{Ev} were set at 347.25 K and T_{Abs} varying from 394.15 to 404.15 K. The decrease in COP values with increasing T_{Con} is also consistent with the fact that Cudok et al. noted that the industrial installations they have investigated showed better performances in winter[1], when lower temperatures at the condenser can be reached. In terms of composition, a higher T_{Con} leads to a higher P_{low} and a lower amount of water evaporated at the generator (and more water

in the poor solution, points 8-10). This in turn gives lower COP values. Overall, even though water/LiBr can offer more useful heat via higher COP values, the range of temperature at which the AHT can be operated with DESs made of ammonium and chloride is a bit wider.

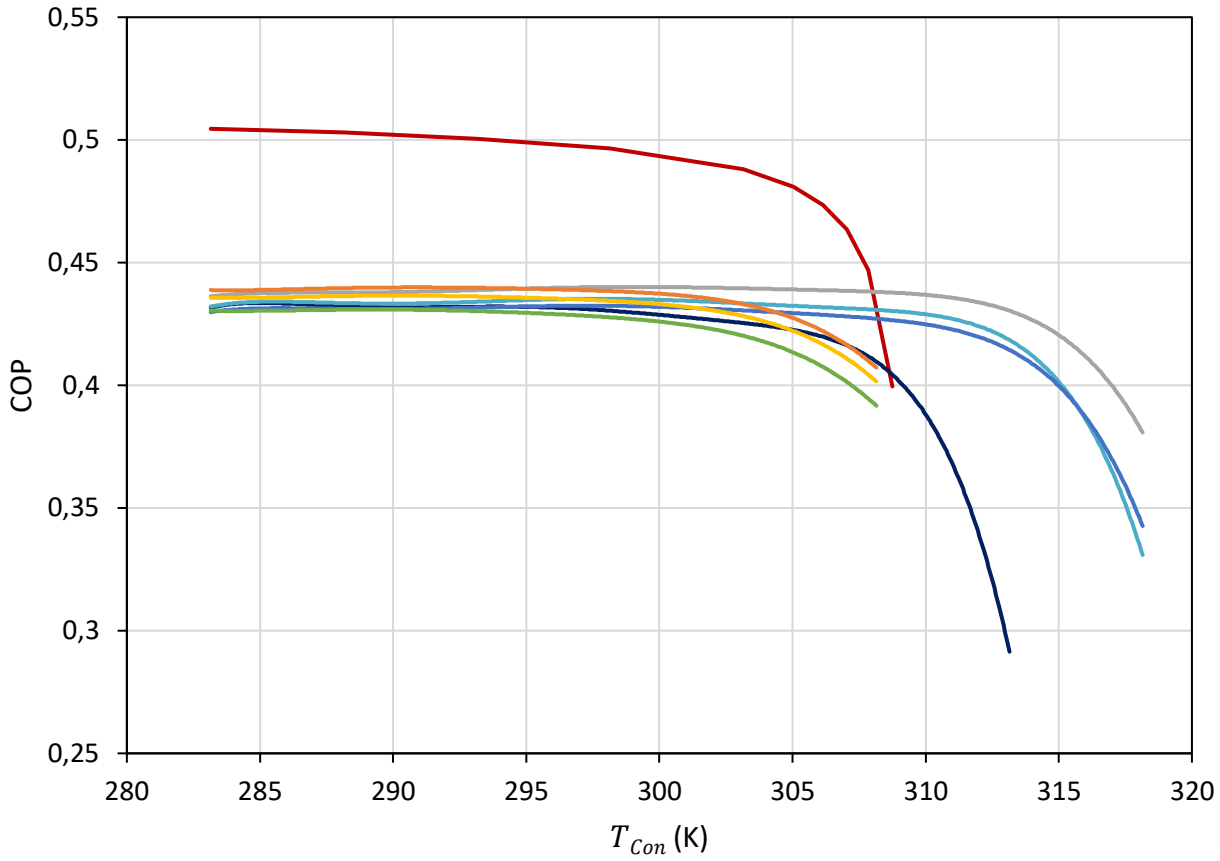

Figure 5.6. Influence of the temperature of the condenser on the coefficient of performance in the AHT simulations – $T_{Gen} = T_{Ev} = 353\ K$, $T_{Abs} = 403\ K$ – Comparison between working fluids. Water as refrigerant.
Absorbent:
- LiBr[23]
- 1-Ethyl-3-methylimidazolium methylphosphonate[23]
- Glycerol : Choline chloride [2:1]
- Glycerol : Tetramethylammonium chloride [2:1]
- Glycerol : Tetraethylammonium chloride [2:1]
- Glycerol : Betaine [1:2]
- Glycerol : Betaine [1:1]
- Glycerol : Betaine [2:1]

5.3.3.2 Influence of T_{Gen} and T_{Ev}

The performances of the AHT were studied for a temperature of the waste heat ranging from 333.15 to 353.15 K, with T_{Con} and T_{Abs} set to 293.15 K and 403.15 K, respectively. The

evolution of the COP with T_{Gen} (or T_{Ev}) can be found in **Figure 5.7** and is similar for all of the working fluids: higher COP values are obtained when the temperature of the waste heat is high. Logically, it is easier to upgrade heat when the temperature of the input source is increased. Composition-wise, an increase in T_{Ev} causes an increase in P_{high} and a higher absorption of water by the poor solution (higher concentration of water in the rich solution, points 5 to 7). This results in higher COP values. One can also observe that when the temperature of the heat input becomes too low, COP values decrease drastically. This is also very close to what Horuz and Kurt obtained with water/LiBr[32]. As for the influence of T_{Con}, the range at which the COP remains acceptable before the drop is wider for chloride-based DESs compared to betaine-based DESs and LiBr, even though the COPs of the latter reach higher values. DESs with glycerol and ammonium chloride can indeed be used with waste heat around 340.15 K while LiBr requires a temperature of at least 348.15 K. In this way, replacing LiBr by DESs would make it easier to work around the waste heat and expand the applicability of the process to more types of effluents. Noticeably, only the IL [EMIM][MPH] seems to still provides good COP values around 335 K.

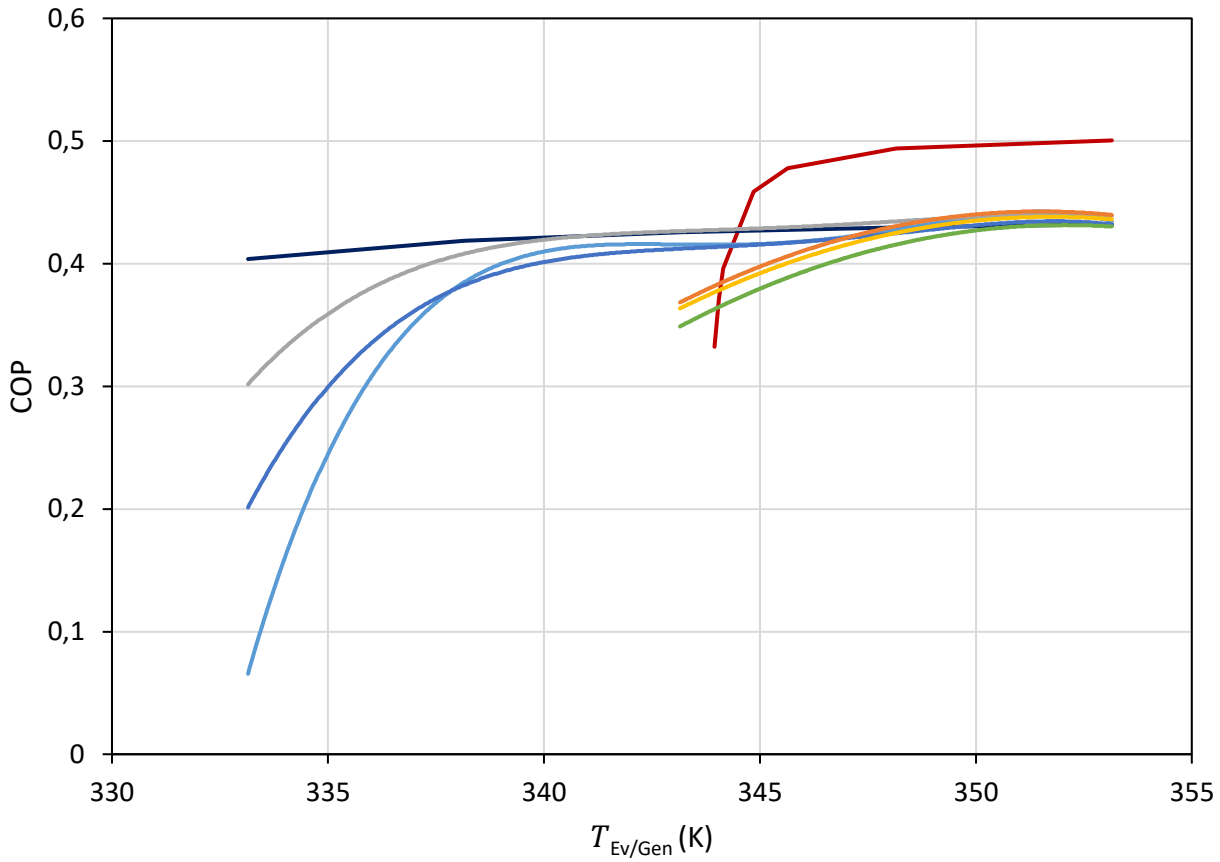

Figure 5.7. Influence of the temperature of the evaporator and generator on the coefficient of performance in the AHT simulations– $T_{Con} = 293\ K$, $T_{Abs} = 403\ K$ – Comparison between working fluids. Water as refrigerant.
Absorbent:
- LiBr[23]
- 1-Ethyl-3-methylimidazolium methylphosphonate[23]
- Glycerol : Choline chloride [2:1]
- Glycerol : Tetramethylammonium chloride [2:1]
- Glycerol : Tetraethylammonium chloride [2:1]
- Glycerol : Betaine [1:2]
- Glycerol : Betaine [1:1]
- Glycerol : Betaine [2:1]

5.3.3.3 Influence of T_{Abs}

Figure 5.8 provides the COP as a function of the temperature of the output heat at the absorber. T_{Abs} ranges from 373.15 to 423.15 K with T_{Con} set to 293.15 K and T_{Gen} and T_{Ev} set to 353.15 K. Overall, the COP decreases as T_{Abs} increases. LiBr COP values remain around 0.5 before dropping while the COP values of the other fluids decreases starting from around 0.46. This is in line with the fact that the higher T_{Abs} becomes, the more difficult it is to retain good

performances. This can also be observed with the evolution of the circulation ratio as a function of T_{Abs} which has been displayed for the DES in **Figure 5.9**. Starting from values around 5 at 373.15 K, f increases with T_{Abs}. The trend is very similar to the one that Rivera et al. observed with water/LiBr and different operating conditions[33]. With a higher T_{Abs}, more energy needs to be released by the absorption phenomenon and the working fluid needs to circulate more between the generator and the absorber, leading to higher f values and higher costs. It should be noted that the circulation ratio of the DESs made of betaine increases more compared to the DESs with ammonium chloride, and especially from 400 K, underlying again their lesser performances.

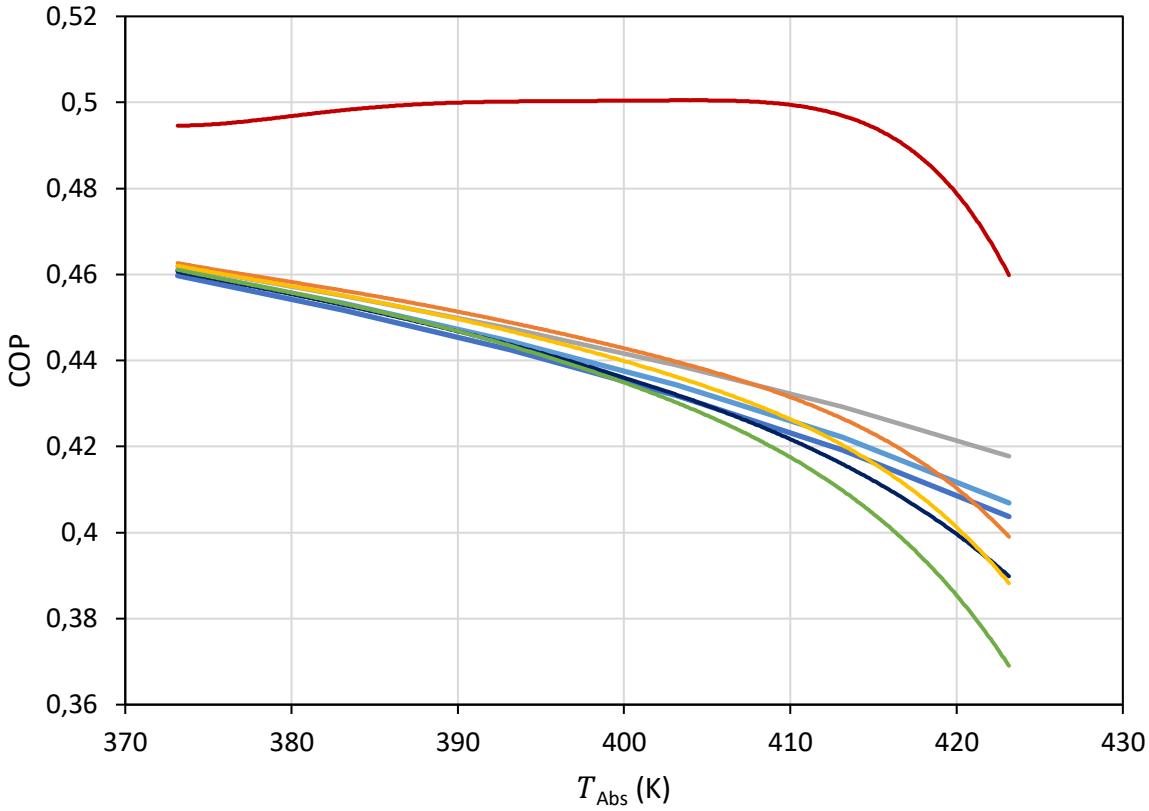

Figure 5.8. Influence of the temperature of the absorber on the coefficient of performance in the AHT simulations– $T_{Con} = 293\ K$, $T_{Gen} = T_{Ev} = 353\ K$ – Comparison between working fluids. Water as refrigerant.
Absorbent:
- LiBr[23]
- 1-Ethyl-3-methylimidazolium methylphosphonate[23]
- Glycerol : Choline chloride [2:1]
- Glycerol : Tetramethylammonium chloride [2:1]
- Glycerol : Tetraethylammonium chloride [2:1]
- Glycerol : Betaine [1:2]
- Glycerol : Betaine [1:1]
- Glycerol : Betaine [2:1]

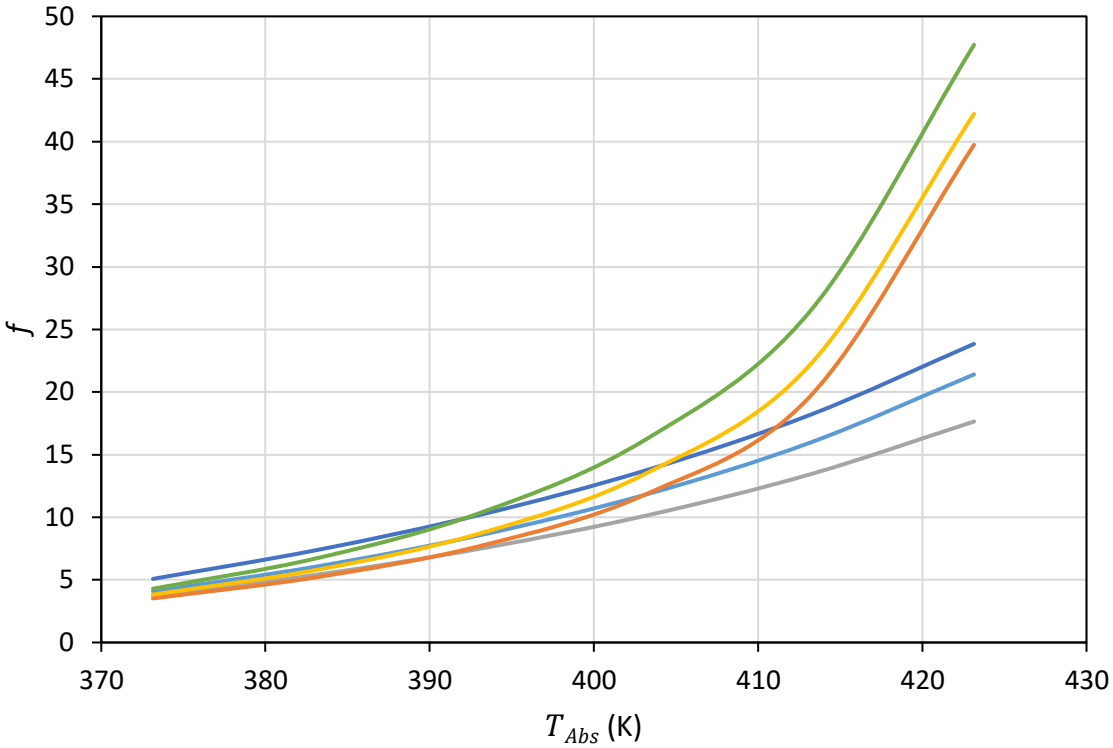

Figure 5.9. Influence of the temperature of the absorber on the circulation ratio in the AHT simulations– $T_{Con} = 293\ K$, $T_{Gen} = T_{Ev} = 353\ K$ – Comparison between working fluids. Water as refrigerant.
Absorbent:
- Glycerol : Choline chloride [2:1]
- Glycerol : Tetramethylammonium chloride [2:1]
- Glycerol : Tetraethylammonium chloride [2:1]
- Glycerol : Betaine [1:2]
- Glycerol : Betaine [1:1]
- Glycerol : Betaine [2:1]

5.4 Conclusion

In this work, a tool based on COSMOC-SAC (+OH-ClBr) and group contribution methods is proposed to simulate water/DES working fluids in AHT processes. A total of 32 working pairs made of DESs and water have been investigated to gauge their capacity to upgrade heat as part of an AHT process. The impact of various operating temperatures as well as a better understanding of the influence of the components on the results were explored by comparing the performance criteria of the water/DESs working fluids. Their performances were also compared to the more traditional water/LiBr. Overall, within the simulations the values of

COP for water/LiBr proved to be higher than the ones with the investigated DESs. However, working fluids involving DESs allow to work within a bigger range of temperature. In particular, they retain good performances at higher temperature in the condenser and can upgrade waste heat flows that have a lower temperature compared to LiBr, potentially expanding the field of application for AHT or rending the implementation of the process easier. This work allowed to showcase the applicability of the AHT model based on COSMO-SAC (+OH-ClBr) and group contributions. The tool presented in this work gives the possibility of screening potentially any DES and perform a first selection of DESs as absorbent before further experimental testing. The calculations have been tested with some of the most common DESs. First results show that smaller components with high HBA ratio lead to better performances. As more DESs are investigated, the pool of material to research on will be expanded. Then, would remain to study the suitability of the fluids, in particular in terms of viscosity for the potential pressure drop and thermal stability. Thanks to the flexibility of DESs, it should be possible to develop a working fluid with high performances and good availability.

5.5 Nomenclature

Abbreviations

AHT	Absorption heat transformer
COP	Coefficient of performance (-)
COSMO	COnductor-like Screening Model
COSMO-SAC	COSMO segment activity coefficient
DES	Deep eutectic solvent
EMIM	1-Ethyl-3-methylimidazolium
HBA	Hydrogen bond acceptor
HBD	Hydrogen bond donor
IL	Ionic liquid
LiBr	Lithium bromide
MPH	Methylphosphonate
SHE	Solution heat exchanger
TEA	Tetraethylammonium cation
TMA	Tetramethylammonium cation
VLE	Vapour-liquid equilibrium

Symbols

c_p	Heat capacity (kJ.kg^{-1}.K^{-1})
f	Circulation ratio (-)
h	Enthalpy (kJ.kg^{-1})
$\dot{m}$	Mass flow rate (kg.s^{-1})
P	Pressure (Pa)
$\dot{Q}$	Heat flow (kW)
q	Heat output per unit mass of refrigerant (kJ.kg^{-1})
R	Gas constant (kJ.mol^{-1}K^{-1})
T	Temperature (K)
x	Molar fraction in the liquid phase (-)
x_m	Mass fraction in the liquid phase (-)
z	Mass fraction of vapour in the liquid vapour mixture (-)

Superscripts

DES	Deep eutectic solvent
w	Water

Subscripts

Abs	Absorber
C	Critical
Con	Condenser
Ev	Evaporator
Gen	Generator

$high$	High pressure (absorber or evaporator) or temperature (absorber)
liq	Liquid
low	Low pressure (condenser or generator) or temperature (condenser)
LV	Liquid vapour mixture
$medium$	Medium temperature (generator or evaporator)
mix	Mixture
$poor$	Fluid poor in refrigerant
ref	Reference
$rich$	Fluid rich in refrigerant
sat	Saturated
vap	Vapour

Greek letters

γ	Activity coefficient
Δh_{vap}	Enthalpy of vaporization (kJ.kg^{-1})
Δt	Gross lift temperature (K)
ΔT_{min}	Minimum temperature difference between the hot and cold streams of the SHE (K)
ρ	Density (kg.m^{-3})

References

(1) Cudok, F.; Giannetti, N.; Ciganda, J. L. C.; Aoyama, J.; Babu, P.; Coronas, A.; Fujii, T.; Inoue, N.; Saito, K.; Yamaguchi, S.; Ziegler, F. Absorption Heat Transformer - State-of-the-Art of Industrial Applications. *Renewable and Sustainable Energy Reviews* **2021**, *141*, 110757. https://doi.org/10.1016/j.rser.2021.110757.

(2) Sun, J.; Fu, L.; Zhang, S. A Review of Working Fluids of Absorption Cycles. *Renewable and Sustainable Energy Reviews* **2012**, *16*, 1899–1906.

(3) Wu, W.; Wang, B.; Shi, W.; Li, X. An Overview of Ammonia-Based Absorption Chillers and Heat Pumps. *Renewable and Sustainable Energy Reviews* **2014**, *31*, 681–707. https://doi.org/10.1016/j.rser.2013.12.021.

(4) Arshi Banu, P. S.; Sudharsan, N. M. Review of Water Based Vapour Absorption Cooling Systems Using Thermodynamic Analysis. *Renewable and Sustainable Energy Reviews* **2018**, *82*, 3750–3761. https://doi.org/10.1016/j.rser.2017.10.092.

(5) Kurem, E.; Horuz, I. A Comparison between Ammonia-Water and Water-Lithium Bromide Solutions in Absorption Heat Transformers. *International Communications in Heat and Mass Transfer* **2001**, *28* (3), 427–438. https://doi.org/10.1016/S0735-1933(01)00247-0.

(6) Wang, K.; Abdelaziz, O.; Kisari, P.; Vineyard, E. A. State-of-the-Art Review on Crystallization Control Technologies for Water/LiBr Absorption Heat Pumps. *International Journal of Refrigeration* **2011**, *34* (6), 1325–1337. https://doi.org/10.1016/j.ijrefrig.2011.04.006.

(7) Bandrés, I.; Royo, F. M.; Gascón, I.; Castro, M.; Lafuente, C. Anion Influence on Thermophysical Properties of Ionic Liquids: 1-Butylpyridinium Tetrafluoroborate and 1-Butylpyridinium Triflate. *J. Phys. Chem. B* **2010**, *114* (10), 3601–3607. https://doi.org/10.1021/jp9120707.

(8) Vogl, T.; Goodrich, P.; Jacquemin, J.; Passerini, S.; Balducci, A. The Influence of Cation Structure on the Chemical–Physical Properties of Protic Ionic Liquids. *J. Phys. Chem. C* **2016**, *120* (16), 8525–8533. https://doi.org/10.1021/acs.jpcc.6b01945.

(9) Khamooshi, M.; Parham, K.; Atikol, U. Overview of Ionic Liquids Used as Working Fluids in Absorption Cycles. *Advances in Mechanical Engineering* **2013**, *5*, 620592. https://doi.org/10.1155/2013/620592.

(10) Zhang, X.; Hu, D. Performance Analysis of the Single-Stage Absorption Heat Transformer Using a New Working Pair Composed of Ionic Liquid and Water. *Applied*

Thermal Engineering **2012**, *37*, 129–135. https://doi.org/10.1016/j.applthermaleng.2011.11.006.

(11) Ayou, D. S.; Currás, M. R.; Salavera, D.; García, J.; Bruno, J. C.; Coronas, A. Performance Analysis of Absorption Heat Transformer Cycles Using Ionic Liquids Based on Imidazolium Cation as Absorbents with 2,2,2-Trifluoroethanol as Refrigerant. *Energy Conversion and Management* **2014**, *84*, 512–523. https://doi.org/10.1016/j.enconman.2014.04.077.

(12) Abumandour, E.-S.; Mutelet, F.; Alonso, D. Performance of an Absorption Heat Transformer Using New Working Binary Systems Composed of {ionic Liquid and Water}. *Applied Thermal Engineering* **2016**, *94*, 579–589. https://doi.org/10.1016/j.applthermaleng.2015.10.107.

(13) Chen, W.; Liang, S. Thermodynamic Analysis of Absorption Heat Transformers Using [Mmim]DMP/H 2 O and [Mmim]DMP/CH 3 OH as Working Fluids. *Applied Thermal Engineering* **2016**, *99*, 846–856. https://doi.org/10.1016/j.applthermaleng.2016.01.135.

(14) Merkel, N.; Bücherl, M.; Zimmermann, M.; Wagner, V.; Schaber, K. Operation of an Absorption Heat Transformer Using Water/Ionic Liquid as Working Fluid. *Applied Thermal Engineering* **2018**, *131*, 370–380. https://doi.org/10.1016/j.applthermaleng.2017.11.147.

(15) Abumandour, E.-S.; Mutelet, F.; Alonso, D. Thermodynamic Properties Assessment of Working Mixtures {water + Alkylphosphonate Based Ionic Liquids} as Innovative Alternatives Working Pairs for Absorption Heat Transformers. *Applied Thermal Engineering* **2020**, *181*, 115943. https://doi.org/10.1016/j.applthermaleng.2020.115943.

(16) Pham, T. P. T.; Cho, C.-W.; Yun, Y.-S. Environmental Fate and Toxicity of Ionic Liquids: A Review. *Water Research* **2010**, *44* (2), 352–372. https://doi.org/10.1016/j.watres.2009.09.030.

(17) Kunz, W.; Häckl, K. The Hype with Ionic Liquids as Solvents. *Chemical Physics Letters* **2016**, *661*, 6–12. https://doi.org/10.1016/j.cplett.2016.07.044.

(18) Abbott, A. P.; Capper, G.; Davies, D. L.; Rasheed, R. K.; Tambyrajah, V. Novel Solvent Properties of Choline Chloride/Urea MixturesElectronic Supplementary Information (ESI) Available: Spectroscopic Data. See Http://Www.Rsc.Org/Suppdata/Cc/B2/B210714g/. *Chem. Commun.* **2003**, No. 1, 70–71. https://doi.org/10.1039/b210714g.

(19) Abbott, A. P.; Boothby, D.; Capper, G.; Davies, D. L.; Rasheed, R. K. Deep Eutectic Solvents Formed between Choline Chloride and Carboxylic Acids: Versatile Alternatives

to Ionic Liquids. *J. Am. Chem. Soc.* **2004**, *126* (29), 9142–9147. https://doi.org/10.1021/ja048266j.

(20) Guajardo, N.; Müller, C. R.; Schrebler, R.; Carlesi, C.; Domínguez de María, P. Deep Eutectic Solvents for Organocatalysis, Biotransformations, and Multistep Organocatalyst/Enzyme Combinations. *ChemCatChem* **2016**, *8* (6), 1020–1027. https://doi.org/10.1002/cctc.201501133.

(21) Khandelwal, S.; Tailor, Y. K.; Kumar, M. Deep Eutectic Solvents (DESs) as Eco-Friendly and Sustainable Solvent/Catalyst Systems in Organic Transformations. *Journal of Molecular Liquids* **2016**, *215*, 345–386. https://doi.org/10.1016/j.molliq.2015.12.015.

(22) Marcus, Y. *Deep Eutectic Solvents*; Springer International Publishing: Cham, 2019. https://doi.org/10.1007/978-3-030-00608-2.

(23) Nessakh, F. Z.; Mutelet, F.; Negadi, A. Efficiency of Two Working Fluids Constituted of a Deep Eutectic Solvent and Water in Absorption Heat Transformer. *Intl J of Energy Research* **2022**, er.8658. https://doi.org/10.1002/er.8658.

(24) Abedin, R.; Heidarian, S.; Flake, J. C.; Hung, F. R. Computational Evaluation of Mixtures of Hydrofluorocarbons and Deep Eutectic Solvents for Absorption Refrigeration Systems. *Langmuir* **2017**, *33* (42), 11611–11625. https://doi.org/10.1021/acs.langmuir.7b02003.

(25) Haghbakhsh, R.; Peyrovedin, H.; Raeissi, S.; Duarte, A. R. C.; Shariati, A. Energy Conservation in Absorption Refrigeration Cycles Using DES as a New Generation of Green Absorbents. *Entropy* **2020**, *22* (4), 409. https://doi.org/10.3390/e22040409.

(26) Haghbakhsh, R.; Peyrovedin, H.; Raeissi, S.; Duarte, A. R. C.; Shariati, A. Investigating the Performance of Novel Green Solvents in Absorption Refrigeration Cycles: Energy and Exergy Analyses. *International Journal of Refrigeration* **2020**, *113*, 174–186. https://doi.org/10.1016/j.ijrefrig.2020.01.013.

(27) Shen, V. K.; Siderius, D. W.; Krekelberg, W. P.; Hatch, H. W. *NIST Standard Reference Simulation Website, NIST Standard Reference Database Number 173, National Institute of Standards and Technology, Gaithersburg MD, 20899, http://doi.org/10.18434/T4M88Q*. NIST. https://www.nist.gov/ (accessed 2021-10-18).

(28) Di Pietro, T.; Cesari, L.; Mutelet, F. Modified Version of the COSMO-SAC Model for the Prediction of Vapour-Liquid Equilibria of Mixtures Containing Halogen Compounds. *Fluid Phase Equilibria*. Accepted. Cf. chapter 3.

(29) *DIPPR. Data Compilation of Pure Compound Properties, Version 12.3.0*; The Design Institute for Physical property Data (DIPPR), 2018.

(30) Di Pietro, T.; Cesari, L.; Mutelet, F. Group Contribution Models for Densities and Heat Capacities of Deep Eutectic Solvents. To be submitted. Cf. chapter 4.

(31) Hansen, B. B.; Spittle, S.; Chen, B.; Poe, D.; Zhang, Y.; Klein, J. M.; Horton, A.; Adhikari, L.; Zelovich, T.; Doherty, B. W.; Gurkan, B.; Maginn, E. J.; Ragauskas, A.; Dadmun, M.; Zawodzinski, T. A.; Baker, G. A.; Tuckerman, M. E.; Savinell, R. F.; Sangoro, J. R. Deep Eutectic Solvents: A Review of Fundamentals and Applications. *Chem. Rev.* **2021**, *121* (3), 1232–1285. https://doi.org/10.1021/acs.chemrev.0c00385.

(32) Horuz, I.; Kurt, B. Absorption Heat Transformers and an Industrial Application. *Renewable Energy* **2010**, *35* (10), 2175–2181. https://doi.org/10.1016/j.renene.2010.02.025.

(33) Rivera, W.; Cerezo, J.; Rivero, R.; Cervantes, J.; Best, R. Single Stage and Double Absorption Heat Transformers Used to Recover Energy in a Distillation Column of Butane and Pentane. *Int. J. Energy Res.* **2003**, *27* (14), 1279–1292. https://doi.org/10.1002/er.943.

Conclusion et perspectives

Conclusion et perspectives

Dans le cadre de la revalorisation énergétique de la chaleur fatale, ce travail de thèse a porté sur le remplacement des fluides de travail dans les thermotransformateurs à absorption. Le choix s'est porté sur l'étude des solvants eutectiques profonds (SEPs), solvants novateurs et attractifs étant donné leur flexibilité et les possibilités offertes par le grand nombre de constituants envisageables. L'adaptabilité de leurs propriétés pose alors comme défi la connaissance des propriétés de ces solvants, capitale pour le développement et le dimensionnement des procédés industriels. Il apparaît utopique et coûteux d'obtenir une large banque de données expérimentales nécessaire à la sélection des meilleurs solvants pour l'application dans les pompes à chaleur. Pour cette technologie, les propriétés requises étant la masse volumique, la capacité thermique et les équilibres liquide-vapeur des mélanges de travail. Avec pour objectif de s'émanciper du besoin de générer cette grande quantité de données, une approche multi-échelle a été menée dans le but de produire un outil capable de prédire les propriétés thermodynamiques ainsi que les performances de SEPs couplés à de l'eau au sein d'un thermotransformateur à absorption.

Tout d'abord, l'approche a été développée à l'échelle moléculaire dans le but d'en apprendre plus sur les interactions entre les constituants qui forment les SEPs. A travers l'exemple de deux SEPs basés sur le chlorure de choline, l'étude menée au moyen de la théorie de la fonctionnelle de la densité a permis de mettre en évidence l'importance des liaisons hydrogène entre les groupes hydroxyles et les atomes halogènes pouvant faire partie de SEPs tel que l'atome de chlore.

Ces résultats nous ont conduit à proposer une modification du modèle COSMO SAC (2010) par le biais de l'ajout de paramètres correspondant aux liaisons hydrogène entre atomes d'hydrogène issus de groupes hydroxyles et atomes de chlore ou de brome. Avec le développement du modèle COSMO-SAC (+OH-ClBr), l'objectif était de mieux modéliser les

équilibres de phases de mélanges contenant des SEPs, notamment les équilibres liquide-vapeur {eau + SEP}. Ainsi, une nette amélioration de la précision des prédictions des équilibres liquide-vapeur a pu être observée.

Deux méthodes de contributions de groupes ont été spécifiquement développés pour les SEPs pour déterminer leur masse volumique et leur capacité thermique. Cette approche offre une très bonne représentation de ces propriétés, avec une déviation moyenne de 1.95 % pour la masse volumique et de 3.09 % pour la capacité thermique. Ces modèles sont d'autant plus intéressants lorsque les bases de données sont étendues.

Le modèle COSMO-SAC (+OH-ClBr) et les méthodes de contributions de groupes ont enfin été intégrés à un outil de prédiction de performances d'un thermotransformateur à absorption fonctionnant avec un fluide de travail constitué d'eau et de SEP. Cette méthode a été validée par comparaison des résultats obtenus avec une méthode plus traditionnelle, basée sur l'utilisation du modèle NRTL et des corrélations empiriques ajustées sur des données expérimentales. Cet outil permet une présélection de mélanges de travail. Un premier screening de 32 fluides de travail eau/SEP a montré que ces mélanges pouvaient atteindre des performances proches de celles du mélange traditionnel eau/LiBr. De plus, cette étude indique que les SEPs avec une faible masse molaire et un plus haut ratio en accepteur de liaisons hydrogène conduisent à de meilleures performances. Le mélange eau/{éthylene glycol : tetramethylammonium chloride} ratio [2 :1] a ainsi conduit aux meilleurs résultats.

La suite logique du screening de mélanges de travail est une étude expérimentale basée sur les meilleurs résultats théoriques. D'une part pour pousser la validation des modèles et de l'outil de présélection, d'autre part pour étudier plus en profondeur la pertinence et l'applicabilité des mélanges choisis. Ainsi, un certain nombre de questions doivent être posées, notamment du point de vue des propriétés des SEPs qui influent directement sur la viabilité et la durée de vie d'une installation industrielle. Entre autres, est-ce que la corrosivité,

l'inflammabilité et la viscosité des mélanges choisis sont adaptées ?

Du point de vue des modèles utilisés, les pistes d'amélioration suivantes peuvent être envisagées. La dynamique moléculaire pourrait être employée afin de faire le lien entre échelle microscopique et des propriétés macroscopiques. Cela permettrait notamment d'étudier des systèmes contenant un plus grand nombre de molécules. Au sein des modèles de type COSMO, de nouvelles formes de liaisons et d'interactions (liaisons hydrogènes spécifiques, liaisons halogènes, etc...) décrites à l'aide de nouveaux paramètres peuvent permettre une meilleure modélisation des mélanges. Concernant les modèles de contributions de groupes, l'ajout de nouveaux groupes au fur et à mesure que les bases de données seront étendues permettra d'étendre la gamme de molécules pouvant être modélisées.

La modélisation du thermotransformateur à absorption peut également bénéficier d'une amélioration via l'ajout du calcul des propriétés d'excès des composés, potentiellement utiles pour le calcul des enthalpies de mélange. Il s'agirait par exemple de voir si suffisamment de données sont disponibles afin de développer un modèle de contributions de groupes supplémentaire pour les SEPs. Une analyse de sensibilité est également à mener afin d'étudier l'impact de la précision des modèles mis en place sur les performances du thermotransformateur à absorption.

Finalement, la méthodologie présentée dans ce rapport, ici appliquée aux thermotransformateurs à absorption, peut être étendue à d'autres machines thermiques, notamment les machines frigorifiques.

Annexes

Annexes

Annexe A : Influence of water on the conformation and interactions within two chloride-based deep eutectic solvents : a density functional theory investigation

A.1. Input Keywords

A.1.1 Optimization and frequency

opt freq b3lyp/6-311++g(d,p) nosymm geom=connectivity empiricaldispersion=gd3bj

Apart from the calculations for the molecules by themselves (choline cation, phenol, glycolic acid), the following keyword was also added to account for the BSSE correction:

Counterpoise = N, with N the number of fragments considered (2 for choline chloride, 4 for choline chloride and two phenols, etc…).

The fragment number for each atom was also detailed in the Gaussian calculation window, as well as the charge and multiplicity for the whole group of molecules, then for each segment.

For the thermochemistry in particular, temperature was set to 298.15 K and pressure to 1.00000 atm.

A.1.2 NBO calculations

b3lyp/6-311++g(d,p) nosymm pop=(nbo,reg,chelpg) geom=connectivity empiricaldispersion=gd3bj

1.3 Basis set description: 6-311++G(d,p)

6-311G uses different sizes of basis functions (combinations of gaussian functions) to approximate orbitals. It comprises pure 5-component d functions and 7-component f functions. It is a polarized basis set that allows the orbitals to change both size and shape. It is also a triple zeta basis set that adds extra valence functions, namely 3 sizes of orbital s and p functions.

The '++' part adds diffuse functions. They allow orbitals to occupy larger region of space and are important for systems with electrons than are relatively far from the nucleus, for example systems with lone pairs, anions and excited states. The second '+' adds diffuse functions to the

hydrogen atoms.

'(d,p)' indicates that polarization functions have been added to heavy atoms while p functions have been added to hydrogen atoms. This is used when the hydrogen atoms are the site of interest and when final, accurate energy calculations are needed.

A.2. Choline cation

A.2.1 Energies

The geometry optimization and frequency calculations allow to derive several energies for a system. The lower the energy, the more stable is the corresponding conformation. This energy can be ZPE corrected to become E_0, which is the sum of the electronic and zero-point energies. The free energy G corresponds to the sum of the electronic and thermal free energies. When comparing conformations, ΔE is the difference between the energy of the investigated conformation and the energy of the most stable conformation. Energies are provided in hartree in the output files from the Gaussian software, with:

$$1\ hartree = 1\ au = 2625.5\ \text{kJ.mol}^{-1} \quad (1)$$

Table S.A1. Electronic, ZPE corrected and thermal free energies and the relative corresponding energies for three conformers of the choline cation

Conformation	Energy (au)	E_0 (au)	ΔE ZPE corrected (kJ.mol^{-1})	G (au)	ΔG (kJ.mol^{-1})
Gauche	-328.820622	-328.623314	0	-328.655584	0
Anti	-328.812969	-328.616459	17.998	-328.648484	18.64
Anti with the C-C-O-H dihedral angle set to -90°	-328.810849	-328.614471	23.217	-328.648148	19.52

$E_0 = E_{elec} + ZPE$ = sum of electronic and zero-point energies
$G = H - TS$ = sum of electronic and thermal free energies

A.2.2 Partial charge analysis

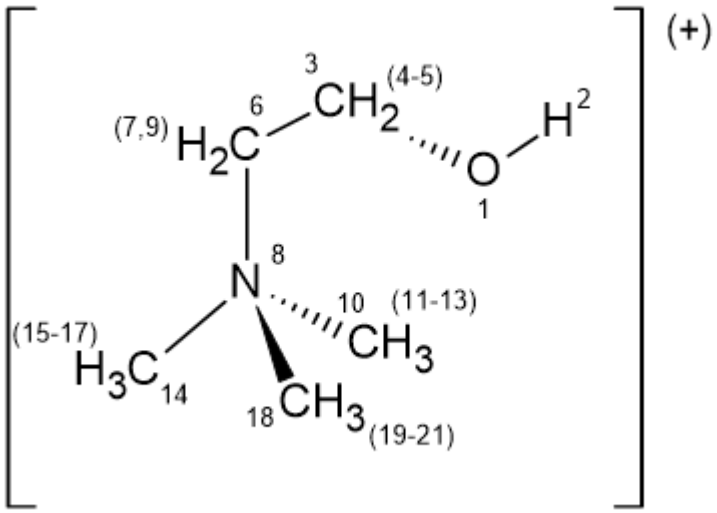

Figure S.A1. Numbering of the atoms in the gauche conformer of the choline cation

Table S.A2. Charge distribution for the gauche conformer of the choline cation

	Charge distribution with the corresponding method (e)	
Atom	NBO	CHelpG
O^1	-0.75258	-0.652973
H^2	0.48966	0.446582
C^3	-0.05068	0.253389
H^4	0.17564	0.019457
H^5	0.20342	0.060858
C^6	-0.17271	-0.162222
H^7	0.2267	0.156018
N^8	-0.34536	0.148631
H^9	0.22648	0.111657
C^{10}	-0.35081	-0.242541
H^{11}	0.21732	0.143218
H^{12}	0.21956	0.149518
H^{13}	0.25562	0.174987
C^{14}	-0.34408	-0.31191
H^{15}	0.22572	0.157901
H^{16}	0.226	0.171341
H^{17}	0.22236	0.169909
C^{18}	-0.35432	-0.299809
H^{19}	0.23482	0.176265
H^{20}	0.22101	0.170115
H^{21}	0.22622	0.159609
Total	**0.99999**	**1.000000**

3. Choline chloride

3.1. Conformations

Table S.A3. 3D structure of the eight choline chloride conformations along with their relative (BSSE and ZPE corrected) energies

Conformation	ChCl_A	ChCl_B
Optimized structure	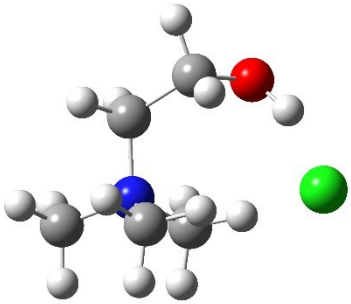	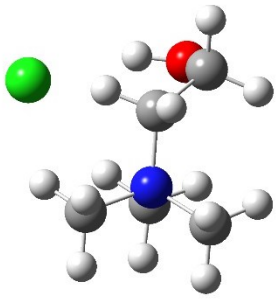
ΔE (kJ.mol^{-1})	0.000	1.633
Conformation	ChCl_C	ChCl_D
Optimized structure	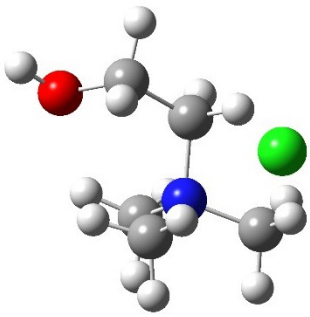	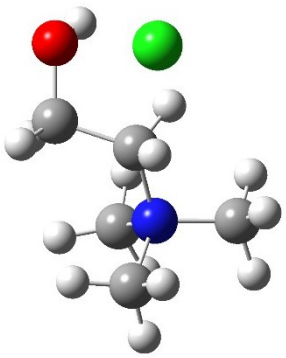
ΔE (kJ.mol^{-1})	12.461	20.655

Conformation	ChCl_E	ChCl_F
Optimized structure	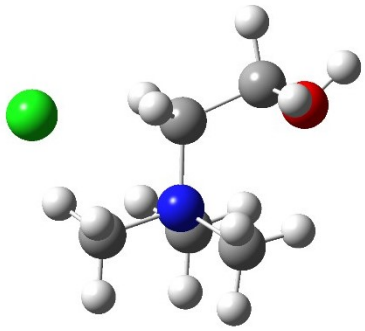	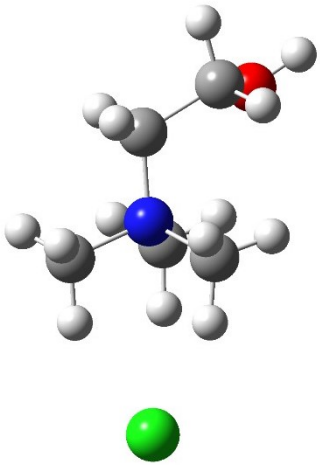
ΔE (kJ.mol^{-1})	28.227	29.366
Conformation	ChCl_G	ChCl_H
Optimized structure	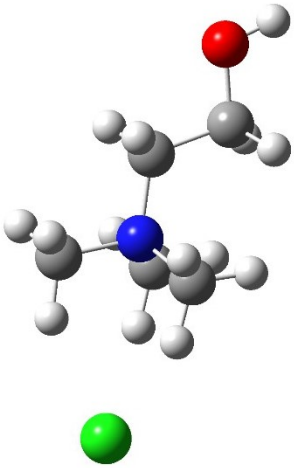	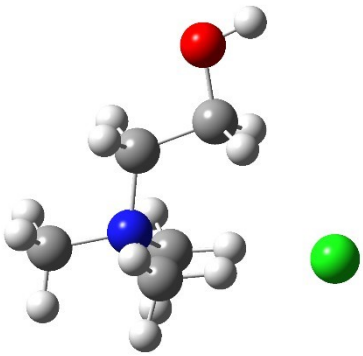
ΔE (kJ.mol^{-1})	33.008	37.629

A.3.2. Energies

For systems containing several molecules or fragments such as choline chloride, the counterpoise keyword allows to obtain BSSE corrected energies to account for the basis set superposition error.

Table S.A4. Electronic, ZPE corrected and thermal free energies and the relative corresponding energies for the eight conformers of the choline chloride

Conformation	Counterpoise corrected energy (au)	BSSE energy (au)	BSSE energy (kJ.mol^{-1})	E_0 (au)	ΔE counterpoise and ZPE corrected (kJ.mol^{-1})	G (au)	ΔG (kJ.mol^{-1})
ChCl_A	-789.281267	0.001300	3.413	-789.083606	0.000	-789.118631	0.00
ChCl_B	-789.280870	0.001335	3.505	-789.083019	1.633	-789.118185	1.17
ChCl_C	-789.276529	0.001187	3.116	-789.078747	12.461	-789.114507	10.83
ChCl_D	-789.27366	0.001294	3.397	-789.075733	20.655	-789.112167	16.97
ChCl_E	-798.269840	0.001092	2.867	-789.072647	28.227	-789.108731	25.99
ChCl_F	-789.269444	0.001056	2.773	-789.072177	29.366	-789.108528	26.53
ChCl_G	-789.267715	0.001063	2.791	-789.070797	33.008	-789.108274	27.19
ChCl_H	-789.266152	0.001165	3.059	-789.069139	37.629	-789.105748	33.82

$E_0 = E_{elec} + ZPE$ = sum of electronic and zero-point energies
$G = H - TS$ = sum of electronic and thermal free energies
$E_{CP} = E_{elec} + BSSE$ = Counterpoise corrected energy

4. Phenol

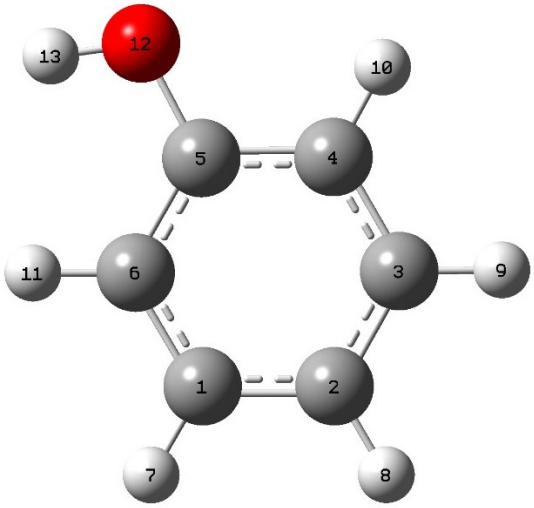

Figure S.A2. Most stable conformation of the molecule of phenol, with numbered atoms

The most stable conformation for the molecule of phenol is presented **Figure S.A2**. It displays the hydroxyl group in the plane of the benzene ring with an angle of 0° (or 180°) for the C-C-O-H dihedron. This result is consistent with the studies from Feller et al. [1] and Cesari et al. [2].

Table S.A5. Charge distribution of the molecule of phenol

	Charge distribution with the corresponding method (e)	
Atom	NBO	CHelpG
C^1	-0.18273	-0.009399
C^2	-0.23635	-0.169025
C^3	-0.18148	-0.034184
C^4	-0.25202	-0.245961
C^5	0.31420	0.462964
C^6	-0.28447	-0.314937
H^7	0.20428	0.083287
H^8	0.20566	0.095212
H^9	0.20450	0.081778
H^{10}	0.21727	0.147348
H^{11}	0.19959	0.120317
O^{12}	-0.67434	-0.638221
H^{13}	0.46589	0.420820
Total	**0.00000**	**0.00000**

Charges range from -0.67 to 0.47 e with the NBO method and from -0.64 to 0.46 e for the CHelpG method. The charge distributions indicate with both methods a high negative charge on the atom of oxygen and a positive charge on the atom of hydrogen from the hydroxyl group. It can also be noticed that the atom of carbon linked to the atom of oxygen is the only positively charged atom of carbon. This relates to the oxygen atom being a strong electronegative site.

A.5. DES 1: Choline chloride + 2 Phenol

Table S.A6. 3D structure of the eight most stable conformations of DES 1 along with their relative (BSSE and ZPE corrected) energies

Conformation	DES1_A	DES1_B
Optimized structure	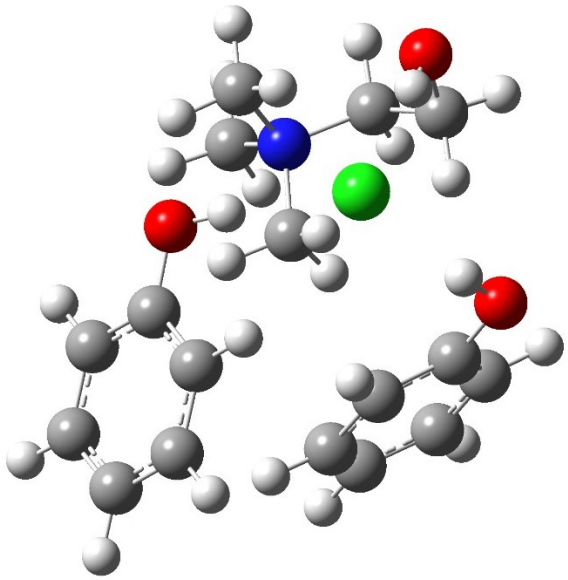	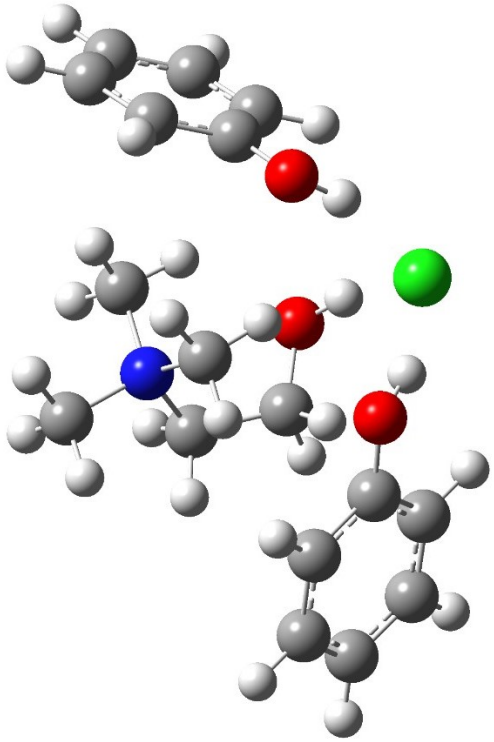
ΔE (kJ.mol^{-1})	0.000	3.628

Conformation	DES1_C	DES1_D
Optimized structure	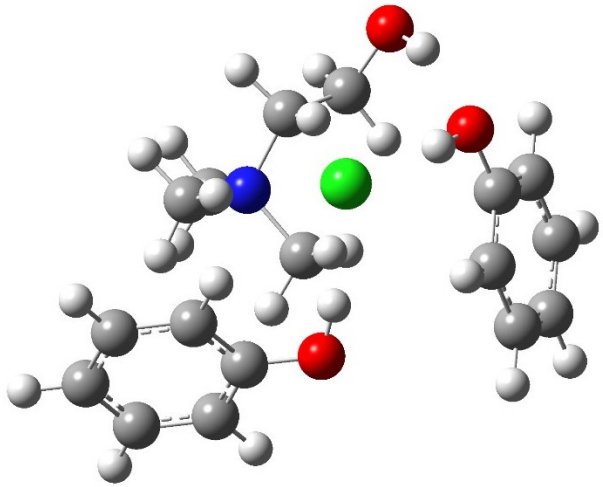	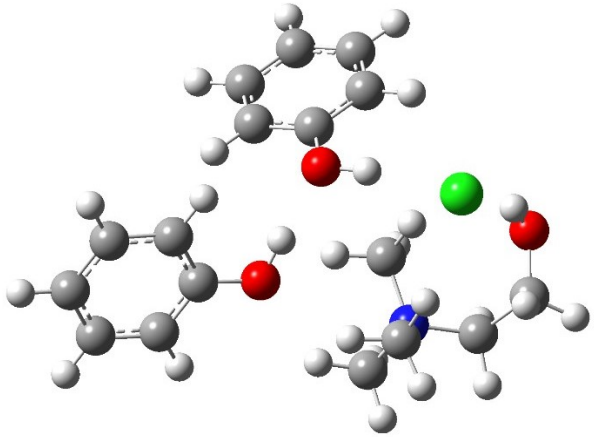
ΔE (kJ.mol^{-1})	4.684	8.793

Conformation	DES1_E	DES1_F
Optimized structure	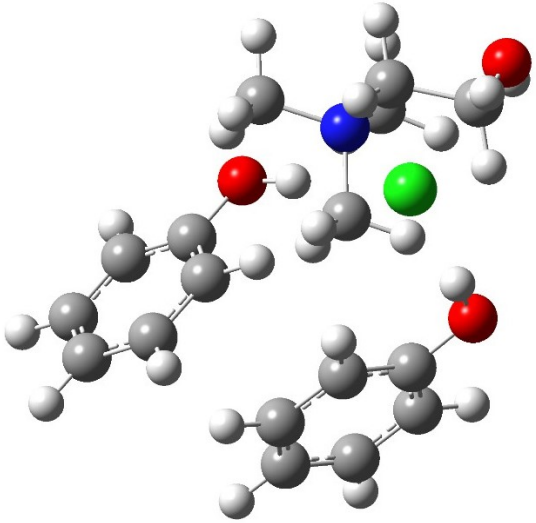	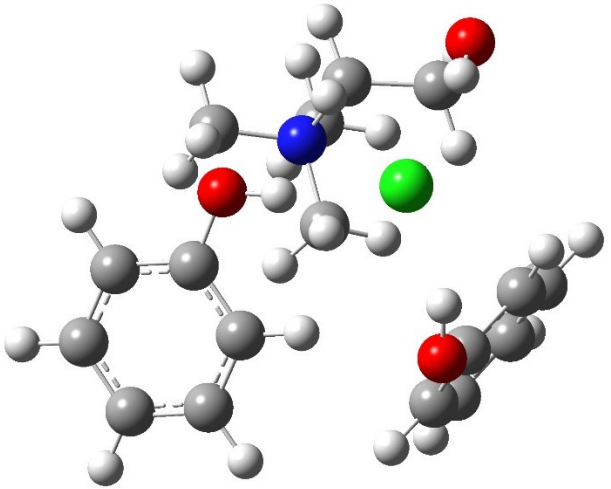
ΔE (kJ.mol^{-1})	9.068	10.686

Conformation	DES1_G	DES1_H
Optimized structure	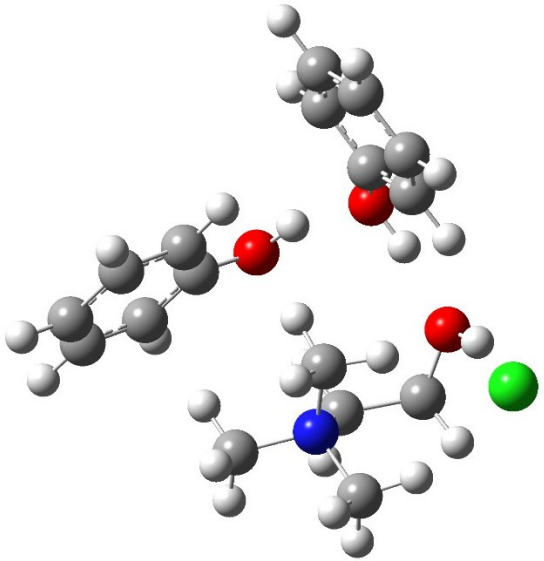	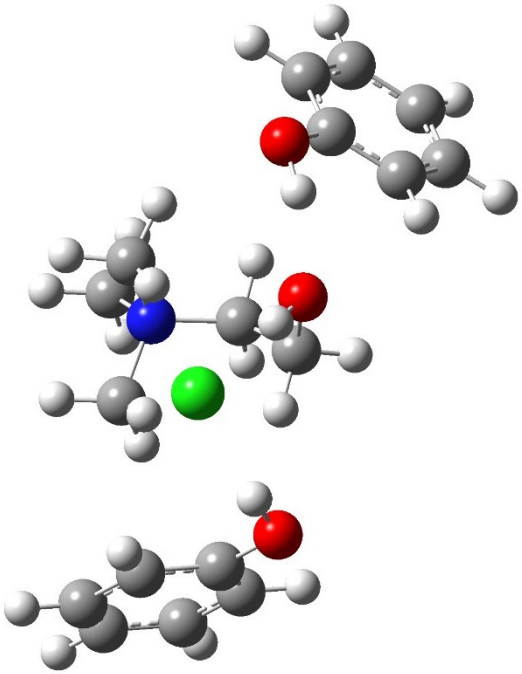
ΔE (kJ.mol^{-1})	13.892	14.414

Table S.A7. Electronic, ZPE corrected and thermal free energies and the relative corresponding energies for the different conformations of DES 1

Conformation	Counterpoise corrected energy (au)	BSSE energy (au)	BSSE energy (kJ.mol^{-1})	E_0 (au)	ΔE counterpoise and ZPE corrected (kJ.mol^{-1})	G (au)	ΔG (kJ.mol^{-1})
DES1_A	-1404.496540	0.005148	13.516	-1404.086847	0.000	-1404.143861	0.33
DES1_B	-1404.494870	0.004946	12.985	-1404.085263	3.628	-1404.143988	0.00
DES1_C	-1404.495412	0.005297	13.907	-1404.085212	4.684	-1404.142248	4.57
DES1_D	-1404.493102	0.005026	13.196	-1404.083376	8.793	-1404.14313	2.25
DES1_E	-1404.493137	0.004953	13.004	-1404.083198	9.068	-1404.140698	8.64
DES1_F	-1404.492417	0.005094	13.374	-1404.082723	10.686	-1404.14052	9.11
DES1_G	-1404.492410	0.006054	15.895	-1404.082462	13.892	-1404.138689	13.91
DES1_H	-1404.491315	0.005162	13.553	-1404.081371	14.414	-1404.137319	17.51

A.6. Cluster 1: DES 1 + Water

Table S.A8. 3D structure of the eight most stable conformations of the first cluster along with their relative (BSSE and ZPE corrected) energies

Conformation	Cluster1_A	Cluster1_B
Optimized structure	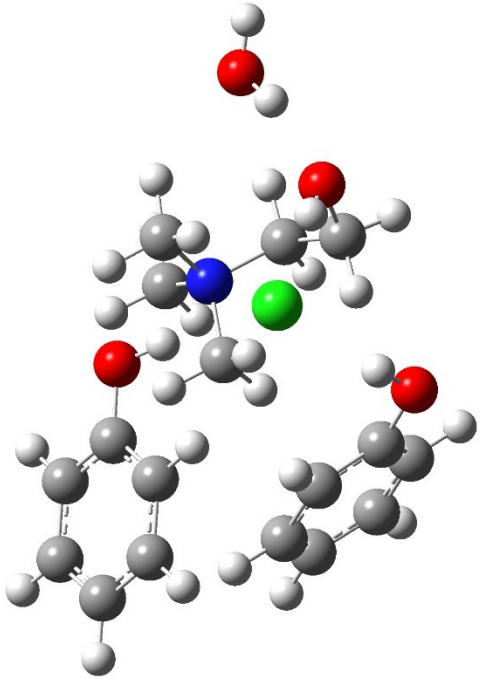	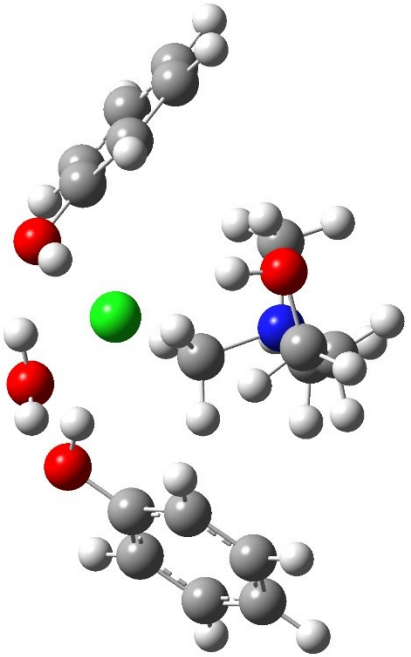
ΔE (kJ.mol^{-1})	0.000	1.003

Conformation	Cluster1_C	Cluster1_D
Optimized structure	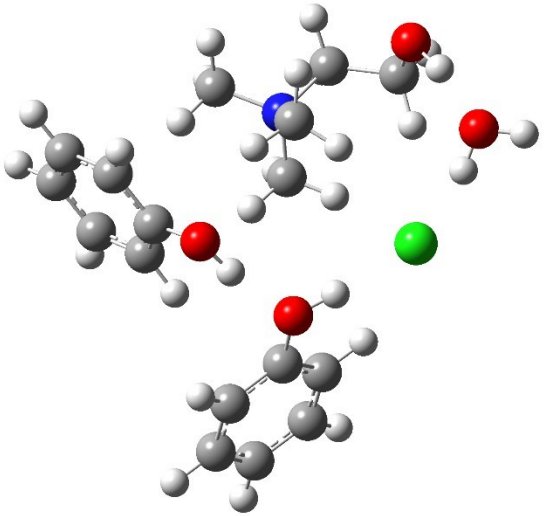	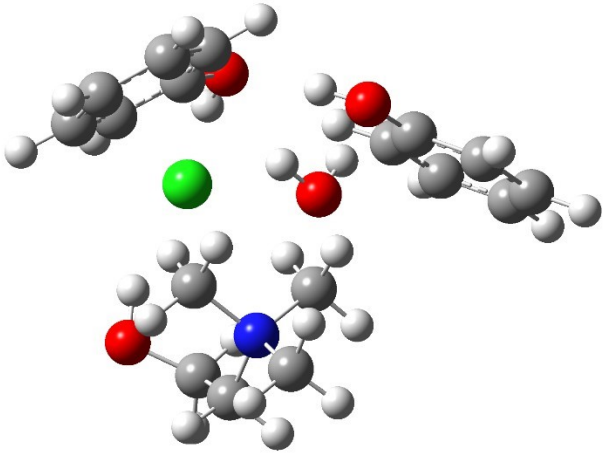
ΔE (kJ.mol^{-1})	1.927	2.100

Conformation	Cluster1_E	Cluster1_F
Optimized structure	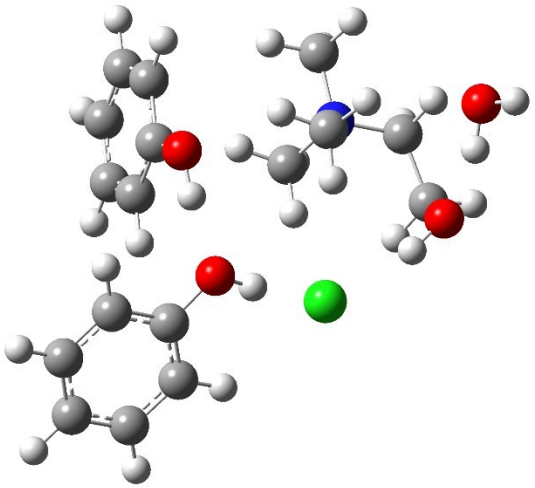	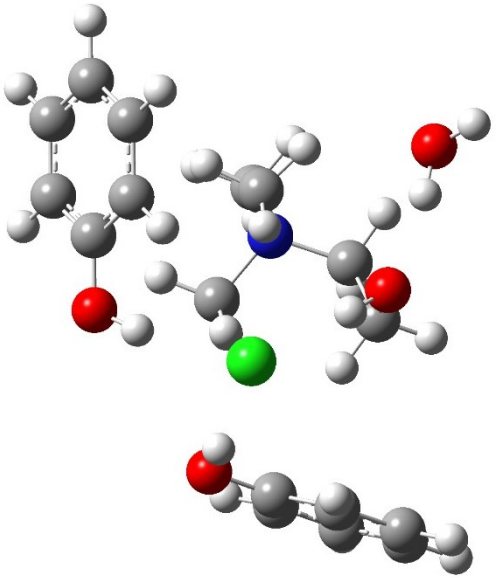
ΔE (kJ.mol^{-1})	3.426	5.850

Conformation	Cluster1_G	Cluster1_H
Optimized structure	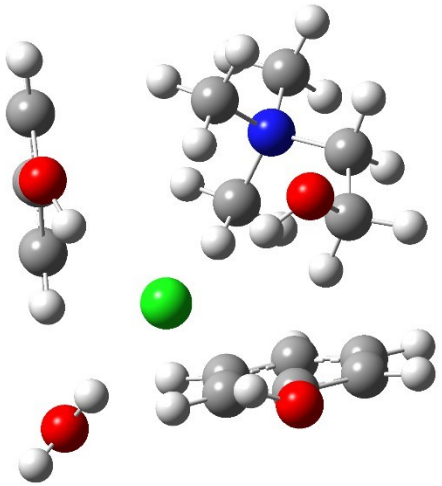	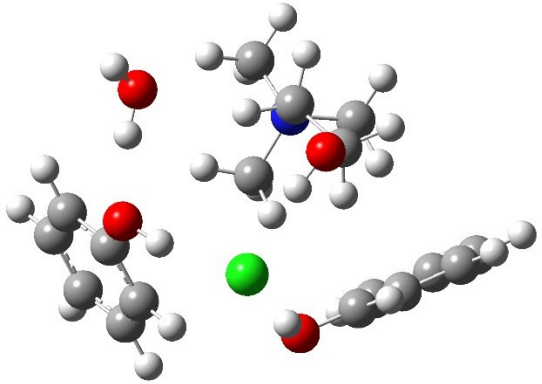
ΔE (kJ.mol^{-1})	8.966	13.170

Table S.A9. Electronic, ZPE corrected and thermal free energies and the relative corresponding energies for the different conformations of the cluster DES 1 + Water

Conformation	Counterpoise corrected energy (au)	BSSE energy (au)	BSSE energy (kJ.mol^{-1})	E_0 (au)	ΔE counterpoise and ZPE corrected (kJ.mol^{-1})	G (au)	ΔG (kJ.mol^{-1})
Cluster1_A	-1480.974326	0.006708	17.612	-1480.539352	0.000	-1480.599778	4.17
Cluster1_B	-1480.974274	0.006968	18.294	-1480.539230	1.003	-1480.599519	4.85
Cluster1_C	-1480.973172	0.006996	18.368	-1480.538906	1.927	-1480.598767	6.83
Cluster1_D	-1480.974208	0.007530	19.770	-1480.539374	2.100	-1480.600188	3.10
Cluster1_E	-1480.972922	0.006888	18.084	-1480.538227	3.426	-1480.597640	9.79
Cluster1_F	-1480.971205	0.006532	17.150	-1480.536948	5.850	-1480.601368	0.00
Cluster1_G	-1480.96981	0.006717	17.635	-1480.535946	8.966	-1480.596830	11.91
Cluster1_H	-1480.968818	0.007172	18.830	-1480.534800	13.170	-1480.596941	11.62

A.7. Glycolic acid

Two conformations for the molecule of glycolic acid have been obtained and are presented in **Table S.A10**. Both conformations are in a plane. The most stable conformation favours a hydrogen bond between the double bonded atom of oxygen and the atom of hydrogen from the alcohol function, whereas the second conformation displays a hydrogen bond between the two hydroxyl groups. In both cases, the alcohol function plays the role of the HBD.

Table S.A10. 3D structure of the two glycolic acid conformations and their relative energies (ZPE corrected)

Conformation	Gly_A	Gly_B
Optimized structure	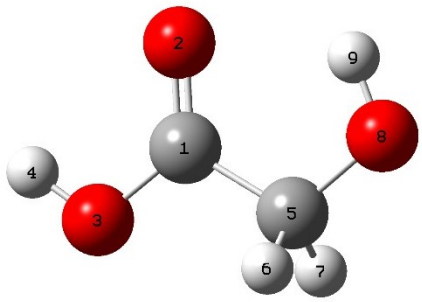	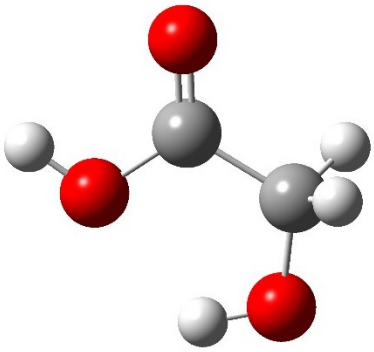
ΔE (kJ.mol^{-1})	0.000	9.662

The charge distributions of the first conformation of glycolic acid are presented in **Table S.A11**. They are compared to the one obtained by van den Bruinhorst et al. [3] who used a Hartree-Fock method with the 6-31G* basis set and the Mertz−Singh−Kollman (MSK) scheme.

Table S.A11. Charge distribution of the most stable conformation Gly_A of glycolic acid

	Charge distribution with the corresponding method (e)		
Atom	NBO	CHelpG	MSK from [3]
C^1	0.77873	0.666208	0.6815
O^2	-0.61101	-0.553324	-0.5282
O^3	-0.67797	-0.668810	-0.5845
H^4	0.48758	0.471603	0.3969
C^5	-0.12288	0.294832	0.2421
H^6	0.19663	0.029477	0.0196
H^7	0.19667	0.029530	0.0200
O^8	-0.72526	-0.661318	-0.6434
H^9	0.47750	0.391802	0.3960
Total	**0.00000**	**0.000000**	**0.0000**

All methods predict comparable charge distributions in terms of sign and order of magnitude of the charges, apart from the carbon C^5 which has a negative charge with the NBO method and a positive one with the CHelpG and MSK schemes. Both schemes share close results. Aside from this, there is a disagreement between the methods on the most charged atom of oxygen. The NBO and MSK calculations predict a low charge of -0.73 e and -0.64 e on the oxygen O^8 from the hydroxyl group while with the CHelpG scheme, it is found that the oxygen O^3 linked to the hydrogen in the carboxyl group is the most negatively charged (-0.67 e). This makes it unclear which site would be the most preferred hydrogen bond acceptor, although both O^3 and O^8 seem preferable and are more negatively charged compared to O^2. In contrast, the most positively charged atom of hydrogen for both methods is the atom H^4 from the carboxyl group.

A.8. DES 2: Choline chloride + Glycolic acid

Table S.A12. 3D structure of the eight most stable conformations of DES 2 along with their relative (BSSE and ZPE corrected) energies

Conformation	DES2_A	DES2_B
Optimized structure	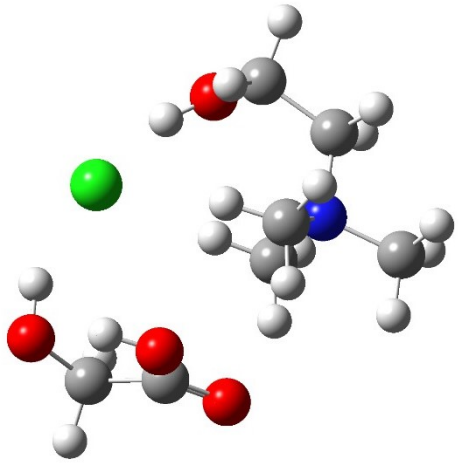	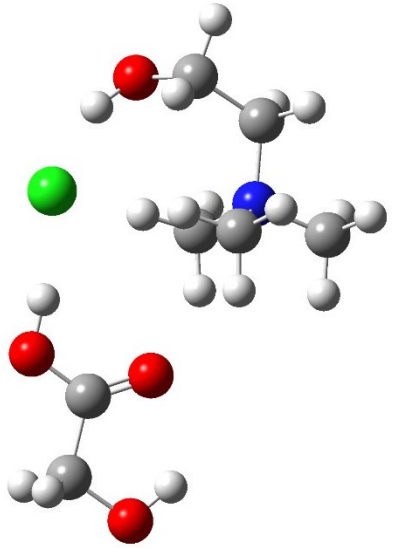
ΔE (kJ.mol^{-1})	0.000	0.585

Conformation	DES2_C	DES2_D
Optimized structure	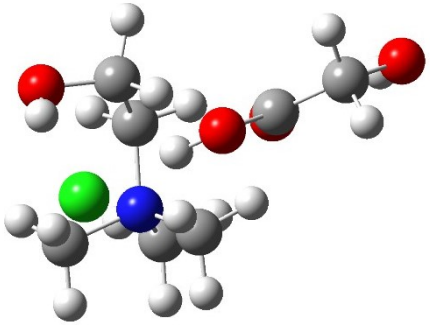	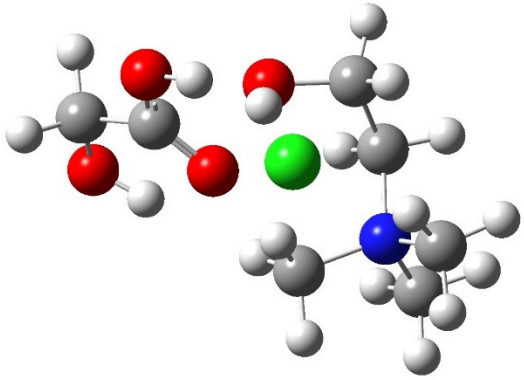
ΔE (kJ.mol^{-1})	3.736	9.578

Conformation	DES2_E	DES2_F
Optimized structure	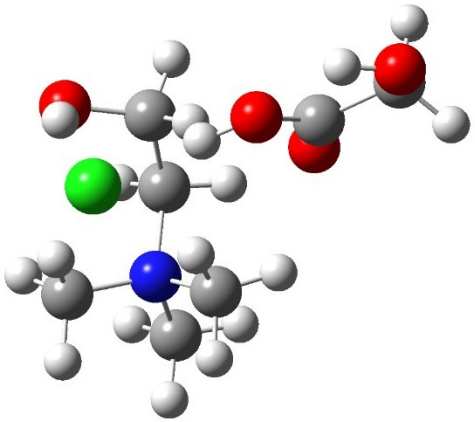	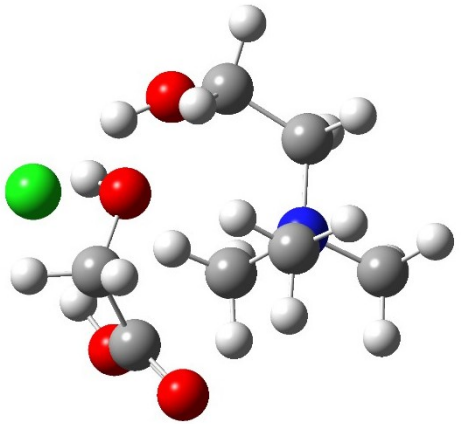
ΔE (kJ.mol^{-1})	9.714	15.036

Conformation	DES2_G	DES2_H
Optimized structure	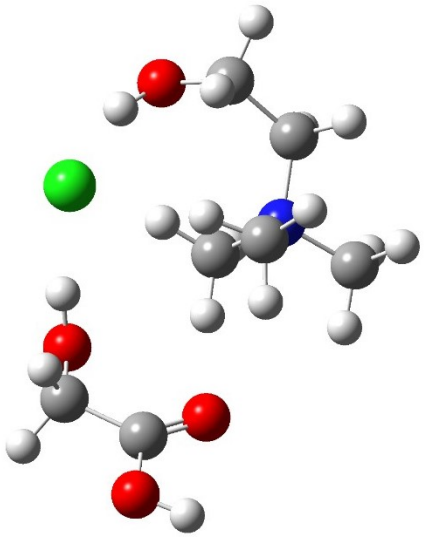	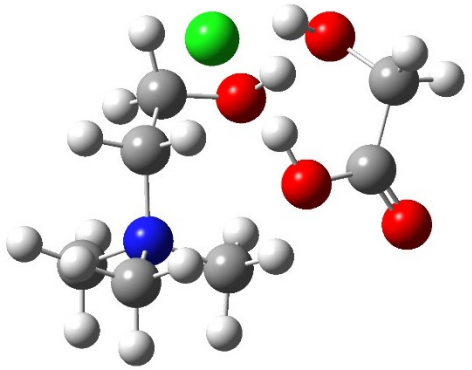
ΔE (kJ.mol^{-1})	15.217	16.764

Table S.A13. Electronic, ZPE corrected and thermal free energies and the relative corresponding energies for the different conformations of DES 2

Conformation	Counterpoise corrected energy (au)	BSSE energy (au)	BSSE energy (kJ.mol^{-1})	E_0 (au)	ΔE counterpoise and ZPE corrected (kJ.mol^{-1})	G (au)	ΔG (kJ.mol^{-1})
DES2_A	-1093.726402	0.002827	7.422	-1093.458863	0.000	-1093.504054	2.87
DES2_B	-1093.724004	0.002577	6.766	-1093.458390	0.585	-1093.505149	0.00
DES2_C	-1093.722638	0.002641	6.934	-1093.457254	3.736	-1093.504401	1.96
DES2_D	-1093.721590	0.003234	8.491	-1093.455622	9.578	-1093.501589	9.35
DES2_E	-1093.720196	0.002516	6.606	-1093.454852	9.714	-1093.502049	8.14
DES2_F	-1093.720551	0.003374	8.858	-1093.453683	15.036	-1093.499492	14.85
DES2_G	-1093.719493	0.002817	7.396	-1093.453057	15.217	-1093.499654	14.43
DES2_H	-1093.720438	0.004016	10.544	-1093.453667	16.764	-1093.499846	13.92

A.9. Cluster 2: DES 2 + Water

Table S.A14. 3D structure of the eight most stable conformations of the second cluster along with their relative (BSSE and ZPE corrected) energies

Conformation	Cluster2_A	Cluster2_B
Optimized structure	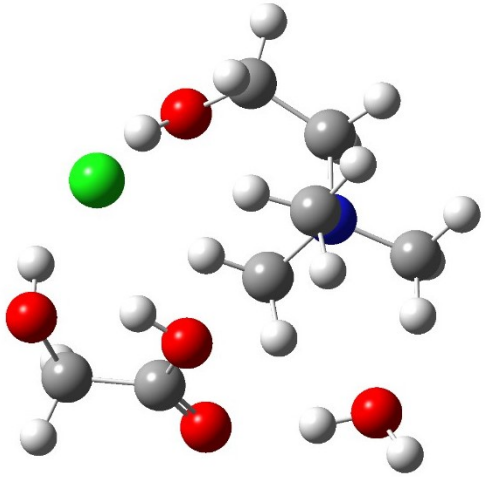	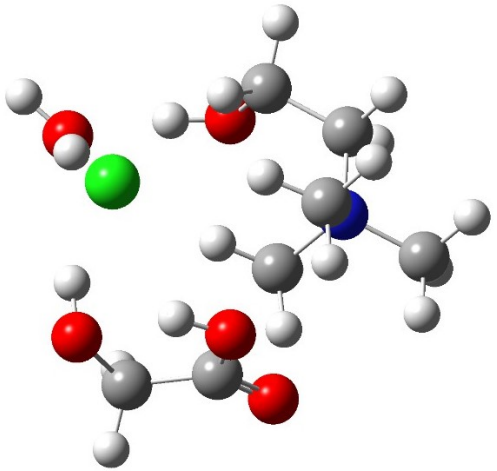
ΔE (kJ.mol^{-1})	0.000	1.738

Conformation	Cluster2_C	Cluster2_D
Optimized structure	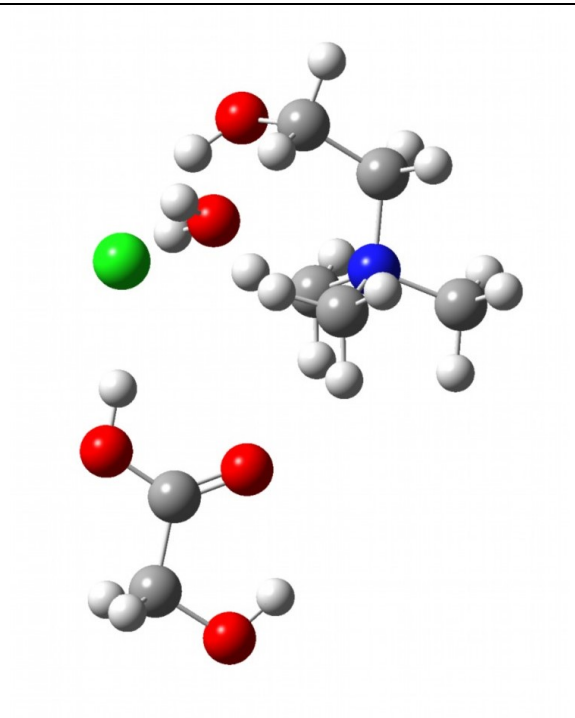	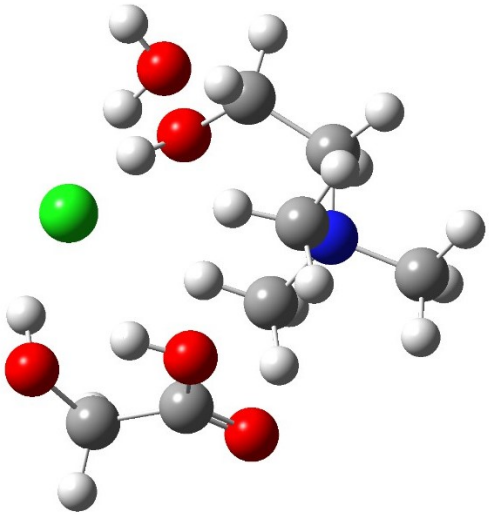
ΔE (kJ.mol^{-1})	4.421	4.511

Conformation	Cluster2_E	Cluster2_F
Optimized structure	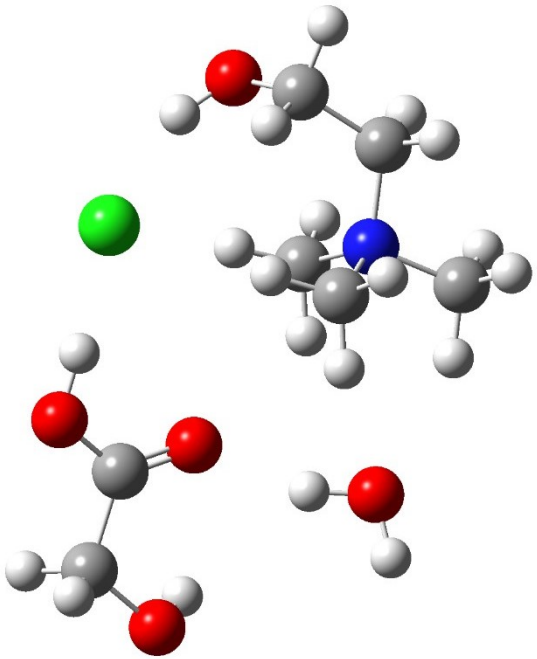	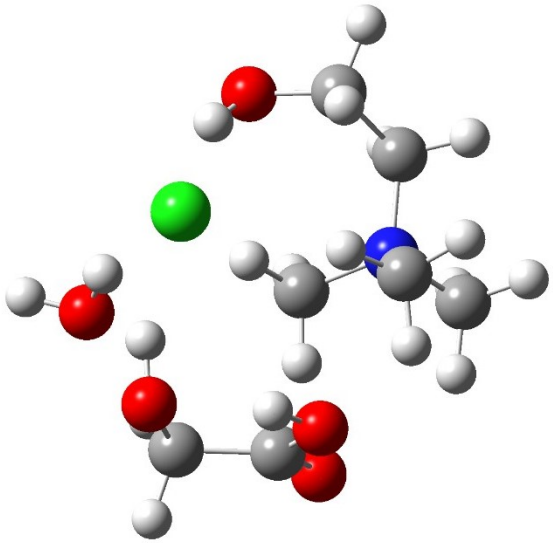
ΔE (kJ.mol^{-1})	5.949	8.785

Conformation	Cluster2_G	Cluster2_H
Optimized structure	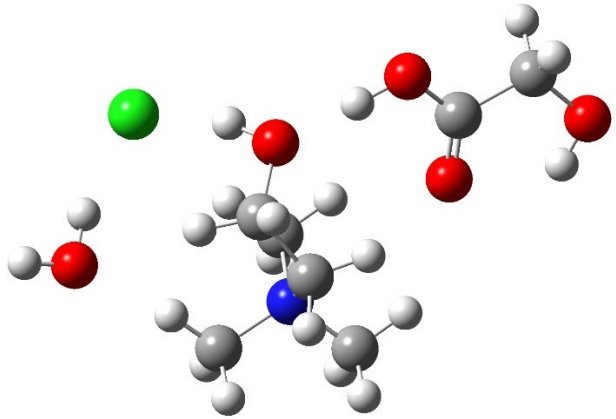	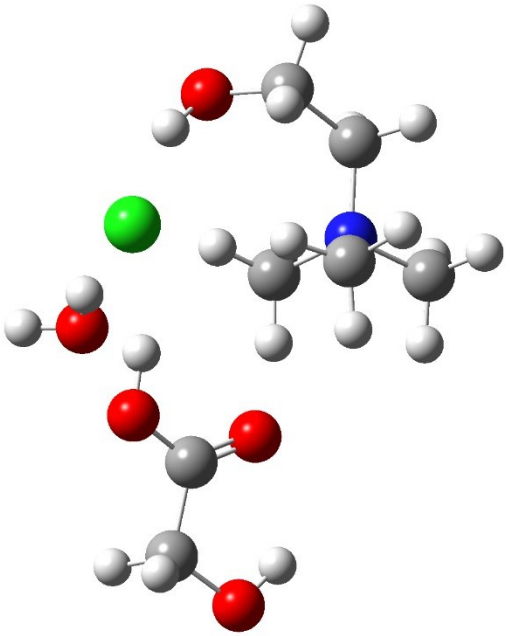
ΔE (kJ.mol^{-1})	9.342	12.818

Table S.A15. Electronic, ZPE corrected and thermal free energies and the relative corresponding energies for the different conformations of the cluster DES 2+Water

Conformation	Counterpoise corrected energy (au)	BSSE energy (au)	BSSE energy (kJ.mol^{-1})	E_0 (au)	ΔE counterpoise and ZPE corrected (kJ.mol^{-1})	G (au)	ΔG (kJ.mol^{-1})
Cluster2_A	-1170.205152	0.004465	11.723	-1169.913165	0.000	-1169.963291	0.00
Cluster2_B	-1170.204605	0.004583	12.033	-1169.912621	1.738	-1169.962988	0.80
Cluster2_C	-1170.200480	0.003684	9.672	-1169.910700	4.421	-1169.963055	0.62
Cluster2_D	-1170.202852	0.004118	10.812	-1169.911100	4.511	-1169.961319	5.18
Cluster2_E	-1170.200715	0.004046	10.623	-1169.910480	5.949	-1169.961873	3.72
Cluster2_F	-1170.201425	0.004316	11.332	-1169.909670	8.785	-1169.959122	10.95
Cluster2_G	-1170.199972	0.004380	11.500	-1169.909522	9.342	-1169.960235	8.02
Cluster2_H	-1170.197356	0.003811	10.006	-1169.907629	12.818	-1169.959536	9.86

A.10. Binding energies

A.10.1 Isolated molecules

Table S.A16. Energies (ZPE corrected) and free energies of the optimized geometries of the isolated molecules investigated in this work

Molecule	Optimized structure	E_0 (au)	G (au)
Choline ion (gauche conformation)	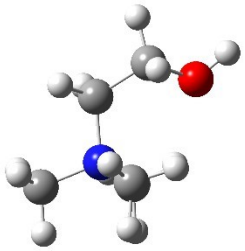	-328.623314	-328.655584
Chloride ion		-460.303727	-460.318750
Phenol	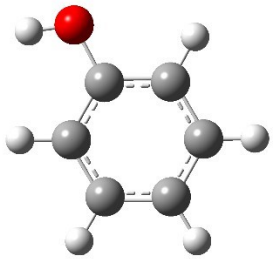	-307.475655	-307.504702
Glycolic acid	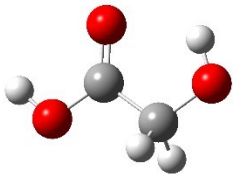	-304.343763	-304.372611

Water		-76.437816	-76.456113

A.10.2 Values for the binding energies

Table S.A17. Binding energies of the different systems from this work

System	Binding energy ΔE_b (kJ.mol^{-1})
Choline chloride	-407.65
Choline chloride + 2 Phenol (DES 1)	-126.24
Choline chloride + Glycolic acid (DES 2)	-78.68
Choline chloride + 2 Phenol + Water (Cluster 1)	-34.47
Choline chloride + Glycolic acid + Water (Cluster 2)	-20.55

References

[1] D. Feller, M.W. Feyereisen, Ab initio study of hydrogen bonding in the phenol-water system, J. Comput. Chem. 14 (1993) 1027–1035. https://doi.org/10.1002/jcc.540140904.

[2] L. Cesari, L. Canabady-Rochelle, F. Mutelet, Computational study on the molecular conformations of phenolic compounds, Struct. Chem. 29 (2017) 179–194. https://doi.org/10.1007/s11224-017-1017-9.

[3] A. van den Bruinhorst, T. Spyriouni, J.-R. Hill, M.C. Kroon, Experimental and Molecular Modeling Evaluation of the Physicochemical Properties of Proline-Based Deep Eutectic Solvents, J. Phys. Chem. B. 122 (2018) 369–379. https://doi.org/10.1021/acs.jpcb.7b09540.

Annexe B : Modified version of the COSMO-SAC model for the prediction of vapour-liquid equilibria of mixtures containing halogen compounds

B.1. Generation of COSMO files with Gaussian 9: key words input

BVP86/TZVP/DGA1 opt=(MAXCYC=99) scf=(tight,novaracc) SCRF=COSMO NoSymm geom=connectivity

--Link1--

BVP86/TZVP/DGA1 scf=(tight,novaracc) SCRF=COSMORS guess=read geom=checkpoint NoSymm

B.2. Databases

Table S.B18. Average deviations for the entirety of the VLE database

System	Range of temperature (K)	Number of data points	Average Deviation COSMO-SAC 2010 (%)	Average Deviation COSMO-SAC OH-Cl (%)	Average Deviation COSMO-SAC OH-Br (%)	Average Deviation COSMO-SAC OH-ClBr (%)	Reference
{Ethylene glycol:[Choline][Chloride]} [2:1] + Water	303.15 – 343.15	20	19.07	5.07	2.86	5.00	[1]
{Glycerol:[Choline][Chloride]} [2:1] + Water	298.15 – 338.15	86	30.87	5.44	13.41	5.35	[2]
{Phenol:[Choline][Chloride]} [2:1] + Water	298.15 – 333.15	80	20.93	4.74	15.79	4.82	[2]
{Glycolic acid:[Choline][Chloride]} [3:1] + Water	373.1 - 388	15	4.29	9.27	8.96	9.22	[3]
{Glycolic acid:[Choline][Chloride]} [3:1] + Acetonitrile	354.7 – 376.5	14	8.24	6.89	6.83	6.81	[3]
{Glycolic acid:[Tetramethyl ammonium][Chloride]} [3:1] + Water	373.1 – 398.8	15	14.09	4.6	5.12	4.66	[4]
{Glycolic acid :[Tetramethyl ammonium]	354.7 – 381.4	14	4.59	11.19	10.98	11.1	[4]

[Chloride]} [3:1] + Acetonitrile							
{D-(+)-Glucose:[Choline] [Chloride]} [1:2] + Water	367.56 – 372.64	10	3.22	1.32	1.28	1.31	[5]
[EMIM] [Chloride] + Water	355.58 – 435.03	92	131.98	4.96	7.77	4.59	[6]
[BMIM] [Chloride] + Water	354.92 – 429.69	79	125.56	4.5	7.22	4.31	[6]
[HMIM] [Chloride] + Water	354.64 – 405.3	101	47.34	3.36	1.3	3.05	[6]
[Choline] [Chloride] + Water	355.11 – 411.12	50	46.56	11.57	8.07	11.14	[6]
[EMIM] [Chloride] + Ethanol	334.8 – 392.85	82	91.69	30.88	31.69	31.46	[6]
[BMIM] [Chloride] + Ethanol	334.77 – 405.89	90	122.38	43.42	47.24	44.24	[6]
[HMIM] [Chloride] + Ethanol	335.15 – 411.86	75	133.30	46.36	51.46	47.28	[6]
[Choline] [Chloride] + Ethanol	334.81 – 353.06	53	1.48	0.54	0.58	0.54	[6]
[BMIM] [Bromide] + 1-Butanol	353.15 – 373.15	15	3.33	7.97	8.17	7.86	[7]
[BMIM] [Chloride] + Ethanol	351.44 – 412.61	13	105.46	31.32	37.86	32.15	[8]
[BMIM] [Chloride] + Water	373.15 – 441.11	30	54.89	1.98	3.92	1.69	[8]
[BMIM] [Chloride] + Methanol	320.8 – 361.74	69	32.57	16.52	18.69	21.19	[9]
[BMIM] [Chloride] + 1-Propanol	352.75 - 410.89	66	67.53	6.85	11.02	7.46	[9]
[BMIM] [Chloride] + 2-Propanol	338.67 – 388.75	100	53.31	18.68	19.23	19.02	[9]
[BMIM] [Chloride] + 1-Butanol	372.25 – 431	58	52.34	4.33	9.49	4.68	[9]
[BMIM] [Chloride] + 2-Butanol	354.75 – 398.75	87	38.36	5.28	7.11	5.39	[9]
[BMIM] [Chloride] + 2-Methylpropan-2-ol	338.58 – 384.21	64	50.59	22.06	22.07	22.35	[9]
[BMIM] [Chloride] + 2-Methylpropan-1-ol	362.85 - 420.94	60	79.16	15.32	21.85	16.07	[9]
[BMIM] [Chloride] + 1-Pentanol	389.91 – 444.55	64	50.21	6.58	7.48	6.12	[9]
{Malonic acid:[Choline] [Chloride]} [2:1] + Water	303.15 – 343.15	20	17.15	6.59	3.39	6.50	[1]
1-Chlorobutane + 1-Octanol	278.15 – 323.15	100	8.88	9.13	9.37	9.14	[10]
1-Chlorobutane + 1-Decanol	283.15 – 323.15	99	8.79	9.1	9.36	9.11	[10]
1-Chlorobutane + 1-Propanol	318.15 – 338.15	30	4.93	5.25	5.04	5.26	[11]
Heptane + 1-Propanol + 1-	318.15	45	4.07	4.27	4.37	4.28	[11]

Chlorobutane							
{Malic acid:[Choline] [Chloride]} [1:1] + Water	303.2 – 343.2	25	7.37	6.23	10.63	6.29	[12]
{Malonic acid:[Choline] [Chloride]} [1:1] + Water	303.2 – 343.2	25	3.71	5.00	7.63	5.04	[12]
{Malic acid:[Choline] [Chloride]} [1:1] + Water	373.1 – 385.6	15	4.37	7.38	6.91	7.30	[13]
{Malic acid:[Choline] [Chloride]} [1:1] + Acetonitrile	354.7 – 374.3	14	1.36	10.32	10.32	10.26	[13]
{Lactic acid:[Choline] [Chloride]} [2:1] + Propan-2-ol	307.2 – 354.5	23	8.03	8.02	8.08	8.02	[14]
{Glycolic acid:[Choline] [Chloride]} [3:1] + Propan-2-ol	306.8 – 355.3	23	8.77	8.61	8.60	8.61	[14]
1,2-Dichloroethane + 1-Hexanol	355.15 – 428.45	17	16.43	14.65	14.75	14.67	[15]
1,1,2,2,2-Tetrachloroethane + 1-Hexanol	417.25 – 428.45	16	2.88	2.71	2.73	2.71	[15]
Trichloroethene + 1-Hexanol	358.45 – 428.45	16	15.44	15.20	15.21	15.20	[15]
Tetrachloroethene + 1-Hexanol	392.15 – 428.45	16	11.24	11.14	11.15	11.14	[15]
1-Butanol + Chlorobenzene	389.1 – 402.5	8	7.82	7.59	7.61	7.59	[16]
2-Methylpropan-1-ol + Chlorobenzene	379.4 – 402.5	8	11.29	10.98	11.00	10.98	[16]
2-Methylpropan-2-ol + Chlorobenzene	355.1 – 402.5	11	4.52	4.55	4.55	4.55	[16]
1,2-Dichloroethane + 3-Methylphenol	354.95 – 472.95	11	18.86	11.60	12.53	11.70	[17]
1,1,1-Trichloroethane + 3-Methylphenol	345.35 – 472.95	7	51.16	48.41	48.58	48.44	[17]
1,1,2,2-Tetrachloroethane + 3-Methylphenol	413.55 – 472.95	11	7.16	9.50	9.05	9.46	[17]
Tetrachloroethene + 3-Methylphenol	391.89 – 472.95	11	2.54	2.09	2.15	2.10	[17]
1-Bromopropane + Acetic acid	344.75 – 383.05	29	79.88	75.56	75.50	75.60	[18]
1-Bromopropane + Propanoic acid	345.7 – 411.32	40	15.36	10.97	11.05	11.01	[18]
1-Bromopropane + Acetic acid + Propanoic acid	346.75 – 406.55	79	58.86	53.53	53.78	53.59	[18]
[C1C2PIP] [Bromide] + Water	338.15 – 368.15	89	7.25	1.23	1.35	1.20	[19]

[1-Ethylpyridinium] [Bromide] + Water	338.15 – 368.15	76	28.62	3.49	3.10	3.54	[19]
[C2OHPY] [Bromide] + Water	338.15 – 368.16	46	16.29	2.37	2.69	2.31	[19]
[C1C2MOR] [Bromide] + Water	338.15 – 368.17	87	23.65	3.16	2.38	3.16	[19]
[C1C2OHMOR] [Bromide] + Water	338.15 – 368.18	70	10.97	1.76	2.23	1.71	[19]
[Choline] [Bromide] + Water	338.15 – 368.19	49	25.95	2.85	3.15	2.78	[19]
[MMIM] [Chloride] + Water	287.15 – 437.45	79	196.43	42.41	34.28	42.47	[20]
[C2OHMIM] [Chloride] + Water	300.73 – 406.45	49	47.97	10.31	6.84	10.27	[21]
[BMIM] [Bromide] + Water	304.8 – 457.4	64	567.50	25.91	14.96	25.23	[22]
[C1C3PYR] [Bromide] + Water	338.15 – 368.15	64	10.01	1.37	1.58	1.34	[23]
[BMPYR] [Bromide] + Water	338.15 – 368.15	61	17.40	1.95	1.82	1.93	[23]
[C1C5PYR] [Bromide] + Water	338.15 – 368.15	54	17.68	1.78	1.78	1.76	[23]
[C1C3MOR] [Bromide] + Water	338.15 – 368.15	70	6.63	1.40	1.64	1.37	[24]
[C1C4MOR] [Bromide] + Water	338.15 – 368.15	56	6.54	1.15	1.37	1.13	[24]
[C1C5MOR] [Bromide] + Water	338.15 – 368.15	86	7.91	1.49	1.60	1.46	[24]
[C1C5PIP] [Bromide] + Water	338.15 – 368.15	62	10.83	1.96	2.34	1.91	[24]
Methanol + 1-Bromopropane	339.45 – 354.85	14	64.04	62.51	62.36	62.52	[25]
2-Propanol + 1-Bromopropane	327.62 – 339.78	26	43.65	43.95	44.03	43.95	[25]
Methanol + 2-Propanol + 1-Bromopropane	328.35 – 350.35	80	6.48	6.93	7.02	6.93	[25]
2-Methylpropan-2-ol + 1-Bromopropane	341.58 – 353.65	23	3.26	3.48	3.51	3.48	[26]
Methanol + 1-Bromopropane + Methyl methacrylate	328.85 – 368.5	72	6.75	7.04	7.11	7.04	[27]
Methanol + Acetonitrile + 1-Bromopropane	327.7 – 347.85	84	6.14	6.30	6.34	6.30	[28]
[BMIM] [Bromide] + Water	355.24 – 399.88	65	24.16	1.86	2.03	1.80	[29]
1-Bromopropane + 2-Methylpropan-1-ol	345.18 – 377.84	12	2.26	1.28	1.29	1.27	[30]

Table S.B19. Description of the dataset used to assess the performances of COSMO-SAC (+OH-Cl) and COSMO-SAC (+OH-ClBr) and not used in the optimization (dataset B)

System	Temperature range (K)	Number of data points	Reference
{Ethylene glycol:[Choline] [Chloride]} [2:1] + Water	303.15 – 343.15	20	[1]
{Glycolic acid:[Choline] [Chloride]} [3:1] + Water	373.1 - 388	15	[3]
{Glycolic acid:[Choline] [Chloride]} [3:1] + Acetonitrile	354.7 – 376.5	14	[3]
{Glycolic acid:[Tetramethyl ammonium] [Chloride]} [3:1] + Water	373.1 – 398.8	15	[4]
{Glycolic acid:[Tetramethyl ammonium] [Chloride]} [3:1] + Acetonitrile	354.7 – 381.4	14	[4]
{D-(+)-Glucose:[Choline] [Chloride]} [1:2] + Water	367.56 – 372.64	10	[5]
[BMIM] [Chloride] + Water	354.92 – 429.69	79	[6]
[HMIM] [Chloride] + Water	354.64 – 405.3	101	[6]
[Choline] [Chloride] + Water	355.11 – 411.12	50	[6]
[EMIM] [Chloride] + Ethanol	334.8 – 392.85	82	[6]
[BMIM] [Chloride] + Ethanol	334.77 – 405.89	90	[6]
[HMIM] [Chloride] + Ethanol	335.15 – 411.86	75	[6]
[Choline] [Chloride] + Ethanol	334.81 – 353.06	53	[6]
[BMIM] [Chloride] + Ethanol	351.44 – 412.61	13	[8]
[BMIM] [Chloride] + Water	373.15 – 441.11	30	[8]
[BMIM] Chloride] + 2-Methylpropan-2-ol	338.58 – 384.21	64	[9]
[BMIM] [Chloride] + 2-Methylpropan-1-ol	362.85 - 420.94	60	[9]
{Malonic acid:[Choline] [Chloride]} [2:1] + Water	303.15 – 343.15	20	[1]
1-Chlorobutane + 1-Octanol	278.15 – 323.15	100	[10]
1-Chlorobutane + 1-Decanol	283.15 – 323.15	99	[10]
1-Chlorobutane + 1-Propanol	318.15 – 338.15	30	[11]
Heptane + 1-Propanol + 1-Chlorobutane	318.15	45	[11]
{Malic acid:[Choline] [Chloride]} [1:1] + Water	303.2 – 343.2	25	[12]
{Malonic acid:[Choline] [Chloride]} [1:1] + Water	303.2 – 343.2	25	[12]
{Malic acid:[Choline] [Chloride]} [1:1] + Water	373.1 – 385.6	15	[13]
{Malic acid:[Choline] [Chloride]} [1:1] + Acetonitrile	354.7 – 374.3	14	[13]
{Lactic acid:[Choline] [Chloride]} [2:1] + Propan-2-ol	307.2 – 354.5	23	[14]
{Glycolic acid:[Choline] [Chloride]} [3:1] + Propan-2-ol	306.8 – 355.3	23	[14]
1,2-Dichloroethane	355.15 – 428.45	17	[15]

+ 1-Hexanol			
1,1,2,2,2-Tetrachloroethane + 1-Hexanol	417.25 – 428.45	16	[15]
Trichloroethene + 1-Hexanol	358.45 – 428.45	16	[15]
Tetrachloroethene + 1-Hexanol	392.15 – 428.45	16	[15]
1-Butanol + Chlorobenzene	389.1 – 402.5	8	[16]
2-Methylpropan-1-ol + Chlorobenzene	379.4 – 402.5	8	[16]
2-Methylpropan-2-ol + Chlorobenzene	355.1 – 402.5	11	[16]
1,2-Dichloroethane + 3-Methylphenol	354.95 – 472.95	11	[17]
1,1,1-Trichloroethane + 3-Methylphenol	345.35 – 472.95	7	[17]
1,1,2,2-Tetrachloroethane + 3-Methylphenol	413.55 – 472.95	11	[17]
Tetrachloroethene + 3-Methylphenol	391.89 – 472.95	11	[17]
[MMIM] [Chloride] + Water	287.15 – 437.45	79	[20]
[C2OHMIM] [Chloride] + Water	300.73 – 406.45	49	[21]

Table S.B20. Description of the dataset used to assess the performances of COSMO-SAC (+OH-Br) and COSMO-SAC (+OH-ClBr) and not used in the optimization (dataset D)

System	Temperature range (K)	Number of data points	Reference
[BMIM] [Bromide] + 1-Butanol	353.15 – 373.15	15	[7]
1-Bromopropane + Acetic acid + Propanoic acid	346.75 – 406.55	79	[18]
[C1C3PYR] [Bromide] + Water	338.15 – 368.15	64	[23]
[BMPYR] [Bromide] + Water	338.15 – 368.15	61	[23]
[C1C5PYR] [Bromide] + Water	338.15 – 368.15	54	[23]
[C1C3MOR] [Bromide] + Water	338.15 – 368.15	70	[24]
[C1C4MOR] [Bromide] + Water	338.15 – 368.15	56	[24]
[C1C5MOR] [Bromide] + Water	338.15 – 358.15	64	[24]
[C1C5PIP] [Bromide] + Water	338.15 – 368.15	62	[24]
Methanol + 2-Propanol + 1-Bromopropane	328.35 – 350.35	80	[25]
Methanol + 1-Bromopropane + Methyl methacrylate	328.85 – 368.5	72	[27]
Methanol + Acetonitrile + 1-Bromopropane	327.7 – 347.85	84	[28]
1-Bromopropane + 2-Methylpropan-1-ol	345.18 – 377.84	12	[30]

Table S.B21. RMSD for the entire LLE database

System	Temperature (K)	Number of data points*	RMSD COSMO-SAC 2010	RMSD COSMO-SAC OH-ClBr	Reference
{Glucose:[Choline] [Chloride]} [1:1] + Hexane + Benzene	298.15	10	0.04	0.04	[31]
{Glucose: [Choline] [Chloride]} [1:1] + Hexane + Toluene	298.15	13	0.03	0.03	[31]
{Glycerol: [Choline] [Chloride]} [2:1] + Heptane + Ethanol	298.15	11	0.02	0.02	[32]
{Levulinic acid: [Choline] [Chloride]} [2:1] + Heptane + Ethanol	298.15	11	0.05	0.05	[32]
{Ethylene glycol: [Choline] [Chloride]} [2:1] + Heptane + Ethanol	298.15	11	0.04	0.04	[32]
{Levulinic acid: [Tetrabutylammonium] [Bromide]} [2:1] + Ethanol + Hexane	298.15	6	0.09	0.09	[33]
{Levulinic acid: [Tetrabutylammonium] [Bromide]} [2:1] + Ethanol + Heptane	298.15	6	0.07	0.07	[33]
{Levulinic acid: [Tetrabutylammonium] [Bromide]} [2:1] + Ethanol + Octane	298.15	6	0.06	0.06	[33]
{Levulinic acid: [Choline] [Chloride]} [2:1] + Hexane + Ethanol	298.15	8	0.03	0.03	[34]
{Ethylene glycol: [Choline] [Chloride]} [2:1] + Hexane + Ethanol	298.15	9	0.02	0.02	[34]
{Malonic acid: [Choline] [Chloride]} [1:1] + Hexane + Ethanol	298.15	9	0.07	0.10	[34]
{Glycerol:[Tetramethylammonium] [Chloride]} [2:1] + Hexane + Benzene	298.15	10	0.11	0.11	[35]
{Glycerol:[Tetraethylammonium] [Chloride]} [2:1] + Hexane + Benzene	298.15	8	0.18	0.18	[35]
{Ethylene glycol:[Tetraethylammonium] [Chloride]} [2:1] + Hexane + Benzene	298.15	6	0.17	0.17	[35]
{Ethylene glycol:[Tetrabutylammonium] [Chloride} [2:1] + Hexane + Benzene	298.15	8	0.09	0.09	[35]
{Glycerol:[Tetrahexylammonium] [Chloride]} [2:1] + Hexane + Benzene	298.15	8	0.18	0.18	[35]

{Ethylene glycol:[Tetrahexylammonium] [Chloride]} [2:1] + Hexane + Benzene	298.15	7	0.01	0.01	[35]
{Phenol: [Choline] [Chloride]} [3:1] + Toluene + Heptane	303.2	6	0.02	0.02	[36]
{Phenol: [Choline] [Chloride]} [4:1] + Toluene + Heptane	303.2	6	0.02	0.02	[36]
{Phenol: [Choline] [Chloride]} [3:1] + Toluene + Hexane	303.2	6	0.02	0.02	[36]
{Phenol: [Choline] [Chloride]} [4:1] + Toluene + Hexane	303.2	6	0.02	0.02	[36]
{1,2-Propanediol: [Choline] [Chloride]} [3:1] + Hexane + Ethanol	298.15	7	0.03	0.02	[37]
{1,2-Propanediol:Water: [Choline] [Chloride]} [3:3:1] + Hexane + Ethanol	298.15	6	0.02	0.03	[37]
{1,2-Propanediol: [Choline] [Chloride]} [3:1] + Heptane + Ethanol	298.15	6	0.01	0.01	[37]
{1,2-Propanediol:Water: [Choline] [Chloride]} [3:3:1] + Heptane + Ethanol	298.15	6	0.01	0.01	[37]
{Malic acid: [Choline] [Chloride]} [1:1] + Heptane + Methanol	298.15	5	0.03	0.03	[38]
{Malic acid: [Choline] [Chloride]} [1:1] + Toluene + Methanol	298.15	5	0.10	0.10	[38]
{Levulinic acid: [Choline] [Chloride]} [2:1] + Heptane + Toluene	298.15	12	0.04	0.04	[39]
{Levulinic acid:[Benzylcholine] [Chloride]} [2:1] + Heptane + Toluene	298.15	10	0.05	0.05	[39]
{Levulinic acid:[Tetrabutylammonium] [Chloride]} [2:1] + Heptane + Toluene	298.15	10	0.11	0.11	[39]
{Oxalic acid: [Choline] [Chloride]} [1:1] + Hexane + Ethanol	293.15	6	0.01	0.01	[40]
{Oxalic acid: [Choline] [Chloride]} [1:1] + Hexane + Ethanol	313.15	6	0.03	0.04	[40]
{Malonic acid: [Choline] [Chloride]} [1:1] + Hexane + Ethanol	293.15	5	0.05	0.06	[40]
{Malonic acid: [Choline] [Chloride]} [1:1] + Hexane + Ethanol	313.15	5	0.05	0.06	[40]
{Ethylene glycol:[Tetrabutylammonium]	298.15	10	0.01	0.01	[41]

[Bromide]} [2:1] + Pyridine + Hexadecane					
{Ethylene glycol:[Tetrabutylammonium] [Bromide]} [2:1] + Quinoline + Hexadecane	298.15	10	0.01	0.01	[41]
{Ethylene glycol:[Tetrabutylphosphonium] [Bromide]} [2:1] + Pyridine + Hexadecane	298.15	10	0.01	0.01	[41]
{Ethylene glycol:[Tetrabutylphosphonium] [Bromide]} [2:1] + Quinoline + Hexadecane	298.15	10	0.01	$4.8.10^{-3}$	[41]
{Ethylene glycol:[Choline] [Chloride]} [5:1] + Hexadecane + Benzene	298.15	7	0.03	0.03	[42]
{Ethylene glycol:[Choline] [Chloride]} [5:1] + Hexadecane + Benzene	308.15	7	0.03	0.03	[42]
{Ethylene glycol:[Choline] [Chloride]} [7:1] + Hexadecane + Benzene	298.15	7	0.03	0.03	[42]
{Ethylene glycol:[Choline] [Chloride]} [7:1] + Hexadecane + Benzene	308.15	7	0.03	0.03	[42]
{Dithylene glycol:[Choline] [Chloride]} [5:1] + Hexadecane + Benzene	298.15	7	0.06	0.06	[42]
{Diethylene glycol:[Choline] [Chloride]} [5:1] + Hexadecane + Benzene	308.15	7	0.06	0.06	[42]
{Diethylene glycol:[Choline] [Chloride]} [7:1] + Hexadecane + Benzene	298.15	7	0.06	0.06	[42]
{Diethylene glycol:[Choline] [Chloride]} [7:1] + Hexadecane + Benzene	308.15	7	0.06	0.07	[42]
{Trithylene glycol:[Choline] [Chloride]} [5:1] + Hexadecane + Benzene	298.15	7	0.10	0.10	[42]
{Triethylene glycol:[Choline] [Chloride]} [5:1] + Hexadecane + Benzene	308.15	7	0.10	0.10	[42]
{Triethylene glycol:[Choline] [Chloride]} [7:1] + Hexadecane + Benzene	298.15	7	0.11	0.11	[42]
{Triethylene glycol:[Choline] [Chloride]} [7:1] + Hexadecane + Benzene	308.15	7	0.11	0.11	[42]
{Ethylene glycol:[Choline] [Chloride]} [5:1] + Cyclohexane + Benzene	298.15	7	0.05	0.05	[42]

{Ethylene glycol:[Choline] [Chloride]} [5:1] + Cyclohexane + Benzene	308.15	7	0.05	0.06	[42]
{Ethylene glycol:[Choline] [Chloride]} [7:1] + Cyclohexane + Benzene	298.15	7	0.05	0.05	[42]
{Ethylene glycol:[Choline] [Chloride]} [7:1] + Cyclohexane + Benzene	308.15	7	0.05	0.05	[42]
{Diethylene glycol:[Choline] [Chloride]} [5:1] + Cyclohexane + Benzene	298.15	7	0.11	0.11	[42]
{Diethylene glycol:[Choline] [Chloride]} [5:1] + Cyclohexane + Benzene	308.15	7	0.11	0.11	[42]
{Diethylene glycol:[Choline] [Chloride]} [7:1] + Cyclohexane + Benzene	298.15	7	0.11	0.11	[42]
{Diethylene glycol:[Choline] [Chloride]} [7:1] + Cyclohexane + Benzene	308.15	7	0.11	0.12	[42]
{Triethylene glycol:[Choline] [Chloride]} [5:1] + Cyclohexane + Benzene	298.15	7	0.17	0.17	[42]
{Triethylene glycol:[Choline] [Chloride]} [5:1] + Cyclohexane + Benzene	308.15	7	0.17	0.17	[42]
{Triethylene glycol:[Choline] [Chloride]} [7:1] + Cyclohexane + Benzene	298.15	7	0.18	0.18	[42]
{Triethylene glycol:[Choline] [Chloride]} [7:1] + Cyclohexane + Benzene	308.15	6	0.18	0.19	[42]
{Ethylene glycol:[Choline] [Chloride]} [5:1] + Hexadecane + Thiophene	298.15	7	0.06	0.06	[42]
{Ethylene glycol:[Choline] [Chloride]} [5:1] + Hexadecane + Thiophene	308.15	7	0.06	0.06	[42]
{Ethylene glycol:[Choline] [Chloride]} [7:1] + Hexadecane + Thiophene	298.15	7	0.06	0.06	[42]
{Ethylene glycol:[Choline] [Chloride]} [7:1] + Hexadecane + Thiophene	308.15	7	0.06	0.06	[42]
{Diethylene glycol:[Choline] [Chloride]} [5:1] + Hexadecane + Thiophene	298.15	7	0.11	0.11	[42]
{Diethylene glycol:[Choline] [Chloride]} [5:1] + Hexadecane + Thiophene	308.15	7	0.11	0.11	[42]
{Diethylene glycol:[Choline] [Chloride]} [7:1] + Hexadecane + Thiophene	298.15	7	0.11	0.11	[42]

{Diethylene glycol:[Choline] [Chloride]} [7:1] + Hexadecane + Thiophene	308.15	7	0.11	0.11	[42]
{Triethylene glycol:[Choline] [Chloride]} [5:1] + Hexadecane + Thiophene	298.15	7	0.14	0.14	[42]
{Triethylene glycol:[Choline] [Chloride]} [5:1] + Hexadecane + Thiophene	308.15	7	0.14	0.14	[42]
{Triethylene glycol:[Choline] [Chloride]} [7:1] + Hexadecane + Thiophene	298.15	7	0.21	0.20	[42]
{Triethylene glycol:[Choline] [Chloride]} [7:1] + Hexadecane + Thiophene	308.15	7	0.14	0.14	[42]
{Ethylene glycol:[Choline] [Chloride]} [5:1] + Cyclohexane + Thiophene	298.15	7	0.11	0.11	[42]
{Ethylene glycol:[Choline] [Chloride]} [5:1] + Cyclohexane + Thiophene	308.15	7	0.11	0.11	[42]
{Ethylene glycol:[Choline] [Chloride]} [7:1] + Cyclohexane + Thiophene	298.15	7	0.10	0.10	[42]
{Ethylene glycol:[Choline] [Chloride]} [7:1] + Cyclohexane + Thiophene	308.15	7	0.10	0.10	[42]
{Diethylene glycol:[Choline] [Chloride]} [5:1] + Cyclohexane + Thiophene	298.15	7	0.18	0.18	[42]
{Diethylene glycol:[Choline] [Chloride]} [5:1] + Cyclohexane + Thiophene	308.15	7	0.18	0.18	[42]
{Diethylene glycol:[Choline] [Chloride]} [7:1] + Cyclohexane + Thiophene	298.15	7	0.18	0.18	[42]
{Diethylene glycol:[Choline] [Chloride]} [7:1] + Cyclohexane + Thiophene	308.15	7	0.18	0.17	[42]
{Triethylene glycol:[Choline] [Chloride]} [5:1] + Cyclohexane + Thiophene	298.15	5	0.19	0.19	[42]
{Triethylene glycol:[Choline] [Chloride]} [5:1] + Cyclohexane + Thiophene	308.15	5	0.18	0.18	[42]
{triethylene glycol:[Choline] [Chloride]} [7:1] + Cyclohexane + Thiophene	298.15	5	0.19	0.19	[42]
{Triethylene glycol:[Choline] [Chloride]} [7:1] + Cyclohexane + Thiophene	308.15	5	0.19	0.18	[42]
{Ethylene glycol:[Tetrahexylammonium]	298.15	6	0.06	0.06	[43]

[Bromide]} [2:1] + Hexane + Benzene					
{Ethylene glycol:[Tetrahexylammonium] [Bromide]} [2:1] + Hexane + Benzene	308.15	5	0.05	0.05	[43]
{Glycerol:[Tetrahexylammonium] [Bromide]} [2:1] + Hexane + Benzene	298.15	6	0.07	0.06	[43]
{Glycerol:[Tetrahexylammonium] [Bromide]} [2:1] + Hexane + Benzene	308.15	10	0.07	0.07	[43]
{Ethylene glycol:[Tetrabutylammonium] [Bromide]} [8:1] + Ethylbenzene + Octane	298.15	9	0.03	0.03	[44]
{Pyridine:Ethylene glycol:[Tetrabutylammonium] [Bromide]} [4:4:1] + Ethylbenzene + Octane	298.15	8	0.10	0.10	[44]
{Pyridine:Ethylene glycol:[Tetrabutylammonium] [Bromide]} [4:6:1] + Ethylbenzene + Octane	298.15	9	0.09	0.09	[44]
{Pyridine:Ethylene glycol:[Tetrabutylammonium] [Bromide]} [6:4:1] + Ethylbenzene + Octane	298.15	7	0.11	0.11	[44]
{Glycolic acid:[Choline] [Chloride]} [1:1] + Hexane + Ethanol	298.15	10	0.04	0.04	[45]
{Glycolic acid:[Choline] [Chloride]} [1:1] + Hexane + Ethanol	308.15	9	0.05	0.05	[45]
{L-Lactic acid:[Choline] [Chloride]} [2:1] + Hexane + Ethanol	298.15	9	0.03	0.03	[45]
{L-Lactic acid:[Choline] [Chloride]} [2:1] + Hexane + Ethanol	308.15	9	0.03	0.04	[45]
{Glycolic acid:[Choline] [Chloride]} [1:1] + Heptane + Ethanol	298.15	8	0.05	0.06	[45]
{Glycolic acid:[Choline] [Chloride]} [1:1] + Heptane + Ethanol	308.15	9	0.06	0.07	[45]
{L-Lactic acid:[Choline] [Chloride]} [2:1] + Heptane + Ethanol	298.15	9	0.02	0.03	[45]
{L-Lactic acid:[Choline] [Chloride]} [2:1] + Heptane + Ethanol	308.15	9	0.04	0.05	[45]

{Ethylene glycol:[Choline] [Chloride]} [2:1] + Hexane + Benzene	303	7	0.11	0.11	[46]
{Ethylene glycol:[Choline] [Chloride]} [3:1] + Hexane + Benzene	303	7	0.13	0.13	[46]
{Glycerol:[Choline] [Chloride]} [2:1] + Hexane + Benzene	303	7	0.21	0.20	[46]
{Glycerol:[Choline] [Chloride]} [3:1] + Hexane + Benzene	303	7	0.22	0.22	[46]

*Binary points and the data for which the algorithm could not converge have been excluded

Table S.B22. RMSD for the entire SLE database

System	Temperature (K)	Number of data points*	RMSD COSMO-SAC 2010	RMSD COSMO-SAC OH-ClBr	Reference
[Choline] [Chloride] + [EMIM] [Chloride]	303.4 – 525.7	18	0.03	0.04	[47]
[Choline] [Chloride] + [BMPYR] [Chloride]	419.6 – 560.7	20	0.06	0.04	[47]
[Choline] [Chloride] + [Benzylcholine] [Chloride]	305.7 – 535.7	18	0.05	0.05	[47]
(1,10-Decanediol:[Acetylcholine] [Chloride]) [2.5:1] + 2-Phenylethanol	246.2 – 338.1	19	0.11	0.12	[48]
[Choline] [Chloride] + [Tetrabutylammonium] [Chloride]	316.3 – 520.4	17	0.08	0.09	[47]
[Choline] [Chloride] + [1-(2-Hydroxyethyl)-3-methylimidazolium] [Chloride]	323.5 – 517.4	18	0.02	0.02	[47]
Choline chloride + Choline acetate	313.3 – 557.2	15	NA	0.06	[47]
[C1C3PYR] [Bromide] + Water	247.59 – 476.68	40	0.26	0.22	[23]
[BMPYR] [Bromide] + Water	250.56 – 487.67	24	0.25	0.22	[23]
[C1C5PYR] [Bromide] + Water	252.49 – 431.55	18	0.29	0.26	[23]
[C1C3MOR] [Bromide] + Water	235.57 – 453.94	37	0.24	0.19	[24]
[C1C4MOR] [Bromide] + Water	237.26 – 484.47	21	0.23	0.18	[24]
[C1C5MOR] [Bromide] + Water	244.56 – 467	24	0.22	0.19	[24]
[C1C5PIP] [Bromide] + Water	256.16 – 446.8	16	0.18	0.14	[24]
[EMIM] [Bromide] + Water	243.6 – 273.1	18	0.26	0.23	[49]

[C1C6MOR] [Bromide] + Diethylene glycol	291.5 – 428.3	14	0.35	0.25	[50]
[C1C6MOR] [Bromide] + Triethylene glycol	300.7 – 428.3	17	0.35	0.22	[50]
[Tetramethylammonium] [Chloride] + Decanoic acid	303.75 – 612.87	8	0.21	0.11	[51]
[Tetramethylammonium] [Chloride] + Lauric acid	312.55 – 612.87	11	0.23	0.13	[51]
[Tetramethylammonium] [Chloride] + Tetradecanoic acid	317.15 – 612.87	12	0.29	0.13	[51]
[Tetramethylammonium] [Chloride] + Palmitic acid	331.36 – 612.87	13	0.22	0.21	[51]
[Tetramethylammonium] [Chloride] + Stearic acid	337.95 – 612.87	7	0.33	0.17	[51]
[Tetraethylammonium] [Chloride] + Decanoic acid	301.66 – 526.78	5	0.26	0.14	[51]
[Tetraethylammonium] [Chloride] + Lauric acid	303.82 – 526.78	9	0.22	0.10	[51]
[Tetraethylammonium] [Chloride] + Tetradecanoic acid	311.71 – 526.78	8	0.33	0.06	[51]
[Tetraethylammonium] [Chloride] + Palmitic acid	319.93 – 526.78	6	0.33	0.16	[51]
[Tetraethylammonium] [Chloride] + Stearic acid	321.65 – 526.78	6	0.31	0.11	[51]
[Tetrapropylammonium] [Chloride] + Decanoic acid	295.57 – 503.07	6	0.29	0.11	[51]
[Tetrapropylammonium] [Chloride] + Lauric acid	295.7 – 503.07	11	0.32	0.19	[51]
[Tetrapropylammonium] [Chloride] + Tetradecanoic acid	303.65 – 503.07	12	0.37	0.12	[51]
[Tetrapropylammonium] [Chloride] + Palmitic acid	304.02 – 503.07	8	0.33	0.12	[51]
[Tetrapropylammonium] [Chloride] + Stearic acid	327.25 – 503.07	6	0.36	0.08	[51]
[Choline] [Chloride] + [Choline] [Propanoate]	324.2 – 560.7	13	NA	0.02	[47]
[Choline] [Chloride] + [Choline] [Butanoate]	320.5 – 555.8	8	NA	0.08	[47]

*Binary points and the data for which the algorithm could not converge have been excluded

References

[1] S.-H. Wu, A.R. Caparanga, R.B. Leron, M.-H. Li, Vapor pressure of aqueous choline chloride-based deep eutectic solvents (ethaline, glyceline, maline and reline) at 30–70°C, Thermochim. Acta. 544 (2012) 1–5. https://doi.org/10.1016/j.tca.2012.05.031.

[2] F.Z. Nessakh, Etude de nouveaux fluides de travail constitués de solvants eutectiques profonds pour les pompes à chaleur, Ph.D. Thesis, Université de Tlemcen, Algeria, Université de Lorraine, France, 2022.

[3] B. Sharma, N. Singh, T. Jain, J.P. Kushwaha, P. Singh, Acetonitrile Dehydration via Extractive Distillation Using Low Transition Temperature Mixtures as Entrainers, J. Chem. Eng. Data. 63 (2018) 2921–2930. https://doi.org/10.1021/acs.jced.8b00228.

[4] B. Sharma, N. Singh, J.P. Kushwaha, Ammonium-based deep eutectic solvent as entrainer for separation of acetonitrile–water mixture by extractive distillation, J. Mol. Liq. 285 (2019) 185–193. https://doi.org/10.1016/j.molliq.2019.04.089.

[5] M. Moghimi, A. Roosta, Physical properties of aqueous mixtures of (choline chloride + glucose) deep eutectic solvents, J. Chem. Thermodyn. 129 (2019) 159–165. https://doi.org/10.1016/j.jct.2018.09.029.

[6] P.J. Carvalho, I. Khan, A. Morais, J.F.O. Granjo, N.M.C. Oliveira, L.M.N.B.F. Santos, J.A.P. Coutinho, A new microebulliometer for the measurement of the vapor–liquid equilibrium of ionic liquid systems, Fluid Phase Equilibria. 354 (2013) 156–165. https://doi.org/10.1016/j.fluid.2013.06.015.

[7] M. Teodorescu, Isothermal Vapor + Liquid Equilibrium and Thermophysical Properties for 1-Butyl-3-methylimidazolium Bromide + 1-Butanol Binary System, Ind. Eng. Chem. Res. 53 (2014) 13522–13528. https://doi.org/10.1021/ie502247d.

[8] N. Calvar, B. González, E. Gómez, Á. Domínguez, Vapor−Liquid Equilibria for the Ternary System Ethanol + Water + 1-Butyl-3-methylimidazolium Chloride and the Corresponding Binary Systems at 101.3 kPa, J. Chem. Eng. Data. 51 (2006) 2178–2181. https://doi.org/10.1021/je060293x.

[9] N. Chouireb, I. Khan, E.A. Crespo, M.B. Oliveira, F. Llovell, L.F. Vega, O. Tafat-Igoudjilene, A.A. Kaci, L.M.N.B.F. Santos, P.J. Carvalho, J.A.P. Coutinho, Evaluation of the solvent structural effect upon the vapor –liquid equilibrium of [C4C1im][Cl] + alcohols, Fluid Phase Equilibria. 440 (2017) 36–44. https://doi.org/10.1016/j.fluid.2017.02.016.

[10] R. Garriga, S. Martínez, P. Pérez, M. Gracia, Isothermal (vapour+liquid) equilibrium at several temperatures of (1-chlorobutane+1-octanol, or 1-decanol), J. Chem. Thermodyn. 36 (2004) 59–69. https://doi.org/10.1016/j.jct.2003.09.009.

[11] F.A. Ashraf, J.H. Vera, Vapor-liquid equilibria for the ternary system n-Heptane/n-Propanol/l, chlorobutane and its constituent binaries at 318.15 and 338.15 K, Can. J. Chem. Eng. 59 (1981) 89–95. https://doi.org/10.1002/cjce.5450590111.

[12] S. Gholami, A. Roosta, Experimental Study and Modeling of Bubble Point of Aqueous Mixtures of Deep Eutectic Solvents Based on Dicarboxylic Acids and Choline Chloride, J. Chem. Eng. Data. 65 (2020) 2743–2750. https://doi.org/10.1021/acs.jced.0c00070.

[13] B. Sharma, N. Singh, J.P. Kushwaha, Natural Deep Eutectic Solvent-Mediated Extractive Distillation for Separation of Acetonitrile + Water Azeotropic Mixture, J. Chem. Eng. Data. 65 (2020) 1497–1505. https://doi.org/10.1021/acs.jced.9b00932.

[14] N.R. Rodriguez, M.C. Kroon, Isopropanol dehydration via extractive distillation using low transition temperature mixtures as entrainers, J. Chem. Thermodyn. 85 (2015) 216–221. https://doi.org/10.1016/j.jct.2015.02.003.

[15] K.S. Reddy, A.V.N. Swamy, T.E.V. Prasad, D.H.L. Prasad, Vapor−Liquid Equilibria of Binary Mixtures Formed by Hexan-1-ol with Chloroethanes and Chloroethenes at 95.6 kPa, J. Chem. Eng. Data. 55 (2010) 2073–2076. https://doi.org/10.1021/je9000608.

[16] T.E. Vittal Prasad, D.G. Reddi, D.H.L. Prasad, Vapor-Liquid Equilibria for Chlorobenzene with Butan-1-ol, 2-Methylpropan-1-ol and 2-Methylpropan-2-ol at 94.6 kPa, Phys. Chem. Liq. 38 (2000) 635–641. https://doi.org/10.1080/00319100008030311.
[17] T.E. Vittal Prasad, A. Phanibhushan, D.H.L. Prasad, Bubble temperature measurements on m-cresol with some chlorohydrocarbons, Fluid Phase Equilibria. 153 (1998) 81–85. https://doi.org/10.1016/S0378-3812(98)00406-3.
[18] J. Wisniak, A. Tamir, Vapor-liquid equilibrium in the systems propyl bromide-acetic acid, propyl bromide-propionic acid and propyl bromide-acetic acid-propionic acid, J. Chem. Eng. Data. 27 (1982) 430–435. https://doi.org/10.1021/je00030a019.
[19] M. Królikowska, K. Paduszyński, M. Zawadzki, (Vapor + liquid) phase equilibria of an aqueous solution of bromide-based ionic liquids – measurements, correlations and application to absorption cycles, Fluid Phase Equilibria. 494 (2019) 201–211. https://doi.org/10.1016/j.fluid.2019.05.003.
[20] J. Wang, D. Zheng, L. Fan, L. Dong, Vapor Pressure Measurement for the Water + 1,3-Dimethylimidazolium Chloride System and 2,2,2-Trifluoroethanol + 1-Ethyl-3-methylimidazolium Tetrafluoroborate System, J. Chem. Eng. Data. 55 (2010) 2128–2132. https://doi.org/10.1021/je900738e.
[21] N. Nie, D. Zheng, L. Dong, Y. Li, Thermodynamic Properties of the Water + 1-(2-Hydroxylethyl)-3-methylimidazolium Chloride System, J. Chem. Eng. Data. 57 (2012) 3598–3603. https://doi.org/10.1021/je3007953.
[22] K.-S. Kim, S.-Y. Park, S. Choi, H. Lee, Vapor Pressures of the 1-Butyl-3-methylimidazolium Bromide + Water, 1-Butyl-3-methylimidazolium Tetrafluoroborate + Water, and 1-(2-Hydroxyethyl)-3-methylimidazolium Tetrafluoroborate + Water Systems, J. Chem. Eng. Data. 49 (2004) 1550–1553. https://doi.org/10.1021/je034210d.
[23] M. Zawadzki, M. Królikowska, P. Lipiński, Physicochemical and thermodynamic characterization of N -alkyl- N -methylpyrrolidinium bromides and its aqueous solutions, Thermochim. Acta. 589 (2014) 148–157. https://doi.org/10.1016/j.tca.2014.05.028.
[24] M. Zawadzki, M. Królikowska, J. Antonowicz, P. Lipiński, M. Karpińska, Physicochemical and thermodynamic properties of the {1-alkyl-1-methylmorpholinium bromide, [C1Cn=3,4,5MOR]Br, or 1-methyl-1-pentylpiperidinium bromide, [C1C5PIP]Br+water} binary systems, J. Chem. Thermodyn. 98 (2016) 324–337. https://doi.org/10.1016/j.jct.2016.03.030.
[25] J. Wisniak, A. Tamir, Vapor-liquid equilibria at 760 mmHg in the system methanol-2-propanol-propyl bromide and its binaries, J. Chem. Eng. Data. 30 (1985) 339–344. https://doi.org/10.1021/je00041a032.
[26] J. Wisniak, A. Tamir, Vapor-liquid equilibria at 760 mm Hg in the systems propyl bromide-tert-butyl alcohol and propyl bromide-p-xylene, J. Chem. Eng. Data. 33 (1988) 106–108. https://doi.org/10.1021/je00052a012.
[27] J. Wisniak, A. Tamir, Vapor-liquid equilibria at 760 mmHg in the ternary system methonal- propyl bromide-methyl methacrylate, J. Chem. Eng. Data. 33 (1988) 376–379. https://doi.org/10.1021/je00053a041.
[28] A. Tamir, J. Wisniak, Vapor-liquid equilibria at 760 mm mercury in the ternary system methanol-acetonitrile-propyl bromide, J. Chem. Eng. Data. 32 (1987) 291–293. https://doi.org/10.1021/je00049a002.
[29] H. Passos, I. Khan, F. Mutelet, M.B. Oliveira, P.J. Carvalho, L.M.N.B.F. Santos, C. Held, G. Sadowski, M.G. Freire, J.A.P. Coutinho, Vapor–Liquid Equilibria of Water + Alkylimidazolium-Based Ionic Liquids: Measurements and Perturbed-Chain Statistical Associating Fluid Theory Modeling, Ind. Eng. Chem. Res. 53 (2014) 3737–3748. https://doi.org/10.1021/ie4041093.
[30] J. Wisniak, Isobaric vapor-liquid equilibria in the binary systems propyl bromide-i-butanol, propyl bromide-l-chlorobutane and 1-chlorobutane-methyl ethyl ketone, (n.d.) 8.
[31] K.A. Kurnia, N.A. Athirah, F.J.M. Candieiro, B. Lal, Phase Behavior of Ternary Mixtures {Aliphatic Hydrocarbon + Aromatic Hydrocarbon + Deep Eutectic Solvent}: A Step Forward toward

"Greener" Extraction Process, Procedia Eng. 148 (2016) 1340–1345. https://doi.org/10.1016/j.proeng.2016.06.582.
[32] F.S. Oliveira, A.B. Pereiro, L.P.N. Rebelo, I.M. Marrucho, Deep eutectic solvents as extraction media for azeotropic mixtures, Green Chem. 15 (2013) 1326. https://doi.org/10.1039/c3gc37030e.
[33] M.K. Hadj-Kali, H.F. Hizaddin, I. Wazeer, L. El blidi, S. Mulyono, M.A. Hashim, Liquid-liquid separation of azeotropic mixtures of ethanol/alkanes using deep eutectic solvents: COSMO-RS prediction and experimental validation, Fluid Phase Equilibria. 448 (2017) 105–115. https://doi.org/10.1016/j.fluid.2017.05.021.
[34] E.J. Sa, B.-S. Lee, B.H. Park, Extraction of ethanol from mixtures with n-hexane by deep eutectic solvents of choline chloride + levulinic acid, + ethylene glycol, or + malonic acid, J. Mol. Liq. 316 (2020) 113877. https://doi.org/10.1016/j.molliq.2020.113877.
[35] N.R. Rodriguez, T. Gerlach, D. Scheepers, M.C. Kroon, I. Smirnova, Experimental determination of the LLE data of systems consisting of {hexane + benzene + deep eutectic solvent} and prediction using the Conductor-like Screening Model for Real Solvents, J. Chem. Thermodyn. 104 (2017) 128–137. https://doi.org/10.1016/j.jct.2016.09.021.
[36] A. Hosseini, R. Haghbakhsh, S. Raeissi, Experimental Investigation of Liquid–Liquid Extraction of Toluene + Heptane or Toluene + Hexane Using Deep Eutectic Solvents, J. Chem. Eng. Data. 64 (2019) 3811–3820. https://doi.org/10.1021/acs.jced.9b00237.
[37] J. Vuksanović, M.Lj. Kijevčanin, I.R. Radović, Effect of water addition on extraction ability of eutectic solvent choline chloride+ 1,2-propanediol for separation of hexane/heptane+ethanol systems, Korean J. Chem. Eng. 35 (2018) 1477–1487. https://doi.org/10.1007/s11814-018-0030-z.
[38] J.M. Vuksanović, N.M. Todorović, M.L. Kijevčanin, S.P. Šerbanović, I.R. Radović, Experimental investigation and modeling of thermophysical and extraction properties of choline chloride + DL-malic acid based deep eutectic solvent, J. Serbian Chem. Soc. 82 (2017) 1287–1302.
[39] A.S.L. Gouveia, F.S. Oliveira, K.A. Kurnia, I.M. Marrucho, Deep Eutectic Solvents as Azeotrope Breakers: Liquid–Liquid Extraction and COSMO-RS Prediction, ACS Sustain. Chem. Eng. 4 (2016) 5640–5650. https://doi.org/10.1021/acssuschemeng.6b01542.
[40] A.A. Samarov, M.A. Smirnov, M.P. Sokolova, E.N. Popova, A.M. Toikka, Choline chloride based deep eutectic solvents as extraction media for separation of n-hexane–ethanol mixture, Fluid Phase Equilibria. 448 (2017) 123–127. https://doi.org/10.1016/j.fluid.2017.03.029.
[41] H.F. Hizaddin, M.K. Hadj-Kali, A. Ramalingam, M. Ali Hashim, Extractive denitrogenation of diesel fuel using ammonium- and phosphonium-based deep eutectic solvents, J. Chem. Thermodyn. 95 (2016) 164–173. https://doi.org/10.1016/j.jct.2015.12.009.
[42] H. Shekaari, M.T. Zafarani-Moattar, B. Mohammadi, Liquid–Liquid Equilibria for Benzene/Thiophene + Cyclohexane/Hexadecane + Deep Eutectic Solvents: Data and Correlation, J. Chem. Eng. Data. 64 (2019) 3904–3918. https://doi.org/10.1021/acs.jced.9b00313.
[43] N.R. Rodriguez, P.F. Requejo, M.C. Kroon, Aliphatic–Aromatic Separation Using Deep Eutectic Solvents as Extracting Agents, Ind. Eng. Chem. Res. 54 (2015) 11404–11412. https://doi.org/10.1021/acs.iecr.5b02611.
[44] H.F. Hizaddin, M. Sarwono, M.A. Hashim, I.M. Alnashef, M.K. Hadj-Kali, Coupling the capabilities of different complexing agents into deep eutectic solvents to enhance the separation of aromatics from aliphatics, J. Chem. Thermodyn. 84 (2015) 67–75. https://doi.org/10.1016/j.jct.2014.12.024.
[45] N.R. Rodriguez, B.S. Molina, M.C. Kroon, Aliphatic+ethanol separation via liquid–liquid extraction using low transition temperature mixtures as extracting agents, Fluid Phase Equilibria. 394 (2015) 71–82. https://doi.org/10.1016/j.fluid.2015.03.017.
[46] M.A. Usman, O.K. Fagoroye, T.O. Ajayi, A.J. Kehinde, Ternary liquid–liquid equilibrium data for n-Hexane-Benzene-DES (choline chloride/ethylene glycol, choline chloride/glycerol, choline chloride/urea) at 303 K and 101.3 kPa, Appl. Petrochem. Res. 10 (2020) 125–137. https://doi.org/10.1007/s13203-020-00252-w.

[47] L. Fernandez, L.P. Silva, M.A.R. Martins, O. Ferreira, J. Ortega, S.P. Pinho, J.A.P. Coutinho, Indirect assessment of the fusion properties of choline chloride from solid-liquid equilibria data, Fluid Phase Equilibria. 448 (2017) 9–14. https://doi.org/10.1016/j.fluid.2017.03.015.
[48] U. Domańska, P. Okuniewska, A. Markowska, Phase equilibrium in binary systems of ionic liquids, or deep eutectic solvents with 2-phenylethanol (PEA), or water, Fluid Phase Equilibria. 424 (2016) 68–78. https://doi.org/10.1016/j.fluid.2015.10.016.
[49] E. Vataščin, V. Dohnal, Phase equilibria of (water + [EMIM] bromide) and (water + [EMIM] tosylate), Fluid Phase Equilibria. 483 (2019) 84–91. https://doi.org/10.1016/j.fluid.2018.11.001.
[50] M. Królikowski, K. Sankiewicz, New experimental data on (solid + liquid) phase equilibria of N-hexyl-N-methylmorholinium bromide with glycols and sulfolane. The use of these binary systems in a sulfur extraction, J. Mol. Liq. 263 (2018) 366–374. https://doi.org/10.1016/j.molliq.2018.05.017.
[51] P.V.A. Pontes, E.A. Crespo, M.A.R. Martins, L.P. Silva, C.M.S.S. Neves, G.J. Maximo, M.D. Hubinger, E.A.C. Batista, S.P. Pinho, J.A.P. Coutinho, G. Sadowski, C. Held, Measurement and PC-SAFT modeling of solid-liquid equilibrium of deep eutectic solvents of quaternary ammonium chlorides and carboxylic acids, Fluid Phase Equilibria. 448 (2017) 69–80. https://doi.org/10.1016/j.fluid.2017.04.007.

Annexe C : Group contribution models for densities and heat capacities of deep eutectic solvents

Table S.C23. List of the systems found in the datasets for the densities of DESs along with the corresponding number of data points available

System	Number of data points
1,2-Decanediol : Thymol	1
1-Napthol : Menthol	1
1-Tetradecanol : Menthol	1
Acetylcholine chloride : 1,2,4-Triazole	7
Acetylcholine chloride : Fructose	13
Acetylcholine chloride : Glucose	13
Acetylcholine chloride : Guaiacol	12
Acetylcholine chloride : Imidazole	21
Acetylcholine chloride : Levulinic acid	15
Acetylcholine chloride : Mannose	13
Acetylcholine chloride : Ribose	13
Acetylcholine chloride : Xylose	13
Alanine : Lactic acid	15
Alanine : Malic acid	14
Allyltriphenylphosphonium bromide : Diethylene glycol	33
Allyltriphenylphosphonium bromide : Triethylene glycol	33
Atropine : Thymol	1
Benzyldimethyl(2-hydroxyethyl)ammonium chloride : Fructose	13
Benzyldimethyl(2-hydroxyethyl)ammonium chloride : Glucose	13
Benzyldimethyl(2-hydroxyethyl)ammonium chloride : Mannose	13
Benzyldimethyl(2-hydroxyethyl)ammonium chloride : Ribose	13
Benzyldimethyl(2-hydroxyethyl)ammonium chloride : Xylose	13
Benzyltributylammonium chloride : Diethylene glycol	13
Benzyltributylammonium chloride : Ethylene glycol	13
Benzyltributylammonium chloride : Glycerol	13
Benzyltributylammonium chloride : Triethylene glycol	13
Benzyltriethylammonium chloride : Oxalic acid	9
Benzyltrimethylammonium chloride : 1,2-Butanediol	7
Benzyltrimethylammonium chloride : 1,6-Hexanediol	7
Benzyltrimethylammonium chloride : Diethylene glycol	13
Benzyltrimethylammonium chloride : Ethylene glycol	20
Benzyltrimethylammonium chloride : Glycerol	20
Benzyltrimethylammonium chloride : Triethylene glycol	13
Benzyltripropylammonium chloride : Ethylene Glycol	11
Benzyltripropylammonium chloride : Glycerol	11
Benzyltripropylammonium chloride : Lactic acid	11

Benzyltripropylammonium chloride : Phenol	11
Betaine : Lactic acid	36
Betaine : Lactic acid : Water	11
Betaine : Levulinic acid	11
Betaine : Malic acid	10
Betaine: Citric acid : Water	11
Camphor : Capric acid	1
Camphor : Formic acid	1
Carvacrol : Capric acid	1
Carvone : Borneol	1
Carvone : Camphor	1
Carvone : Capric acid	1
Carvone : Decanoic acid	1
Carvone : Heptanoic acid	1
Carvone : Menthol	1
Carvone : Nonanoic acid	1
Carvone : Octanoic acid	1
Carvone : Salol	1
Carvone : Thymol	1
Choline chloride : 1,2-Propanediol	44
Choline chloride : 1,2-Propanediol : Water	1
Choline chloride : 1,3-Propanediol	54
Choline chloride : 1,4-Butanediol	66
Choline chloride : 2,3-Butanediol	26
Choline chloride : 2,6-Dimethylphenol	5
Choline chloride : 3-Methylphenol	5
Choline chloride : 4-Ethylphenol	5
Choline chloride : Acetamide	1
Choline chloride : Benzilic acid	9
Choline chloride : Citric acid	2
Choline chloride : Diethylene glycol	8
Choline chloride : Diglycolic acid	9
Choline chloride : Ethylene glycol	152
Choline chloride : Fructose	49
Choline chloride : Fructose : Water	2
Choline chloride : Furfuryl alcohol	12
Choline chloride : Glucose	31
Choline chloride : Glucose : Water	2
Choline chloride : Glutaric acid	13
Choline chloride : Glycerol	109
Choline chloride : Glycerol : Water	1
Choline chloride : Glycolic acid	13
Choline chloride : Guaiacol	12
Choline chloride : Lactic acid	141
Choline chloride : Levulinic acid	36

Choline chloride : Malic acid	1
Choline chloride : Malic acid : Water	1
Choline chloride : Malonic acid	27
Choline chloride : Maltose : Water	1
Choline chloride : Mannose	13
Choline chloride : Monochloroacetic acid	11
Choline chloride : Ninhydrin	9
Choline chloride : o-Cresol	10
Choline chloride : Oxalic acid	17
Choline chloride : p-Chlorophenol	14
Choline chloride : p-Cresol	14
Choline chloride : Phenol	58
Choline chloride : Propionic acid	11
Choline chloride : p-Toluenesulfonic acid	1
Choline chloride : Resorcinol	23
Choline chloride : Ribose	13
Choline chloride : Sorbitol	1
Choline chloride : Sorbitol : Water	1
Choline chloride : Sucrose	2
Choline chloride : Sucrose : Water	2
Choline chloride : Tartaric acid	2
Choline chloride : Trichloroacetic acid	11
Choline chloride : Triethylene glycol	15
Choline chloride : Urea	106
Choline chloride : Urea : L-Arginine	48
Choline chloride : Urea : Tetraethylene glycol	35
Choline chloride : Xylitol	1
Choline chloride : Xylitol : Water	1
Choline chloride : Xylose	15
Choline chloride : Xylose : Water	2
Citric acid : Glucose	1
Citric acid : Sucrose	1
Citronellol : Capric acid	1
Decanoic acid : Atropine	1
Decanoic acid : Menthol	2
Diethylamine hydrochloride : Guaiacol	12
Dodecanoic acid : Atropine	1
Dodecanoic acid : Decanoic acid	10
Dodecanoic acid : Octanoic acid	16
EMIM chloride : Ethylene glycol	15
EMIM chloride : Imidazole	28
Ethylamine hydrochloride : Acetamide	15
Eugenol : Capric acid	1
Fenchone : Capric acid	1
Geraniol : Capric acid	1

Glucose : Tartaric acid	1
Glycolic acid : Xylitol	20
Lactic acid : Glucose : Water	1
Linalool : Capric acid	1
Malic acid : β-Alanine : Water	1
Menthol : 2-Methyl-2,4-pentanediol	9
Menthol : 3-hydroxybenzoic acid	7
Menthol : Acetic acid	14
Menthol : Butyric acid	1
Menthol : Capric acid	20
Menthol : Caprylic acid	21
Menthol : Decanoic acid	17
Menthol : Diphenyl ether	8
Menthol : Dodecanoic acid	10
Menthol : Ethanolamine : Acetic acid	9
Menthol : Formic acid	1
Menthol : Hexanoic acid	1
Menthol : Lactic acid	15
Menthol : Lauric acid	46
Menthol : Levulinic acid	1
Menthol : Myristic acid	16
Menthol : Octanoic acid	17
Menthol : Oleic acid	1
Menthol : Oleyl alcohol	20
Menthol : Palmitic acid	13
Menthol : Propionic acid	1
Menthol : Pyruvic acid	13
Menthol : Salol	1
Menthol : Sesamol	7
Menthol : Stearic acid	13
Menthol : β-Citronellol	1
Menthol: 1-Decanol	9
Menthol: Thymol	7
Methyltrioctylammonium bromide : Decanoic acid	8
Methyltrioctylammonium chloride : Decanoic acid	8
Methyltriphenylphosphonium bromide : Ethylene glycol	64
Methyltriphenylphosphonium bromide : Glycerol	64
Methyltriphenylphosphonium bromide : Triethylene glycol	3
N,N-Diethylethanolammonium chloride : Ethylene glycol	68
N,N-Diethylethanolammonium chloride : Glycerol	68
Ninhydrin : 1-Nonanol	9
Ninhydrin : Tetrabutylammonium chloride	18
Proline : Lactic acid	11
Proline : Levulinic acid	11
Proline : Malic acid : Water	1

Tetrabutylammonium bromide : Levulinic acid	15
Tetrabutylammonium bromide : 1-Nonanol	9
Tetrabutylammonium bromide : 3-Amino-1-propanol	27
Tetrabutylammonium bromide : Polyethylene Glycol 200	20
Tetrabutylammonium bromide : Polyethylene Glycol 400	20
Tetrabutylammonium bromide : Polyethylene Glycol 600	20
Tetrabutylammonium chloride : 3-Amino-1-propanol	27
Tetrabutylammonium chloride : Arginine	18
Tetrabutylammonium chloride : Aspartic acid	18
Tetrabutylammonium chloride : Decanoic acid	8
Tetrabutylammonium chloride : Ethylene glycol	32
Tetrabutylammonium chloride : Glutamic acid	18
Tetrabutylammonium chloride : Glycerol	21
Tetrabutylammonium chloride : Lactic acid	6
Tetrabutylammonium chloride : Levulinic acid	15
Tetrabutylammonium chloride : Phenylacetic acid	11
Tetrabutylammonium chloride : Polyethylene glycol (400)	11
Tetrabutylammonium chloride : Propionic acid	11
Tetrabutylammonium chloride : Triethylene glycol	28
Tetrabutylammonium hydrogen sulfate : 1-Nonanol	9
Tetrabutylammonium hydrogen sulfate : Benzilic acid	9
Tetrabutylammonium hydrogen sulfate : Diglycolic acid	9
Tetrabutylammonium hydrogen sulfate : Ninhydrin	9
Tetraethylammonium bromide : Benzilic acid	9
Tetraethylammonium bromide : Levulinic acid	15
Tetraethylammonium chloride : 3-Amino-1-propanol	27
Tetraethylammonium chloride : Lactic acid	6
Tetraethylammonium chloride : Levulinic acid	15
Tetraheptylammonium chloride : Decanoic acid	8
Tetrahexylammonium bromide : Ethylene glycol	11
Tetrahexylammonium bromide : Glycerol	11
Tetramethylammonium chloride : Lactic acid	6
Tetraoctylammonium bromide : Decanoic acid	8
Tetraoctylammonium chloride : Decanoic acid	8
Tetrapropylammonium bromide : Benzilic acid	9
Thymol : 10-Undecylenic acid	6
Thymol : Camphor	3
Thymol : Capric acid	18
Thymol : Caprylic acid	20
Thymol : Coumarin	2
Thymol : Decanoic acid	4
Thymol : Lauric acid	15
Thymol : Menthol	2
Thymol : Myristic acid	13
Thymol : Palmitic acid	13

Thymol : Stearic acid	12
Thymol : β-Citronellol	1
Thymol: 1-Decanol	9
Thymol: 2-Methyl-2,4-pentanediol	9
Triethylammonium chloride : 4-Methylphenol	1
Triethylammonium chloride : Glycolic acid	1
Triethylammonium chloride : Phenol	1
Trimethylglycine : 2-Chlorobenzoic acid	4
Trimethylglycine : 2-Furoic acid	5
Trimethylglycine : 4-Chlorobenzoic acid	4
Trimethylglycine : Benzoic acid	3
Trimethylglycine : Glycolic acid	5
Trimethylglycine : Mandelic acid	5
Trimethylglycine : Oxalic acid	4
Trimethylglycine : Phenylacetic acid	5
Total	**3266**

Table S.C24. Dataset used in the optimization of the parameters for the density group contribution model (Dataset D1) with the average deviations between experimental and calculated densities

System	Ratio	Temperature range (K)	Number of data points	Average deviation (%)	Reference
{[Choline][Chloride]:Urea}	[0.4:0.6]	303.15 - 353.15	6	1.23	[1]
	[0.333:0.667]	298.15 - 358.15	7	1.93	
	[0.286:0.714]	303.15 - 353.15	6	0.65	
{[Choline][Chloride]:Glycerol}	[0.5:0.5]	298.15 - 368.15	15	3.15	[2]
	[0.33:0.67]		15	0.61	
	[0.25:0.75]		15	1.79	
{[Choline][Chloride]:Ethylene glycol}	[0.36:0.64]	298.15 - 368.15	15	0.85	[2]
	[0.33:0.67]		15	0.53	
	[0.28:0.72]		15	0.01	
{[N,N-Diethylethanolammonium] [Chloride]:Glycerol}	[0.33:0.67]	298.15 - 368.15	15	0.08	[2]
	[0.25:0.75]		15	2.72	
	[0.2:0.8]		15	3.95	
{[N,N-Diethylethanolammonium] [Chloride]:Ethylene glycol}	[0.33:0.67	298.15 - 368.15	15	2.26	[2]
	[0.25:0.75]		15	1.58	
	[0.2:0.8]		15	1.38	
{[Methyltriphenylphosphonium] [Bromide]:Ethylene glycol}	[0.25:0.75]	298.15 - 368.15	15	0.38	[2]
	[0.2:0.8]		15	1.62	
	[0.16:0.84]		15	2.68	
{[Tetrabutylammonium][Chloride] :Glycerol}	[0.25:0.75]	293.15 - 353.15	7	10.46	[3]
	[0.2:0.8]		7	9.99	
	[0.167:0.833]		7	9.69	
{[Tetrabutylammonium][Chloride] :Triethylene glycol}	[0.5:0.5]	293.15 - 353.15	7	1.32	[3]
	[0.667:0.333]		7	1.94	
	[0.75:0.25]		7	2.21	

	[0.8:0.2]		7	2.53	
{[Benzyltrimethylammonium][Chloride]:1,6-Hexanediol}	[0.5:0.5]	293.15 - 323.15	7	3.55	[4]
{[Benzyltrimethylammonium][Chloride]:Glycerol}	[0.5:0.5]	293.15 - 323.15	7	0.38	[4]
{[Benzyltrimethylammonium][Chloride]:1,2-Butanediol}	[0.5:0.5]	293.15 - 323.15	7	1.85	[4]
{[Choline][Chloride]:Glycerol}	[0.333:0.667]	293.15	1	2.33	[5]
	[0.5:0.5]	298.15	1	2.95	
{[Choline][Chloride]:Fructose}	[0.667:0.333]	298.15	1	3.71	[5]
{[Methyltriphenylphosphonium][Bromide]:Ethylene glycol}	[0.2:0.8]	298.15	1	4.74	[5]
	[0.25:0.75]		1	0.33	
{[N,N-Diethylethanolammonium][Chloride]:Glycerol}	[0.333:0.667]	298.15	1	2.81	[5]
	[0.25:0.75]		1	2.68	
{[N,N-Diethylethanolammonium][Chloride]:Ethylene glycol}	[0.25:0.75]	298.15	1	0.27	[5]
	[0.2:0.8]		1	0.46	
{[Choline][Chloride]:Urea}	[0.333:0.667]	293.15	1	1.79	[5]
{[Choline][Chloride]:Phenol}	[0.25:0.75]	298.15	1	1.03	[5]
{[Choline][Chloride]:Lactic acid}	[0.333:0.667]	298.15	1	0.58	[5]
{[Choline][Chloride]:2,3-Butanediol}	[0.2:0.8]	303.15 - 343.15	9	5.41	[6]
	[0.25:0.75]		9	5.25	
{[Choline][Chloride]:1,3-Propanediol}	[0.2:0.8]	303.15 - 343.15	9	1.87	[6]
	[0.25:0.75]		9	2.08	
{[Choline][Chloride]:Urea}	[0.333:0.667]	308.15 - 363.15	12	0.08	[7]
{[Tetrabutylammonium][Bromide]:Polyethylene glycol 200	[0.3205:0.6795]	298.15 - 343.15	10	0.76	[8]
	[0.2469:0.7531]		10	0.76	
{[Tetrabutylammonium][Bromide]:Polyethylene glycol 600	[0.3236:0.6764]	298.15 - 343.15	10	0.64	[8]
	[0.2415:0.7585]		10	0.98	
{[Choline][Chloride]:D-Ribose}	[0.5:0.5]	293.15 - 353.15	13	0.68	[9]
{[Choline][Chloride]:D-Mannose}	[0.5:0.5]	293.15 - 353.15	13	0.37	[9]
{[Choline][Chloride]:D-Fructose}	[0.5:0.5]	293.15 - 353.15	13	2.35	[9]
{[Acetylcholine][Chloride]:D-Xylose}	[0.5:0.5]	293.15 - 353.15	13	1.13	[9]
{[Acetylcholine][Chloride]:D-Ribose}	[0.5:0.5]	293.15 - 353.15	13	0.48	[9]
{[Acetylcholine][Chloride]:D-Glucose}	[0.5:0.5]	293.15 - 353.15	13	0.20	[9]
{[Benzyldimethyl(2-hydroxyethyl)ammonium][Chloride]:D-Ribose}	[0.5:0.5]	293.15 - 353.15	13	2.50	[9]
{[Benzyldimethyl(2-hydroxyethyl)ammonium][Chloride]:D-Mannose}	[0.5:0.5]	293.15 - 353.15	13	2.30	[9]
{[Benzyldimethyl(2-hydroxyethyl)ammonium][Chloride]:D-Fructose}	[0.5:0.5]	293.15 - 353.15	13	1.59	[9]

{[Acetylcholine][Chloride]:Levulinic acid}	[0.25:0.75]	303.15 - 333.15	4	1.07	[10]
{[Tetraethylammonium][Chloride]:Levulinic acid}	[0.25:0.75]	303.15 - 333.15	4	0.07	[10]
{[Tetraethylammonium][Bromide]:Levulinic acid}	[0.25:0.75]	303.15 - 333.15	4	3.83	[10]
{[Tetrabutylammonium][Chloride]:Levulinic acid}	[0.25:0.75]	303.15 - 333.15	4	3.21	[10]
{[Tetrabutylammonium][Bromide]:Levulinic acid}	[0.25:0.75]	303.15 - 333.15	4	0.15	[10]
{[Allyltriphenylphosphonium][Bromide]:Diethylene glycol}	[0.2:0.8]	293.15 - 343.15	11	1.37	[11]
	[0.091:0.909]		11	0.98	
	[0.059:0.941]		11	1.58	
{[Allyltriphenylphosphonium][Bromide]:Triethylene glycol}	[0.2:0.8]	293.15 - 343.15	11	2.56	[11]
	[0.091:0.909]		11	0.57	
	[0.059:0.941]		11	1.12	
{[Benzyltripopylammonium][Chloride]:Phenol	[0.25:0.75]	293.15 - 343.15	11	1.35	[12]
{[Benzyltripopylammonium][Chloride]:Lactic acid	[0.25:0.75]	293.15 - 343.15	11	1.90	[12]
{[Benzyltripopylammonium][Chloride]:Glycerol	[0.25:0.75]	293.15 - 343.15	11	1.45	[12]
{L-Proline:Levulinic acid}	[0.333:0.667]	293.15 - 343.15	11	0.44	[13]
{L-Proline:DL-Lactic acid}	[0.5:0.5]	293.15 - 343.15	11	0.06	[13]
{Betaine:DL-Lactic acid}	[0.333:0.667]	298.15 - 343.15	10	0.42	[13]
	[0.167:0.833]	293.15 - 343.15	11	1.95	[13]
{Betaine:DL-Levulinic acid}	[0.333:0.667]	293.15 - 343.15	11	0.01	[13]
{Betaine:DL-Lactic acid:Water}	[0.333:0.333:0.333]	293.15 - 343.15	11	4.44	[13]
{Betaine:Citric acid:Water}	[0.222:0.111:0.667]	293.15 - 343.15	11	$8.5*10^{-3}$	[13]
{[Choline][Chloride]:2,3-Butanediol}	[0.25:0.75]	293.15 - 323.15	4	4.03	[14]
	[0.2:0.8]		4	4.25	
{[Choline][Chloride]:1,2-Propanediol}	[0.25:0.75]	293.15 - 323.15	4	3.49	[14]
	[0.2:0.8]		4	2.77	
{[Choline][Chloride]:D-Fructose}	[0.5:0.5]	298.15 - 358.15	7	4.29	[15]
	[0.6:0.4]		7	1.65	
	[0.667:0.333]		7	0.50	
	[0.714:0.286]		7	2.01	
{[Choline][Chloride]:Triethylene glycol}	[0.333:0.667]	303.15 - 353.15	6	0.25	[16]
{[Choline][Chloride]:Urea}	[0.333:0.667]	293.15 - 363.15	8	0.25	[17]
{[Choline][Chloride]:Ethylene glycol}	[0.333:0.667]	298.15 - 333.15	8	0.57	[18]
{[Choline][Chloride]:Glycerol}	[0.333:0.667]	298.15 - 333.15	8	0.46	[18]
{[Choline][Chloride]:Ethylene glycol}	[0.333:0.667]	308.15 - 363.15	12	0.60	[19]
{[Choline][Chloride]:Glycerol}	[0.333:0.667]	283.15 - 363.15	9	0.36	[20]
{[Choline][Chloride]:Glycolic acid}	[0.5:0.5]	293.15 - 353.15	13	0.20	[21]
{[Choline][Chloride]:Oxalic acid}	[0.5:0.5]	293.15 - 348.15	12	1.29	[21]

{[Choline][Chloride]:Glutaric acid}	[0.5:0.5]	293.15 - 353.15	13	2.48	[21]
{[Choline][Chloride]:Furfuryl alcohol}	[0.25:0.75]	303.15 - 333.15	4	1.00	[22]
	[0.2:0.8]		4	0.73	
	[0.167:0.833]		4	0.51	
{[Choline][Chloride]:Phenol}	[0.333:0.667]	293.15 - 318.15	6	0.08	[23]
	[0.25:0.75]		6	0.89	
	[0.2:0.8]		6	1.35	
	[0.167:0.833]		6	1.64	
	[0.143:0.857]		6	1.84	
{[Choline][Chloride]:Phenol}	[0.333:0.667]	293.15 - 333.15	9	1.93	[24]
{[Choline][Chloride] :p-Chlorophenol}	[0.333:0.667]	293.15 - 333.15	9	0.56	[24]
{[Choline][Chloride]:Urea}	[0.333:0.667]	298.15 - 353.15	12	$9.2*10^{-3}$	[25]
{[Choline][Chloride]:Urea :L-Arginine}	[0.328:0.656 :0.016]	298.15 - 353.15	12	$6.2*10^{-3}$	[25]
	[0.323:0.645 :0.032]		12	$4.3*10^{-3}$	
	[0.317:0.635 :0.048]		12	0.04	
	[0.3125:0.625 :0.0625]		12	0.09	
{[Choline][Chloride]:Urea}	[0.333:0.667]	293.15 - 323.15	4	0.08	[26]
{[Tetrabutylammonium][Chloride] :Propionic acid}	[0.333:0.667]	288.15 - 338.15	11	4.86	[27]
{[Tetrabutylammonium][Chloride] :Polyethylene glycol 400}	[0.333:0.667]	288.15 - 338.15	11	1.73	[27]
{[Tetrabutylammonium][Chloride] :Phenylacetic acid}	[0.333:0.667]	288.15 - 338.15	11	0.67	[27]
{[Tetrahexylammonium][Bromide] :Ethylene glycol}	[0.333:0.667]	293.15 - 343.15	11	3.22	[28]
{[Tetrahexylammonium][Bromide] :Glycerol}	[0.333:0.667]	293.15 - 343.15	11	5.53	[28]
{[Choline][Chloride]:Urea}	[0.333:0.667]	293.15 - 338.15	10	0.10	[29]
{[Choline][Chloride]:Urea}	[0.333:0.667]	303.15 - 358.15	5	0.21	[30]
{[Choline][Chloride]:Urea}	[0.333:0.667]	298.15 - 323.15	6	0.05	[31]
{[Choline][Chloride]:Urea}	[0.333:0.667]	303.15 - 353.15	7	0.02	[32]
{[Choline][Chloride]:Urea}	[0.333:0.667]	298.15 - 333.15	8	0.02	[33]
{[Choline][Chloride]:Glycerol}	[0.33:0.67]	298.15 - 328.15	7	0.56	[34]
{[Choline][Chloride]:Ethylene glycol}	[0.33:0.67]	298.15 - 328.15	7	0.48	[34]
{[Choline][Chloride]:Fructose}	[0.33:0.67]	298.15 - 328.15	7	2.99	[34]
{[Choline][Chloride]:Glucose}	[0.33:0.67]	298.15 - 328.15	7	1.29	[34]
{[Methyltriphenylphosphonium] [Bromide]:Ethylene glycol}	[0.2:0.8]	298.15 - 328.15	7	5.92	[34]
{[N,N-Diethylethanolammonium] [Chloride]:Glycerol}	[0.2:0.8]	298.15 - 328.15	7	2.62	[34]
{[N,N-Diethylethanolammonium] [Chloride]:Ethylene glycol}	[0.25:0.75]	298.15 - 328.15	7	0.26	[34]
{[N,N-Diethylethanolammonium] [Chloride]:Glycerol}	[0.333:0.667]	298.15 - 343.15	10	0.38	[35]

{[N,N-Diethylethanolammonium][Chloride]:Ethylene glycol}	[0.333:0.667]	298.15 - 343.15	10	0.85	[35]
{[Choline][Chloride]:Glycerol}	[0.333:0.667]	298.15 - 323.15	6	0.50	[36]
{Menthol:Ethanolamine:Acetic acid}	[0.143:0.286:0.571]	293.15 - 333.15	9	0.81	[37]
{DL-Menthol:Acetic acid}	[0.5:0.5]	293.15 - 353.15	13	5.20	[38]
{DL-Menthol:Pyruvic acid}	[0.333:0.667]	293.15 - 353.15	13	10.06	[38]
{DL-Menthol:Lactic acid}	[0.333:0.667]	293.15 - 353.15	13	3.91	[38]
{Menthol:Decanoic acid}	[0.5:0.5]	298.15	1	0.55	[39]
{Menthol:Oleic acid}	[0.5:0.5]	298.15	1	0.47	[39]
{Menthol:Salol}	[0.5:0.5]	298.15	1	3.74	[39]
{DL-Menthol:Diphenyl ether}	[0.455:0.545]	293.15 - 363.15	8	2.59	[40]
{Thymol:2-Methyl-2,4-pentanediol}	[0.667:0.333]	293.15 - 353.15	9	0.06	[41]
{Thymol:1-Decanol}	[0.667:0.333]	293.15 - 353.15	9	0.90	[41]
{Menthol:2-Methyl-2,4-pentanediol}	[0.667:0.333]	293.15 - 353.15	9	2.51	[41]
{Menthol:1-Decanol}	[0.667:0.333]	293.15 - 353.15	9	0.06	[41]
{Menthol:Formic acid}	[0.5:0.5]	298.15	1	7.71	[42]
{Menthol:Acetic acid}	[0.5:0.5]	298.15	1	3.73	[42]
{Menthol:Propionic acid}	[0.5:0.5]	298.15	1	2.21	[42]
{Menthol:Butyric acid}	[0.5:0.5]	298.15	1	1.58	[42]
{Menthol:Hexanoic acid}	[0.5:0.5]	298.15	1	3.32	[42]
{Menthol:Octanoic acid}	[0.5:0.5]	298.15	1	1.38	[42]
{Menthol:Lactic acid}	[0.5:0.5]	298.15	1	1.88	[42]
{Menthol:Levulinic acid}	[0.5:0.5]	298.15	1	0.04	[42]
{Decanoic acid:Atropine}	[0.667:0.333]	298.15	1	0.09	[43]
{Decanoic acid:Menthol}	[0.5:0.5]	298.15	1	1.69	[43]
	[0.333:0.667]		1	0.40	
{Dodecanoic acid:Atropine}	[0.667:0.333]	298.15	1	$1.1*10^{-3}$	[43]
{Thymol:Coumarin}	[0.667:0.333]	298.15	1	0.32	[43]
	[0.5:0.5]		1	1.69	
{Thymol:Menthol}	[0.5:0.5]	298.15	1	2.83	[43]
	[0.333:0.667]		1	2.60	
{1-Tetradecanol:Menthol}	[0.333:0.667]	298.15	1	2.25	[43]
{1,2-Decanediol:Thymol}	[0.333:0.667]	298.15	1	0.44	[43]
{1-Naphtol:Menthol}	[0.333:0.667]	298.15	1	0.63	[43]
{Atropine:Thymol}	[0.333:0.667]	298.15	1	3.90	[43]
{Menthol:Octanoic acid}	[0.5:0.5]	353.15 - 413.15	5	3.64	[44]
{Menthol:Decanoic acid}	[0.5:0.5]	353.15 - 413.15	5	1.73	[44]
{Menthol:Dodecanoic acid}	[0.667:0.333]	303.15 - 413.15	10	0.41	[44]
{[Benzyltrimethylammonium][Chloride]:Diethylene glycol}	[0.25:0.75]	283.15 - 343.15	13	0.73	[45]
{[Benzyltrimethylammonium][Chloride]:Triethylene glycol}	[0.25:0.75]	283.15 - 343.15	13	0.95	[45]
{[Benzyltrimethylammonium][Chloride]:Glycerol}	[0.25:0.75]	283.15 - 343.15	13	1.10	[45]
{[Benzyltributylammonium][Chloride]:Ethylene glycol}	[0.25:0.75]	283.15 - 343.15	13	2.85	[45]
{[Benzyltributylammonium][Chloride]:Diethylene glycol}	[0.25:0.75]	283.15 - 343.15	13	1.34	[45]

{[Benzyltributylammonium][Chloride]:Triethylene glycol}	[0.25:0.75]	283.15 - 343.15	13	0.47	[45]
{[Benzyltriethylammonium][Chloride]:Acid oxalic}	[0.5:0.5]	293.15 - 333.15	9	1.50	[46]
{[Choline][Chloride]:Trichloroacetic acid}	[0.333:0.667]	288.15 - 338.15	11	1.61	[47]
{[Choline][Chloride]:Monochloroacetic acid}	[0.333:0.667]	288.15 - 338.15	11	4.15	[47]
{[Choline][Chloride]:Propionic acid}	[0.333:0.667]	288.15 - 338.15	11	2.72	[47]
{[Choline][Chloride]:Glycerol}	[0.333:0.667]	278.15 - 363.15	18	0.49	[48]
{Menthol:Lactic acid}	[0.5:0.5]	298	1	3.07	[49]
{Camphor:Formic acid}	[0.5:0.5]	298	1	5.18	[49]
{Menthol:β-Citronellol}	[0.5:0.5]	298	1	$2.2*10^{-3}$	[49]
{Thymol:β-Citronellol}	[0.5:0.5]	298	1	0.79	[49]
{[Tetrabutylammonium][Chloride]:Decanoic acid}	[0.333:0.667]	288.15 - 323.15	8	2.87	[50]
{[Methyltrioctylammonium][Chloride]:Decanoic acid}	[0.333:0.667]	288.15 - 323.15	8	0.48	[50]
{[Tetraheptylammonium][Chloride]:Decanoic acid}	[0.333:0.667]	288.15 - 323.15	8	0.71	[50]
{[Tetraoctylammonium][Chloride]:Decanoic acid}	[0.333:0.667]	288.15 - 323.15	8	2.67	[50]
{[Methyltrioctylammonium][Bromide]:Decanoic acid}	[0.333:0.667]	288.15 - 323.15	8	0.09	[50]
{[Tetraoctylammonium][Bromide]:Decanoic acid}	[0.333:0.667]	288.15 - 323.15	8	2.41	[50]
{[Triethylammonium][Chloride]:Glycolic acid}	[0.25:0.75]	298.15	1	9.58	[51]
{[Triethylammonium][Chloride]:Phenol}	[0.25:0.75]	298.15	1	0.05	[51]
{[Triethylammonium][Chloride]:4-Methylphenol}	[0.25:0.75]	298.15	1	0.15	[51]
{[Choline][Chloride]:Glycerol}	[0.333:0.667]	298.15	1	0.35	[52]
{[Choline][Chloride]:Ethylene glycol}	[0.333:0.667]	298.15	1	1.18	[52]
{[N,N-Diethylethanolammonium][Chloride]:Glycerol}	[0.333:0.667]	298.15	1	0.11	[52]
{[N,N-Diethylethanolammonium][Chloride]:Ethylene glycol}	[0.333:0.667]	298.15	1	0.78	[52]
{Malic acid:[Choline][Chloride]:Water}	[0.25:0.25:0.5]	313.15	1	3.10	[53]
{Glycerol:[Choline][Chloride]:Water}	[0.5:0.25:0.25]	313.15	1	2.17	[53]
{Malic acid:β-Alanine:Water}	[0.2:0.2:0.6]	313.15	1	8.16	[53]
{Proline:Malic acid:Water}	[0.2:0.2:0.6]	313.15	1	1.49	[53]
{Fructose:[Choline][Chloride]:Water}	[0.166:0.417:0.417]	313.15	1	2.58	[53]
{Sucrose:[Choline][Chloride]:Water}	[0.111:0.444:0.444]	313.15	1	3.35	[53]

{1,2-Propanediol :[Choline][Chloride] :Water}	[0.333:0.333 :0.333]	313.15	1	8.36	[53]
{Lactic acid:[Choline][Chloride] :Water}	[0.556:0.111 :0.333]	313.15	1	3.18	[53]
{Sorbitol:[Choline][Chloride] :Water}	[0.154:0.385 :0.461]	313.15	1	7.02	[53]
{Xylitol:[Choline][Chloride] :Water}	[0.167:0.333 :0.5]	313.15	1	6.81	[53]
{[Choline][Chloride]:Phenol}	[0.333:0.667]	323.15	1	0.35	[54]
	[0.25:0.75]		1	1.44	
	[0.2:0.8]		1	1.94	
{[Choline][Chloride]:Diethylene glycol}	[0.25:0.75]	293.15 - 323.15	4	0.41	[54]
	[0.2:0.8]		4	0.58	
{[Choline][Chloride]:Triethylene glycol}	[0.25:0.75]	293.15 - 323.15	4	0.73	[54]
	[0.2:0.8]		4	0.26	
{[Tetramethylammonium] [Chloride]:Lactic acid}	[0.333:0.667]	293.15 - 318.15	6	0.33	[55]
{[Tetraethylammonium] [Chloride]:Lactic acid}	[0.333:0.667]	293.15 - 318.15	6	1.21	[55]
{[Tetrabutylammonium] [Chloride]:Lactic acid}	[0.333:0.667]	293.15 - 318.15	6	6.10	[55]
{[Choline] [Chloride]:Lactic acid}	[0.435:0.565]	298.15 - 363.15	14	1.73	[56]
	[0.4:0.6]		14	0.92	
	[0.333:0.667]		14	0.51	
	[0.286:0.714]		14	0.54	
	[0.25:0.75]		14	0.81	
	[0.222:0.778]		14	1.18	
	[0.167:0.833]		14	1.95	
	[0.111:0.889]		14	2.69	
	[0.091:0.909]		14	2.97	
	[0.0625 :0.9375]		14	2.87	
{Carvacrol:Capric acid}	[0.5:0.5]	298	1	1.38	[57]
{Carvone:Capric acid}	[0.5:0.5]	298	1	2.53	[57]
{Thymol:Capric acid}	[0.5:0.5]	298	1	1.60	[57]
{Eugenol:Capric acid}	[0.5:0.5]	298	1	4.59	[57]
{Menthol:Capric acid}	[0.5:0.5]	298	1	0.68	[57]
{Frenchone:Capric acid}	[0.5:0.5]	298	1	1.13	[57]
{Camphor:Capric acid}	[0.5:0.5]	298	1	0.07	[57]
{Citronellol:Capric acid}	[0.5:0.5]	298	1	4.81	[57]
{Geraniol:Capric acid}	[0.5:0.5]	298	1	4.17	[57]
{Linalool:Capric acid}	[0.5:0.5]	298	1	6.71	[57]
{Carvone:Heptanoic acid}	[0.6:0.4]	298.15	1	1.65	[58]
{Carvone:Octanoic acid}	[0.8:0.2]	298.15	1	0.07	[58]
{Carvone:Nonanoic acid}	[0.74:0.26]	298.15	1	$7.6*10^{-11}$	[58]
{Carvone:Decanoic acid}	[0.89:0.11]	298.15	1	1.30	[58]
{Carvone:Camphor}	[0.73:0.27]	298.15	1	2.52	[58]
{Carvone:Menthol}	[0.76:0.24]	298.15	1	2.28	[58]
{Carvone:Borneol}	[0.86:0.14]	298.15	1	2.71	[58]

{Carvone:Thymol}	[0.5:0.5]	298.15	1	2.89	[58]
{Carvone:Salol}	[0.5:0.5]	298.15	1	2.19	[58]
{[1-Ethyl-3-methylimidazolium][Chloride]:Imidazole}	[0.667:0.333]	298.2 - 358.2	7	0.01	[59]
	[0.5:0.5]		7	0.05	
	[0.333:667]		7	$8.1*10^{-3}$	
	[0.25:0.75]		7	0.11	
{[Tetrabutylammonium][Bromide]:3-Amino-1-propanol}	[0.2:0.8]	293.15 - 333.15	9	1.94	[60]
	[0.143:0.857]		9	1.74	
	[0.111:0.889]		9	1.52	
{[Tetraethylammonium][Chloride]:3-Amino-1-propanol}	[0.2:0.8]	293.15 - 333.15	9	0.13	[60]
	[0.143:0.857]		9	0.03	
	[0.111:0.889]		9	0.02	
{[Tetrabutylammonium][Chloride]:3-Amino-1-propanol}	[0.2:0.8]	293.15 - 333.15	9	1.46	[60]
	[0.143:0.857]		9	1.22	
	[0.111:0.889]		9	1.05	
{[Choline][Chloride]:Ninhydrin}	[0.571:0.429]	293.15 - 333.15	9	0.43	[61]
{[Tetrabutylammonium][Hydrogen sulfate]:Ninhydrin}	[0.571:0.429]	293.15 - 333.15	9	0.87	[61]
{[Tetrabutylammonium][Bromide]:1-Nonanol}	[0.2:0.8]	293.15 - 333.15	9	1.29	[62]
{[Tetrabutylammonium][Hydrogen sulfate]:1-Nonanol}	[0.2:0.8]	293.15 - 333.15	9	0.30	[62]
{Ninhydrin:1-Nonanol}	[0.25:0.75]	293.15 - 333.15	9	4.96	[62]
{[Choline][Chloride]:Benzilic acid}	[0.5:0.5]	293.15 - 333.15	9	1.50	[63]
{[Tetraethylammonium][Bromide]:Benzilic acid}	[0.5:0.5]	293.15 - 333.15	9	2.76	[63]
{[Tetrapropylammonium][Bromide]:Benzilic acid}	[0.5:0.5]	293.15 - 333.15	9	0.20	[63]
{[Tetrabutylammonium][Hydrogen sulfate]:Benzilic acid}	[0.5:0.5]	293.15 - 333.15	9	0.02	[63]
{[Tetrabutylammonium][Chloride]:Glutamic acid}	[0.889:0.111]	303.15 - 353.15	6	0.03	[64]
	[0.9:0.1]		6	0.26	
	[0.909:0.091]		6	0.36	
{[Tetrabutylammonium][Chloride]:Aspartic acid}	[0.9:0.1]	303.15 - 353.15	6	0.03	[64]
	[0.909:0.091]		6	0.03	
	[0.917:0.083]		6	0.11	
{[Tetrabutylammonium][Chloride]:Arginine}	[0.857:0.143]	303.15 - 353.15	6	0.19	[64]
	[0.875:0.125]		6	0.81	
	[0.889:0.111]		6	0.52	
{[Choline][Chloride]:Ethylene glycol}	[0.33:0.67]	293.15 - 308.15	4	0.68	[65]
{[Choline][Chloride]:Ethylene glycol}	[0.33:0.67]	283.15 - 363.15	9	0.86	[66]
{[Choline][Chloride]:Oxalic acid}	[0.5:0.5]	293.15 - 308.15	4	2.68	[65]
{[Choline][Chloride]:Glycerol}	[0.5:0.5]	298.15	1	2.38	[67]
	[0.34:0.66]		1	0.54	
	[0.25:0.75]		1	1.64	
{[Choline][Chloride]:Ethylene glycol}	[0.36:0.64]	298.15	1	0.71	[67]
	[0.34:0.66]		1	0.56	
	[0.28:0.72]		1	0.04	

{[N,N-Diethylethanolammonium][Chloride]:Glycerol}	[0.34:0.66]	298.15	1	1.06	[67]
	[0.25:0.75]		1	2.73	
	[0.2:0.8]		1	3.82	
{[N,N-Diethylethanolammonium][Chloride]:Ethylene glycol}	[0.28:0.72]	298.15	1	0.36	[67]
	[0.25:0.75]		1	0.05	
	[0.2:0.8]		1	0.46	
{[Methyltriphenylphosphonium][Bromide]:Ethylene glycol}	[0.25:0.75]	298.15	1	0.35	[67]
	[0.2:0.8]		1	1.58	
	[0.16:0.84		1	2.68	
{[Methyltriphenylphosphonium][Bromide]:Triethylene glycol}	[0.25:0.75]	298.15	1	3.07	[67]
	[0.2:0.8]		1	1.88	
	[0.16:0.84		1	0.86	
{[Acetylcholine][Chloride]:1,2,4-Triazole}	[0.5:0.5]	303.15 - 363.15	7	3.48	[68]
{[Acetylcholine][Chloride]:Imidazole}	[0.4:0.6]	303.15 - 363.15	7	1.02	[68]
	[0.333:0.667]		7	1.03	
	[0.25:0.75]		7	2.99	
{[Choline][Chloride]:Guaiacol}	[0.25:0.75]	293.15 - 323.15	4	6.05	[69]
	[0.2:0.8]		4	6.79	
	[0.167:0.833]		4	6.89	
{Diethylamine hydrochloride:Guaiacol}	[0.25:0.75]	293.15 - 323.15	4	4.18	[69]
	[0.2:0.8]		4	4.92	
	[0.167:0.833]		4	5.29	
{[Acetylcholine][Chloride]:Guaiacol}	[0.25:0.75]	293.15 - 323.15	4	6.39	[69]
	[0.2:0.8]		4	6.92	
	[0.167:0.833]		4	7.64	
{[Acetylcholine][Chloride]:Levulinic acid}	[0.5:0.5]	293.15 - 343.15	11	0.81	[70]
{[Tetraethylammonium][Chloride]:Levulinic acid}	[0.5:0.5]	293.15 - 343.15	11	1.11	[70]
{[Tetraethylammonium][Bromide]:Levulinic acid}	[0.5:0.5]	293.15 - 343.15	11	1.94	[70]
{[Tetrabutylammonium][Chloride]:Levulinic acid}	[0.5:0.5]	293.15 - 343.15	11	1.04	[70]
{[Tetrabutylammonium][Bromide]:Levulinic acid}	[0.5:0.5]	293.15 - 343.15	11	0.81	[70]
{[Choline][Chloride]:Urea}	[0.333:0.667]	303.15	1	0.60	[71]
{[Choline][Chloride]:Acetamide}	[0.333:0.667]	303.15	1	7.48	[71]
{[Choline][Chloride]:Ethylene glycol}	[0.333:0.667]	303.15	1	0.58	[71]
{[Choline][Chloride]:Glycerol}	[0.333:0.667]	303.15	1	0.20	[71]
{[Choline][Chloride]:Triethylene glycol}	[0.2:0.8]	303.15	1	0.71	[71]
{[Choline][Chloride]:Xylitol}	[0.5:0.5]	303.15	1	2.98	[71]
{[Choline][Chloride]:D-Sorbitol}	[0.5:0.5]	303.15	1	3.85	[71]
{[Choline][Chloride]:p-Toluenesulfonic acid}	[0.5:0.5]	303.15	1	3.78	[71]
{[Choline][Chloride]:Oxalic acid}	[0.5:0.5]	303.15	1	0.08	[71]
{[Choline][Chloride]:Malic acid}	[0.5:0.5]	303.15	1	0.28	[71]
{[Choline][Chloride]:Citric acid}	[0.5:0.5]	303.15	1	2.17	[71]

{[Choline][Chloride]:Sucrose :Water}	[0.417:0.166 :0.417]	303.15	1	1.40	[71]
{[Choline][Chloride]:Fructose :Water}	[0.417:0.166 :0.417]	303.15	1	2.92	[71]
{[Choline][Chloride]:Maltose :Water}	[0.417:0.166 :0.417]	303.15	1	2.12	[71]
{[Methyltriphenylphosphonium] [Bromide]:Ethylene glycol}	[0.2:0.8]	298.15 - 358.15	7	1.61	[72]
{Menthol:Caprylic acid}	[0.6:0.4]	278.15 - 373.15	20	2.26	[73]
{Menthol:Myristic acid}	[0.8:0.2]	298.15 - 373.15	16	1.43	[73]
{Menthol:Palmitic acid}	[0.85:0.15]	313.15 - 373.15	13	2.06	[73]
{Menthol:Stearic acid}	[0.9:0.1]	313.15 - 373.15	13	2.18	[73]
{Thymol:Capric acid}	[0.5:0.5]	293.15 - 373.15	17	0.88	[73]
{Thymol:Lauric acid}	[0.55:0.45]	303.15 - 373.15	15	0.77	[73]
{Thymol:Myristic acid}	[0.75:0.25]	313.15 - 373.15	13	2.77	[73]
{Thymol:Palmitic acid}	[0.8:0.2]	313.15 - 373.15	13	3.40	[73]
{Menthol:Thymol}	[0.5:0.5]	298.15 - 353.15	7	2.32	[74]
{Menthol:Sesamol}	[0.5:0.5]	298.15 - 353.15	7	1.40	[74]
{Menthol:3-Hydroxybenzoic acid}	[0.875:0.125]	298.15 - 353.15	7	0.20	[74]
{Menthol:Octanoic acid}	[0.5:0.5]	293.15 - 343.15	11	3.13	[75]
{Menthol:Decanoic acid}	[0.5:0.5]	293.15 - 343.15	11	1.94	[75]
{Dodecanoic acid:Decanoic acid}	[0.333:0.667]	298.15 - 343.15	10	4.99	[75]
{[Choline][Chloride]:Citric acid}	[0.5:0.5]	296.15	1	5.14	[76]
{[Choline][Chloride]:D-(+)-Sucrose}	[0.8:0.2]	296.15	1	4.59	[76]
	[0.5:0.5]		1	2.66	
{[1-Ethyl-3-methylimidazolium] [Chloride]:Ethylene glycol}	[0.667:0.333]	293.15 - 333.15	5	0.05	[77]
	[0.5:0.5]		5	0.71	
	[0.333:0.667]		5	1.12	
{[Choline][Chloride]:Resorcinol}	[0.333:0.667]	283.15 - 338.15	23	2.52	[78]
{Thymol:Camphor}	[0.7:0.3]	298.15	1	4.33	[79]
	[0.6:0.4]		1	5.10	
	[0.5:0.5]		1	6.89	
{Thymol:10-Undecylenic acid}	[0.7:0.3]	298.15	1	0.34	[79]
	[0.6:0.4]		1	1.99	
	[0.5:0.5]		1	3.40	
	[0.333:0.667]		1	5.40	
	[0.25:0.75]		1	6.29	
	[0.2:0.8]		1	6.94	
{Thymol:Decanoic acid}	[0.6:0.4]	298.15	1	0.71	[79]
	[0.5:0.5]		1	0.22	
	[0.333:0.667]		1	1.16	
	[0.25:075]		1	2.27	
{[Choline][Chloride]:Diglycolic acid}	[0.5:0.5]	293.15 - 333.15	9	1.33	[80]
{[Tetrabutylammonium][Hydrogen sulfate]:Diglycolic acid}	[0.5:0.5]	293.15 - 333.15	9	0.82	[80]
{Betaine:Lactic acid}	[0.5:0.5]	293.15 - 363.15	15	0.50	[81]
{Alanine:Malic acid}	[0.5:0.5]	298.15 - 363.15	14	14.25	[81]
{[Choline][Chloride]:Phenol}	[0.25:0.75]	293.15 - 333.15	5	1.05	[82]
	[0.2:0.8]		5	1.54	

{[Choline][Chloride]:Ethylene glycol}	[0.333:0.667]	283.15 - 323.15	5	0.61	[83]
{[Choline][Chloride]:Ethylene glycol}	[0.333:0.667]	333.15	1	0.64	[84]
{[Choline][Chloride]:Ethylene glycol}	[0.333:0.667]	283.15 - 363.15	9	0.54	[85]
{[Choline][Chloride]:Glycerol}	[0.333:0.667]	283.15 - 363.15	9	0.70	[85]
{[Choline][Chloride]:Urea}	[0.333:0.667]	293.15 - 363.15	8	0.04	[85]
{Ninhydrin:[Tetrabutylammonium][Chloride]}	[0.571:0.429]	293.15 - 333.15	9	2.38	[86]
	[0.4:0.6]		9	2.91	
{[Choline][Chloride]:Phenol}	[0.333:0.667]	298.15	1	0.20	[87]
	[0.25:0.75]		1	0.96	
	[0.2:0.8]		1	1.45	
	[0.167:0.833]		1	1.72	
	[0.143:0.857]		1	1.97	
{[Choline][Chloride]:2,6-Dimethylphenol}	[0.333:0.667]	298.15	1	6.96	[87]
	[0.25:0.75]		1	8.37	
	[0.2:0.8]		1	9.20	
	[0.167:0.833]		1	8.78	
	[0.143:0.857]		1	10.07	
{[Choline][Chloride]:Urea}	[0.333:0.667]	298 - 358	5	0.46	[88]
{[Choline][Chloride]:Urea:Tetraethylene glycol}	[0.317:0.633:0.05]	298 - 358	5	0.31	[88]
	[0.3:0.6:0.1]		5	0.37	
	[0.267:0.533:0.2]		5	0.22	
	[0.283:0.567:0.15]		5	0.19	
	[0.2:0.4:0.4]		5	0.07	
	[0.133:0.267:0.6]		5	0.60	
	[0.067:0.133:0.8]		5	1.56	
{[Choline][Chloride]:Ethylene glycol}	[0.333:0.667]	293.15 - 333.15	9	0.60	[89]
	[0.250:0.750]		9	0.19	
	[0.200:0.800]		9	0.70	
	[0.167:0.833]		9	0.95	
	[0.143:0.857]		9	1.23	
{[Choline][Chloride]:1,2-Propanediol}	[0.303:0.697]	293.15 - 333.15	9	3.77	[89]
	[0.200:0.800]		9	3.03	
	[0.167:0.833]		9	3.02	
	[0.143:0.857]		9	3.02	
{[Choline][Chloride]:1,3-Propanediol}	[0.249:0.751]	293.15 - 333.15	9	2.15	[89]
	[0.200:0.800]		9	1.96	
	[0.167:0.833]		9	1.79	
	[0.143:0.857]		9	1.78	
		Total	**2607**		

Table S.C25. Description of the dataset used to assess the performances of the density group contribution model (Dataset D2, not used in the optimization) with the average deviations between experimental and calculated densities

System	Ratio	Temperature range (K)	Number of data points	Average deviation (%)	Reference
{[Methyltriphenylphosphonium][Bromide]:Glycerol}	[0.33:0.67]	298.15 - 368.15	15	4.23	[2]
	[0.25:0.75]		15	1.44	
	[0.2:0.8]		15	0.01	
{[Tetrabutylammonium][Chloride]:Ethylene glycol}	[0.333:0.667]	293.15 - 353.15	7	6.44	[3]
	[0.25:0.75]		7	7.39	
	[0.2:0.8]		7	7.96	
{[Benzyltrimethylammonium][Chloride]:Ethylene glycol}	[0.5:0.5]	293.15 - 323.15	7	0.64	[4]
{[Choline][Chloride]:Ethylene glycol}	[0.333:0.667]	293.15	1	1.41	[5]
	[0.286:0.714]	298.15	1	0.01	
{[Choline][Chloride]:Glucose}	[0.667:0.333]	298.15	1	0.64	[5]
{[Methyltriphenylphosphonium][Bromide]:Glycerol}	[0.333:0.667]	298.15	1	5.72	[5]
	[0.2:0.8]		1	0.01	
{[Choline][Chloride]:Malonic acid}	[0.5:0.5]	303.15	1	4.46	[5]
{[Choline][Chloride]:1,4-Butanediol}	[0.2:0.8]	303.15 - 343.15	9	3.61	[6]
	[0.25:0.75]		9	3.71	
{[Tetrabutylammonium][Bromide]:Polyethylene glycol 400	[0.3115 :0.6885]	298.15 - 343.15	10	0.18	[8]
	[0.2506 :0.7494]		10	0.12	
{[Choline][Chloride]:D-Xylose}	[0.5:0.5]	293.15 - 353.15	13	0.69	[9]
{[Choline][Chloride]:D-Glucose}	[0.5:0.5]	293.15 - 353.15	13	0.06	[9]
{[Acetylcholine][Chloride]:D-Mannose}	[0.5:0.5]	293.15 - 353.15	13	0.53	[9]
{[Acetylcholine][Chloride]:D-Fructose}	[0.5:0.5]	293.15 - 353.15	13	2.29	[9]
{[Benzyldimethyl(2-hydroxyethyl)ammonium][Chloride]:D-Xylose}	[0.5:0.5]	293.15 - 353.15	13	3.28	[9]
{[Benzyldimethyl(2-hydroxyethyl)ammonium][Chloride]:D-Glucose}	[0.5:0.5]	293.15 - 353.15	13	2.95	[9]
{[Benzyltripopylammonium][Chloride]:Ethylene glycol	[0.25:0.75]	293.15 - 343.15	11	1.42	[12]
{[Choline][Chloride]:1,4-Butanediol}	[0.25:0.75]	293.15 - 323.15	4	3.77	[14]
	[0.2:0.8]		4	3.81	
{[Choline][Chloride]:Glucose}	[0.667:0.333]	303.15 - 353.15	6	0.77	[16]
{[Choline][Chloride]:Malonic acid}	[0.5:0.5]	293.15 - 348.15	12	0.17	[21]
{[Choline][Chloride]:Levulinic acid}	[0.333:0.667]	293.15 - 348.15	12	0.26	[21]
{[Choline][Chloride]:Levulinic acid}	[0.25:0.75]	303.15 - 333.15	4	0.49	[22]
	[0.2:0.8]		4	0.91	
	[0.167:0.833]		4	1.20	
{[Choline][Chloride]:o-Cresol}	[0.333:0.667]	298.2	1	0.29	[23]

	[0.25:0.75]	298.2	1	1.14	
	[0.204:0.796]	298.2	1	1.57	
	[0.167:0.833]	298.2	1	1.94	
	[0.143:0.857]	298.2	1	2.14	
{[Choline][Chloride]:p-Cresol}	[0.333:0.667]	293.15 - 333.15	9	0.53	[24]
{[Tetrabutylammonium][Chloride] :Ethylene glycol}	[0.333:0.667]	288.15 - 338.15	11	4.35	[27]
{[Methyltriphenylphosphonium] [Bromide]:Glycerol}	[0.25:0.75]	298.15 - 328.15	7	1.42	[34]
{DL-Menthol:Lauric acid}	[0.667:0.333]	293.15 - 353.15	13	0.29	[38]
{Menthol:Capric acid}	[0.5:0.5]	298.15	1	0.98	[39]
{DL-Menthol:Oleyl alcohol}	[0.5:0.5]	293.15 - 363.15	8	0.03	[40]
{Menthol:Lauric acid}	[0.5:0.5]	298.15 - 310.15	2	0.58	[90]
	[0.667:0.333]		2	0.11	
	[0.75:0.25]		2	0.47	
	[0.8:0.2]		2	0.70	
	[0.9:0.1]		2	1.05	
{DL-Menthol:Lauric acid	[0.667:0.333]	293.15 - 353.15	7	0.25	[91]
{Dodecanoic acid:Octanoic acid}	[0.25:0.75]	353.15 - 413.15	5	7.02	[44]
{[Benzyltrimethylammonium] [Chloride]:Ethylene glycol}	[0.25:0.75]	283.15 - 343.15	13	0.21	[45]
{[Benzyltributylammonium] [Chloride]:Glycerol}	[0.25:0.75]	283.15 - 343.15	13	3.03	[45]
{Xylose:[Choline][Chloride] :Water}	[0.2:0.4:0.4]	313.15	1	2.71	[53]
{Glucose:[Choline][Chloride] :Water}	[0.166:0.417 :0.417]	313.15	1	3.51	[53]
{[Choline][Chloride]:D-Glucose}	[0.5:0.5]	298.15 - 358.15	2	1.96	[92]
	[0.667:0.333]	358.15	1	0.91	
{[Choline][Chloride]:Malonic acid}	[0.5:0.5]	293.15 - 308.15	4	0.51	[65]
{[Choline][Chloride]:Malonic acid}	[0.33:0.67]	283.15 - 363.15	9	5.06	[66]
{[Choline][Chloride]:1,4- Butanediol}	[0.34:0.66]	298.15	1	3.01	[67]
	[0.28:0.72]		1	2.77	
	[0.25:0.75]		1	2.94	
{[Methyltriphenylphosphonium] [Bromide]:Glycerol}	[0.34:0.66]	298.15	1	4.54	[67]
	[0.25:0.75]		1	1.43	
	[0.2:0.8]		1	0.04	
{[Choline][Chloride]:Levulinic acid}	[0.5:0.5]	293.15 - 343.15	11	1.87	[70]
{[Choline][Chloride] :1,4-Butanediol}	[0.2:0.8]	303.15	1	3.86	[71]
{[Choline][Chloride]:Levulinic acid}	[0.333:0.667]	303.15	1	0.44	[71]
{[Choline][Chloride]:Malonic acid}	[0.5:0.5]	303.15	1	2.66	[71]
{[Choline][Chloride]:Tartaric acid}	[0.5:0.5]	303.15	1	4.45	[71]
{[Choline][Chloride]:Xylose:Water}	[0.333:0.333 :0.333]	303.15	1	0.36	[71]
{[Choline][Chloride]:Glucose :Water}	[0.417:0.166 :0.417]	303.15	1	3.76	[71]
{[Methyltriphenylphosphonium] [Bromide]:Glycerol}	[0.364:0.636]	298.15 - 358.15	7	7.05	[72]
{Trimethylglycine:Glycolic acid}	[0.333:0.667]	298.15 - 388.15	5	5.93	[93]

{Trimethylglycine:Oxalic acid}	[0.333:0.667]	348.15 - 388.15	4	1.91	[93]
{Trimethylglycine:D-(+)-Mandelic acid}	[0.333:0.667]	298.15 - 388.15	5	1.72	[93]
{Trimethylglycine:Phenylacetic acid}	[0.333:0.667]	298.15 - 388.15	5	2.18	[93]
{Trimethylglycine:2-Furoic acid}	[0.333:0.667]	303.15 - 363.15	5	1.87	[93]
{Trimethylglycine:2-Chlorobenzoic acid}	[0.333:0.667]	338.15 - 373.15	4	6.04	[93]
{Trimethylglycine:4-Chlorobenzoic acid}	[0.333:0.667]	338.15 - 373.15	4	4.53	[93]
{Trimethylglycine:Benzoic acid}	[0.333:0.667]	353.15 - 373.15	3	4.63	[93]
{Ethylamine hydrochloride:Acetamide}	[0.5:0.5]	313.15 - 353.15	5	1.66	[94]
	[0.333:0.667]		5	3.26	
	[0.25:0.75]		5	5.87	
{Menthol:Capric acid}	[0.6:0.4]	283.15 - 373.15	19	1.14	[73]
{Menthol:Lauric acid}	[0.75:0.25]	298.15 - 373.15	16	0.61	[73]
{Dodecanoic acid:Octanoic acid}	[0.25:0.75]	293.15 - 343.15	11	7.05	[75]
{Menthol:Oleyl alcohol}	[0.5:0.5]	298.15 - 353.15	12	0.03	[95]
{[Choline][Chloride]:D-(+)-Glucose}	[0.5:0.5]	296.15	1	0.42	[76]
{[Choline][Chloride]:L-(+)-Tartaric acid}	[0.667:0.333]	296.15	1	2.39	[76]
{[Choline][Chloride]:D-(+)-Xylose}	[0.667:0.333]	296.15	1	0.31	[76]
	[0.75:0.25]		1	0.49	
{Citric acid:D-(+)-Sucrose}	[0.5:0.5]	296.15	1	8.40	[76]
{Citric acid:D-(+)-Glucose}	[0.5:0.5]	296.15	1	0.73	[76]
{D-(+)-Glucose: L-(+)-Tartaric acid}	[0.5:0.5]	296.15	1	3.67	[76]
{Thymol:Caprylic acid}	[0.421:0.579]	278.15 - 373.15	20	3.30	[73]
{Thymol:Stearic acid}	[0.9:0.1]	318.15 - 373.15	12	3.97	[73]
{Glycolic acid:Xylitol}	[0.5:0.5]	303.15 - 343.15	5	9.88	[96]
	[0.333:0.667]		5	7.32	
	[0.25:0.75]		5	5.91	
	[0.2:0.8]		5	4.93	
{Betaine:Malic acid}	[0.5:0.5]	318.15 - 363.15	10	0.68	[81]
{Alanine:Lactic acid}	[0.5:0.5]	293.15 - 363.15	15	12.64	[81]
{[Choline][Chloride]:o-Cresol}	[0.333:0.667]	298.15	1	0.31	[87]
	[0.25:0.75]		1	0.62	
	[0.2:0.8]		1	1.24	
	[0.167:0.833]		1	1.66	
	[0.143:0.857]		1	1.98	
{[Choline][Chloride] :3-Methylphenol}	[0.333:0.667]	298.15	1	0.25	[87]
	[0.25:0.75]		1	0.69	
	[0.2:0.8]		1	1.30	
	[0.167:0.833]		1	1.75	
	[0.143:0.857]		1	1.99	
{[Choline][Chloride]:p-Cresol}	[0.333:0.667]	298.15	1	0.22	[87]
	[0.25:0.75]		1	0.76	
	[0.2:0.8]		1	1.36	
	[0.167:0.833]		1	1.75	
	[0.143:0.857]		1	2.07	
	[0.333:0.667]	298.15	1	5.73	[87]

{[Choline][Chloride] :4-Ethylphenol}	[0.25:0.75]		1	6.45	
	[0.2:0.8]		1	7.27	
	[0.167:0.833]		1	7.72	
	[0.143:0.857]		1	7.67	
{[Choline][Chloride] :p-Chlorophenol}	[0.333:0.667]	298.15	1	0.04	[87]
	[0.25:0.75]		1	0.24	
	[0.2:0.8]		1	0.38	
	[0.167:0.833]		1	0.43	
	[0.143:0.857]		1	0.52	
{[Choline][Chloride] :1,4-Butanediol}	[0.248:0.752]	293.15 - 333.15	9	3.89	[89]
	[0.200:0.800]		9	3.73	
	[0.167:0.833]		9	3.69	
	[0.142:0.858]		9	3.71	
		Total	**659**		

Table S.C26. List of the systems found in the datasets for the heat capacities of DESs along with the corresponding number of data points available

System	Number of data points
Betaine : Ethylene glycol	10
Choline chloride : Citric acid	23
Choline chloride : Ethylene glycol	11
Choline chloride : Fructose	23
Choline chloride : Glucose	23
Choline chloride : Glycerol	36
Choline chloride : Glycerol : Water	25
Choline chloride : Malonic acid	23
Choline chloride : Oxalic acid	23
Choline chloride : Phenol	36
Choline chloride : Resorcinol	23
Choline chloride : Triethylene glycol	23
Choline chloride : Urea	22
Choline chloride : Urea : L-Arginine	44
Lactic acid : Betaine : Water	8
L-Carnitine : Ethylene glycol	10
Malic acid : Betaine : Water	8
Methyltriphenylphosphonium bromide : Ethylene glycol	23
Methyltriphenylphosphonium bromide : Glycerol	23
Methyltriphenylphosphonium bromide : Malonic acid	23
N,N-Diethylethanolammonium chloride : Ethylene glycol	11
N,N-Diethylethanolammonium chloride : Glycerol	11
Tetrabutylammonium chloride : Ethylene glycol	23
Tetrabutylammonium chloride : Glycerol	23
Tetrabutylammonium chloride : Malonic acid	23
Tetrabutylammonium chloride : Triethylene glycol	23
Tetrabutylammonium chloride : Urea	19
Total	**573**

Table S.C27. Dataset used in the optimization of the parameters for the group contribution model for heat capacity (Dataset H1) with the average deviations between calculated and experimental data

System	Ratio	Temperature range (K)	Number of data points	Average deviation (%)	Reference
{[Choline][Chloride]:Triethylene glycol}	[0.333:0.667]	298.15 - 353.15	23	0.35	[97]
{[Choline][Chloride]:Malonic acid}	[0.5:0.5]	298.15 - 353.15	23	0.58	[97]
{[Choline][Chloride]:Citric acid}	[0.333:0.667]	298.15 - 353.15	23	0.18	[97]
{[Choline][Chloride]:Oxalic acid}	[0.333:0.667]	298.15 - 353.15	23	27.53	[97]
{[Choline][Chloride]:Fructose}	[0.667:0.333]	298.15 - 353.15	23	0.86	[97]
{[Choline][Chloride]:Glucose}	[0.667:0.333]	298.15 - 353.15	23	0.47	[97]
{[N,N-Diethylethanolammonium] [Chloride]:Glycerol}	[0.333:0.667]	303.15 - 353.15	11	4.40	[98]
{[N,N-Diethylethanolammonium] [Chloride]:Ethylene glycol}	[0.333:0.667]	303.15 - 353.15	11	0.84	[98]
{[Tetrabutylammonium][Chloride]:Glycerol}	[0.167:0.833]	298.15 - 353.15	23	0.85	[97]
{[Tetrabutylammonium][Chloride]:Urea}	[0.2:0.8]	308.15 - 353.15	19	7.87	[97]
{[Tetrabutylammonium][Chloride]:Ethylene glycol}	[0.25:0.75]	298.15 - 353.15	23	2.21	[97]
{[Tetrabutylammonium][Chloride] :Malonic acid}	[0.25:0.75]	298.15 - 353.15	23	1.31	[97]
{Betaine:Ethylene glycol}	[0.25:0.75]	318.15 - 363.15	10	1.22	[99]
{L-Carnitine:Ethylene glycol}	[0.25:0.75]	318.15 - 363.15	10	4.70	[99]
{[Methyltriphenylphosphonium][Bromide] :Malonic acid}	[0.4:0.6]	298.15 - 353.15	23	0.11	[97]
{[Methyltriphenylphosphonium][Bromide] :Glycerol}	[0.25:0.75]	298.15 - 353.15	23	10.24	[97]
{[Methyltriphenylphosphonium][Bromide] :Ethylene glycol}	[0.2:0.8]	298.15 - 353.15	23	0.09	[97]
{[Choline][Chloride]:Urea}	[0.333:0.667]	303.15 - 353.15	11	0.03	[25]
			11	0.41	[100]
{[Choline][Chloride]:Urea:L-Arginine}	[0.328:0.656 :0.016]	303.15 - 353.15	11	0.03	[25]
	[0.323:0.645 :0.032		11	0.04	
	[0.317:0.635 :0.048]		11	0.03	
	[0.3125:0.625 :0.0625]		11	0.03	
{Lactic acid:Betaine:Water}	[0.4:0.2:0.4]	298.15 - 360.15	8	1.36	[101]
{Malic acid:Betaine:Water}	[0.167:0.333 :0.5]	298.15 - 360.15	8	0.28	[101]
		Total	**419**		

Table S.C28. Dataset not used in the optimization of the parameters for the group contribution model for heat capacity (Dataset H2) with the average deviations between calculated and experimental data

System	Ratio	Temperature range (K)	Number of data points	Average deviation (%)	Reference
{[Choline][Chloride]:Ethylene glycol}	[0.333:0.667]	303.15 - 353.15	11	1.50	[100]
{[Choline][Chloride]:Glycerol}	[0.333:0.667]	303.15 - 353.15	11	3.93	[100]
		278.15 - 338.15	25	2.96	[102]
{[Choline][Chloride]:Glycerol:Water}	[0.250:0.496 :0.254	278.15 - 338.15	25	0.65	[102]
{[Choline][Chloride]:Phenol}	[0.25:0.75]	298.15 - 353.15	23	0.11	[97]
	[0.333:0.667]	303.15 - 361.15	13	8.24	[103]
{[Choline][Chloride]:Resorcinol}	[0.333:0.667]	283.15 - 338.15	23	2.42	[78]
{[Tetrabutylammonium][Chloride] :Triethylene glycol}	[0.5:0.5]	298.15 - 353.15	23	6.07	[97]
		Total	**154**		

Table S.C29. Pool of data D3 used for the comparison between the model of Haghbakhsh et al. [104] and the model presented in this work for the prediction of densities

System	Ratio	Temperature range (K)	Number of data points	Average deviation, Haghbakhsh et al. [121] (%)	Average deviation, this work (%)	Reference
{[Acetylcholine][Chloride] :1,2,4-Triazole}	[0.5:0.5]	303.15 - 363.15	7	0.72	3.48	[71]
{[Acetylcholine][Chloride] :D-Fructose}	[0.5:0.5]	293.15 - 353.15	13	1.03	2.29	[9]
{[Acetylcholine][Chloride] :D-Glucose}	[0.5:0.5]	293.15 - 353.15	13	0.65	0.20	[9]
{[Acetylcholine][Chloride] :D-Mannose}	[0.5:0.5]	293.15 - 353.15	13	0.15	0.53	[9]
{[Acetylcholine][Chloride] :D-Ribose}	[0.5:0.5]	293.15 - 353.15	13	0.25	0.48	[9]
{[Acetylcholine][Chloride] :D-Xylose}	[0.5:0.5]	293.15 - 353.15	13	0.21	0.69	[9]
{[Acetylcholine][Chloride] :Guaiacol}	[0.25:0.75]	293.15 - 323.15	4	0.31	6.39	[72]
	[0.2:0.8]		4	0.32	6.92	
	[0.167:0.833]		4	0.3	7.64	
{[Acetylcholine][Chloride] :Imidazole}	[0.4:0.6]	303.15 - 363.15	7	0.43	1.02	[71]
	[0.333:0.667]		7	0.93	1.03	
	[0.25:0.75]		7	0.76	2.99	
{[Acetylcholine][Chloride] :Levulinic acid}	[0.5:0.5]	293.15 - 343.15	11	1.48	0.81	[73]
	[0.25:0.75]	303.15 - 333.15	4	0.53	1.07	[10]

{[Allyltriphenylphosphonium][Bromide]:Diethylene glycol}	[0.2:0.8]	293.15 - 343.15	11	0.71	1.37	[11]
	[0.091:0.909]		11	0.49	0.98	
	[0.059:0.941]		11	2.09	1.58	
{[Allyltriphenylphosphonium][Bromide]:Triethylene glycol}	[0.2:0.8]	293.15 - 343.15	11	0.68	2.56	[11]
	[0.091:0.909]		11	1.88	0.57	
	[0.059:0.941]		11	0.41	1.12	
{[Benzyltripropylammonium][Chloride]:Ethylene glycol}	[0.25:0.75]	293.15 - 343.15	11	0.68	1.42	[12]
{[Benzyltripropylammonium][Chloride]:Glycerol}	[0.25:0.75]	293.15 - 343.15	11	3.32	1.45	[12]
{[Benzyltripropylammonium][Chloride]:Lactic acid}	[0.25:0.75]	293.15 - 343.15	11	1.92	1.90	[12]
{[Choline][Chloride]:Oxalic acid}	[0.5:0.5]	293.15 - 348.15	12	9.73	1.29	[21]
{[Benzyltripropylammonium][Chloride]:Phenol}	[0.25:0.75]	293.15 - 343.15	11	0.70	1.35	[12]
{Betaine:Lactic acid}	[0.333:0.667]	298.15 - 343.15	10	0.88	0.42	[13]
	[0.167:0.833]	293.15 - 343.15	11	1.09	1.95	
{Betaine:Levulinic acid}	[0.333:0.667]	293.15 - 343.15	11	1.41	$5.5*10^{-3}$	[13]
{[Benzyldimethyl(2-hydroxyethyl)ammonium][Chloride]:D-Fructose}	[0.5:0.5]	293.15 - 353.15	13	1.79	1.59	[9]
{[Benzyldimethyl(2-hydroxyethyl)ammonium][Chloride]:D-Glucose}	[0.5:0.5]	293.15 - 353.15	13	0.26	2.95	[9]
{[Benzyldimethyl(2-hydroxyethyl)ammonium][Chloride]:D-Mannose}	[0.5:0.5]	293.15 - 353.15	13	0.37	2.30	[9]
{[Benzyldimethyl(2-hydroxyethyl)ammonium][Chloride]:D-Ribose}	[0.5:0.5]	293.15 - 353.15	13	0.32	2.50	[9]
{[Benzyldimethyl(2-hydroxyethyl)ammonium][Chloride]:D-Xylose}	[0.5:0.5]	293.15 - 353.15	13	1.30	3.28	[9]
{[Choline][Chloride]:1,2-Propanediol}	[0.25:0.75]	293.15 - 323.15	4	1.01	3.49	[14]
	[0.2:0.8]		4	0.74	2.77	
{[Choline][Chloride]:1,4-Butanediol}	[0.25:0.75]	293.15 - 323.15	4	0.35	3.77	[14]
	[0.2:0.8]		4	0.85	3.81	
		303.15	1		3.86	[74]
{[Choline][Chloride]:2,3-Butanediol}	[0.25:0.75]	293.15 - 323.15	4	0.68	4.03	[14]
	[0.2:0.8]		4	1.22	4.25	
{[Choline][Chloride]:Acetamide}	[0.333:0.667]	303.15	1	3.80	7.48	[74]

{[Choline][Chloride]:Citric acid}	[0.5:0.5]	303.15	1	11.57	2.17	[74]
	[0.5:0.5]	296.15	1		5.14	[82]
{[Choline][Chloride]:Fructose}	[0.5:0.5]	298.15 - 358.15	7	4.24	4.29	[15]
	[0.4:0.6]		7	2.66	1.65	
	[0.333:0.667]		7	1.29	0.50	
	[0.286:0.714]		7	0.34	2.01	
{[Choline][Chloride]:Glucose}	[0.5:0.5]	296.15	1	0.63	0.42	[82]
	[0.667:0.333]	303.15 - 353.15	6	1.18	0.77	[16]
{[Choline][Chloride]:Mannose}	[0.5:0.5]	293.15 - 353.15	13	0.13	0.37	[9]
{[Choline][Chloride]:Ribose}	[0.5:0.5]	293.15 - 353.15	13	0.66	0.68	[9]
{[Choline][Chloride]:D-Sorbitol}	[0.5:0.5]	303.15	1	4.31	3.85	[74]
{[Choline][Chloride]:D-Sucrose}	[0.5:0.5]	296.15	1	1.44	2.67	[82]
{[Choline][Chloride]:D-Xylose}	[0.667:0.333]	296.15	1	19.28	0.31	[82]
{[Choline][Chloride]:D-Sucrose}	[0.8:0.2]	296.15	1	12.54	4.59	[82]
{[Choline][Chloride]:Xylose}	[0.5:0.5]	293.15 - 353.15	13	0.08	0.69	[9]
	[0.75:0.25]	296.15	1	0.01	0.49	[82]
{[Choline][Chloride]:Ethylene glycol}	[0.36:0.64]	298.15 - 368.15	15	1.08	0.85	[2]
	[0.333:0.667]	298.15 - 333.15	8	0.79	0.57	[18]
		283.15 - 363.15	9		0.86	[69]
		308.15 - 363.15	12		0.60	[19]
		303.15	1		0.58	[74]
	[0.33:0.67]	298.15 - 368.15	15	0.94	0.53	[2]
	[0.28:0.72]		15	0.82	0.01	
{[Choline][Chloride]:Glutaric acid}	[0.5:0.5]	293.15 - 353.15	13	1.55	2.48	[21]
{[Choline][Chloride]:Glycerol}	[0.5:0.5]	298.15 - 368.15	15	2.50	3.15	[2]
	[0.333:0.667]	303.15	1	0.99	0.20	[74]
		298.15 - 333.15	8		0.46	[18]
		283.15 - 363.15	9		0.36	[20]
	[0.33:0.67]	298.15 - 368.15	15	0.76	0.61	[2]
	[0.25:0.75]	298.15 - 368.15	15	0.77	1.79	

{[Choline][Chloride]:Glycolic acid}	[0.5:0.5]	293.15 - 353.15	13	1.22	0.20	[21]
{[Choline][Chloride]:Guaiacol}	[0.25:0.75]	293.15 - 323.15	4	0.66	6.05	[72]
	[0.2:0.8]		4	0.85	6.79	
	[0.167:0.833]		4	0.52	6.89	
{[Choline][Chloride]:Levulinic acid}	[0.5:0.5]	293.15 - 343.15	11	0.80	1.87	[73]
	[0.333:0.667]	303.15	1	0.75	0.44	[74]
		293.15 - 348.15	12		0.26	[21]
	[0.25:0.75]	303.15 - 333.15	4	0.41	0.49	[22]
	[0.2:0.8]		4	0.91	0.91	
	[0.167:0.833]		4	2.60	1.20	
{[Choline][Chloride]:Malonic acid}	[0.5:0.5]	303.15	1	2.41	1.47	[74]
		293.15 - 348.15	12		0.17	[21]
	[0.333:0.667]	283.15 - 363.15	9	3.67	5.06	[69]
{[Choline][Chloride]:Furfuryl alcohol}	[0.25:0.75]	303.15 - 333.15	4	0.45	1.00	[22]
	[0.2:0.8]		4	0.46	0.73	
	[0.167:0.833]		4	0.42	0.51	
{[Choline][Chloride]:o-Cresol}	[0.333:0.667]	298.2	1	1.47	0.29	[23]
	[0.25:0.75]		1	0.83	1.14	
	[0.204:0.796]		1	0.71	1.57	
	[0.167:0.833]		1	0.91	1.9	
	[0.143:0.857]		1	1.40	2.1	
{[Choline][Chloride]:Oxalic acid}	[0.5:0.5]	303.15	1	2.09	0.08	[74]
{[Choline][Chloride]:p-Chlorophenol}	[0.333:0.667]	293.15 - 333.15	9	0.68	0.56	[24]
{[Choline][Chloride]:p-Cresol}	[0.333:0.667]	293.15 - 333.15	9	3.38	0.53	[24]
{[Choline][Chloride]:Phenol}	[0.333:0.667]	293.15 - 318.15	6	0.42	0.46	[23]
	[0.25:0.75]		6	0.38	0.89	
	[0.2:0.8]		6	0.42	1.35	
	[0.167:0.833]		6	0.29	1.64	
	[0.143:0.857]		6	0.42	1.84	
{[Choline][Chloride]:p-Toluenesulfonic acid}	[0.5:0.5]	303.15	1	0.12	3.78	[74]
	[0.5:0.5]	303.15	1	4.98	4.45	[74]

{[Choline][Chloride]:Tartaric acid}	[0.667:0.333]	296.15	1	9.94	2.39	[82]
{[Choline][Chloride]:Triethylene glycol}	[0.333:0.667]	303.15 - 353.15	6	1.63	0.25	[16]
{[Choline][Chloride]:Triethylene glycol}	[0.2:0.8]	303.15	1	1.69	0.71	[74]
{[Choline][Chloride]:Urea}	[0.333:0.667]	303.15	1	0.58	0.60	[74]
		293.15 - 363.15	8		0.25	[17]
		298.15 - 353.15	12		$9.2*10^{-3}$	[25]
{[Choline][Chloride]:Xylitol}	[0.5:0.5]	303.15	1	1.90	2.98	[74]
{Citric acid:D-Glucose}	[0.5:0.5]	296.15	1	2.52	0.73	[82]
{D-Glucose:Tartaric acid}	[0.5:0.5]	296.15	1	5.05	3.67	[82]
{Diethylamine hydrochloride :Guaiacol}	[0.25:0.75]	293.15 - 323.15	4	0.53	4.18	[72]
	[0.2:0.8]		4	0.44	4.92	
	[0.167:0.833]		4	0.53	5.29	
{L-Proline:Lactic acid}	[0.5:0.5]	293.15 - 343.15	11	0.66	0.06	[13]
{L-Proline:Levulinic acid}	[0.333:0.667]	293.15 - 343.15	11	0.63	0.44	[13]
{[Methyltriphenylphosphonium] [Bromide] : Ethylene glycol}	[0.25:0.75]	298.15 - 368.15	15	1.25	0.38	[2]
	[0.2:0.8]	298.15 - 368.15	15	0.73	1.62	[2]
		298.15 - 358.15	7		1.61	[75]
	[0.16:0.84]	298.15 - 368.15	15	0.70	2.68	[2]
{[Methyltriphenylphosphonium] [Bromide] : Glycerol}	[0.364:0.636]	298.15 - 358.15	7	0.87	7.05	[75]
	[0.33:0.67]	298.15 - 368.15	15	0.87	4.23	[2]
	[0.25:0.75]	298.15 - 368.15	15	0.75	1.44	
	[0.2:0.8]	298.15 - 368.15	15	1.31	0.01	
{[N,N-Diethylethanolammonium] [Chloride]:Ethylene glycol}	[0.333:0.667]	298.15 - 343.15	10	0.76	0.85	[35]
	[0.33:0.67]	298.15 - 368.15	15	1.40	2.26	[2]
	[0.25:0.75]	298.15 - 368.15	15	1.02	1.58	
	[0.2:0.8]	298.15 - 368.15	15	1.32	1.38	
	[0.333:0.667]	298.15 - 343.15	10	0.67	0.38	[35]

{[N,N-Diethylethanolammonium][Chloride]:Glycerol}	[0.33:0.67]	298.15 - 368.15	15	1.35	0.08	[2]
	[0.25:0.75]	298.15 - 368.15	15	1.05	2.72	
	[0.2:0.8]	298.15 - 368.15	15	1.12	3.95	
{[Tetrabutylammonium][Chloride]:Arginine}	[0.857:0.143]	303.15 - 353.15	6	0.99	0.19	[67]
	[0.875:0.125]		6	0.59	0.81	
	[0.889:0.111]		6	0.40	0.52	
{[Tetrabutylammonium][Chloride]:Aspartic acid}	[0.9:0.1]	303.15 - 353.15	6	0.43	0.03	[67]
	[0.909:0.091]		6	0.68	0.03	
	[0.917:0.083]		6	1.40	0.11	
{[Tetrabutylammonium][Chloride]:Ethylene glycol}	[0.333:0.667]	293.15 - 353.15	7	9.10	6.44	[3]
	[0.25:0.75]		7	8.81	7.39	
	[0.2:0.8]		7	12.15	7.96	
{[Tetrabutylammonium][Chloride]:Glutamic acid}	[0.889:0.111]	303.15 - 353.15	6	0.72	0.17	[67]
	[0.9:0.1]		6	0.51	0.26	
	[0.909:0.091]		6	0.51	0.36	
{[Tetrabutylammonium][Chloride]:Glycerol}	[0.25:0.75]	293.15 - 353.15	7	3.85	10.46	[3]
	[0.2:0.8]		7	2.17	9.99	
	[0.167:0.833]		7	1.40	9.69	
{[Tetrabutylammonium][Chloride]:Phenylacetic acid}	[0.333:0.667]	288.15 - 338.15	11	0.66	0.67	[27]
{[Tetrabutylammonium][Chloride]:Propionic acid}	[0.333:0.667]	288.15 - 338.15	11	6.23	4.86	[27]
{[Tetrabutylammonium][Chloride]:Triethylene glycol}	[0.5:0.5]	293.15 - 353.15	7	5.32	1.32	[3]
	[0.667:0.333]		7	1.14	1.94	
	[0.75:0.25]		7	1.24	2.21	
	[0.8:0.2]		7	2.38	2.53	
{[Tetraethylammonium][Bromide]:Levulinic acid}	[0.5:0.5]	293.15 - 343.15	11	3.89	1.94	[73]
{[Tetraethylammonium][Chloride]:Levulinic acid}	[0.5:0.5]	293.15 - 343.15	11	0.79	1.11	[73]
{[Tetrahexylammonium][Bromide]:Ethylene glycol}	[0.333:0.667]	293.15 - 343.15	11	3.18	3.22	[28]
{[Tetrahexylammonium][Bromide]:Glycerol}	[0.333:0.667]	293.15 - 343.15	11	0.99	5.53	[28]
{Trimethylglycine:2-Chlorobenzoic acid}	[0.333:0.667]	338.15 - 373.15	4	1.36	6.04	[76]
{Trimethylglycine:4-Chlorobenzoic acid}	[0.333:0.667]	338.15 - 373.15	4		4.53	[76]

{Trimethylglycine:Benzoic acid}	[0.333:0.667]	353.15 - 373.15	3	1.42	4.63	[76]
{Trimethylglycine:D-(+)-Mandelic acid}	[0.333:0.667]	298.15 - 388.15	5	0.85	1.72	[76]
{Trimethylglycine:Phenylacetic acid}	[0.333:0.667]	298.15 - 388.15	5	1.17	2.18	[76]
		Total	**1239**			

Table S.C30. Pool of data H3 used for the comparison between the model of Haghbakhsh et al. [104] and the model presented in this work for the prediction of heat capacities

System	Ratio	Temperature range (K)	Number of data points	Average deviation, Haghbakhsh et al. [121] (%)	Average deviation, this work (%)	Reference
{Betaine:Ethylene glycol}	[0.25:0.75]	318.15 - 363.15	10	0.42	1.22	[99]
{[Choline][Chloride]:Citric acid}	[0.333:0.667]	298.15 - 353.15	23	0.26	0.18	[97]
{[Choline][Chloride]:Ethylene glycol}	[0.333:0.667]	303.15 - 353.15	11	2.5	1.5	[101]
{[Choline][Chloride]:Fructose}	[0.667:0.333]	298.15 - 353.15	23	0.89	0.86	[97]
{[Choline][Chloride]:Glucose}	[0.667:0.333]	298.15 - 353.15	23	0.47	0.47	[97]
{[Choline][Chloride]:Glycerol}	[0.333:0.667]	303.15 - 353.15	11	2.74	3.93	[101]
		278.15 - 338.15	25		2.96	[103]
{[Choline][Chloride]:Malonic acid}	[0.5:0.5]	298.15 - 353.15	23	4.27	0.58	[97]
{[Choline][Chloride]:Oxalic acid}	[0.5:0.5]	298.15 - 353.15	23	32.97	27.53	[97]
{[Choline][Chloride]:Phenol}	[0.25:0.75]	298.15 - 353.15	23	0.5	0.11	[97]
{[Choline] [Chloride]:Triethylene glycol}	[0.333:0.667]	298.15 - 353.15	23	0.57	0.35	[97]
{[Choline][Chloride]:Urea}	[0.333:0.667]	303.15 - 353.15	11	0.63	0.41	[101]
		303.15 - 353.15	11		0.03	[25]
{L-Carnitine:Ethylene glycol}	[0.25:0.75]	318.15 - 363.15	10	1.05	4.7	[99]
{[Methyltriphenylphosphonium] [Bromide]:Ethylene glycol}	[0.2:0.8]	298.15 - 353.15	23	0.5	0.09	[97]
{[Methyltriphenylphosphonium] [Bromide]:Glycerol}	[0.25:0.75]	298.15 - 353.15	23	1.51	10.24	[97]

{[Methyltriphenylphosphonium] [Bromide]:Malonic acid}	[0.4:0.6]	298.15 - 353.15	23	1.31	0.11	[97]
{[N,N-Diethylethanolammonium] [Chloride]:Ethylene glycol}	[0.333:0.667]	303.15 - 353.15	11	0.57	0.84	[98]
{[N,N-Diethylethanolammonium] [Chloride]:Glycerol}	[0.333:0.667]	303.15 - 353.15	11	0.32	4.4	[98]
{[Tetrabutylammonium] [Chloride]:Ethylene glycol}	[0.25:0.75]	298.15 - 353.15	23	2.08	2.21	[97]
{[Tetrabutylammonium] [Chloride]:Glycerol}	[0.167:0.833]	298.15 - 353.15	23	0.58	0.85	[97]
{[Tetrabutylammonium] [Chloride]:Malonic acid}	[0.25:0.75]	298.15 - 353.15	23	2.54	1.31	[97]
{[Tetrabutylammonium] [Chloride]:Triethylene glycol}	[0.5:0.5]	298.15 - 353.15	23	2.88	6.07	[97]
{[Tetrabutylammonium] [Chloride]:Urea}	[0.8:0.2]	308.15 - 353.15	19	0.35	7.87	[97]
		Total	**452**			

References

[1] F.S. Mjalli, Molar volume of eutectic solvents as a function of molar composition and temperature, Chin. J. Chem. Eng. 24 (2016) 1779–1785. https://doi.org/10.1016/j.cjche.2016.05.047.

[2] K. Shahbaz, S. Baroutian, F.S. Mjalli, M.A. Hashim, I.M. AlNashef, Densities of ammonium and phosphonium based deep eutectic solvents: Prediction using artificial intelligence and group contribution techniques, Thermochim. Acta. 527 (2012) 59–66. https://doi.org/10.1016/j.tca.2011.10.010.

[3] F.S. Mjalli, J. Naser, B. Jibril, V. Alizadeh, Z. Gano, Tetrabutylammonium Chloride Based Ionic Liquid Analogues and Their Physical Properties, J. Chem. Eng. Data. 59 (2014) 2242–2251. https://doi.org/10.1021/je5002126.

[4] H.B. Balaraman, S.K. Rathnasamy, Thermophysical and Molar Volume Aberration of Amphiphilic Eutectic Mix of Bivalent Diols and Ammonium-Ionic Liquid, J. Chem. Eng. Data. 64 (2019) 3307–3315. https://doi.org/10.1021/acs.jced.9b00134.

[5] F.S. Mjalli, K. Shahbaz, I.M. AlNashef, Modified Rackett equation for modelling the molar volume of deep eutectic solvents, Thermochim. Acta. 614 (2015) 185–190. https://doi.org/10.1016/j.tca.2015.06.026.

[6] X. Deng, X. Duan, L. Gong, D. Deng, Ammonia Solubility, Density, and Viscosity of Choline Chloride–Dihydric Alcohol Deep Eutectic Solvents, J. Chem. Eng. Data. 65 (2020) 4845–4854. https://doi.org/10.1021/acs.jced.0c00386.

[7] V. Agieienko, R. Buchner, Variation of Density, Viscosity, and Electrical Conductivity of the Deep Eutectic Solvent Reline, Composed of Choline Chloride and Urea at a Molar Ratio of 1:2, Mixed with Dimethylsulfoxide as a Cosolvent, J. Chem. Eng. Data. 65 (2020) 1900–1910. https://doi.org/10.1021/acs.jced.9b01105.

[8] S.P. Ijardar, Deep eutectic solvents composed of tetrabutylammonium bromide and PEG: Density, speed of sound and viscosity as a function of temperature, J. Chem. Thermodyn. 140 (2020) 105897. https://doi.org/10.1016/j.jct.2019.105897.

[9] C. Florindo, M.M. Oliveira, L.C. Branco, I.M. Marrucho, Carbohydrates-based deep eutectic solvents: Thermophysical properties and rice straw dissolution, J. Mol. Liq. 247 (2017) 441–447. https://doi.org/10.1016/j.molliq.2017.09.026.
[10] D. Deng, Y. Jiang, X. Liu, Z. Zhang, N. Ai, Investigation of solubilities of carbon dioxide in five levulinic acid-based deep eutectic solvents and their thermodynamic properties, J. Chem. Thermodyn. 103 (2016) 212–217. https://doi.org/10.1016/j.jct.2016.08.015.
[11] H. Ghaedi, M. Ayoub, S. Sufian, B. Lal, A.M. Shariff, Measurement and correlation of physicochemical properties of phosphonium-based deep eutectic solvents at several temperatures (293.15 K–343.15 K) for CO 2 capture, J. Chem. Thermodyn. 113 (2017) 41–51. https://doi.org/10.1016/j.jct.2017.05.020.
[12] A. Basaiahgari, S. Panda, R.L. Gardas, Acoustic, volumetric, transport, optical and rheological properties of Benzyltripropylammonium based Deep Eutectic Solvents, Fluid Phase Equilibria. 448 (2017) 41–49. https://doi.org/10.1016/j.fluid.2017.03.011.
[13] P.B. Sánchez, B. González, J. Salgado, J. José Parajó, Á. Domínguez, Physical properties of seven deep eutectic solvents based on l-proline or betaine, J. Chem. Thermodyn. 131 (2019) 517–523. https://doi.org/10.1016/j.jct.2018.12.017.
[14] Y. Chen, N. Ai, G. Li, H. Shan, Y. Cui, D. Deng, Solubilities of Carbon Dioxide in Eutectic Mixtures of Choline Chloride and Dihydric Alcohols, J. Chem. Eng. Data. 59 (2014) 1247–1253. https://doi.org/10.1021/je400884v.
[15] A. Hayyan, F.S. Mjalli, I.M. AlNashef, T. Al-Wahaibi, Y.M. Al-Wahaibi, M.A. Hashim, Fruit sugar-based deep eutectic solvents and their physical properties, Thermochim. Acta. 541 (2012) 70–75. https://doi.org/10.1016/j.tca.2012.04.030.
[16] F.S. Mjalli, O. Ahmad, Density of aqueous choline chloride-based ionic liquids analogues, Thermochim. Acta. 647 (2017) 8–14. https://doi.org/10.1016/j.tca.2016.11.008.
[17] A. Yadav, S. Pandey, Densities and Viscosities of (Choline Chloride + Urea) Deep Eutectic Solvent and Its Aqueous Mixtures in the Temperature Range 293.15 K to 363.15 K, J. Chem. Eng. Data. 59 (2014) 2221–2229. https://doi.org/10.1021/je5001796.
[18] R.B. Leron, A.N. Soriano, M.-H. Li, Densities and refractive indices of the deep eutectic solvents (choline chloride + ethylene glycol or glycerol) and their aqueous mixtures at the temperature ranging from 298.15 to 333.15 K, J. Taiwan Inst. Chem. Eng. 43 (2012) 551–557. https://doi.org/10.1016/j.jtice.2012.01.007.
[19] A.R. Harifi-Mood, R. Buchner, Density, viscosity, and conductivity of choline chloride + ethylene glycol as a deep eutectic solvent and its binary mixtures with dimethyl sulfoxide, J. Mol. Liq. 225 (2017) 689–695. https://doi.org/10.1016/j.molliq.2016.10.115.
[20] A. Yadav, S. Trivedi, R. Rai, S. Pandey, Densities and dynamic viscosities of (choline chloride+glycerol) deep eutectic solvent and its aqueous mixtures in the temperature range (283.15–363.15)K, Fluid Phase Equilibria. 367 (2014) 135–142. https://doi.org/10.1016/j.fluid.2014.01.028.
[21] C. Florindo, F.S. Oliveira, L.P.N. Rebelo, A.M. Fernandes, I.M. Marrucho, Insights into the Synthesis and Properties of Deep Eutectic Solvents Based on Cholinium Chloride and Carboxylic Acids, ACS Sustain. Chem. Eng. 2 (2014) 2416–2425. https://doi.org/10.1021/sc500439w.
[22] M. Lu, G. Han, Y. Jiang, X. Zhang, D. Deng, N. Ai, Solubilities of carbon dioxide in the eutectic mixture of levulinic acid (or furfuryl alcohol) and choline chloride, J. Chem. Thermodyn. 88 (2015) 72–77. https://doi.org/10.1016/j.jct.2015.04.021.
[23] W. Guo, Y. Hou, S. Ren, S. Tian, W. Wu, Formation of Deep Eutectic Solvents by Phenols and Choline Chloride and Their Physical Properties, J. Chem. Eng. Data. 58 (2013) 866–872. https://doi.org/10.1021/je300997v.
[24] J. Zhu, K. Yu, Y. Zhu, R. Zhu, F. Ye, N. Song, Y. Xu, Physicochemical properties of deep eutectic solvents formed by choline chloride and phenolic compounds at T = (293.15 to 333.15) K: The influence of electronic effect of substitution group, J. Mol. Liq. 232 (2017) 182–187. https://doi.org/10.1016/j.molliq.2017.02.071.

[25] F. Chemat, H. Anjum, A.M. Shariff, P. Kumar, T. Murugesan, Thermal and physical properties of (Choline chloride + urea +l-arginine) deep eutectic solvents, J. Mol. Liq. 218 (2016) 301–308. https://doi.org/10.1016/j.molliq.2016.02.062.

[26] R. Haghbakhsh, S. Raeissi, Densities and volumetric properties of (choline chloride + urea) deep eutectic solvent and methanol mixtures in the temperature range of 293.15–323.15 K, J. Chem. Thermodyn. 124 (2018) 10–20. https://doi.org/10.1016/j.jct.2018.04.010.

[27] H.-Zhen. Su, J.-Mei. Yin, Q.-Shan. Liu, C.-Ping. Li, [1] 大连大学环境与化学工程学院,辽宁大连116622,[1] College of Chemical Engineering and the Environment, Dalian University, Dalian 116622, Liaoning Province, P. R. China, [2] 沈阳农业大学理学院,沈阳110866,[2] School of Science, Shenyang Agricultural University, Shenyang 110866, P. R. China, Properties of Four Deep Eutectic Solvents: Density, Electrical Conductivity, Dynamic Viscosity and Refractive Index, Acta Phys.-Chim. Sin. 31 (2015) 1468–1473. https://doi.org/10.3866/PKU.WHXB201506111.

[28] N.R. Rodriguez, P.F. Requejo, M.C. Kroon, Aliphatic–Aromatic Separation Using Deep Eutectic Solvents as Extracting Agents, Ind. Eng. Chem. Res. 54 (2015) 11404–11412. https://doi.org/10.1021/acs.iecr.5b02611.

[29] V. Agieienko, R. Buchner, Densities, Viscosities, and Electrical Conductivities of Pure Anhydrous Reline and Its Mixtures with Water in the Temperature Range (293.15 to 338.15) K, J. Chem. Eng. Data. 64 (2019) 4763–4774. https://doi.org/10.1021/acs.jced.9b00145.

[30] D. Dhingra, Bhawna, S. Pandey, Effect of lithium chloride on the density and dynamic viscosity of choline chloride/urea deep eutectic solvent in the temperature range (303.15–358.15) K, J. Chem. Thermodyn. 130 (2019) 166–172. https://doi.org/10.1016/j.jct.2018.10.003.

[31] R.B. Leron, M.-H. Li, High-pressure density measurements for choline chloride: Urea deep eutectic solvent and its aqueous mixtures at T= (298.15 to 323.15) K and up to 50 MPa, J. Chem. Thermodyn. 54 (2012) 293–301. https://doi.org/10.1016/j.jct.2012.05.008.

[32] W.C. Su, D.S.H. Wong, M.H. Li, Effect of Water on Solubility of Carbon Dioxide in (Aminomethanamide + 2-Hydroxy- *N* , *N* , *N* -trimethylethanaminium Chloride), J. Chem. Eng. Data. 54 (2009) 1951–1955. https://doi.org/10.1021/je900078k.

[33] Y. Xie, H. Dong, S. Zhang, X. Lu, X. Ji, Effect of Water on the Density, Viscosity, and CO_2 Solubility in Choline Chloride/Urea, J. Chem. Eng. Data. 59 (2014) 3344–3352. https://doi.org/10.1021/je500320c.

[34] F.S. Mjalli, G. Vakili-Nezhaad, K. Shahbaz, I.M. AlNashef, Application of the Eötvos and Guggenheim empirical rules for predicting the density and surface tension of ionic liquids analogues, Thermochim. Acta. 575 (2014) 40–44. https://doi.org/10.1016/j.tca.2013.10.017.

[35] K.R. Siongco, R.B. Leron, M.-H. Li, Densities, refractive indices, and viscosities of N,N-diethylethanol ammonium chloride–glycerol or –ethylene glycol deep eutectic solvents and their aqueous solutions, J. Chem. Thermodyn. 65 (2013) 65–72. https://doi.org/10.1016/j.jct.2013.05.041.

[36] R.B. Leron, D.S.H. Wong, M.-H. Li, Densities of a deep eutectic solvent based on choline chloride and glycerol and its aqueous mixtures at elevated pressures, Fluid Phase Equilibria. 335 (2012) 32–38. https://doi.org/10.1016/j.fluid.2012.08.016.

[37] N. Chaabene, K. Ngo, M. Turmine, V. Vivier, New hydrophobic deep eutectic solvent for electrochemical applications, J. Mol. Liq. 319 (2020) 114198. https://doi.org/10.1016/j.molliq.2020.114198.

[38] B.D. Ribeiro, C. Florindo, L.C. Iff, M.A.Z. Coelho, I.M. Marrucho, Menthol-based Eutectic Mixtures: Hydrophobic Low Viscosity Solvents, ACS Sustain. Chem. Eng. 3 (2015) 2469–2477. https://doi.org/10.1021/acssuschemeng.5b00532.

[39] M. Nedaei, A.R. Zarei, S.A. Ghorbanian, Development of a new emulsification microextraction method based on solidification of settled organic drop: application of a novel ultra-hydrophobic tailor-made deep eutectic solvent, New J. Chem. 42 (2018) 12520–12529. https://doi.org/10.1039/C8NJ02219D.

[40] P. Dehury, U. Mahanta, T. Banerjee, Comprehensive Assessment on the Use of Boron Nitride-Based Nanofluids Comprising Eutectic Mixtures of Diphenyl Ether and Menthol for Enhanced Thermal Media, ACS Sustain. Chem. Eng. 8 (2020) 14595–14604. https://doi.org/10.1021/acssuschemeng.0c05648.

[41] G. Almustafa, R. Sulaiman, M. Kumar, I. Adeyemi, H.A. Arafat, I. AlNashef, Boron extraction from aqueous medium using novel hydrophobic deep eutectic solvents, Chem. Eng. J. 395 (2020) 125173. https://doi.org/10.1016/j.cej.2020.125173.

[42] L.-T. Wang, Q. Yang, Q. Cui, X.-H. Fan, M.-Z. Dong, M.-Z. Gao, M.-J. Lv, J.-Y. An, D. Meng, X.-H. Zhao, Y.-J. Fu, Recyclable menthol-based deep eutectic solvent micellar system for extracting phytochemicals from Ginkgo biloba leaves, J. Clean. Prod. 244 (2020) 118648. https://doi.org/10.1016/j.jclepro.2019.118648.

[43] D.J.G.P. van Osch, C.H.J.T. Dietz, J. van Spronsen, M.C. Kroon, F. Gallucci, M. van Sint Annaland, R. Tuinier, A Search for Natural Hydrophobic Deep Eutectic Solvents Based on Natural Components, ACS Sustain. Chem. Eng. 7 (2019) 2933–2942. https://doi.org/10.1021/acssuschemeng.8b03520.

[44] O.G. Sas, G.R. Ivaniš, M.Lj. Kijevčanin, B. González, A. Domínguez, I.R. Radović, High pressure densities and derived thermodynamic properties of deep eutectic solvents with menthol and saturated fatty acids, J. Chem. Thermodyn. 162 (2021) 106578. https://doi.org/10.1016/j.jct.2021.106578.

[45] A. Basaiahgari, S. Panda, R.L. Gardas, Effect of Ethylene, Diethylene, and Triethylene Glycols and Glycerol on the Physicochemical Properties and Phase Behavior of Benzyltrimethyl and Benzyltributylammonium Chloride Based Deep Eutectic Solvents at 283.15–343.15 K, J. Chem. Eng. Data. 63 (2018) 2613–2627. https://doi.org/10.1021/acs.jced.8b00213.

[46] M.B. Taysun, E. Sert, F.S. Atalay, Effect of Hydrogen Bond Donor on the Physical Properties of Benzyltriethylammonium Chloride Based Deep Eutectic Solvents and Their Usage in 2-Ethyl-Hexyl Acetate Synthesis as a Catalyst, J. Chem. Eng. Data. 62 (2017) 1173–1181. https://doi.org/10.1021/acs.jced.6b00486.

[47] Y. Cui, C. Li, J. Yin, S. Li, Y. Jia, M. Bao, Design, synthesis and properties of acidic deep eutectic solvents based on choline chloride, J. Mol. Liq. 236 (2017) 338–343. https://doi.org/10.1016/j.molliq.2017.04.052.

[48] V. Agieienko, R. Buchner, A Comprehensive Study of Density, Viscosity, and Electrical Conductivity of (Choline Chloride + Glycerol) Deep Eutectic Solvent and Its Mixtures with Dimethyl Sulfoxide, J. Chem. Eng. Data. 66 (2021) 780–792. https://doi.org/10.1021/acs.jced.0c00869.

[49] C. Fan, Y. Liu, T. Sebbah, X. Cao, A Theoretical Study on Terpene-Based Natural Deep Eutectic Solvent: Relationship between Viscosity and Hydrogen-Bonding Interactions, Glob. Chall. 5 (2021) 2000103. https://doi.org/10.1002/gch2.202000103.

[50] D.J.G.P. van Osch, L.F. Zubeir, A. van den Bruinhorst, M.A.A. Rocha, M.C. Kroon, Hydrophobic deep eutectic solvents as water-immiscible extractants, Green Chem. 17 (2015) 4518–4521. https://doi.org/10.1039/C5GC01451D.

[51] C. Fan, L. Wen, Y. Shan, Y. Shan, X. Cao, Why do ammonium salt/phenol-based deep eutectic solvents show low viscosity?, Arab. J. Chem. 15 (2022) 103512. https://doi.org/10.1016/j.arabjc.2021.103512.

[52] L. Bahadori, M.H. Chakrabarti, N.S.A. Manan, M.A. Hashim, F.S. Mjalli, I.M. AlNashef, N. Brandon, The Effect of Temperature on Kinetics and Diffusion Coefficients of Metallocene Derivatives in Polyol-Based Deep Eutectic Solvents, PLOS ONE. 10 (2015) e0144235. https://doi.org/10.1371/journal.pone.0144235.

[53] Y. Dai, J. van Spronsen, G.-J. Witkamp, R. Verpoorte, Y.H. Choi, Natural deep eutectic solvents as new potential media for green technology, Anal. Chim. Acta. 766 (2013) 61–68. https://doi.org/10.1016/j.aca.2012.12.019.

[54] G. Li, D. Deng, Y. Chen, H. Shan, N. Ai, Solubilities and thermodynamic properties of CO2 in choline-chloride based deep eutectic solvents, J. Chem. Thermodyn. 75 (2014) 58–62. https://doi.org/10.1016/j.jct.2014.04.012.

[55] L.F. Zubeir, M.H.M. Lacroix, M.C. Kroon, Low Transition Temperature Mixtures as Innovative and Sustainable CO_2 Capture Solvents, J. Phys. Chem. B. 118 (2014) 14429–14441. https://doi.org/10.1021/jp5089004.

[56] M. Francisco, A. van den Bruinhorst, L.F. Zubeir, C.J. Peters, M.C. Kroon, A new low transition temperature mixture (LTTM) formed by choline chloride+lactic acid: Characterization as solvent for CO2 capture, Fluid Phase Equilibria. 340 (2013) 77–84. https://doi.org/10.1016/j.fluid.2012.12.001.

[57] C. Fan, T. Sebbah, Y. Liu, X. Cao, Terpenoid-capric acid based natural deep eutectic solvent: Insight into the nature of low viscosity, Clean. Eng. Technol. 3 (2021) 100116. https://doi.org/10.1016/j.clet.2021.100116.

[58] K. Li, J.H. Nam, S. Kang, Y. Liu, J. Lee, Carvone and its eutectic mixtures as novel, biodegradable, and tunable solvents to extract hydrophobic compounds in substitution for volatile toxic solvents, Food Chem. 374 (2022) 131630. https://doi.org/10.1016/j.foodchem.2021.131630.

[59] Z.-L. Li, L.-S. Zhou, Y.-H. Wei, H.-L. Peng, K. Huang, Highly Efficient, Reversible, and Selective Absorption of SO_2 in 1-Ethyl-3-methylimidazolium Chloride Plus Imidazole Deep Eutectic Solvents, Ind. Eng. Chem. Res. 59 (2020) 13696–13705. https://doi.org/10.1021/acs.iecr.0c01451.

[60] B. Nowosielski, M. Jamrógiewicz, J. Łuczak, M. Śmiechowski, D. Warmińska, Experimental and predicted physicochemical properties of monopropanolamine-based deep eutectic solvents, J. Mol. Liq. 309 (2020) 113110. https://doi.org/10.1016/j.molliq.2020.113110.

[61] K.A. Omar, R. Sadeghi, Novel ninhydrin-based deep eutectic solvents for amino acid detection, J. Mol. Liq. 303 (2020) 112644. https://doi.org/10.1016/j.molliq.2020.112644.

[62] K.A. Omar, R. Sadeghi, Novel Nonanol-Based deep eutectic solvents: Thermophysical properties and their applications in Liquid-Liquid extraction and amino acid detection, J. Mol. Liq. 336 (2021) 116359. https://doi.org/10.1016/j.molliq.2021.116359.

[63] K.A. Omar, R. Sadeghi, Novel benzilic acid-based deep-eutectic-solvents: Preparation and physicochemical properties determination, Fluid Phase Equilibria. 522 (2020) 112752. https://doi.org/10.1016/j.fluid.2020.112752.

[64] F.S. Mjalli, Novel amino acids based ionic liquids analogues: Acidic and basic amino acids, J. Taiwan Inst. Chem. Eng. 61 (2016) 64–74. https://doi.org/10.1016/j.jtice.2015.12.020.

[65] H. Shekaari, M.T. Zafarani-Moattar, M. Mokhtarpour, S. Faraji, Volumetric and compressibility properties for aqueous solutions of choline chloride based deep eutectic solvents and Prigogine–Flory–Patterson theory to correlate of excess molar volumes at T = (293.15 to 308.15) K, J. Mol. Liq. 289 (2019) 111077. https://doi.org/10.1016/j.molliq.2019.111077.

[66] A. Yadav, J.R. Kar, M. Verma, S. Naqvi, S. Pandey, Densities of aqueous mixtures of (choline chloride+ethylene glycol) and (choline chloride+malonic acid) deep eutectic solvents in temperature range 283.15–363.15K, Thermochim. Acta. 600 (2015) 95–101. https://doi.org/10.1016/j.tca.2014.11.028.

[67] K. Shahbaz, F.S.G. Bagh, F.S. Mjalli, I.M. AlNashef, M.A. Hashim, Prediction of refractive index and density of deep eutectic solvents using atomic contributions, Fluid Phase Equilibria. 354 (2013) 304–311. https://doi.org/10.1016/j.fluid.2013.06.050.

[68] D. Deng, X. Liu, B. Gao, Physicochemical Properties and Investigation of Azole-Based Deep Eutectic Solvents as Efficient and Reversible SO_2 Absorbents, Ind. Eng. Chem. Res. 56 (2017) 13850–13856. https://doi.org/10.1021/acs.iecr.7b02478.

[69] X. Liu, B. Gao, Y. Jiang, N. Ai, D. Deng, Solubilities and Thermodynamic Properties of Carbon Dioxide in Guaiacol-Based Deep Eutectic Solvents, J. Chem. Eng. Data. 62 (2017) 1448–1455. https://doi.org/10.1021/acs.jced.6b01013.

[70] G. Li, Y. Jiang, X. Liu, D. Deng, New levulinic acid-based deep eutectic solvents: Synthesis and physicochemical property determination, J. Mol. Liq. 222 (2016) 201–207. https://doi.org/10.1016/j.molliq.2016.07.039.
[71] B.-Y. Zhao, P. Xu, F.-X. Yang, H. Wu, M.-H. Zong, W.-Y. Lou, Biocompatible Deep Eutectic Solvents Based on Choline Chloride: Characterization and Application to the Extraction of Rutin from *Sophora japonica*, ACS Sustain. Chem. Eng. 3 (2015) 2746–2755. https://doi.org/10.1021/acssuschemeng.5b00619.
[72] M.A. Kareem, F.S. Mjalli, M.A. Hashim, I.M. AlNashef, Phosphonium-Based Ionic Liquids Analogues and Their Physical Properties, J. Chem. Eng. Data. 55 (2010) 4632–4637. https://doi.org/10.1021/je100104v.
[73] M.A.R. Martins, E.A. Crespo, P.V.A. Pontes, L.P. Silva, M. Bülow, G.J. Maximo, E.A.C. Batista, C. Held, S.P. Pinho, J.A.P. Coutinho, Tunable Hydrophobic Eutectic Solvents Based on Terpenes and Monocarboxylic Acids, ACS Sustain. Chem. Eng. 6 (2018) 8836–8846. https://doi.org/10.1021/acssuschemeng.8b01203.
[74] S.A. Mat Hussin, P. Varanusupakul, S. Shahabuddin, B. Yih Hui, S. Mohamad, Synthesis and characterization of green menthol-based low transition temperature mixture with tunable thermophysical properties as hydrophobic low viscosity solvent, J. Mol. Liq. 308 (2020) 113015. https://doi.org/10.1016/j.molliq.2020.113015.
[75] O.G. Sas, M. Castro, Á. Domínguez, B. González, Removing phenolic pollutants using Deep Eutectic Solvents, Sep. Purif. Technol. 227 (2019) 115703. https://doi.org/10.1016/j.seppur.2019.115703.
[76] R. Craveiro, I. Aroso, V. Flammia, T. Carvalho, M.T. Viciosa, M. Dionísio, S. Barreiros, R.L. Reis, A.R.C. Duarte, A. Paiva, Properties and thermal behavior of natural deep eutectic solvents, J. Mol. Liq. 215 (2016) 534–540. https://doi.org/10.1016/j.molliq.2016.01.038.
[77] J. Zhu, Y. Xu, X. Feng, X. Zhu, A detailed study of physicochemical properties and microstructure of EmimCl-EG deep eutectic solvents: Their influence on SO2 absorption behavior, J. Ind. Eng. Chem. 67 (2018) 148–155. https://doi.org/10.1016/j.jiec.2018.06.025.
[78] L. Lomba, F. Tucciarone, B. Giner, M. Artal, C. Lafuente, Thermophysical characterization of choline chloride: Resorcinol and its mixtures with water, Fluid Phase Equilibria. 557 (2022) 113435. https://doi.org/10.1016/j.fluid.2022.113435.
[79] P. Makoś, A. Przyjazny, G. Boczkaj, Hydrophobic deep eutectic solvents as “green” extraction media for polycyclic aromatic hydrocarbons in aqueous samples, J. Chromatogr. A. 1570 (2018) 28–37. https://doi.org/10.1016/j.chroma.2018.07.070.
[80] K.A. Omar, R. Sadeghi, Novel diglycolic acid-based deep eutectic solvents and their applications as a rust remover, J. Mol. Liq. 312 (2020) 113380. https://doi.org/10.1016/j.molliq.2020.113380.
[81] T. Altamash, M.S. Nasser, Y. Elhamarnah, M. Magzoub, R. Ullah, H. Qiblawey, S. Aparicio, M. Atilhan, Gas solubility and rheological behavior study of betaine and alanine based natural deep eutectic solvents (NADES), J. Mol. Liq. 256 (2018) 286–295. https://doi.org/10.1016/j.molliq.2018.02.049.
[82] A. Hosseini, R. Haghbakhsh, S. Raeissi, Experimental Investigation of Liquid–Liquid Extraction of Toluene + Heptane or Toluene + Hexane Using Deep Eutectic Solvents, J. Chem. Eng. Data. 64 (2019) 3811–3820. https://doi.org/10.1021/acs.jced.9b00237.
[83] R. Haghbakhsh, S. Raeissi, Experimental investigation on the volumetric properties of mixtures of the deep eutectic solvent of Ethaline and methanol in the temperature range of 283.15 to 323.15 K, J. Chem. Thermodyn. 147 (2020) 106124. https://doi.org/10.1016/j.jct.2020.106124.
[84] R. Haghbakhsh, S. Raeissi, A study of non-ideal mixtures of ethanol and the (1 choline chloride +2 ethylene glycol) deep eutectic solvent for their volumetric behaviour, J. Chem. Thermodyn. 150 (2020) 106219. https://doi.org/10.1016/j.jct.2020.106219.
[85] E.A. Crespo, J.M.L. Costa, A.M. Palma, B. Soares, M.C. Martín, J.J. Segovia, P.J. Carvalho, J.A.P. Coutinho, Thermodynamic characterization of deep eutectic solvents at high pressures, Fluid Phase Equilibria. 500 (2019) 112249. https://doi.org/10.1016/j.fluid.2019.112249.

[86] A. Kianpour, K.A. Omar, R. Sadeghi, Novel Deep Eutectic Solvents: Physical Properties and Their Application in Amino Acid Detection, J. Chem. Eng. Data. (2022) acs.jced.2c00152. https://doi.org/10.1021/acs.jced.2c00152.
[87] P. Makoś, G. Boczkaj, Deep eutectic solvents based highly efficient extractive desulfurization of fuels – Eco-friendly approach, J. Mol. Liq. 296 (2019) 111916. https://doi.org/10.1016/j.molliq.2019.111916.
[88] A. Kadyan, K. Behera, S. Pandey, Hybrid green nonaqueous media: tetraethylene glycol modifies the properties of a (choline chloride + urea) deep eutectic solvent, RSC Adv. 6 (2016) 29920–29930. https://doi.org/10.1039/C6RA03726G.
[89] N.F. Gajardo-Parra, V.P. Cotroneo-Figueroa, P. Aravena, V. Vesovic, R.I. Canales, Viscosity of Choline Chloride-Based Deep Eutectic Solvents: Experiments and Modeling, J. Chem. Eng. Data. 65 (2020) 5581–5592. https://doi.org/10.1021/acs.jced.0c00715.
[90] R. Craveiro, L. Meneses, L. Durazzo, Â. Rocha, J.M. Silva, R.L. Reis, S. Barreiros, A.R.C. Duarte, A. Paiva, Deep Eutectic Solvents for Enzymatic Esterification of Racemic Menthol, ACS Sustain. Chem. Eng. 7 (2019) 19943–19950. https://doi.org/10.1021/acssuschemeng.9b05434.
[91] R. Verma, T. Banerjee, Liquid–Liquid Extraction of Lower Alcohols Using Menthol-Based Hydrophobic Deep Eutectic Solvent: Experiments and COSMO-SAC Predictions, Ind. Eng. Chem. Res. 57 (2018) 3371–3381. https://doi.org/10.1021/acs.iecr.7b05270.
[92] A. Hayyan, F.S. Mjalli, I.M. AlNashef, Y.M. Al-Wahaibi, T. Al-Wahaibi, M.A. Hashim, Glucose-based deep eutectic solvents: Physical properties, J. Mol. Liq. 178 (2013) 137–141. https://doi.org/10.1016/j.molliq.2012.11.025.
[93] F. Cardellini, M. Tiecco, R. Germani, G. Cardinali, L. Corte, L. Roscini, N. Spreti, Novel zwitterionic deep eutectic solvents from trimethylglycine and carboxylic acids: characterization of their properties and their toxicity, RSC Adv. 4 (2014) 55990–56002. https://doi.org/10.1039/C4RA10628H.
[94] J.-Y. Zhang, K. Huang, Densities and viscosities of, and NH3 solubilities in deep eutectic solvents composed of ethylamine hydrochloride and acetamide, J. Chem. Thermodyn. 139 (2019) 105883. https://doi.org/10.1016/j.jct.2019.105883.
[95] P. Dehury, R.K. Chaudhary, T. Banerjee, A. Dalal, Evaluation of Thermophysical Properties of Menthol-Based Deep Eutectic Solvent as a Thermal Fluid: Forced Convection and Numerical Studies, Ind. Eng. Chem. Res. 58 (2019) 20125–20133. https://doi.org/10.1021/acs.iecr.9b01836.
[96] B. Liu, J. Tian, Investigation of Glycolic Acid Natural Deep Eutectic Solvents with Strong Proton Donors for Ammonia Capture and Separation, Ind. Eng. Chem. Res. 60 (2021) 11600–11610. https://doi.org/10.1021/acs.iecr.1c01456.
[97] J. Naser, F.S. Mjalli, Z.S. Gano, Molar Heat Capacity of Selected Type III Deep Eutectic Solvents, J. Chem. Eng. Data. 61 (2016) 1608–1615. https://doi.org/10.1021/acs.jced.5b00989.
[98] K.R. Siongco, R.B. Leron, A.R. Caparanga, M.-H. Li, Molar heat capacities and electrical conductivities of two ammonium-based deep eutectic solvents and their aqueous solutions, Thermochim. Acta. 566 (2013) 50–56. https://doi.org/10.1016/j.tca.2013.05.023.
[99] K. Zhang, H. Li, S. Ren, W. Wu, Y. Bao, Specific Heat Capacities of Two Functional Ionic Liquids and Two Functional Deep Eutectic Solvents for the Absorption of SO_2, J. Chem. Eng. Data. 62 (2017) 2708–2712. https://doi.org/10.1021/acs.jced.7b00102.
[100] R.B. Leron, M.-H. Li, Molar heat capacities of choline chloride-based deep eutectic solvents and their binary mixtures with water, Thermochim. Acta. 530 (2012) 52–57. https://doi.org/10.1016/j.tca.2011.11.036.
[101] V.I.B. Castro, F. Mano, R.L. Reis, A. Paiva, A.R.C. Duarte, Synthesis and Physical and Thermodynamic Properties of Lactic Acid and Malic Acid-Based Natural Deep Eutectic Solvents, J. Chem. Eng. Data. 63 (2018) 2548–2556. https://doi.org/10.1021/acs.jced.7b01037.
[102] D. Lapeña, L. Lomba, M. Artal, C. Lafuente, B. Giner, The NADES glyceline as a potential Green Solvent: A comprehensive study of its thermophysical properties and effect of water inclusion, J. Chem. Thermodyn. 128 (2019) 164–172. https://doi.org/10.1016/j.jct.2018.07.031.

[103] F.Z. Nessakh, Etude de nouveaux fluides de travail constitués de solvants eutectiques profonds pour les pompes à chaleur, Ph.D. Thesis, Université de Tlemcen, Algeria, Université de Lorraine, France, 2022.
[104] R. Haghbakhsh, S. Raeissi, A.R.C. Duarte, Group contribution and atomic contribution models for the prediction of various physical properties of deep eutectic solvents, Sci. Rep. 11 (2021) 6684. https://doi.org/10.1038/s41598-021-85824-z.

Annexe D : Performances of an Absorption Heat Transformer cycle with water/deep eutectic solvents working fluids: modelling and screening of a database

D.1. Coefficients from the DIPPR to calculate the thermodynamics properties of water

The temperature-dependent equations for the heat capacity and enthalpy of vapour of water are:

$$C_p^w = A + B * T + C * T^2 + D * T^3 + E * T^4 \quad (1)$$

$$\Delta h_{vap} = A * \left(1 - \frac{T}{T_C^w}\right)^{B+C*\frac{T}{T_C^w}+D*\left(\frac{T}{T_C^w}\right)^2+E*\left(\frac{T}{T_C^w}\right)^3} \quad (2)$$

With T_C^w= 647.096 K, the critical temperature of water.

Table S.D31. Parameters from the DIPPR[1] for the determination of the properties of water

Property	A	B	C	D	E
C_p^w (J.kmol^{-1}.K^{-1})	276370	-2090.1	8.125	-0.014116	9.3701.10^{-6}
Δh_{vap} (J.kmol^{-1})	5.66.10^7	0.612041	-0.625697	0.398804	/

D.2. Operating conditions at points 6,7 and 10

A first hypothesis is made concerning the temperature at point 10, after the solution poor in refrigerant exits the SHE:

$$T_{10} = T_5 - \Delta T_{min} \quad (3)$$

There is a liquid mixture if $P_{sat}^w(T_{10}) < P_{10} = P_{high}$, otherwise it is a case of a mixture of vapour and liquid. The energy balance of the SHE gives:

$$h_6 = \frac{\dot{m}_5 . h_5 - \dot{m}_9 . h_9 - \dot{m}_{10} h_{10}}{\dot{m}_6} \quad (4)$$

T_6 must ensure that:

$$h_6 = h_{mix}\left(T_6, P_{high}, x_{m,rich}^w\right) \quad (5)$$

Hypothesis #1 is validated if:

$$T_6 - T_9 > \Delta T_{min} \tag{6}$$

If not, a second hypothesis is made where the solution rich in refrigerant exits the SHE:

$$T_6 = T_9 - \Delta T_{min} \tag{7}$$

Eq. 5 is used to derive h_6. Then, h_{10} is obtained from Eq. 4:

$$h_{10} = \frac{\dot{m}_5 . h_5 + \dot{m}_9 . h_9 - \dot{m}_6 h_6}{\dot{m}_{10}} \tag{8}$$

A temperature $T_{10,sat}$ is evaluated so that:

$$P_{sat}^{w}(T_{10,sat}) * \gamma^{w} * x_{poor}^{w} = P_{10} = P_{high} \tag{9}$$

If $h_{mix}(T_{10,sat}, P_{high}, x_{m,poor}^{w}) < h_{10}$ from Eq. 8, then there is a mixture of liquid and vapour and T_{10} must ensure that:

$$h_{10} = h_{LV}(T_{10}, P_{high}, x_{m,poor}^{w}) \tag{10}$$

Otherwise, point 10 corresponds to a liquid mixture and T_{10} is evaluated so that:

$$h_{10} = h_{mix}(T_{10}, P_{high}, x_{m,poor}^{w}) \tag{11}$$

Once the points 6 and 10 are determined, the point 7 is investigated. A temperature $T_{7,sat}$ is evaluated so that:

$$P_{sat}^{w}(T_{7,sat}) * \gamma^{w} * x_{rich}^{w} = P_7 = P_{low} \tag{12}$$

Since the valve is considered isenthalpic, $h_6 = h_7$ and the equilibrium condition is evaluated using the value of h_6 previously obtained. If $h_{mix}(T_{7,sat}, P_{low}, x_{m,rich}^{w}) < h_6$, the fluid is a mixture of liquid and vapour and T_7 is determined so that:

$$h_7 = h_{LV}(T_7, P_{high}, x_{m,rich}^{w}) \tag{13}$$

Otherwise, the fluid at point 7 is a liquid mixture, which means that T_7 is evaluated using:

$$h_7 = h_{mix}(T_7, P_{high}, x_{m,rich}^{w}) \tag{14}$$

D.3. Influence of T_{Con} (T_{Low})

Table S.D32. COP values obtained at various T_{Con} within the AHT simulations with $T_{Ev/Gen}$ set to 353.15 K and T_{Abs} to 403.15 K, with water as refrigerant and various absorbents

Absorbent			T_{Con} (K)							
Compound #1	**Compound #2**	**Ratio**	**283.15**	**288.15**	**293.15**	**298.15**	**303.15**	**308.15**	**313.15**	**318.15**
LiBr[2]	/	/	0.505	0.503	0.500	0.496	0.488	0.437	NA	NA
[EMIM][MPH][2]	/	/	0.432	0.432	0.432	0.430	0.425	0.410	0.291	NA
Glycerol	Choline chloride	[2:1]	0.432	0.433	0.434	0.435	0.434	0.430	0.419	0.331
	TMA chloride	[2:1]	0.436	0.438	0.439	0.440	0.440	0.438	0.430	0.381
	TEA chloride	[2:1]	0.430	0.431	0.432	0.432	0.431	0.427	0.415	0.343
	Betaine	[1:2]	0.439	0.440	0.440	0.438	0.433	0.407	NA	NA
		[1:1]	0.436	0.436	0.436	0.434	0.428	0.402	NA	NA
		[2:1]	0.430	0.431	0.430	0.428	0.420	0.392	NA	NA

D.4. Influence of T_{Gen} and T_{Ev}

Table S.D33. COP values obtained at various $T_{Ev/Gen}$ within the AHT simulations with T_{Con} set to 293.15 K and T_{Abs} to 403.15 K, with water as refrigerant and various absorbents

	$T_{Ev/Gen}$ (K)						
Absorbent	**343.95**	**344.05**	**344.15**	**344.85**	**345.65**	**348.15**	**353.15**
LiBr[2]	0.332	0.371	0.396	0.459	0.478	0.494	0.500

Absorbent			$T_{Ev/Gen}$ (K)				
Compound #1	**Compound #2**	**Ratio**	**333.15**	**338.15**	**343.15**	**348.15**	**353.15**
[EMIM][MPH][2]	/	/	0.404	0.419	0.426	0.430	0.432
Glycerol	Choline chloride	[2:1]	0.066	0.385	0.416	0.428	0.434
	TMA chloride	[2:1]	0.302	0.408	0.427	0.434	0.439
	TEA chloride	[2:1]	0.201	0.382	0.412	0.425	0.432
	Betaine	[1:2]	NA	NA	0.368	0.431	0.440
		[1:1]	NA	NA	0.363	0.425	0.436
		[2:1]	NA	NA	0.349	0.416	0.430

D.5. Influence of T_{Abs}

Table S.D34. COP values obtained at various T_{Abs} within the AHT simulations with T_{Con} set to 293.15 K and $T_{Ev/Gen}$ set to 353.15 K, with water as refrigerant and various absorbents

Absorbent			T_{Abs} (K)					
Compound #1	**Compound #2**	**Ratio**	**373.15**	**383.15**	**393.15**	**403.15**	**413.15**	**423.15**
LiBr[2]	/	/	0.495	0.498	0.500	0.500	0.497	0.460
[EMIM][MPH] [2]	/	/	0.461	0.453	0.444	0.432	0.416	0.390
Glycerol	Choline chloride	[2:1]	0.461	0.453	0.445	0.434	0.422	0.407
	TMA chloride	[2:1]	0.462	0.455	0.447	0.439	0.429	0.418
	TEA chloride	[2:1]	0.460	0.452	0.443	0.432	0.419	0.404
	Betaine	[1:2]	0.463	0.456	0.449	0.440	0.426	0.399
		[1:1]	0.462	0.455	0.447	0.436	0.420	0.388
		[2:1]	0.461	0.453	0.443	0.430	0.410	0.369

Table S.D35. Circulation ratio values obtained at various T_{Abs} within the AHT simulations with T_{Con} set to 293.15 K and $T_{Ev/Gen}$ set to 353.15 K, with water as refrigerant and various absorbents

Absorbent			T_{Abs} (K)					
Compound #1	**Compound #2**	**Ratio**	**373.15**	**383.15**	**393.15**	**403.15**	**413.15**	**423.15**
Glycerol	Choline chloride	[2:1]	4.09	6.08	8.60	11.81	15.95	21.40
	TMA chloride	[2:1]	3.73	5.41	7.51	10.12	13.42	17.65
	TEA chloride	[2:1]	5.08	7.39	10.22	13.74	18.17	23.84
	Betaine	[1:2]	3.52	5.22	7.73	11.83	19.63	39.74
		[1:1]	3.83	5.81	8.74	13.48	22.15	42.21
		[2:1]	4.29	6.73	10.38	16.21	26.43	47.72

Reference

(1) *DIPPR. Data Compilation of Pure Compound Properties, Version 12.3.0*; The Design Institute for Physical property Data (DIPPR), 2018.

(2) Nessakh, F. Z.; Mutelet, F.; Negadi, A. Efficiency of Two Working Fluids Constituted of a Deep Eutectic Solvent and Water in Absorption Heat Transformer. *Intl J of Energy Research* **2022**, er.8658. https://doi.org/10.1002/er.8658.

Approche multi-échelle pour la modélisation de fluides de travail des procédés de revalorisation de la chaleur fatale

Résumé

Le secteur industriel produit une quantité importante de chaleur fatale généralement rejetée dans l'atmosphère. Aujourd'hui, il existe différentes technologies pour revaloriser cette énergie perdue. Il est notamment possible de produire de la chaleur à haute température (120 – 150 °C) à partir d'une source de chaleur à température moyenne (typiquement 60 – 80 °C) en utilisant un type particulier de pompe à chaleur à absorption (PACA) : le thermotransformateur de chaleur à absorption. Malheureusement, les mélanges de travail actuellement utilisés (eau/bromure de lithium ou ammoniac/eau) présentent de nombreux inconvénients (corrosion, toxicité, risque de cristallisation…) qui empêchent le développement de ces technologies.

Ce travail porte sur l'étude de couples de travail eau/solvant eutectique profond (SEP) en tant que solution alternative verte et bon marché. Une méthodologie originale basée sur une approche multi-échelle est proposée afin de modéliser les propriétés de nombreux SEP sans avoir besoin de recourir à une étude expérimentale coûteuse. Dans un premier temps, des calculs de chimie quantique ont été réalisés afin de mieux comprendre la structure moléculaire des différents constituants des mélanges de travail et les interactions mises en jeu. L'importance de la liaison hydrogène entre l'ion chlorure et les groupes hydroxyles a ainsi été mise en avant dans les configurations moléculaires les plus stables des SEP {chlorure de choline : phénol} et {chlorure de choline : acide glycolique}. Suite à ces observations, une version modifiée du modèle COSMO-SAC (COnductor-like Screening MOdel segment activity coefficient) prenant en compte les possibles liaisons hydrogène entre les atomes de chlore ou de brome et les groupes hydroxyles a été développée. La prédiction des équilibres liquide-vapeur de mélanges contenant des atomes de chlore ou de brome a ainsi pu être améliorée. Des modèles de contributions de groupes ont également été développés pour prédire deux propriétés clef des SEPs : la masse volumique et la capacité thermique.

Ces modèles ont ensuite été intégrés à un outil de simulation de procédés et ont permis d'évaluer les performances de 32 fluides de travail eau/SEP dans des thermotransformateurs à absorption. Les résultats obtenus sont proches de ceux des mélanges traditionnels.

Mots-clef : thermotransformateur à absorption, solvants eutectiques profonds, revalorisation énergétique, chaleur fatale, modèles prédictifs

Abstract

Industries produce a significant amount of waste heat usually rejected in the atmosphere. As of today, it is possible to produce high temperature heat (120-150°C) from medium temperature heat (60-80°C) by using a particular kind of absorption heat pumps: the absorption heat transformers (PACA type II or AHT). Unfortunately, traditional working fluids (water/lithium bromide or ammonia/water) display numerous drawbacks (corrosion, toxicity, risk of crystallization…) which hinder the development of these technologies.

This study focuses on the working fluids water/deep eutectic solvents (DESs) as a green and cheap solution of replacement. Using an innovative method based on a multiscale approach, this work aims at modelling the properties of many DESs without the need of a comprehensive and costly experimental investigation. At first, quantum chemical calculations were performed in order to get a better understanding of the molecular structure of different components of working fluids and the interactions between them. The importance of the hydrogen bond between the chloride ion and the hydroxyl groups has been highlighted in the most stable conformations of the DESs {choline chloride : phenol} and {choline chloride : glycolic acid}. From these observations, a modified version of the COSMO-SAC (COnductor-like Screening MOdel segment activity coefficient) model taking into account the possible hydrogen bonds between atoms of chlorine or bromine and hydroxyl groups was developed. This model improves the prediction of the vapour-liquid equilibria of mixtures with chlorine and bromine atoms, including DESs. Group contribution models have also been developed to predict two key properties of DESs: the density and the heat capacity.

These models have been implemented in a simulation tool to evaluate the performances of 32 water/DES working fluids in AHT. Their performances are close to those of the traditional working fluids.

Key words: absorption heat transformer, deep eutectic solvents, energy recovery, waste heat, predictive models